The ecology of soil viruses: abundance, distribution, diversity and impact on microbial community structure

A Dissertation Presented for the

Doctor of Philosophy

Degree

The University of Tennessee, Knoxville

Xiaolong Liang

December 2019

DEDICATION

To my parents, Shunxue Liang and Xiubo Xue, and my beloved Yingyue Zhang.

ACKNOWLEDGEMENTS

The body of work in this dissertation reflects the dedication and support from many. My sincere thanks to my supervisor, Dr. Mark Radosevich, for his incredible passion and vision through the entire course of my research. He is unselfish and always supportive like an academic father. He has always inspired me in both research and life. Having Dr. Radosevich as my PhD supervisor is one of the happiest things in my life.

I sincerely thank my committee members, Dr. Jie Zhuang, Dr. Jennifer DeBruyn and Dr. Steven Wilhelm. They have constantly provided constructive feedback and support over the years. They also gave valuable suggestions on my academic career. I am also grateful to Dr. Yusong Wang and Regan Wagner for the wonderful time and discussion we had in and outside the lab.

I also thank China Scholarship Council for the financial support of my four years in UTK and sincere thank Dr. John Stier and Dr. Zhuang who recruited me into my current PhD program. It has been an incredible journey of friendship and personal development. Over the years, I have had many amazing friends in campus, and it has been such an amazing memory of being through all the years together.

I am a Ph.D. because of my supportive and loving family. Thank you, Yingyue, for always being with me in life, in work, and in spirit. Your love, tenacity, and patience are unparalleled. The home with you and Lydia is the warmest place in my life. Thank you, Mom and Dad, for all you have done for me and the unconditional love making it possible for everything I have been able to do.

ABSTRACT

Viruses as a critical biotic component in all ecosystems have exhibited pronounced ecological significance. The global abundance of viruses in the biosphere has been estimated at 1 x 10^{31}, with 90-95% of these viruses residing in soil and/or sedimentary environments. Despite the apparent greater abundance and diversity, soil virology is under-investigated relative to other environments such as marine and freshwater habitats and soil viral genomic data are underrepresented in public repositories of genetic information. In this dissertation, we investigated the viral abundance, diversity, and virus-host interactions in natural soils and the simulated stimulated subsurface bioremediation environments. We used epifluorescence microscopy counting, mitomycin C-induction assays, viral metagenomics sequencing, random amplified polymorphic DNA technique, bacterial 16S rRNA gene amplicons sequencing, and bioinformatics tools and revealed the viral ecology in the soils. Viral abundance and virus-to-bacteria ratio decreased with soil depth in the natural Ultisol, Alfisol, and Mollisol. The bacterial community composition and diversity significantly correlated with viral abundance, virus-to-bacteria ratio, and lysogenic fraction. The inducible lysogenic fractions among bacterial hosts increased with soil depth, indicating lysogeny became the more dominant reproduction strategy for autochthonous soil bacteriophages in deeper soil. The surface soil viromes had higher relative abundances of *Microviridae* (ssDNA virus) compared with the subsurface soil virome. Meanwhile, subsurface soils had higher relative abundances of dsDNA viruses, auxiliary metabolic genes and genes potentially encoding proteins of bacteriophage structural components and replication machinery than surface soils. The results in the simulated subsurface bioremediation systems showed that acetate availability was important in influencing viral abundance, community composition and interactions with microbial hosts. The increased viral abundance coincided with an increase in relative abundance of Fe(III)-reducing bacteria in areas of the columns exhibiting the most Fe(III) reduction. The research in this dissertation furthers our understanding of microbial ecology and has broader implications as the nature of virus-bacteria interactions is of fundamental interest.

TABLE OF CONTENTS

LIST OF TABLES

LIST OF FIGURES

CHAPTER I

Introduction

Publication Note

This chapter is a version of an article in preparation for submission to a Springer book, Biocommunication of Phages, by Xiaolong Liang and Mark Radosevich.

My contribution to this work was literature collection, review, and most of the writing of the manuscript.

Background

In the microbial world, bacteriophages (also known as phages, viruses that infect and replicate within prokaryotes) are ubiquitous and extremely abundant in the environment. Considerable research has revealed that viruses greatly influence microbial diversity and functions (Williamson et al., 2005; 2017; Breitbart et al., 2018; Emerson et al., 2018; Liang et al., 2019c). Phages may impose top-down control over host populations through predation and drive evolutionary processes of microbial communities. Phages have diverse life histories and can be classified into two general categories, i.e., virulent and temperate. While in the extracellular stage, phages are metabolically inactive and act as colloidal particles passively transported via hydrodynamic forces in the environment. When a phage encounters a suitable host cell and initiates viral infection, the phage genome is injected into the host cell entering an intracellular stage, in which virulent phages take control of the transcription and translation machinery in the cell for virion production ultimately leading to cell lysis. In contrast, temperate phages have two general replication-cycle options (either lytic or lysogenic) in the intracellular stage, and the phage can enter the lytic cycle and eventually destroy its host, releasing progeny virions, or follow the lysogenic pathway as the phage genome integrates into its host genome and stably maintains as a prophage and replicates with the host cell divides (Feiner et al., 2015). Temperate phages have the ability to select replication strategies pursuing either the lytic or lysogenic replication pathways depending on environmental and physiological conditions of the host cell (Goldberg et al., 2014; Brum et al., 2016; Howard-Varona et al. 2017). Analysis of the mechanisms underlying the lysis-lysogeny decisions in phage communities is the basis for formative work on phage-host interactions and phage ecological roles (Weitz et al., 2008; Liang and Radosevich, 2019).

The switch between lysis and lysogeny of temperate phages is critical for potential influence of phage infection on host populations and environmental processes and has thus aroused surging interest and exploration on this topic. Several hypothesized models addressing the correlations of phage abundances and replication strategies with host abundances have been previously reported. The Kill-the-Winner (KtW) model proposed that lytic infections lead to steep collapses of the most dominant bacterial populations,

while lysogeny is promoted at low host density, and the paradigm is supported by a wide range of studies (Thomas et al., 2011; Weitz and Wilhelm, 2012; Payet and Suttle, 2013; Silpe and Bassler, 2019). However, a recent study by Knowles et al. (2016) observed low viral abundance at high host densities and attributed the nonlinear relationship to suppressed lytic phage-host dynamics. The increased prevalence of lysogeny at increasing host abundance led to proposal of the Piggyback-the-Winner (PtW) model wherein temperate dynamics dominate over lytic cycles in systems with high host cell densities leading to fewer viruses and more microbes. This work subsequently sparked a debate on viral lysis and lysogeny in natural systems concerning the analysis and interpretation of largely empirical measurements (Weitz et al., 2017). Knowles et al. (2017) took a further step by exploring the correlation of chemical agent based induction estimates of environmental lysogeny with host density and proposed that the fraction of chemically inducible bacterial cells is generally insensitive to host cell densities, and concluded that more innovative methods are needed to investigate the viral lysis-lysogeny decisions.

Microbial communication is important in linking microbial membership to microbially-mediated processes such as biofilm formation, pathogenicity, antibiotic production, symbiosis, conjugation, and elemental cycling. Hall et al. (2018) proposed a framework for understanding the mechanisms of microbiomes influencing the habitat in which the microbial characteristics (i.e., abundance, diversity and functional processes) are linked to the system-level processes. The cell-to-cell communication among bacteria through chemical signal molecules is well known as quorum sensing in which bacteria can regulate gene expression coordinating group behaviors based on cell population density (Waters and Bassler, 2005). Quorum sensing signals may also play a role in lytic-lysogenic decisions (Ghosh et al., 2009; Patterson et al., 2016; Høyland-Kroghsbo et al., 2017). Diverse microbially released molecules serve as the language of microbial communication and are crucial in regulating group behaviors and ecological function. Phages are extremely small (normally with 20-70 nm diameter and up-to-200 nm length) and must depend on their host cell system for replication, thus phage communication if/when it occurs, most likely occurs during the infection state in host cells (Abedon, 2017). Despite the tremendous efforts in exploring environmental virology, phage communication and the

mechanisms of phage functioning remain underexplored making phages "dark matter" in microbial ecology (Roux et al., 2015). In this review, recent progress in phage ecology including phage distribution, diversity, molecular basis of phage communication, and influence of phage infection on microbial communities are discussed with emphasis directed on phage-bacterial interactions at both molecular and community levels.

Approaches for ecological investigation of phages

The ecological importance of phages had long been overlooked, but the discovery of the exceedingly high phage abundances in aquatic environments and more recently soils propelled a significant increase in viral ecology research. Indeed, viruses are recognized as the most abundant lifeforms on earth with an estimated global abundance or 10^{31} virions in the biosphere (Breitbart and Rohwer, 2005; Williamson et al., 2017). Restricted by the inefficiency of phage extraction and counting methods, investigations of phage abundance and distribution in many terrestrial ecosystems (e.g., soil and sediment environments) has lagged behind those of aquatic environments but steady recent progress suggests that Earth's soils harbor an even greater abundance and diversity of viruses than the world's oceans (Williamson et al., 2017). Assessment of virus abundances in soils is complicated by soil heterogeneity and difficulties optimizing efficient extraction protocols applicable to a wide variety of soils. This has made assessment of geographical distributions and inter-study comparisons difficult. (Williamson et al., 2013 and 2017).

Beyond direct microscopic counting, molecular methods based on structural or functional marker genes and metagenomics/metatranscriptomics have been employeed for characterizing phage alpha- and beta-diversity, functional potential, and evolutionary history. Virome sequencing has been used for assessing viral community diversity and potential ecological functions (Brum and Sullivan, 2015; Paez-Espino et al., 2016; Enault et al., 2017; Segobola et al., 2018; Gregory et al., 2019; Dally et al., 2019). These efforts have revealed that the viral communities are highly diverse across all types of ecosystems and have critical roles in microbial mortality, gene transfer, auxiliary metabolic genes (AMGs) mediated metabolic reprogramming and global elemental cycling. Besides directly sequencing viral DNA samples, mining viral sequences from publicly available

microbial genomes and metagenomes is also valuable (Roux et al., 2015a, b). Roux et al. (2015b) tried to resolve phage-host interactions from publicly available microbial genomic data, and their work led to identification of 12,498 microbial host-linked high-confidence viral genomes and augmentation of public virus genome databases. The authors' efforts also identified viral sequences from 13 bacterial phyla in which groups no viral sequences were reported before. Notably, mining viral genomes from microbial genomes was also important in taxonomically identifying the 'unknown' sequence space in viromes, and Roux et al. (2015) identified 7–38% of such type of virome sequences with the recovered viral sequences from microbial genomes.

While metagenomics and classical phage isolation studies have contributed to better understanding of viral ecology, identifying the hosts of most viruses remains a challenge (Tadmor et al., 2011; Allers et al., 2013). Tadmor et al. (2011) employed microfluidic digital PCR targeting a phage and bacterial gene to explore single-cell level phage-host interactions in the termite hindgut. With this method, the authors were able to find the diversity of specific viral marker alleles (terminase gene) co-localized with SSU rRNA genes and revealed genus-wide infection patterns (Tadmor et al., 2011).

For better understanding of phage-host interactions, Allers et al. (2013) developed a technique known as "phageFISH" to detect and visualize intra- and extra-cellular phage DNA. PhageFISH was optimized from the geneFISH technique that consists of gene detection (based on in situ hybridization of double‐stranded DNA probes) and rRNA detection (based on hybridization of horseradish peroxidase‐labelled oligonucleotide probes) (Allers et al., 2013). The phageFISH protocol can identify and quantify both the intracellular replicating phages and extracellular free phages, along with the host cells and also has a high gene detection efficiency of more than 92%. Moreover, phageFISH can show the relative abundance of infected cells and the single‐cell relative extent of phage infection by measuring the area of phage signal.

Substantial progress has been made in virology studies with diverse model systems of virus-host cultivation, experimental and bioinformatic methods generated viral ecology studies, and modelling framework incorporating viruses. However, challenges remain, and future efforts are in earnest need in better understanding of virus-host ecology. Conceptual

models describing the functions of viruses in nutrient and elemental cycling require empirical studies of characterizing viral lysis released dissolved organic matter and corresponding recycling by microorganisms. Taxonomic assignment to viral sequences and annotation of virome contigs require expansion of viral genome database. Viral ecology studies in soil ecosystems, deep terrestrial biosphere and other understudied environments are needed to catalogue viral diversity and examine virus-host interaction dynamics.

Phage abundance and distribution

Phages contacting and subsequently infecting host cells is the basis for the propagation of phages. The opportunity and/or probability of phage-host contact varies depending on the nature of the environment and the abundance of phages and host cells. For example, phages and host cells may be freely dispersed in aquatic environments for virus-host contact and interactions. In contrast, the heterogeneous porous nature of soils can impose physical barriers to phage-host encounters. Here, attachment/detachment to/from mineral and organic surfaces of phages and hosts can dictate phage-host contact rates. Further, phages due to their much smaller size may become spatially separated and sequestered from their host cells in small pores that restrict entry to relatively larger host cells. Therefore, the pore-scale hydrology and moisture content of soil become extremely important factors affecting phage-host contact rates. The phage-host contact rate is assumed to be proportional to virus and microbial cell abundances and, thus estimates of microbial cell abundance may be used to predict phage-host contact rate and phage production (Wigington et al., 2016). Microbial host cell densities also influence phages' reproduction strategy decisions. The relationship between phages and their microbial hosts and the influence of phages on microbial community dynamics and biogeochemical processes are primarily based on the relative abundance of phages and microbial cells. Virus-to-bacterium ratio (VBR) has been used in many studies to represent the contact rates between phages and host cells and infer the strength of phages' influence in prokaryotic communities (Williamson et al., 2005; 2007; Våge et al., 2016; Wigington et al., 2016; Parikka et al., 2017; Emerson et al., 2018). Phage abundances were reported to be

positively correlated with host cell densities (Brum et al., 2016; Edwards et al., 2016; Pan et al., 2017; Liang et al., 2019a); however a broad range of VBR implies a loose connection between phage abundances and microbial cell abundances, and the sublinear relationship showing a lower VBR at increasing microbial densities is attributed to a combination of exogeneous factors (e.g., temperature, eutrophic conditions and radiation) and endogenous factors (e.g., life history traits of viruses and susceptibility of microbes) (Knowles et al., 2016; Weitz et al., 2016; Wigington et al., 2016).

Phage abundances in the environments are influenced by a wide range of factors, and the drivers of phage abundance and distribution in ecosystems are summarized in Table 1.1. Previous studies have shown that the most common factors influencing phage abundance and distribution generally include nutrient availability, temperature, pH, season, host cell density, and human or other biological activities. The conditions in the living environment of phages change continually imposing threats on phage survival. It is important for phages to modulate their population sizes in response to changes in environmental conditions through specific mechanisms. Great efforts have been made in characterizing the mechanism of phages modulating their population dynamics, and the function of phage communication in this process has been demonstrated (Erez et al., 2017; Silpe and Basslar, 2019; Liang et al., 2019b).

Phage-phage communication on phage lysis-lysogeny switching

Cell-cell communication among bacteria using chemical signal molecules (termed "autoinducers"), known as quorum sensing, enables bacteria to monitor the environmental conditions and coordinate a wide range of group behaviors (Waters and Bassler, 2005; Ng and Bassler, 2009). In quorum sensing, bacteria produce, secrete, detect, and respond to autoinducers that carry chemical information, and the communication ultimately synchronizes the gene expression of the group for collective behaviors. In comparison, phage communication associated with infection of bacteria has been much less studied (Abedon, 2017). Phage-phage interactions are diverse and extensively present in nature (Díaz-Muñoz and Koskella, 2014; Díaz-Muñoz SL et al., 2017; Ofir and Sorek, 2018). The reproduction strategy selection is an important feature for phages, and there have been a

Table 1.1: Factors influencing phage abundance and distribution.

Habitat	Factors
Ocean	Nutrient concentrations (Finke et al., 2017) Salinity and temperature (Junger et al., 2018) Prokaryote abundances (Gainer et al., 2017) Organic/inorganic particles (Mojica and Brussaard, 2014) Season (Brum et al., 2016; Gainer et al., 2017) Ultraviolet radiation (Mojica and Brussaard, 2014)
River and lake	Dissolved inorganic carbon (Keshri et al., 2017) Hydrodynamics (turbidity, water transparency, partial pressure of carbon dioxide), dissolved organic carbon (Almeida et al., 2015)
Sediment	Suspended solids, inorganic nutrients (Hewson et al., 2001) Depth in sediment cores (Danovaro et al., 2005) Bacterial densities (Danovaro and Serresi, 2000) Physical-chemical conditions (e.g., temperature; Manini et al., 2008)
Soil	pH (Narr et al., 2017) Total nitrogen content (Narr et al., 2017) Moisture content (Williamson et al., 2005; 2013) Land use (Williamson et al., 2005) Season, water-table height and dissolved oxygen (Ballaud et al., 2016) Organic matter (Amossé et al., 2013) Biological activity (Amossé et al., 2013)
Aquifer & ground water	Trophic conditions (Wilhartitz et al., 2013) Geochemical conditions (e.g., groundwater uranium and DOC; Pan et al., 2017) Abundance of prokaryotic cells (Kyle et al., 2008)
Human body	Sites (Letarov and Kulikov, 2009)

lot of debate on the mechanism of phage lysis-lysogeny decision. However, all the models proposed for predicting phage reproductive strategy and their interactions with host community (eg., KtW and PtW) suggest that phages can sense their host cell density and make decisions accordingly (Knowles et al., 2016; Weitz et al., 2017; Silpe and Bassler, 2019). Meanwhile, lysis-lysogeny decisions occur at both the individual and group levels (Weitz et al., 2008; Zeng et al., 2010). As reported in Zeng et al. (2010), each individual phage, following the infection of host cells by multiple phages, makes a decision between lysis and lysogeny based on the phage particle abundance per cell volume. Then, a precise integration of the decisions by all phages infecting the same cell leads to a group decision, in which lysogeny is only reached by a unanimous ‘‘vote’’ by all phage members (Zeng et al., 2010). All these studies suggest that phages should have specific communication systems for making group decisions.

The first report of a phage-to-phage based communication system by Erez et al. (2017) showed that *Bacillus* phage phi3T encoded hexapeptides are produced during infection of its host cell, and the signal peptides are secreted by host *Bacillus* and accumulate in the local environment. The progeny phages can sense the population level of nearby relatives through the host *Bacillus*-secreted extracellular signals and make lysis-lysogeny decisions accordingly. The small-molecule communication system, termed “arbitrium” system, includes three phage genes (i.e., *aimP*, *aimR*, and *aimX*) that are involved in the production of the peptide signals (AimP*)*, intracellular receptor (AimR) of the peptide, and a negative regulator (AimX) of lysogeny (Fig. 1.1a). The expression of the *aimP* and *aimR* starts immediately upon infection of *Bacillus* host cell, while the expression of *aimX* needs to be activated by AimR. AimX inhibits lysogeny of the phage leading to a lytic cycle. However, AimR, as the arbitrium receptor, can bind to the mature arbitrium molecule preventing activation of *aimX* expression. The *aimP*-encoded peptides are recognized, cleaved, and secreted outside the cell, and the released molecules are further processed into six-amino-acid-long mature arbitrium peptides by host extracellular proteases. The molecular mechanism of phage communication systems was also described in detail by Wang et al. (2018) and del Sol et al. (2019). Upon infection, phages detect the concentration of the signal peptides using the arbitrium receptor AimR and decide on

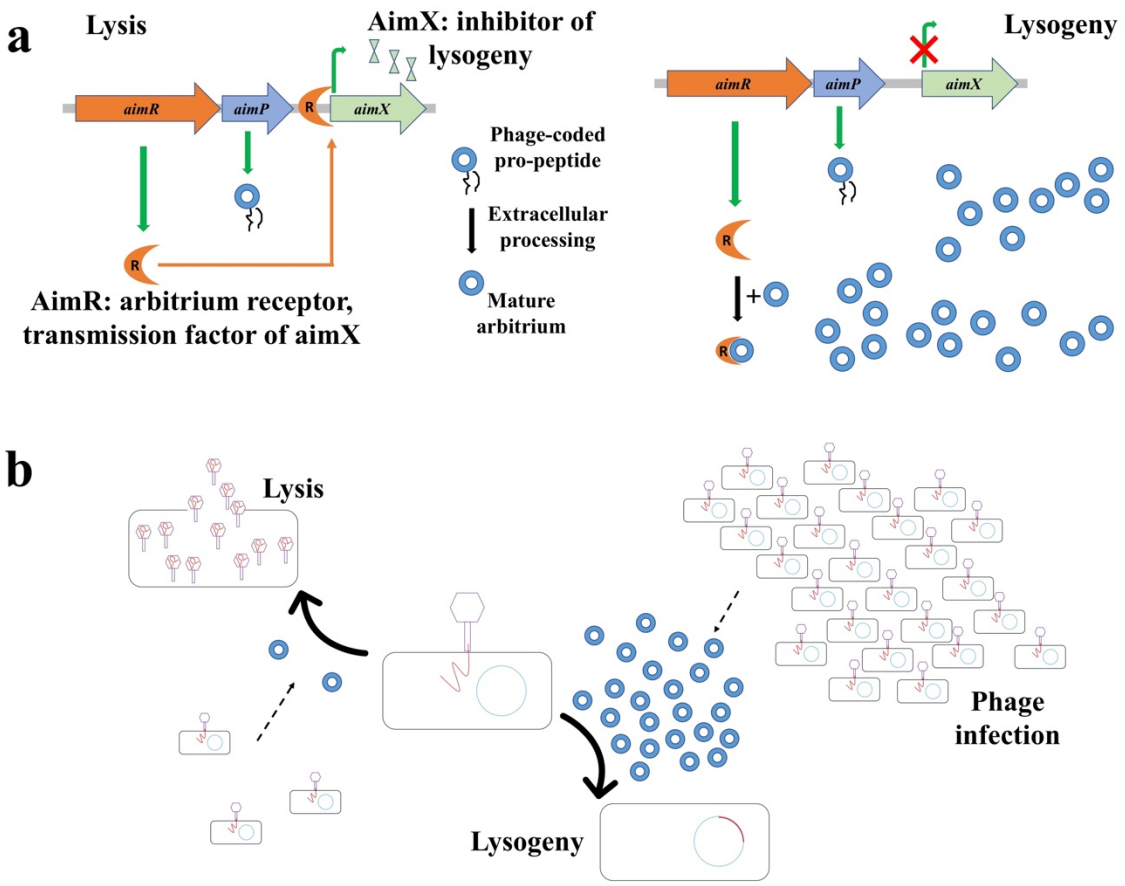

Figure 1.1: Mechanistic model of phage-phage communication for lysis-lysogeny decisions.

whether to lyse or lysogenize the host cell (Fig. 1.1b). High concentrations of arbitrium peptides lead to lysogenic cycles in phage-infected cells, and low concentrations of arbitrium peptides direct phages to lytic reproduction pathways. Thus, the arbitrium communication between phages enables infecting phages to lysogenize and extend the infection period as prophages when potential host cells are mostly phage infected.

Erez et al. (2017) also found that the communication peptide in arbitrium systems is phage-specific and can only influence the closely related phages. Two different phage-encoded communication peptides (SAIRGA and GMPRGA) that are effective in driving infection kinetics of specific *Bacillus* phages in a different fashion have also been reported (Dou et al. 2018). These studies demonstrated that there are multiple molecular mechanisms in determining phage lysis-lysogeny decisions and subtle structural changes of phage-encoded communication peptides can lead to distinct lysis-lysogeny decision pathways. The viral arbitrium communication mechanism has important ecological implications. Previous research showed that lysogeny is favored under conditions of low host cell density and nutrient availability (Ghosh et al., 2008; Thomas et al., 2011; Brum et al., 2016; Touchon et al., 2016), however the arbitrium communication mechanism suggests that high abundances of infected host cells cause high concentrations of arbitrium signal and guide phages into lysogenic cycles. The small-molecule phage communication mechanism may provide indirect evidence and theoretical support for the recently proposed Piggyback-the-Winner model (Knowles et al., 2016; Silveira and Rohwer, 2016; Coutinho et al., 2017).

Phage-host communication on phage lysis-lysogeny switching

The long-term existence of phages depends on prokaryotic hosts, and preliminary efforts have been made to characterize the complicated interactions between bacteria and phages, e.g., parasitic infection, coevolution of arms race dynamics, and symbiosis through metabolic reprograming (Roucourt and Lavigne, 2009; Díaz-Muñoz and Koskella, 2014; De Sordi et al., 2019; Moreno-Gallego et al., 2019). Furthermore, phage reproductive cycles have significant impacts on host populations, physiology, and also phage-host dynamics. Quorum sensing systems, indicative of bacterial density as discussed above,

were reported to activate prophage induction in soil and groundwater bacteria and a model bacterium *E. coli* (Ghosh et al., 2009). The authors also showed that the mechanism of homoserine lactone-based prophage induction was SOS (i.e. *recA*) independent. This study offered the first experimental evidence of cell-density dependent prophage induction indicating that prophage induction mechanisms can also be activated during times of high host cell density when the physiological conditions of potential host cells was favorable for growth.

The new molecular mechanism of quorum sensing-based lysis-lysogeny decisions was recently reported (Silpe and Bassler, 2019). Specifically, the *Vibrio* quorum-sensing signal molecules 3,5-dimethylpyrazin-2-ol (DPO) are used as a que for vibriophage VP882 to determine the host cell density. The mechanistic model for host quorum sensing-based phage reproduction strategy selection, in which phage genes pg55, gp56, gp59, gp62, gp69, gp70, and gp71 are included, is shown in Fig. 2.2. The vibriophage genes gp69, gp70, and gp71 are necessary to execute lysis of the infected host cell. In the lysogeny circuit, Gp59 (shown as cl repressor, Fig. 2.2a) can directly repress the expression of gene 62 which codes the lysis genes-launching protein Q anti-terminator. Host cell lysis is promoted when the concentration of host-produced quorum-sensing DPO is high, and large amounts of DPO-binding $VqmA_{phage}$ protein of vibriophage VP882 bind to DPO and are activated. The DPO-activated $VqmA_{phage}$ binds upstream of gene gp55 activating the expression of Q-tip anti-repressor. Q-tip directly aggregates the cl repressor preventing cl from binding to the promoter of gene 62 which allows normal production of Q anti-terminator. Q activates lysis genes inducing lysis of the host cell. In summary, the host quorum-sensing autoinducer concentration indicating host cell density can guide the lysis-lysogeny decisions of phages (Fig. 2.2b).

The communication between phages and bacteria has significance for microbial ecology (Liang et al, 2019b). As Silpe and Bassler (2019) showed in the model of quorum sensing-mediated viral reproductive strategy selection, lysogeny is favored under conditions of low host cell density, while high host cell density tend to induce lytic cycles of phages. These reports provide strong support for the Kill-the-Winner hypothesis.

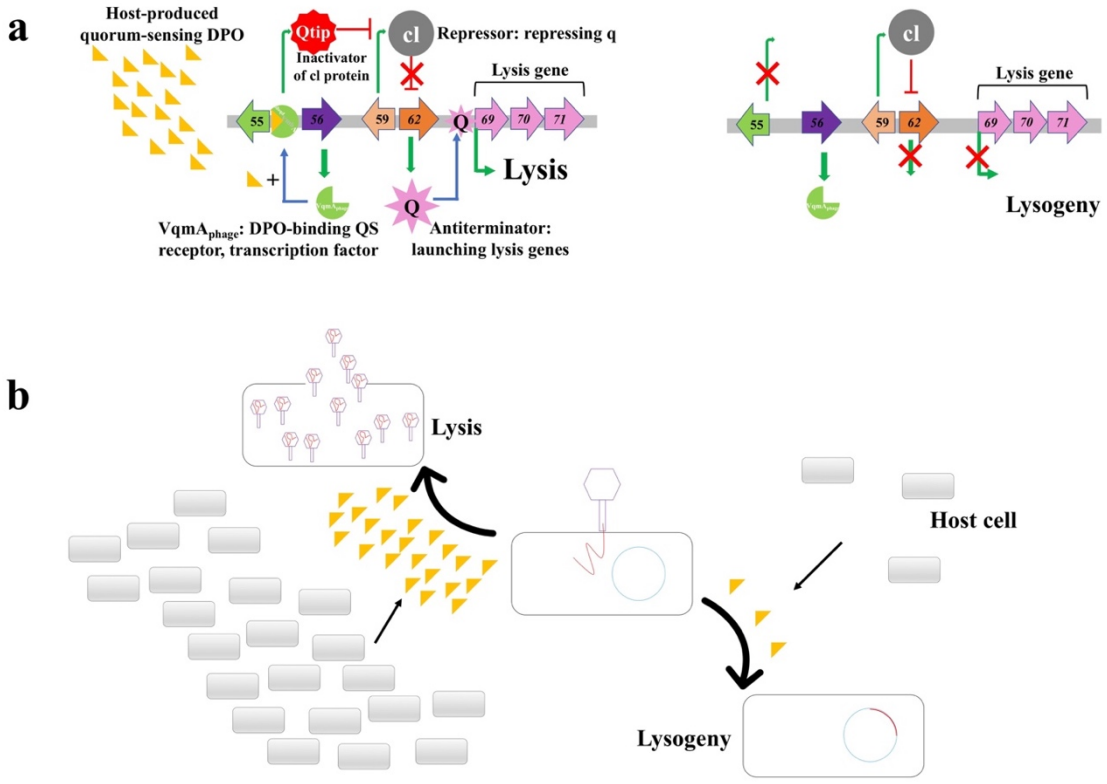

Figure 1.2: Mechanistic model for quorum sensing-mediated lysis-lysogeny decisions.

Phage top-down controls over microbial activity and community diversity

Microbes play substantial roles in biogeochemical cycling on a global scale, and many ecosystem processes are predominately microbially driven. Environmental factors have been demonstrated critical in modulating microbial community diversity, microbial-mediated biogeochemical processes, and interplays among the microbial members executing these processes (Coutinho et al., 2018). As viruses are the most abundant biological entities on the planet, tremendous efforts have been made to determine the ecological roles of viruses, especially prokaryote-infecting phages. As discussed in the introduction section, phages (lytic/temperate) preferentially kill or support their host cells following specific patterns (e.g., Kill-the-Winner and Piggyback-the-Winner) for production of new viral particles affecting microbial population dynamics, community composition, and diversity. Furthermore, phages have been reported to carry auxiliary metabolic genes (AMGs) and express these genes during infection to alter host metabolic pathways which most likely benefit the hosts (Williamson et al., 2017; Coutinho et al., 2018). Thus, characterizing the phage-host relationships is critical in understanding the microbial ecological function (Chow et al., 2014).

In a series of microcosm experiments by Coloma et al. (2017), the introduction of *Nodularia* phages caused an evolution of the cyanobacterial community from a *Nodularia*-dominated population (susceptible to viral lysis) to a *Synechococcu*s-dominated population (resistant to viral lysis). Phages with broad or narrow host ranges can sharply reduce host cell abundances creating opportunity for increased population growth of other species/strains just as the Kill-the-Winner hypothesis suggested. Morella et al. (2018) showed that phages significantly impacted the relative abundance of dominant bacterial community members, and the overall bacterial abundance decreased due to phage-mediated lysis of most abundant and/or fastest-growing bacterial species during initial colonization of a new plant. Phage infections as an important factor of shaping microbial community structure may cause large variation in microbial taxonomic composition (Steffen et al., 2015; Storesund et al., 2015; Louca and Doebeli, 2018). Previous efforts have also demonstrated the importance of phages in microbial respiration (Allen et al., 2010), carbon processing (Trubl et al., 2018), Fe(III)-bioreduction (Liang et al., 2019a),

and nutrient cycling (Weitz and Wilhelm, 2012), yet it is still largely unknown how phage infections influence microbial community function.

Phage-host coevolution

Close interactions between phages and host prokaryotes lead to their dynamic coexistence and coevolution. Phages can mediate horizontal gene transfer and continually contribute to the appearance of new genotypes facilitating the evolution of prokaryotic hosts (Thomas and Nielsen, 2005). Phages as viral predators of prokaryotes constantly attack their hosts to reproduce. In response, the prokaryotes have evolved diverse defense strategies against viral infections for better survival (Dy et al., 2014; Sneed, 2015). In turn, phages may rapidly evolve effective strategies to overcome the infection barriers, resulting in constant cycles of evolutionary arms race between the interacting predator and prey (Koskella and Brockhurst et al., 2014; De Sordi et al., 2019). The parasite-host coevolution battles over every stage of the phage life cycle, i.e., phage attachment to host cell surface, phage DNA entry, and phage replication and release.

The coevolution of phages and prokaryotes influences the population dynamics of both sides and have essential roles in driving and preserving microbial diversity. The frequency of virus‐resistant hosts, that substantially influences the community dynamics, may fluctuate as the phages and prokaryotes coevolve (Coloma et al., 2019). Arms race dynamics (ARD, featuring increasing host resistance and phage infectivity with time) and fluctuating selection dynamics (FSD, characteristic of frequency-based selection of host resistance alleles by phage evolution) are two most commonly considered models for phage-host antagonistic coevolution (Gómez and Buckling, 2011; Scanlan, 2017).

Quorum sensing system can coordinate bacterial group behaviors based on population density and also play an important role in phage-host interactions via influencing the lysis-lysogeny decisions of phages. The impacts of quorum sensing on bacterial susceptibility to phage infection had been overlooked until Høyland-Kroghsbo et al. (2013) reported that the quorum-sensing signals N-acyl-L-homoserine lactones (AHLs) significantly reduced the phage adsorption due to cell-density-dependent down-regulation of the surface phage receptors and drastically increased the frequency of uninfected cells.

Though not reviewed here, the mechanism that quorum sensing affect host resistance against phages also includes strengthening CRISPR-Cas adaptive immune systems in host cells (Patterson et al., 2016; Høyland-Kroghsbo et al., 2017).

Conclusion

Bacteriophages ubiquitous in environments are the most abundant biological entities mostly outnumbering their coexisting microbial cells by 10- to 1000-fold. Phage infections have been demonstrated as a key determinant of microbial population size, composition, structure, and evolution. The impacts of phages over their microbial hosts are closely related with the life properties of phages, typically infection types, morphology, host range, etc. The biology of phages is fundamental to elucidate phage-host relationship and further understanding microbial systems (Clokie et al., 2011). Phages used to be conceived to be too small to have molecular systems for group communication and coordinated behaviors. However, some recent excellent studies have revealed the phage-phage (Erez et al., 2017; Dou et al., 2018; Wang et al., 2018; Sol et al., 2019) and trans-kingdom phage-bacteria (Silpe and Bassler, 2019) communication mechanisms for phage lysis-lysogeny decisions which is a key determinant of phage-host interactions and coevolution.

In this dissertation, we have shown new advances in phage ecology and how molecular level communication systems contribute to phage and microbial host activity, population dynamics, community diversity, and the reciprocal evolution of host immunity and phage anti-immunity. As the discovery of phage communication has greatly inspired microbiologist, a lot more efforts need to be made to unravel the mechanisms and complicated networks of the interconnected microbial systems. The ecological role of phage communication still needs to be addressed. Other than the biological interactions between phages and hosts structuring microbial populations, the inhabiting environment could also impose equal selection pressures on phage and host communities and shape evolutionary trajectories (Gómez and Buckling, 2011). Lab-scale and field-scale experiments should be combined, while the biological interactions and environmental conditions need to be integrated for a better understanding of microbial ecology.

List of References

Abedon ST (2017) Commentary: Communication between Viruses Guides Lysis–Lysogeny Decisions. Front Microbiol 8:983.

Allen B, Willner D, Oechel WC, Lipson D (2010) Top-down control of microbial activity and biomass in an Arctic soil ecosystem. Environ Microbiol 12:642-648.

Allers E, Moraru C, Duhaime MB, Beneze E, Solonenko N, Barrero-Canosa J, Amann R, Sullivan MB (2013) Single-cell and population level viral infection dynamics revealed by phage FISH, a method to visualize intracellular and free viruses. Environ Microbiol 15:2306-2318.

Almeida RM, Roland F, Cardoso SJ, Farjalla VF, Bozelli RL, Barros NO (2015) Viruses and bacteria in floodplain lakes along a major Amazon tributary respond to distance to the Amazon River. Front Microbiol 6:158.

Amossé J, Bettarel Y, Bouvier C, Bouvier T, Duc TT, Thu TD, Jouquet P (2013) The flows of nitrogen, bacteria and viruses from the soil to water compartments are influenced by earthworm activity and organic fertilization (compost vs. vermicompost). Soil Biol Biochem 66:197-203.

Ballaud F, Dufresne A, Francez AJ, Colombet J, Sime-Ngando T, Quaiser A (2016) Dynamics of viral abundance and diversity in a Sphagnum-dominated peatland: temporal fluctuations prevail over habitat. Front Microbiol 6: 1494.

Breitbart M, Bonnain C, Malki K, Sawaya NA (2018) Phage puppet masters of the marine microbial realm. Nat Microbiol 3:754-766.

Breitbart M, Rohwer F (2005) Here a virus, there a virus, everywhere the same virus?. Trends Microbiol 13:278-84.

Brum JR, Hurwitz BL, Schofield O, Ducklow HW, Sullivan MB (2016) Seasonal time bombs: dominant temperate viruses affect Southern Ocean microbial dynamics. ISME J 10:437-449.

Brum JR, Sullivan MB (2015) Rising to the challenge: accelerated pace of discovery transforms marine virology. Nat Rev Microbiol 13:147-159.

Clokie MR, Millard AD, Letarov AV, Heaphy S (2011) Phages in nature. Bacteriophage 1:31-45.

Coloma SE, Dienstbier A, Bamford DH, Sivonen K, Roine E, Hiltunen T (2017) Newly isolated Nodularia phage influences cyanobacterial community dynamics. Environ Microbiol 19:273-286.

Coloma S, Gaedke U, Sivonen K, Hiltunen T (2019) Frequency of virus-resistant hosts determines experimental community dynamics. Ecology 100:e02554.

Coutinho FH, Gregoracci GB, Walter JM, Thompson CC, Thompson FL (2018) Metagenomics sheds light on the ecology of marine microbes and their viruses. Trends Microbiol 11:955-965.

Coutinho FH, Silveira CB, Gregoracci GB, Thompson CC, Edwards RA, Brussaard CP, et al (2017) Marine viruses discovered via metagenomics shed light on viral strategies throughout the oceans. Nat Commun 8:15955.

Daly RA, Roux S, Borton MA, Morgan DM, Johnston MD, Booker AE, et al (2019) Viruses control dominant bacteria colonizing the terrestrial deep biosphere after hydraulic fracturing. Nat Microbiol 4:352-361.

Danovaro R, Serresi M (2000) Viral density and virus-to-bacterium ratio in deep-sea sediments of the Eastern Mediterranean. Appl Environ Microbiol 66:1857-1861.

Danovaro R, Corinaldesi C, Dell'Anno A, Fabiano M, Corselli C (2005) Viruses, prokaryotes and DNA in the sediments of a deep-hypersaline anoxic basin (DHAB) of the Mediterranean Sea. Environ Microbiol 7:586-592.

del Sol FG, Penadés JR, Marina A (2019) Deciphering the Molecular Mechanism Underpinning Phage Arbitrium Communication Systems. Mol Cell 74:59-72.

De Sordi L, Lourenço M, Debarbieux L (2019) The Battle Within: Interactions of Bacteriophages and Bacteria in the Gastrointestinal Tract. Cell Host Microbe 25:210-218.

Dy RL, Richter C, Salmond GP, Fineran PC (2014) Remarkable mechanisms in microbes to resist phage infections. Annu Rev Virol 1:307-331.

Harms A, Diard M (2019) Crowd Controlled—Host Quorum Sensing Drives Phage Decision. Cell Host Microbe 25:179-181.

Díaz-Muñoz SL, Sanjuán R, West S (2017) Conflict, Cooperation, and Communication among Viruses. Cell Host Microbe 22:437-441.

Díaz-Muñoz SL, Koskella B (2014) Bacteria–phage interactions in natural environments. In: Gadd G, Sariaslani S (ed) Advances in applied microbiology, vol 89. Academic Press, San Diego, pp 135-183

Dou C, Xiong J, Gu Y, Yin K, Wang J, Hu Y, et al (2018) Structural and functional insights into the regulation of the lysis–lysogeny decision in viral communities. Nat Microbiol 3:1285-1294.

Edwards RA, McNair K, Faust K, Raes J, Dutilh BE (2016) Computational approaches to predict bacteriophage–host relationships. FEMS Microbiol Rev 40:258-272.

Emerson JB, Roux S, Brum JR, Bolduc B, Woodcroft BJ, Jang HB, et al (2018) Host-linked soil viral ecology along a permafrost thaw gradient. Nat Microbiol 3:870-880.

Enault F, Briet A, Bouteille L, Roux S, Sullivan MB, Petit MA (2017) Phages rarely encode antibiotic resistance genes: a cautionary tale for virome analyses. ISME J 11:237-247.

Erez Z, Steinberger-Levy I, Shamir M, Doron S, Stokar-Avihail A, Peleg Y et al (2017) Communication between viruses guides lysis–lysogeny decisions. Nature 541:488-593.

Feiner R, Argov T, Rabinovich L, Sigal N, Borovok I, Herskovits AA (2015) A new perspective on lysogeny: prophages as active regulatory switches of bacteria. Nat Rev Microbiol 13:641-650.

Finke JF, Hunt BP, Winter C, Carmack EC, Suttle CA (2017) Nutrients and other environmental factors influence virus abundances across oxic and hypoxic marine environments. Viruses 9:152.

Gainer PJ, Pound HL, Larkin AA, LeCleir GR, DeBruyn JM, Zinser ER, Johnson ZI, Wilhelm SW (2017) Contrasting seasonal drivers of virus abundance and production in the North Pacific Ocean. PloS One 12:e0184371.

Ghosh D, Roy K, Williamson KE, White DC, Wommack KE, Sublette KL et al (2008). Prevalence of lysogeny among soil bacteria and presence of 16S rRNA and trzN genes in viral-community DNA. Appl Environ Microbiol 74:495–502.

Ghosh D, Roy K, Williamson KE, Srinivasiah S, Wommack KE, Radosevich M (2009) Acyl-homoserine lactones can induce virus production in lysogenic bacteria: an alternative paradigm for prophage induction. Appl Environ Microbiol 75:7142-7152.

Goldberg GW, Jiang W, Bikard D, Marraffini LA (2014) Conditional tolerance of temperate phages via transcription-dependent CRISPR-Cas targeting. Nature 514:633-637.

Gómez P, Buckling A (2011) Bacteria-phage antagonistic coevolution in soil. Science 332:106-109.

Gregory AC, Zayed AA, Conceição-Neto N, Temperton B, Bolduc B, Alberti A, et al (2019) Marine DNA viral macro-and microdiversity from pole to pole. Cell 177:1109-23.

Hall EK, Bernhardt ES, Bier RL, Bradford MA, Boot CM, Cotner JB, et al (2018) Understanding how microbiomes influence the systems they inhabit. Nat Microbiol 3:977-982.

Hewson I, O'Neil JM, Fuhrman JA, Dennison WC (2001) Virus-like particle distribution and abundance in sediments and overlying waters along eutrophication gradients in two subtropical estuaries. Limnol Oceanogr 46:1734-1746.

Howard-Varona C, Hargreaves KR, Abedon ST, Sullivan MB (2017) Lysogeny in nature: mechanisms, impact and ecology of temperate phages. ISME J 11:1511-1520.

Høyland-Kroghsbo NM, Mærkedahl RB, Svenningsen SL (2013) A quorum-sensing-induced bacteriophage defense mechanism. MBio 4:e00362-12.

Høyland-Kroghsbo NM, Paczkowski J, Mukherjee S, Broniewski J, Westra E, Bondy-Denomy J, Bassler BL (2017) Quorum sensing controls the Pseudomonas aeruginosa CRISPR-Cas adaptive immune system. Proc Natl Acad Sci U S A 114:131-135.

Keshri J, Ram ASP, Colombet J, Perriere F, Thouvenot A, Sime-Ngando T (2017) Differential impact of lytic viruses on the taxonomical resolution of freshwater bacterioplankton community structure. Water Res 124:129-138.

Knowles B, Silveira CB, Bailey BA, Barott K, Cantu VA, Cobián-Güemes AG, et al (2016) Lytic to temperate switching of viral communities. Nature 531:466-470.

Knowles B, Bailey B, Boling L, Breitbart M, Cobián-Güemes A, del Campo J, et al (2017) Variability and host density independence in inductions-based estimates of environmental lysogeny. Nat Microbiol 2:17064.

Koskella B, Brockhurst MA (2014) Bacteria–phage coevolution as a driver of ecological and evolutionary processes in microbial communities. FEMS Microbiol Rev 38:916-931.

Kyle JE, Eydal HS, Ferris FG, Pedersen K (2008) Viruses in granitic groundwater from 69 to 450 m depth of the Äspö hard rock laboratory, Sweden. ISME J 2:571-574.

Letarov A, Kulikov E (2009) The bacteriophages in human-and animal body-associated microbial communities. J Appl Microbiol 107:1-13.

Liang X, Radosevich M (2019) Commentary: A Host-Produced Quorum-Sensing Autoinducer Controls a Phage Lysis-Lysogeny Decision. Front Microbiol 10:1201.

Liang X, Zhuang J, Löffler FE, Zhang Y, DeBruyn J, Wilhelm S, Schaeffer SM, Radosevich M (2019a) Viral and bacterial community responses to stimulated Fe(III)-bioreduction during simulated subsurface bioremediation. Environ Microbiol 21:2043-2055.

Liang X, Wagner RE, Li B, Zhang N, Radosevich M (2019b) Prophage induction mediated by quorum sensing signals alters soil bacterial community structure. bioRxiv 805069.

Liang X, Wagner RE, Zhuang J, DeBruyn JM, Wilhelm SW, Liu F, Yang L, Staton ME, Sherfy AC, Radosevich M (2019c) Viral abundance and diversity vary with depth in a southeastern United States agricultural ultisol. Soil Biol Biochem 137:107546.

Louca S, Doebeli M (2018) Taxonomic variability and functional stability in microbial communities infected by phages. Environ Microbiol 19:3863-3878.

Manini E, Luna GM, Corinaldesi C, Zeppilli D, Bortoluzzi G, Caramanna G, Raffa F, Danovaro R (2008) Prokaryote diversity and virus abundance in shallow hydrothermal vents of the Mediterranean Sea (Panarea Island) and the Pacific Ocean (North Sulawesi-Indonesia). Microb Ecol 55:626-639.

Mojica KD, Brussaard CP (2014) Factors affecting virus dynamics and microbial host–virus interactions in marine environments. FEMS Microbiol Ecol 89:495-515.

Morella NM, Gomez AL, Wang G, Leung MS, Koskella B (2018) The impact of bacteriophages on phyllosphere bacterial abundance and composition. Mol Ecol 27:2025-2038.

Moreno-Gallego JL, Chou SP, Di Rienzi SC, Goodrich JK, Spector TD, Bell JT, Youngblut ND, Hewson I, Reyes A, Ley RE (2019) Virome Diversity Correlates with Intestinal Microbiome Diversity in Adult Monozygotic Twins. Cell Host Microbe 25:261-272.

Ng, WL, Bassler, BL (2009) Bacterial quorum-sensing network architectures. Annu Rev Genet 43:197-222.

Ofir G, Sorek R (2018) Contemporary phage biology: From classic models to new insights. Cell 172:1260-1270.

Paez-Espino D, Eloe-Fadrosh EA, Pavlopoulos GA, Thomas AD, Huntemann M,

Mikhailova N, Rubin E, Ivanova NN, Kyrpides NC (2016) Uncovering Earth's virome. Nature 536:425-430.

Pan D, Nolan J, Williams KH, Robbins MJ, Weber KA (2017) Abundance and Distribution of Microbial Cells and Viruses in an Alluvial Aquifer. Front Microbiol 8:1199.

Parikka KJ, Le Romancer M, Wauters N, Jacquet S (2017) Deciphering the virus-to-prokaryote ratio (VPR): insights into virus–host relationships in a variety of ecosystems. Biol Rev 92:1081-1100.

Patterson AG, Jackson SA, Taylor C, Evans GB, Salmond GP, Przybilski R, Staals RH, Fineran PC (2016) Quorum sensing controls adaptive immunity through the regulation of multiple CRISPR-Cas systems. Mol cell 64:1102-1108.

Payet JP, Suttle CA (2013) To kill or not to kill: the balance between lytic and lysogenic viral infection is driven by trophic status. Limnol Oceanogr 58:465-74.

Roucourt B, Lavigne R (2009) The role of interactions between phage and bacterial proteins within the infected cell: a diverse and puzzling interactome. Environ Microbiol 11:2789-805.

Roux S, Enault F, Hurwitz BL, Sullivan MB (2015a) VirSorter: mining viral signal from microbial genomic data. PeerJ 3:e985.

Roux S, Hallam SJ, Woyke T, Sullivan MB (2015b) Viral dark matter and virus–host interactions resolved from publicly available microbial genomes. Elife 4:e08490.

Roux S, Brum JR, Dutilh BE, Sunagawa S, Duhaime MB, Loy A et al (2016) Ecogenomics and potential biogeochemical impacts of globally abundant ocean viruses. Nature 537:689-693.

Scanlan PD (2017) Bacteria–bacteriophage coevolution in the human gut: implications for microbial diversity and functionality. Trends Microbiol 25:614-623.

Segobola J, Adriaenssens E, Tsekoa T, Rashamuse K, Cowan D (2018) Exploring viral diversity in a unique South African soil habitat. Scientific reports. Sci Rep 8:111.

Silpe JE, Bassler BL (2019) A Host-Produced Quorum-Sensing Autoinducer Controls a Phage Lysis-Lysogeny Decision. Cell 176:1-13.

Silveira CB, Rohwer FL (2016) Piggyback-the-Winner in host-associated microbial communities. NPJ Biofilms Microbi 2:16010.

Seed KD (2015) Battling phages: How bacteria defend against viral attack. PLoS Pathog 11:e1004847.

Steffen MM, Belisle BS, Watson SB, Boyer GL, Bourbonniere RA, Wilhelm SW (2015) Metatranscriptomic evidence for co-occurring top-down and bottom-up controls on toxic cyanobacterial communities. Appl Environ Microbiol 81:3268-76.

Storesund JE, Erga SR, Ray JL, Thingstad TF, Sandaa RA (2015) Top-down and bottom-up control on bacterial diversity in a western Norwegian deep-silled fjord. FEMS Microbiol Ecol 91:fiv076.

Tadmor AD, Ottesen EA, Leadbetter JR, Phillips R (2011) Probing individual environmental bacteria for viruses by using microfluidic digital PCR. Science 333:58-62.

Thomas R, Berdjeb L, Sime-Ngando T, Jacquet S (2011) Viral abundance, production, decay rates and life strategies (lysogeny versus lysis) in Lake Bourget (France). Environ Microbiol 13:616-630.

Thomas CM, Nielsen KM (2005) Mechanisms of, and barriers to, horizontal gene transfer between bacteria. Nat Rev Microbiol 3:711-721.

Touchon M, Bernheim A, Rocha EP (2016) Genetic and life-history traits associated with the distribution of prophages in bacteria. ISME J 10:2744-2754.

Trubl G, Jang HB, Roux S, Emerson JB, Solonenko N, Vik DR, Solden L, Ellenbogen J, Runyon AT, Bolduc B, Woodcroft BJ (2018) Soil viruses are underexplored players in ecosystem carbon processing. mSystems 3:e00076-18.

Våge S, Pree B, Thingstad TF (2016) Linking internal and external bacterial community control gives mechanistic framework for pelagic virus-to-bacteria ratios. Environ Microbiol 18:3932-3948.

Wang Q, Guan Z, Pei K, Wang J, Liu Z, Yin P, Peng D, Zou T (2018) Structural basis of the arbitrium peptide–AimR communication system in the phage lysis–lysogeny decision. Nat Microbiol 3:1266-1273.

Waters CM, Bassler BL (2005) Quorum sensing: cell-to-cell communication in bacteria. Annu. Rev Cell Dev Biol 21:319-346.

Weitz JS, Mileyko Y, Joh RI, Voit EO (2008) Collective decision making in bacterial viruses. Biophys J 95:2673-2680.

Weitz JS, Wilhelm SW (2012) Ocean viruses and their effects on microbial communities and biogeochemical cycles. F1000 Biol Rep 4:17

Weitz JS, Beckett SJ, Brum JR, Cael BB, Dushoff J (2017) Lysis, lysogeny and virus–microbe ratios. Nature 549:E1-E3.

Wigington CH, Sonderegger D, Brussaard CP, Buchan A, Finke JF, Fuhrman JA, et al (2016) Re-examination of the relationship between marine virus and microbial cell abundances. Nat Microbiol 1:15024.

Wilhartitz IC, Kirschner AK, Brussaard CP, Fischer UR, Wieltschnig C, Stadler H, Farnleitner AH (2013) Dynamics of natural prokaryotes, viruses, and heterotrophic nanoflagellates in alpine karstic groundwater. Microbiologyopen 2:633-643.

Williamson KE, Radosevich M, Wommack KE (2005) Abundance and diversity of viruses in six Delaware soils. Appl Environ Microbiol 71:3119-3125.

Williamson KE, Radosevich M, Smith DW, Wommack KE (2007) Incidence of lysogeny within temperate and extreme soil environments. Environ Microbiol 9:2563-2574.

Williamson KE, Corzo KA, Drissi CL, Buckingham JM, Thompson CP, Helton RR (2013) Estimates of viral abundance in soils are strongly influenced by extraction and enumeration methods. Biol Fertil Soils 49:857-869.

Williamson KE, Fuhrmann JJ, Wommack KE, Radosevich M (2017) Viruses in soil ecosystems: an unknown quantity within an unexplored territory. Annu Rev Virol 4:201-219.

Zeng L, Skinner SO, Zong C, Sippy J, Feiss M, Golding I (2010) Decision making at a subcellular level determines the outcome of bacteriophage infection. Cell 141:682-691.

CHAPTER II

Impact of microbial iron oxide reduction on the transport of diffusible tracers and non-diffusible nanoparticles in soils

Publication Note

This chapter was originally published as a peer-reviewed article by Xiaolong Liang, Mark Radosevich, Frank Löffler, Sean M. Schaeffer, and Jie Zhuang in *Chemosphere*.

My contribution to this work was performing lab works (with Yusong Wang), processing the samples, statistical analyses, and most of the writing of the manuscript.

Citation

Liang, X., Radosevich, M., Löffler, F., Schaeffer, S.M. and Zhuang, J., 2019. Impact of microbial iron oxide reduction on the transport of diffusible tracers and non-diffusible nanoparticles in soils. Chemosphere, 220, 391-402.

Abstract

In subsurface bioremediation, electron donor addition promotes microbial Fe(III)-oxide mineral reduction that could change soil pore structure, release colloids, and alter soil surface properties. These processes in turn may impact bioremediation rates and the ultimate fate of contaminants. Columns packed with water-stable, Fe-oxide-rich soil aggregates were infused with acetate-containing artificial groundwater and operated for 20 d or 60 d inside an anoxic chamber. Soluble Fe(II) and soil colloids were detected in the effluent within one week after initiation of the acetate addition, demonstrating Fe(III)-bioreduction and colloid formation. Diffusible Br^-, less diffusible 2,6-difluorobenzoate (DFBA), and non-diffusible silica-shelled silver nanoparticles (SSSNP) were used as tracers in transport experiments before and after the bioreduction. The transport of Br− was not influenced by the bioreduction. DFBA showed earlier breakthrough and less tailing after the bioreduction, suggesting alterations in flow paths and soil surface chemistry during the 20-d bioreduction treatment. Similarly, the bioreduction increased the transport of SSSNP very significantly, with mass recovery increasing from 1.7% to 25.1%. Unexpectedly, the SSSNP was completely retained in the columns when the acetate injection was extended from 20 to 60 d, while the mass recovery of DFBA decreased from 89.1% to 84.1% and Br^- showed no change. The large change in the transport of SSSNP was attributed to soil aggregate breakdown and colloid release (causing mechanical straining of SSSNP) and the exposure of iron oxide surfaces previously unavailable within aggregate interiors (facilitating attachment of SSSNP). These results suggest a time-dependent fashion of microbial effect on the transport of diffusivity-varying tracers.

Introduction

Subsurface bioremediation brought about by electron donor addition creates anoxic conditions that stimulate the growth of iron reducing and/or sulfate reducing bacteria (Chapelle and Lovley, 1992; Si et al., 2015). Subsequently, oxidized forms of iron are reduced to Fe(II), solubilizing iron oxide minerals. The soluble Fe(II) and secondary precipitation of iron (e.g., ferrous hydroxide) can result in abiotic transformation of contaminants and/or the release of colloidal clay and iron mineral colloids (Pedersen et al., 2006; Thompson et al., 2006). Adsorption of contaminants to these colloids may enhance contaminant transport via colloid-facilitated transport (Bose and Sharma, 2002; Zhuang et al., 2003). Additionally, biomass increase and colloid production can cause pore clogging, potentially reducing hydraulic conductivity of the porous medium down gradient from the treatment zone. Alternatively, advective flow paths and increased hydraulic conductivity may trigger substantial soil aggregate breakdown. Thus, altering the indigenous properties of subsurface media may impact coupled processes controlling the fate and transport of contaminants, and cause unintended secondary impacts on the properties of the porous media and groundwater quality (e.g. secondary mineral precipitates, permeability, and microbial activity).

Anaerobic bioremediation is an attractive technology for subsurface soil and water remediation based on cost and effectiveness (Ellis et al., 2000; Coates and Anderson, 2000; Liang et al., 2017). The technology generally aims to create anoxic conditions via addition of soluble electron donors, such as acetate and lactate or higher molecular weight substrates, for stimulating microorganisms that degrade organic contaminants (e.g. chlorinated solvents) and reduce heavy metals and radionuclides to insoluble forms thereby immobilizing them *in situ* (Aulenta et al., 2006). Once anoxic conditions are achieved, anaerobic respiration with available electron acceptors is stimulated leading to biologically-mediated reduction of Fe(III)-oxide minerals (the most common mineral oxide of soils and subsurface environments) and the formation of soluble Fe(II) (Caldwell et al., 1999; Weber et al., 2006; Mejia et al., 2016). Iron oxides, which have diverse crystallinities and reactivity (e.g. ferrihydrite, goethite, lepidocrocite, and hematite), are extensively present in soils (Pedersen et al., 2006; Vink et al., 2017). The indigenous iron

oxides serve a very important role as aggregating agents that "cement" clay particles together into aggregates (Goldberg et al., 1990; Braunschweig et al., 2013). Reduction of Fe(III)-oxides under anoxic conditions may cause disintegration of soil aggregates and generate mobile colloids (Hansel et al., 2005; De-Campos et al., 2009). These processes may disrupt pore structure and alter pore connectivity, flow paths, and permeability (Guan et al., 2017). These alterations could either promote or inhibit the transport of solutes and colloids. Schaider et al. (2014) found that iron oxide aggregates can alter the transport of particulate particles and sequester metals. The formation and mobilization of colloids can act as vectors to facilitate co-transport of solutes and toxic metals in soils and groundwater (McCarthy and McKay, 2004; Maurice and Hocella, 2008; Guan et al., 2017). The reduction of Fe(III)-oxides may also change soil surface properties to influence the reactive transport processes (Hansel et al., 2003; Jardine, 2008).

Transport of solutes and colloids in soil is influenced by the pore structure and surface chemistry of soils, solution chemistry, and hydrological conditions (Zhuang et al., 2005; 2007; 2010; Bradford and Torkzaban, 2008; Mohanty et al., 2016; Pachapur et al., 2016). The influencing mechanisms have been well examined at varying scales from laboratory columns (repacked or undisturbed) to field scale (McKay et al., 2000; Arora et al., 2015; Karadimitriou et al., 2017). Bioremediation treatment may alter aquifer porosity, flow paths, and mineral interfacial properties and in turn change the attenuation and migration of solutes, colloids, and microbial cells; all these may exert feedback effects on microbial bioremediation. Microorganisms, nutrients, or electron donors are generally applied to accelerate in situ bioremediation (Ellis et al., 2000; Lovley 2003; Moon et al., 2017), yet the remediation efficiency is subject to their mobility in porous media (Song et al., 2017). Thus far, few studies have addressed the impacts of biostimulation on the transport of solutes and colloids, making difficult to resolve the low-efficiency problem of bioremediation under field conditions. Therefore, in-depth investigations are needed to understand the potential that biostimulation influences the mobility of solutes and colloids including microorganisms.

The objective of this research was to assess the impact of biologically-mediated Fe(III)-oxide reduction on the transport of solutes and colloids with respect to soil structure

breakdown under saturated flow conditions, shedding light on the interplays of microbial activities with the solutes and colloids migration during bioremediation processes. Breakthrough tests with diffusivity-varying tracers and non-diffusing nanoparticles both before and after acetate-stimulated Fe(III)-bioreduction were conducted to evaluate the alteration of soil surface chemistry and flow pathways. The research provides significant insights into the feedback effects of anoxic bioremediation on the transport of solutes and colloids, microbial distribution, and soil aggregate structure.

Materials and Methods

Porous media

The columns were packed with different porous media, including uncoated and goethite-coated silica sand and water-stable soil aggregates extracted from an iron oxide-rich natural soil. The sand grains had a median diameter (d_{50}) of 0.25 ± 0.01 mm with a trade name Accusand (Grade 50/70, Unimin Corporation, New Canaan, CT, USA). Prior to coating with goethite, the sand was chemically treated to remove natural metal oxides from the grains following the established procedure (Zhuang and Jin, 2003). Goethite synthesis and coating on the cleaned sand were performed as described by Zhuang and Jin (2008). The natural soil was collected from an eroded agricultural site mapped as the Decatur silty clay loam. The Decatur series is a fine, kaolinitic, thermic rhodic Paleudults. Soil aggregates were extracted by wet sieving of the bulk soils through 2,000, 250, and 53 μm sieves using the modified method as described in Zhuang et al. (2008). Two fractions of water-stable soil aggregates, microaggregates (53-250 μm) and macroaggregates (250-2000 μm), were obtained and then air-dried for experimental use. The citrate-bicarbonate-dithionite extractable iron (Mehra and Jackson, 1960) of the bulk soil, microaggregates, and macroaggregates were 5.5%, 4.7% and 5.2% (w/w), respectively, as measured using the ferrozine method (Viollier et al., 2000).

Tracers and nanoparticles

Two diffusible tracers and one non-diffusing nanoparticle were used for transport experiments, including bromide (Br^- in KBr) (ionic diffusible tracer), 2,6-difluorobenzoate (DFBA) (molecular diffusible tracer with lower diffusivity than Br^-) (Mayes et al., 2003), and silica-shelled silver nanoparticles (SSSNP) (non-diffusible particle). The SSSNP was purchased from nanoComposix (http://nanocomposix.com/) and has a core of silver nanoparticles with average diameter of 106 nm. The silver cores are encased in a shell of silica with average thickness of 22 nm, resulting in a total particle diameter of 150 nm. The SSSNP were negatively charged, with a measured zeta potential of -5.7 mV at pH 8. SSSNP were specifically selected as a "non-diffusing" particle and potentially as a non-reactive particle given the silica shell surrounding the silver-core. Advantages to using these shelled particles instead of other previously used particle tracers, such as viruses (e.g., MS-2), are their resistance to biotic and abiotic breakdown, the ease and accuracy of quantification in the effluent samples using graphite furnace atomic absorption spectroscopy, and the convenience to distinguish introduced SSSNP from native soil colloids for mechanistic understanding of transport processes.

Bacterial strain, growth media, and inoculation for stimulated bioreduction

Geobacter species, with capacity to oxidize organic compounds coupled with reduction of iron oxides or other metal minerals, are ubiquitous in subsurface environments (Caccavo et al., 1994). As such, *Geobacter,* and other microorganisms with similar metabolism have been extensively studied and used for anaerobic bioremediation (Lovley 2003; Moon et al., 2017). To ensure active Fe(III) bioreduction, the soil macroaggregates (250-2,000 μm) were inoculated with laboratory-grown culture of *Geobacter sulfurreducens* strain PCA (ATCC 51573; Caccavo et al., 1994) prior to packing the columns. Specifically, *G. sulfurreducens* was grown in mineral salts medium containing 1.0 g of NaCl, 0.5 g of $MgCl_2$, 0.2 g of KH_2PO_4, 0.3 g of NH_4Cl, 0.3 g of KCl, 0.015 g of $CaCl_2$, 1 mg of resazurin, and 2 ml of trace element solution, amended with 5 mM acetate and 10 mM ferric citrate per liter was prepared as described by Löffler et al. (1996). The prepared medium was boiled and transferred to serum bottles while flushing with oxygen-

free 80/20 (v/v) N_2-CO_2, and the pH was adjusted to 7.2 with flow of CO_2. The serum bottles were autoclaved, and filter-sterilized (with a 0.22 μm Millex filter syringe) acetate and ferric citrate were added to the medium to a final concentration of with 5 mM and 10 mM, separately. The serum bottles inoculated with *G. sulfurreducens* were cultured at 30 °C (Löffler et al., 1996). Once the cultures reached stationary phase (3-5 d; optical density at 600 nm = 0.2 to 0.35; cell concentration of approximately 1×10^8 cells per milliliter), 200 ml of culture suspension was centrifuged at 4,248 g, and the bacterial pellet was resuspended in 15 ml of the growth medium in the anaerobic chamber with an 80/20 (v/v) N_2/CO_2 atmosphere. Then, all the resuspended *G. sulfureducens* were uniformly sprayed onto 600 g of air-dried but non-sterile, water-stable soil macroaggregates that were thinly spread on a tray inside the anaerobic chamber. During the application of cell suspension, the aggregates were continuously mixed using a glass rod to achieve uniform inoculation of the bacteria.

Transport experiment

All transport experiments were conducted in plexiglass (acrylic) columns (25 cm in length with an inside diameter of 3.8 cm) with input solution introduced from the bottom of the column in pulse input mode through a peristaltic pump at pore velocity of 24.4 cm/h. Teflon tubing was used throughout the system except for a portion of tygon tubing needed in the pump. The columns were fitted with five ports connected to pressure sensors (Honeywell Sensing and Control, Inc., USA), which were separated by 5-cm intervals along the column length. Real-time data of hydrostatic pressure were collected with data loggers of CR-1000 Measurement and Control Systems (Campbell Scientific, Inc., Logan Utah) to calculate hydraulic conductivity between different sections of the columns according to the difference in pressure. During the transport experiment, liquid effluent was collected from the top of the column into 20-mL glass tubes using Retriever II fraction collectors for determining the concentrations of tracers, iron, and or colloids as described in section 2.5. The protocols for column experiments are shown in Appendix (Table 2.3 and Fig. 2.10).

Three sets of separate transport experiments were conducted using vertical columns under saturated steady-state flow conditions. The first set aimed to evaluate the appropriateness of use of SSSNP as non-diffusible particle tracer and the effect of iron oxide on the transport of tracers and nanoparticles. The experiments included two columns that were wet-packed with uncoated and goethite-coated sands, respectively. The sand columns were flushed with KCl solution (0.67 mM, pH 6.5) prior to the tracer experiments. The input solution for the sand columns contained Br^- (50 mg L^{-1} KBr), DFBA (40 mg L^{-1}), and SSSNP (40 ug L^{-1}) in the KCl solution.

The second set of experiments aimed to evaluate the effect of Fe(III)-bioreduction on the transport of tracers using five columns dry-packed with *Geobactor*-inoculated soil macroaggregates under anoxic conditions (Appendix Fig. 2.11). The experiments included three acetate-stimulated Fe(III)-bioreduction columns (one with 20 d of continuous injection of acetate and two replicates with 60 d of acetate injection) and two control columns (no acetate addition). The 60-d experiments aimed to corroborate the results of bioreduction effects observed from the 20-d experiments. After dry packing, the soil aggregate columns were flushed with carbon dioxide to replace the air in soil pores, followed by flushing with KCl solution (0.67 mM, pH 6.5) to achieve fully saturated conditions without remaining gas pockets. Each column experiment consisted of three phases with constant level of total ionic strength of solutions (2 mM). Before bioreduction, transport experiments with the KCl input solution containing Br^- (85 mg L^{-1} KBr), DFBA (50 mg L^{-1}), and SSSNP (40 μg L^{-1}) were performed in all columns (phase 1). In bioreduction process (phase 2), the columns were flushed with artificial groundwater solution (AGW), which had a total ionic strength of 2 mM and a pH value of 7.5, consisting of $CaCl_2$ (0.075 mM), $MgCl_2$ (0.082 mM), KCl (0.051 mM), and $NaHCO_3$ (1.5 mM), modified from Ferris et al. (2004). The AGW contained trace elements, vitamins, and acetate (bioreduction-stimulated column) or without acetate (control column) (Wolin et al., 1963). Acetate added to the columns served as the electron donor for *Geobacter*. Effluent samples from columns during bioreduction were analyzed for the concentrations of Fe(II), Fe(III) and colloids as described in Section 2.5. After 20 or 60 d of bioreduction, the same transport experiment as that prior to bioreduction was performed (phase 3). Breakthrough

and elution data for Br^-, DFBA, and SSSNP were collected during phases 1 and 3. At the conclusion of the above procedures, the columns were sectioned in 5-cm intervals along the longitudinal flow path of the columns. The distribution of *Geobacter* and readily deducible iron content in soil aggregates from each section were investigated.

The third set of experiments was conducted to examine the effects of aggregate size fractions on the transport of tracers and nanoparticles outside the anoxic chamber without bioreduction treatment (exposed to oxygen), since exposure to aerobic conditions can suppress reduction of iron oxides. The experiments included two columns, which were dry packed with microaggregates and macroaggregates, respectively. The experimental procedures were the same as those used in the second set of column experiments.

Chemical analysis

Bromide concentrations in the effluent fractions were determined using ion chromatography as described elsewhere (Qin et al., 2017). The concentration of DFBA was measured with a modified HPLC method (Galdiga and Greibrokk, 1998). Briefly, DFBA was resolved from other effluent constituents using an Econosphere C-18 RP column (5 μm, 150 mm x 4.6 mm) with isocratic elution using a mobile phase consisting of 95% K-phosphate buffer (5 mM, pH 3) and 5% acetonitrile (v/v) at a flow rate of 1.0 mL min^{-1}. DFBA was quantified using UV absorption at 200 nm and the concentration was calculated via linear regression of peak area of external DFBA standard solutions over a concentration range from 1 to 50 mg L^{-1}. All samples were diluted 1:10 (v/v) in mobile phase to minimize sample matrix effects and filtered through 0.1 μm membrane filters (Merck Millipore Ltd., Cork, Ireland) prior to analysis. SSSNP (with hydrodynamic diameter of 129.8 nm) in effluent fractions were quantified by measuring the concentration of silver by graphite furnace atomic absorption spectrometry using a Perkin-Elmer Graphite Furnance AA equipped with a transversely heated graphite atomizer as described by Fernández et al. (2010). Effluent samples were diluted 10^4 times with deionized water before analysis, and 20 μL of diluted sample was injected with 10 μL of matrix modifier (prepared by dissolving 0.05 mg de Pd and 0.003 mg $Mg(NO_3)_2$ in 10 μL 1% HNO_3). The silver detection program in furnance AA was described in Fernández et al. (2010).

Numerical modeling

The HYDRUS code (Šimůnek et al., 2008) simulating saturated water flow based on the Richards equation was used to simulate the transport of bromide, DFBA, and SSSNP. Transport behaviors of Br^- and 2,6-DFBA were simulated using the classical advection-dispersion equation (ADE). The transport and retention of SSSNP were simulated using the ADE with first-order terms for kinetic retention and release as described in the HYDRUS code. The equation is given in modeling the transport behavior as:

$$\frac{\partial C}{\partial t} + \frac{\rho K_d}{\theta}\frac{\partial C}{\partial t} = D\frac{\partial^2 C}{\partial z^2} - v\frac{\partial C}{\partial z} - \mu C$$

where θ[L^3L^{-3}] is the soil water content, C [M L^{-3}; M represents the units of mass] is the concentration of bromide, DFBA, and SSSNP in the aqueous phase, ρ [M L^{-3}] is the bulk density of soil aggregates, K_d [L^3 M^{-1}] is the adsorption coefficient to soil aggregates, t is time [T, T represents time units], D [L^2 T^{-1}] is the hydrodynamic dispersion coefficient, z [L] is the distance from the inlet of a column, and μ [T^{-1}] is the first-order retention coefficient for tracer transformation processes. For nanoparticle tracer (i.e., SSSNP), the following modified transport equation was used to simulate the transport, attachment, and detachment of nanoparticles.

$$\frac{\partial C}{\partial t} + \frac{\rho}{\theta}\frac{\partial S}{\partial t} = D\frac{\partial^2 C}{\partial z^2} - v\frac{\partial C}{\partial z}$$

where S [M L^{-3}] is the concentration of SSSNP attached to the solid phase. The attachment and detachment of nanoparticles in water-saturated soil aggregates was described by the following first- order kinetic expression:

$$\frac{\rho}{\theta}\frac{\partial S}{\partial t} = k_{att}\psi C - \frac{\rho}{\theta}k_{det}S$$

where k_{att} is the coefficient of SSSNP attachment (T^{-1}), k_{det} is the coefficient of SSSNP detachment (T^{-1}), ψ is a blocking function that is related to the maximum particle attachment capacity, S_{max} (M M^{-1}) which can be calculated using:

$$\psi = \frac{S_{max} - S}{S_{max}}$$

Assessment of soil aggregate properties

Component analysis of soil aggregates were performed by commercial service of Midwest Laboratories Inc. (Omaha, NE, USA). Particle size distribution of soil aggregates was analyzed to indicate the reactivity behaviors of soil aggregates. The procedures and principles were described in Kemper and Rosenau (1986). Fifty grams of air-dried soil aggregates were presoaked in distilled water for 30 min and sieved with a top-down sequence of seven sieves of 2,000, 840, 300, 250, 150, 90, and 53 mm mesh size. The sieves with the contents were oscillated vertically in water with an amplitude of 4 cm at a rate of one oscillation per second for twenty times. The retained aggregates on each sieve after wet-sieving were recovered and dried at 50 °C in a drying oven. The particle size distribution was calculated with dry weight fractions. After bioreduction, dispersion of the aggregates was assessed based on readily reducible iron content. Soil aggregates from each section were homogenized, and 5-g sub-samples were placed in 50-mL centrifuge tubes, in which soil aggregates were shaken vigorously with 40-mL distilled water in an ice-water bath for 30 min (Kemper and Rosenau, 1986; Viollier et al., 2000). The mixtures were centrifuged at 4,248 g for 20 min, and the readily reducible iron in supernatant were determined using a modified Ferrozine method (Stookey, 1970). During column bioreduction experiments, the concentrations of Fe(II) and Fe(III) in the effluent were measured using a modified Ferrozine method (Stookey, 1970). Colloids were determined by centrifuging the effluent sample at 4,248 g for 20 min and measuring the mass of pellets after oven-drying, assuming the mass of dissolved salts was negligible.

DNA extraction and sequencing

To analyze the distribution of *Geobacter* in soil aggregates, DNA was extracted from fractioned soil aggregates using PowerLyser PowerSoil DNA isolation kit (MoBio Laboratories Inv. Carlsbad, California, USA). The DNA samples were quantified using PicoGreen Assay Kit (Carlsbad, CA, USA) and sent out for sequencing at HudsonAlpha

Genomics Services Lab (Huntsville, AL, USA). The V3-V4 region of 16S rRNA gene of bacteria were amplified with primers of 341F_CCTACG GGNGGCWGCAG and 785R_GACTACHVGGGTATCTAATCC) in PCR. Finally, sequencing was performed using 300PE (paired-end) on the Illumina MiSeq platform (Illumina, USA). All methods were performed according to the manufacturers' protocol. Sequences analyses were performed using MOTHUR per standard operating procedure (Kozich et al., 2013). The results of these sequence analyses were used to calculate the relative abundance of *Geobacter* along the flow path in the columns.

Results and Discussion

Effect of iron oxide on transport

The uncoated and goethite-coated quartz sands were used as simple and stable porous systems to evaluate the effect of iron oxide on the transport of tracers and nanoparticles. Br^- was included in the input solution to quantify transport behaviors of a diffusible tracer and to evaluate uniformity and integrity of the column packing in terms of hydrodynamic dispersion. As a conservative tracer, Br^- showed ideal and complete transport behavior in the sand with and without goethite coating (Fig. 2.1). In comparison, the breakthrough of SSSNP from the uncoated sand was slightly retarded relative to that of Br^- and eventually reached a stable maximum relative concentration (max C/C_0) of 0.85. However, almost no SSSNP broke through the goethite-coated sand column. The fitted parameters of the breakthrough curves of SSSNP showed a 14-fold increase in attachment and a 3-fold decrease in detachment of SSSNP in goethite-coated sand compared with the uncoated sand columns. The maximum solid phase concentration of SSSNP was ~20 times higher in the goethite-coated sand than in the uncoated sand, suggesting a strong affinity of the SSSNP to the iron-oxide surface (Table 2.1). The strong attachment of SSSNP to goethite-coated sand in this study was consistent with previous results showing sequestration of silver nanoparticle (no silica-shell) by iron oxides (Sagee et al., 2012; Liang et al., 2013).

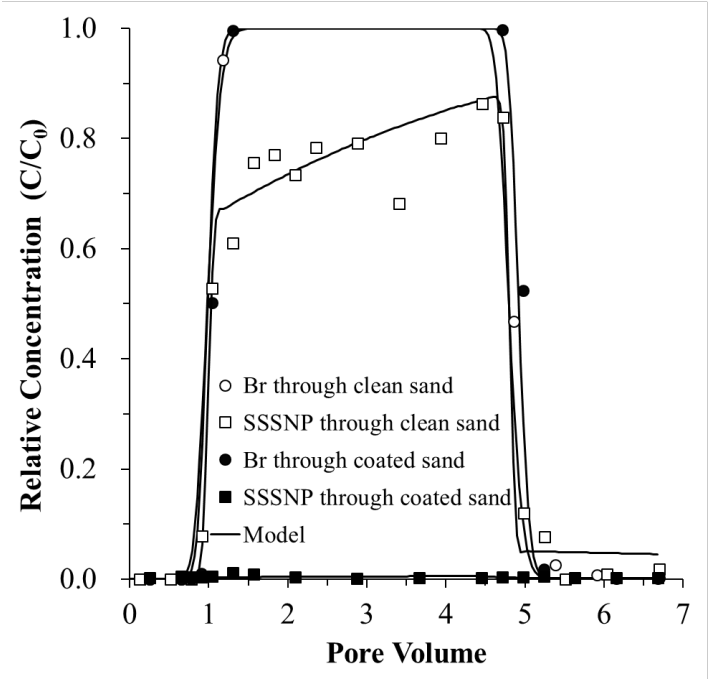

Figure 2.1: Transport of bromide (Br^-) and silica-shelled silver nanoparticles (SSSNP) through goethite-coated and uncoated sands. The concentrations of Br^- and SSSNP are shown over pore volume with columns flushed using KCl solution (0.67 mM, pH 6.5).

Table 2.1: Model fitted parameters for the breakthrough of silica-shelled silver nanoparticles from sand columns.

Silica-shelled silver nanoparticle	Sand	Goethite-coated sand
Maximum solid phase concentration (N_c M^{-1})	0.560	12.000
Attachment coefficient (min^{-1})	0.007	0.100
Detachment coefficient (min^{-1})	0.001	0.0003

Effect of aggregates on transport

To further determine if the change in soil aggregate sizes primarily influences the transport of DFBA and SSSNP in column experiments, transport experiments were conducted in columns packed with water-stable macroaggregates (250-2,000 μm) and microaggregates (53-250 μm) under oxic conditions and without any reduction of Fe(III) oxides. The transport of bromide through both aggregate fractions showed no obvious differences (Fig. 2.2); however, DFBA was retarded in both columns, with larger retardation in the microaggregates (K_d of 0.12) than in the macroaggregates (K_d of 0.06). Since the surface properties of macroaggregates and microaggregates should have been very similar, the larger retardation is ascribed to the greater total surface area and smaller pores of the microaggregates compared to the macroaggregates. The breakthrough of SSSNP was negligible with both columns likely due to the strong interactions of SSSNP with Fe(III) oxides (Fig. 2.2). Similar results of decreased silver nanoparticle mobility in smaller soil aggregates were reported by Sagee et al. (2012), in which the explanation was proposed that the reaction of silver nanoparticles with soil occurs at the aggregate surface, and the smaller aggregates have increased surface area. Aggregate structure has been shown to play an important role in retention of large molecules and nanoparticles with complicated interacting environmental factors (Sagee et al., 2012; Liang et al., 2013). For example, transport of silver nanoparticles in natural soil showed that aggregate size exerted major influence on silver nanoparticle transport, with silver nanoparticle mobility increased in the column of larger soil aggregates (Sagee et al., 2012). The transport and retention of silver nanoparticles in sand columns by Liang et al. (2013) also found that the mobility of silver nanoparticles was enhanced by increase in sand grain size. The soil aggregates used in this study were highly rich in iron oxides and had strong binding capacity for SSSNP, which caused complete retention of SSSNP in both microaggregates and macroaggregates columns. In contrast, the retardation of DFBA increased in the microaggregates.

Effect of short time bioreduction on transport

Soil aggregates rich in iron oxides were used to examine the effect of Fe(III)-bioreduction on transport behaviors of tracers and nanoparticles. The breakthrough of Br^-

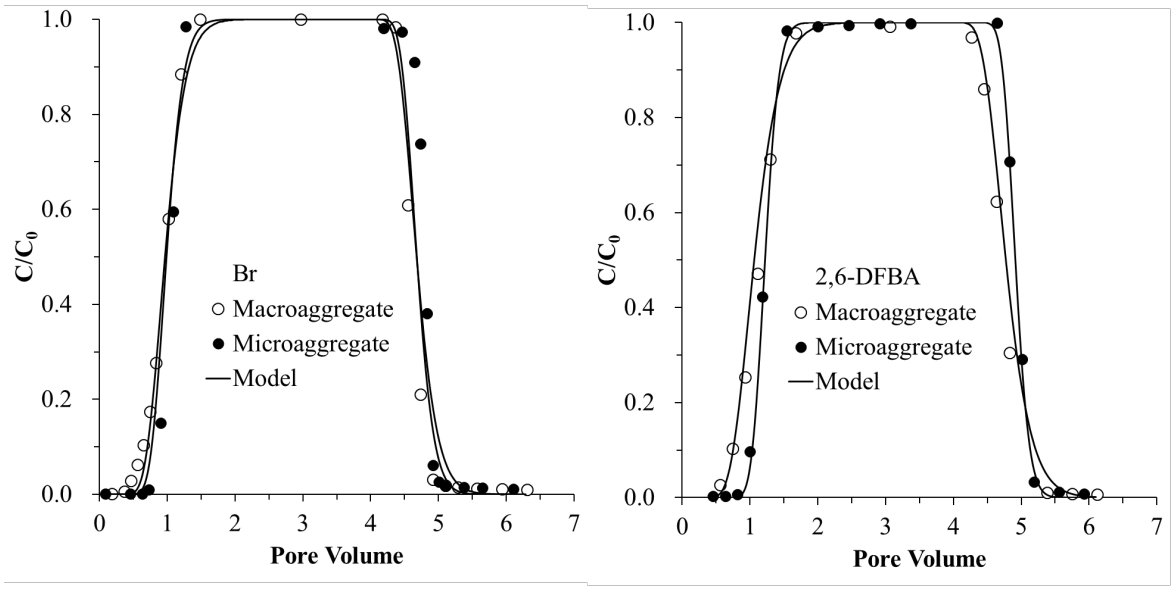

Figure 2.2: Transport of bromide (Br^-) and 2,6-DFBA through columns packed with water-stable macroaggregaes (250-2,000 μm) or water-stable microaggregates (53-250 μm) under oxic conditions without Fe(III)-bioreduction.

occurred at approximately one pore volume before and after the Fe(III)-bioreduction phase (Fig. 2.3), indicating that Fe(III)-bioreduction did not influence the transport of the conservative tracer. Transport of DFBA exhibited some retardation and tailing in the breakthrough experiment before the bioreduction, but the retardation was eliminated after the bioreduction phase (Figs. 2.3 and 2.4). This result suggests that Fe(III)-bioreduction induced either physical and/or chemical changes of the aggregates. Modeling results showed that the estimated dispersivity (D) of DFBA during transport remained similar before and after the Fe(III)-bioreduction phase while the estimated DFBA sorption coefficient (K_d) was about one order of magnitude lower after Fe(III)-bioreduction (Table 2.2). SSSNP exhibited a very pronounced response to the Fe(III)-bioreduction treatment. Almost no breakthrough of SSSNP was observed before Fe(III)-bioreduction (i.e., in phase 1), whereas the relative concentrations (C/C_0) of SSSNP in the effluent reached only 0.3 after the Fe(III)-bioreduction (i.e., in phase 3) (Fig. 2.3). The estimated maximum solid phase concentration of SSSNP in phase 3 was one fourth that in phase 1 with a lower attachment coefficient. The estimated detachment coefficient of SSSNP was 100-fold greater in phase 3 than in phase 1 (Table 2.2). These results indicate that the presence of Fe(III) oxides greatly reduced the mobility of the nanoparticle tracer. Ryan et al. (1999) found that the bacteriophage particles and silica colloids attached to iron oxide-coated sand could be mobilized by anionic surfactant, elevated pH, and reductant, suggesting that iron oxide removal could promote the detachment of colloids and bacteriophage. Vink et al. (2017) showed that arsenic release corresponded to the fractions of readily reducible iron in sediments. At the initial phase of incubation with acetate-supplemented AGW solution, microbially mediated bioreduction released relatively small amount of Fe(II) from soil aggregates, causing certain alteration of the aggregate surface properties. Since the binding capacity for metals and colloids are highly dependent on ferric phases in soils (Pedersen et al., 2006), the reduction of iron oxides can lead to release of certain amount of retained molecules and colloids, such as DFBA and SSSNP.

The detection of soluble Fe(II) in the effluent indicated reduction of soil Fe(III) by *Geobacter* and/or other Fe(III)-reducing bacteria (Fig. 2.4). The increase in effluent Fe(II) concentrations in the first two weeks corresponded to the increase in microbial activity as

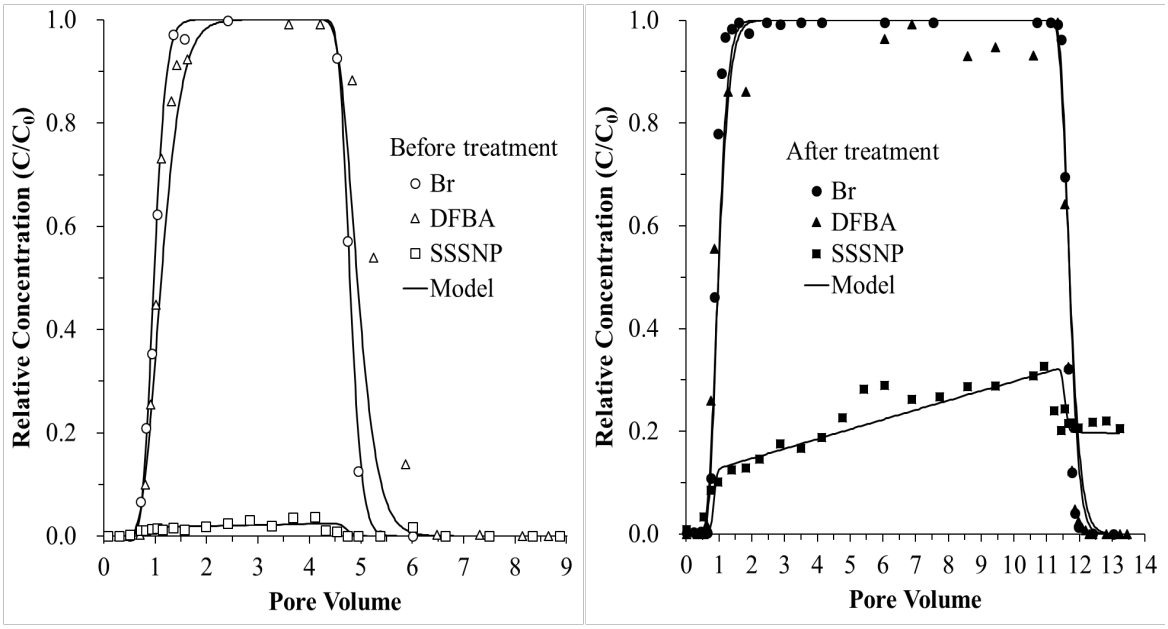

Figure 2.3: Breakthrough curves of bromide (Br^-), 2,6-DFBA, and silica-shelled silver nanoparticles (SSSNP) from columns packed with water-stable soil aggregates before and after the 20-d Fe(III)-bioreduction.

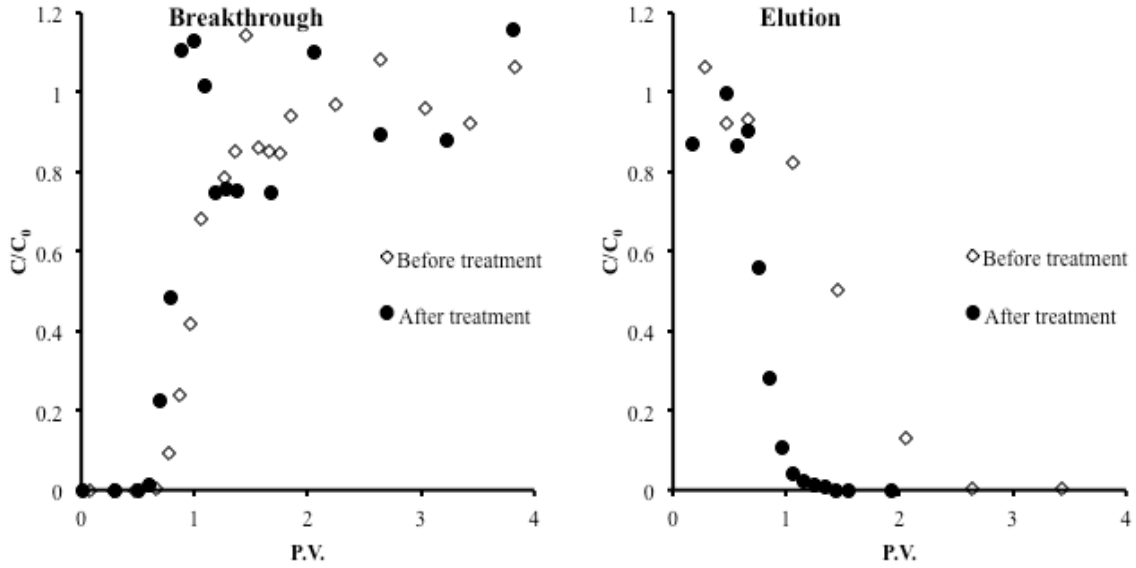

Figure 2.4: Expanded view of breakthrough and elution profiles of 2,6-DFBA before and after the 20-d Fe(III)-bioreduction phase.

Table 2.2: Model fitted parameters for the breakthrough of 2,6-DFBA and silica-shelled silver nanoparticles (SSSNP) from water-stable soil aggregate columns before (Pre-) and after (Post-) Fe(III)-bioreduction.

Tracer	Parameter	[§]Fe(III)-bioreduction phase (20 d)		Fe(III)-bioreduction phase (60 d)					
				Column A		Column B		Column C	
Tracer	Parameter	[#]Pre	*Post	Pre	Post	Pre	Post	Pre	Post
2,6-DFBA	*D* (cm)	1.12	0.93	0.89	0.84	0.85	0.82	0.84	0.83
	K_d (cm^3mg^{-1})	0.086	0.0063	0.014	0.011	0.041	0.031	0.027	0.001
	S_{max}	23.6	5.55	[ϕ] -	-	-	-	-	-
SSSNP	Att. Coeff. (min^{-1})	0.046	0.026	-	-	-	-	-	-
	Detach Coeff. (min^{-1})	$3x10^{-6}$	$7.7x10^{-4}$	-	-	-	-	-	-

[§]Data were collected from a single column.

[#]Tracer transport experiment before stimulation of Fe(III)-bioreduction by injection of acetate.

*Tracer transport experiment after stimulation of Fe(III)-bioreduction by injection of acetate.

[ϕ]Breakthrough of SSSNP was not detected in either acetate-treated or control columns.

D is dispersivity.

Kd is sorption coefficient.

acetate was added to the feed solution (Fig. 2.4). The effluent Fe(II) concentrations plateaued after 20 d of acetate injection, suggesting retardation of Fe(III) bioreduction (Fig. 2.5). The accumulated amount of Fe(II) in the effluent was approximately 0.125 mmol or about 0.04% of the total iron in the column. No Fe(III) oxides or other colloids were detected in the effluent during the 20-d bioreduction treatment. Although only a very small fraction of total Fe(III) was reduced to soluble Fe(II) (assuming there were no secondary precipitation of Fe(II) in the column), the influences of Fe(III) reduction on the transport of DFBA and SSSNP were significant. This effect is attributable to Fe(II) binding to Fe(III) solids and/or the reduction of the most bioavailable Fe(III) on the external surfaces of the aggregates and/or along the advective pathways that are most accessible by less diffusible microorganisms and particle tracers (e.g., SSSNP). Removal of surface iron oxides during bioreduction could reduce positive electric charges and roughness on mineral surfaces (Joe-Wong et al., 2017), causing a decrease in surface deposition of nanoparticles.

An in-situ study investigating the mobility of arsenate in natural groundwater showed that arsenic desorption occurred with reductive dissolution of ferric oxides in ferrihydrite, goethite, and hematite (Zhang et al., 2017). Microbial metabolism can affect the affinity of nanoparticles, and therefore cause the simultaneous releases of Fe and Fe(III)- oxide-bound particles. Similarly, Moon et al. (2017) reported that the genus *Geobacter*, *Anaeromyxobacter*, and *Desulfosporosinus* might play important roles in release of arsenic coupled with iron reduction. In this study, the concentration of Fe(II) in the effluent increased with time during the 20-d treatment demonstrating bioreduction of iron oxides in the acetate-treated soil column. However, without Fe(III) oxides or other colloids detected in the effluent, no evidence of structural breakdown in soil aggregates was observed during the whole bioreduction process. The enhanced transport of SSSNP was most likely attributed to the microbial reduction-induced transformation of iron minerals, resulting in less contact of SSSNP with iron oxides. A very recent study by Xiao et al. (2018) reported that the transformation from less crystalline to more crystalline iron oxides by iron reducing bacterium *Shewanella oneidensis* MR-1 affected the behavior of any species absorbed to the iron oxides, suggesting that the produced Fe(II) can stimulate the reduction and transformation of iron oxide minerals.

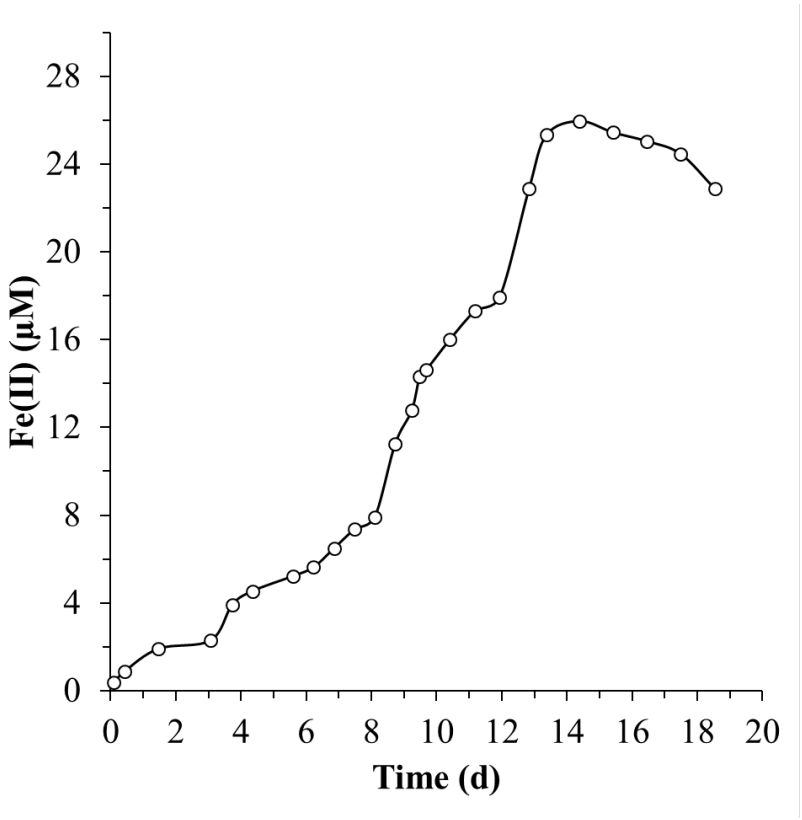

Figure 2.5: Effluent Fe(II) concentration during the acetate injection phase of the 20-d Fe(III)-bioreduction column experiment.

Effect of long time bioreduction on transport

Given only 0.04% of the total iron was detected in the effluent in the 20-d bioreduction experiment, additional aggregate-packed column experiments with the duration of acetate-stimulated Fe(III)-bioreduction extended to 60 d were conducted to further examine the effect of bioreduction on Fe(II) release, aggregate breakdown, and tracer transport. The transport behaviors of bromide and DFBA showed no change after the 60-d Fe(III)-bioreduction treatment, whereas SSSNP were completely retained in the soil aggregates both before and after the 60-d acetate injection (Fig. 2.6 and Table 2.2). These results are inconsistent with the observations made in the short time experiment with 20-d acetate injection, where Fe(III)-bioreduction resulted in earlier breakthrough of DFBA and SSSNP. The longer duration of Fe(III)-bioreduction (60 d) brought about as yet unknown changes to the properties of soil aggregates and resulted in complete retention of the SSSNP particles, though retardation and slow release of the DFBA were not observed in the short time experiment.

The release of soluble Fe(II) in the 60-d experiment was similar to the 20-d experiments during the first 20 d but exhibited a steady increase in the effluent Fe(II) concentration through day 60 (Fig. 2.7). The concentration of soluble Fe(II) reached 300 μM, or more than 10 times the total amount observed at the end of the 20-d Fe(III) bioreduction experiment. The accumulated amount of soluble Fe(II) collected in the effluent was 1.43 mmol or about 0.48% of the total Fe in the soil aggregates within the column. Colloids were first detected in the effluent at 30 d after the acetate injection and continued to increase in concentration during the 60-d Fe(III)-bioreduction treatment, further suggesting that Fe(III)-bioreduction and aggregate breakdown were active throughout the biostimulation phase of the soil column experiment (Fig. 2.7). A small amount of Fe(II) was also detected in the effluent of the control column, indicating that *Geobacter* was able to couple oxidation of the native soil organic carbon with Fe(III) reduction. The inconsistent tracer transport results between the 20-d and 60-d bioreduction experiments very likely arose from the greater aggregate breakdown that occurred during the extended period (day 20-60) than the initial period (day 0-20) of the bioreduction treatment. The aggregate breakdown generated soil colloids, which may have increased

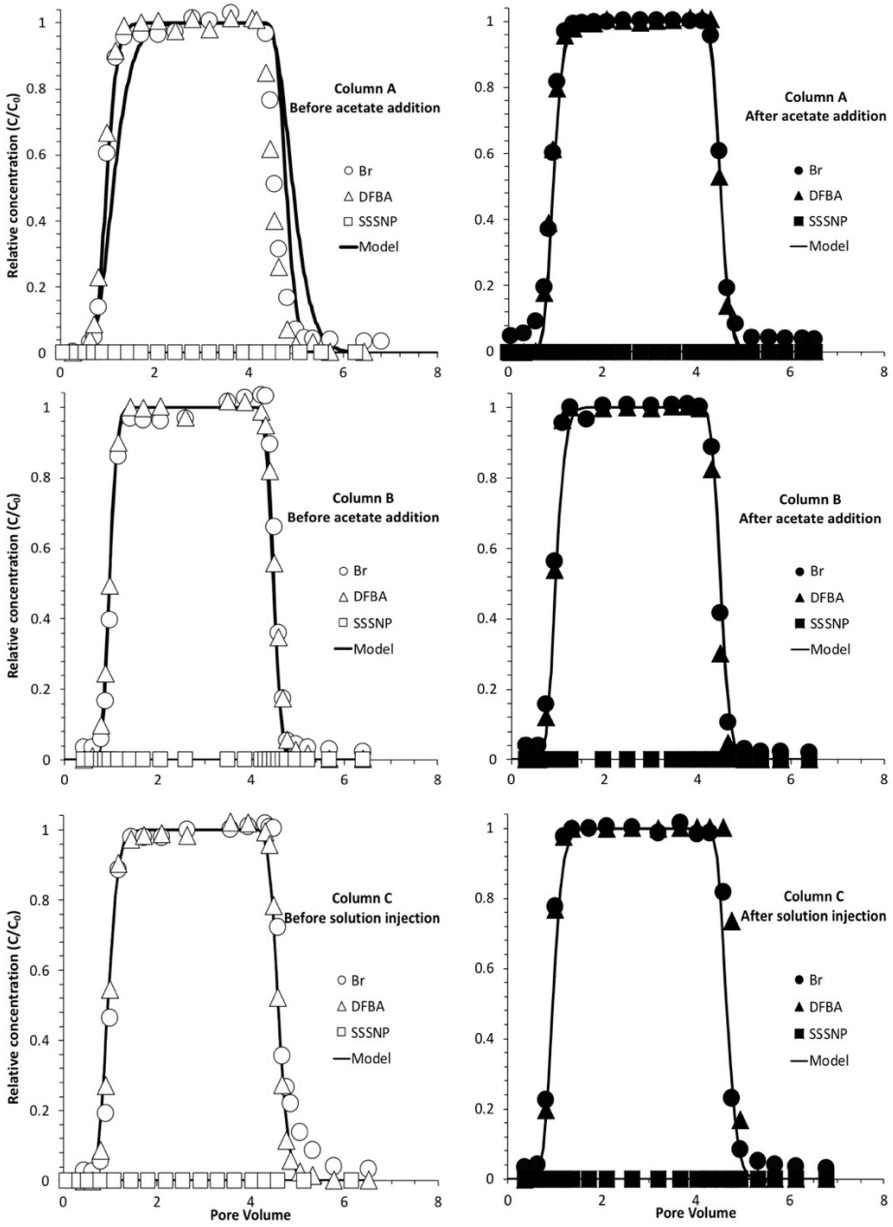

Figure 2.6: Breakthrough curves of bromide (Br^-), 2,6-DFBA, and silica-shelled silver nanoparticles (SSSNP) in pre- (left, a, c, e) and post-acetate (right, b, d, f) treatment transport experiments for 60-d Fe(III)-bioreduction treatment in the columns packed with water-stable macroaggregates (250-2,000 µm). The plots of a, b, c and d are breakthrough curves from replicate acetate-treated columns while the plots of e and f are breakthrough curves from the control column that did not receive acetate injection.

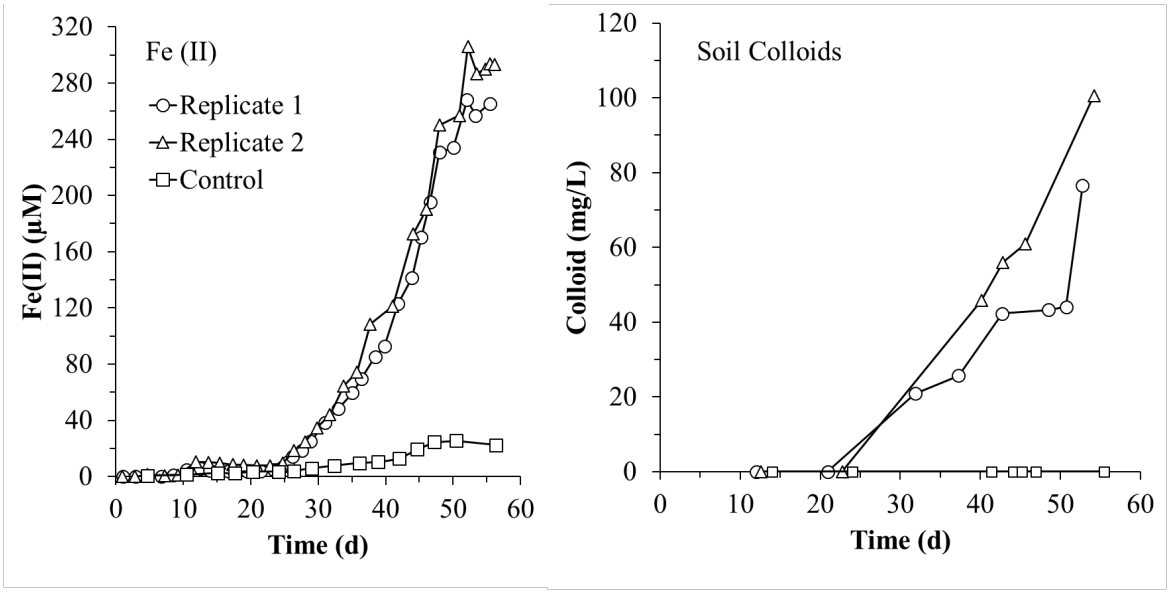

Figure 2.7: Concentrations of released Fe(II) and soil colloids in the effluent during the acetate injection phase of the 60-d Fe(III)-bioreduction column experiments.

mechanical straining of SSSNP in soil pores and may have exposed aggregate interior Fe(III)-oxide surfaces promoting the attachment of SSSNP on positively charged surfaces.

Effect of long time bioreduction on aggregate structure

The above results suggested that the soil aggregates experienced structural breakdown during the 60-d Fe(III)-bioreduction phase with acetate injection. To get direct evidence, we characterized the size distribution of water-stable soil aggregates in each column. The acetate-treated columns contained significantly more soil aggregates with size less than 90 μm than the control column (i.e., no acetate injection) ($P < 0.05$, Fig. 2.8). The aggregate fractions with sizes of 150-2,000 μm in acetate-treated columns were similar to those in the control column. It is obvious that the soil aggregates enduring 60-d bioreduction generated more microaggregates compared to the soil aggregates with 20-d bioreduction.

Our results also show that the bioreduction increased releases of iron and soil colloids. The divergence of soil aggregates along the length of the columns was examined by measuring residual water-extractable total Fe. The readily reducible iron contained in the soil aggregates was much higher in the influent sections of the 60-d acetate-fed columns (A and B) with a range of 20-25 mg g^{-1} compared to the control (Fig. 2.9). The readily reducible iron in the effluent sections of the acetate-fed columns was less than 5 mg g^{-1}. In the control column, the water-extractable iron content ranged between 4.5 and 5.5 mg g^{-1} in the influent sections to less than 1 mg g^{-1} in the effluent section. The amounts of readily reducible iron in the acetate-amended columns exceeded that of the control column by approximately five fold. These trends were very consistent with the distribution of the relative abundance of *Geobacter* in the columns (Fig. 2.9), suggesting that Fe(III)-bioreduction by *Geobacter* contributed to the releases of iron and colloids. Similarly, Shi et al. (2016) observed an increase in the reduction of structural Fe(III) by *G. sulfurreducens* after the addition of an exogenous electron shuttle. These results suggest that soil aggregates could have more structural breakdown at the soil depths receiving more electron donors.

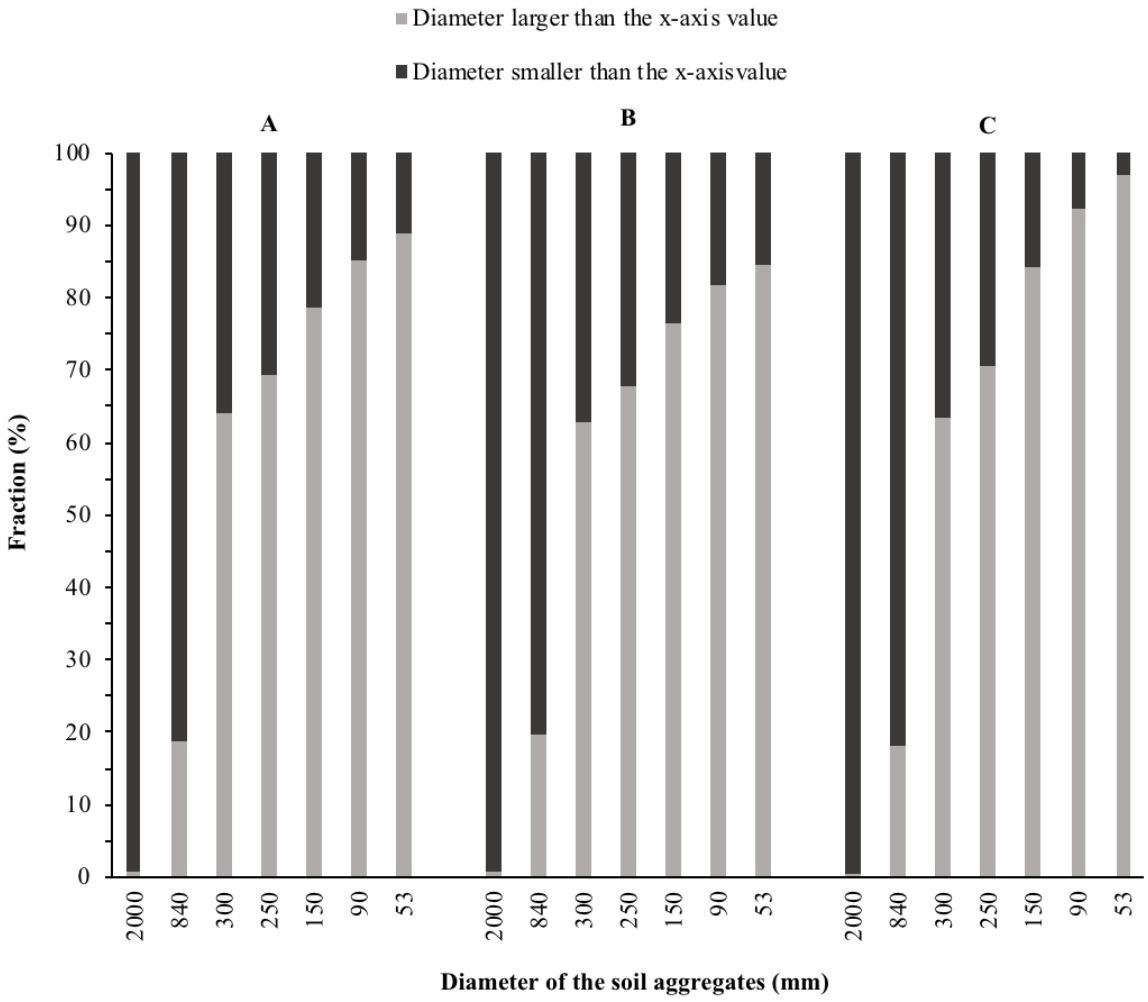

Figure 2.8: The size distribution of soil aggregates from the aggregate-packed columns after the conclusion of the 60-d Fe(III)-bioreduction experiment. Columns A and B received acetate in the feed solution over a 60-d period. Column C was the control column without acetate injection. The group with black color represents soil aggregates with diameter smaller than the x-axis value, while the group with grey color represents soil aggregates with diameter larger than the x-axis value. The fraction was calculated based on dry mass.

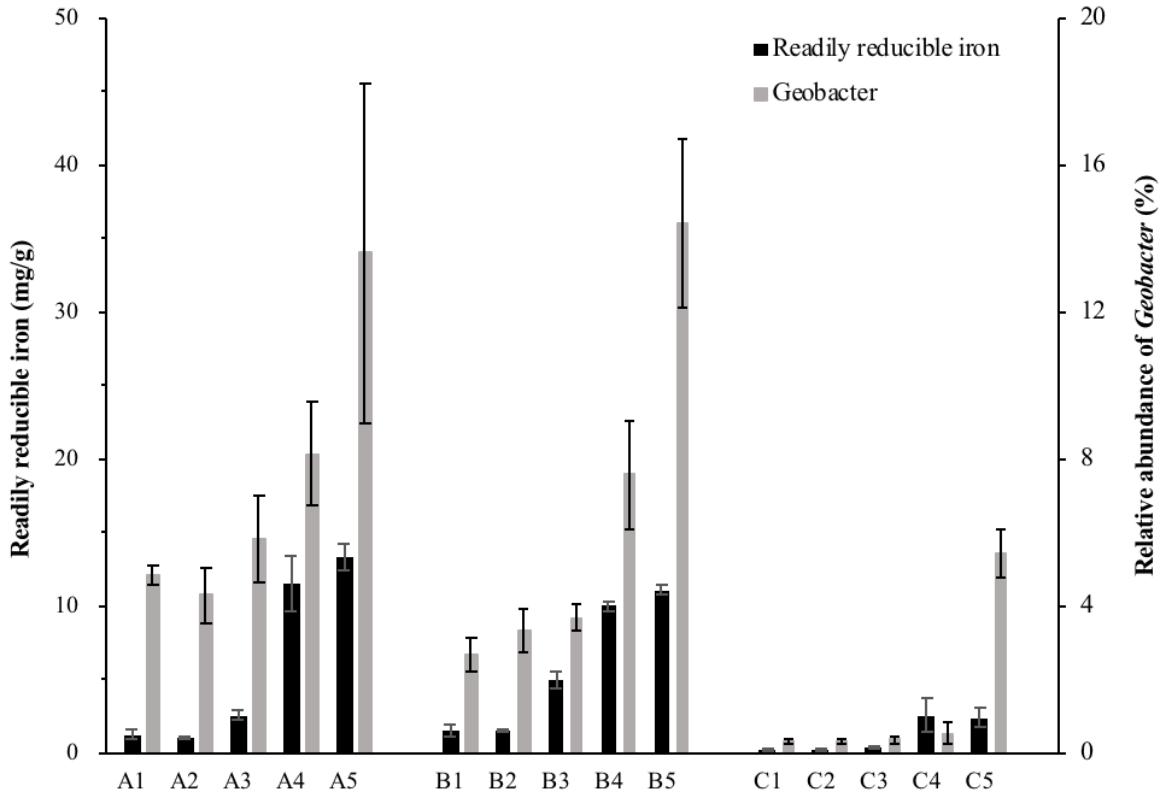

Figure 2.9: Content of readily reducible iron and distribution of iron-reducing bacteria (*Geobacter* determined via sequencing of 16S rRNA gene libraries prepared from soil samples) in five depths of the aggregate-packed columns at the conclusion of the 60-d Fe(III)-bioreduction column experiment. Columns A and B received acetate in the feed solution over a 60-d period. Column C, the control column, did not receive any acetate. Sections 1 and 5 represent samples collected near the effluent and influent ends of the columns, respectively.

Conclusions and Implications

Acetate injection stimulated microbially mediated Fe(III)-oxide reduction, and when delivered for a relatively short duration (i.e. 20 d) it enhanced the transport of an organic molecular tracer (DFBA) and nanoparticle tracers (silica-shelled silver nanoparticles) compared with the transport exhibited prior to acetate injection. However, in the subsequent experiment, when the acetate injection period was extended to 60 d the impact on transport disappeared and the transport of all tracers was identical in acetate-treated and control columns despite significant aggregate structural breakdown in the acetate-treated columns. The limited data suggest that soil aggregates had minimal structural breakdown during the first 20-d bioreduction, and as a result, only Fe(III)-oxides coating the exterior surfaces of the aggregates were reduced, yielding advective flow paths with chemically less reactive surfaces that were unfavorable for the attachment of organic and colloidal tracers on the aggregates. In comparison, more aggregates were dispersed during the 60-d bioreduction experiment, causing exposure of interior Fe(III)-oxide surfaces, generating larger reactive surfaces that were favorable for the attachment of organic and colloidal tracers. As a result, the initial 20-d effect was canceled by the subsequent 40-d of extended acetate injection, leading to similar breakthrough behaviors to those observed before the Fe(III)-bioreduction phase. Electron donor addition during biostimulation cannot continue indefinitely. Thus, upon termination of biostimulation, the treated area will ultimately return to its original redox status as oxygenated groundwater passes through the treatment zone. Future studies should address the influence of Fe(II) re-oxidation on tracer transport in relation to changes in soil properties, such as, pore structure and aggregate surface charges along the flow path.

Conflict of Interest

The authors declare no conflicts of interest.

Acknowledgments

The authors acknowledge with tremendous respect, the contributions of Dr. Phillip Jardine (posthumously) and his collaborators (Drs. Colleen Hansel, Jack Parker, Ungtae

Kim, and Kirk Scheckel) for conceiving and executing the research upon which the current work was founded. This research was financially supported by the Strategic Environmental Research and Development Program (SERDP) under project ER-2130. We also acknowledge the financial support from the China Scholarship Council to support X.L.

List of References

Arora, B., Mohanty, B.P., McGuire, J.T., 2015. An integrated Markov chain Monte Carlo algorithm for upscaling hydrological and geochemical parameters from column to field scale. Sci. Total Environ. 512, 428-443.

Aulenta, F., Majone, M., Tandoi, V., 2006. Enhanced anaerobic bioremediation of chlorinated solvents: environmental factors influencing microbial activity and their relevance under field conditions. J. Chem. Technol. Biotechnol. 81, 1463-1474.

Bose, P., Sharma, A., 2002. Role of iron in controlling speciation and mobilization of arsenic in subsurface environment. Water Res. 36, 4916–4926.

Bradford, S.A., Torkzaban, S., 2008. Colloid transport and retention in unsaturated porous media: a review of interface-, collector-, and pore-scale processes and models. Vadose Zone J. 7, 667-681.

Braunschweig, J., Bosch, J., Meckenstock, R.U., 2013. Iron oxide nanoparticles in geomicrobiology: from biogeochemistry to bioremediation. New Biotechnol. 30, 793-802.

Caccavo, F., Lonergan, D.J., Lovley, D.R., Davis, M., Stolz, J.F., McInerney, M.J., 1994. Geobacter sulfurreducens sp. Nov., a hydrogen- and acetate-oxidizing dissimilatory metal-reducing microorganism. Appl. Environ. Microbiol. 60, 3752-3759.

Caldwell, M.E., Tanner, R.S, Suflita, J.M, 1999. Microbial metabolism of benzene and the oxidation of ferrous iron under anaerobic conditions: implications for bioremediation. Environ. Microbiol. 5, 595-565.

Chapelle, F.H., Lovley, D.R., 1992. Competitive exclusion of sulfate reduction by Fe(lll)-reducing bacteria: a mechanism for producing discrete zones of high-iron ground water. Ground Water 30, 29-36.

Coates, J.D., Anderson, R.T., 2000. Emerging techniques for anaerobic bioremediation of contaminated environments. Trends Biotechnol. 18, 408-412.

De-Camposa, A.B, Mamedovb, A.I., Huang, C.H., 2009. Short-term reducing conditions decrease soil aggregation. Soil Sci. Soc. Am. J. 73, 550-559.

Deng, L., Yuan, P., Liu, D., Annabi-Bergaya, F., Zhou, J., Chen, F., Liu, Z., 2017. Effects of microstructure of clay minerals, montmorillonite, kaolinite and halloysite, on their benzene adsorption behaviors. Appl. Clay Sci. 143, 184-191.

Ellis, D.E., Lutz, E.J., Odom, J.M., Buchanan, R.J., Bartlett, C.L., Lee, M.D., Harkness, M.R., DeWeerd, K.A., 2000. Bioaugmentation for accelerated in situ anaerobic bioremediation. Environ. Sci. Technol. 34, 2254–2260.

Fernández, A., Picouet, P., Lloret, E., 2010. Cellulose-silver nanoparticle hybrid materials to control spoilage-related microflora in absorbent pads located in trays of fresh-cut melon. Int. J. Food Microbiol.

Ferris, F.G., Phoenix, V., Fujita, Y., Smith, R.W., 2004. Kinetics of calcite precipitation induced by ureolytic bacteria at 10 to 20 C in artificial groundwater. Geochim. Cosmochim. Acta 68, 1701-1710.

Galdiga, C.U., Greibrokk, T., 1998. Trace analysis of fluorinated aromatic carboxylic acids in aqueous reservoir fluids by HPLC. J. Liq. Chromatogr. Relat. Technol. 21, 855-868.

Goldberg, S., Kapoor, B.S., Rhoades, J.D., 1990. Effect of aluminum and iron oxides and organic matter on flocculation and dispersion of arid zone soils. Soil Sci. 150, 588-593.

Guan, Z., Tang, X.Y., Nishimura, T., Katou, H., Liu, H.Y., Qing, J., 2017. Surfactant-enhanced flushing enhances colloid transport and alters macroporosity in diesel-contaminated soil. J. Environ. Sci. 64, 197-206.

Hansel, C.M., Benner, S.G., Neiss, J., Dohnalkova, A., Kukkadapu, R.K, Fendorf, S., 2003. Secondary mineralization pathways induced by dissimilatory iron reduction of ferrihydrite under advective flow. Geochim. Cosmochim. Acta 67, 2977–2992.

Hansel, C.M., Benner, S.G., Fendorf, S., 2005. Competing Fe(II)-induced mineralization pathways of ferrihydrite. Environ. Sci. Technol. 39, 7147-7153.

Joe-Wong, C., Brown Jr, G.E., Maher, K., 2017. Kinetics and Products of Chromium (VI) Reduction by Iron (II/III)-Bearing Clay Minerals. Environ. Sci. Technol. 51, 9817-9825.

Karadimitriou, N.K., Joekar-Niasar, V., Brizuela, O.G., 2017. Hydro-dynamic Solute Transport under Two-Phase Flow Conditions. Sci. Rep. 7, 6624.

Kemper W.D., Rosenau R.C., 1986. Aggregate stabilty and size distribution. In: Klute A, ed. Methods of soil analysis, Part 2 chemical and mineralogical methods (2nd edition). Madison: Soil Science Society of America. Fitchburg, WI, pp. 491-515.

Kozich, J.J., Westcott, S.L., Baxter, N.T., Highlander, S.K., Schloss, P.D., 2013. Development of a dual-index sequencing strategy and curation pipeline for analyzing amplicon sequence data on the MiSeq Illumina sequencing platform. Appl. Environ. Microbiol. 79, 5112-5120.

Jardine, P.M., 2008. Influence of coupled processes on contaminant fate and transport in subsurface environments. Adv. Agron. 99, 1-99.

Liang, X., Shi, R., Radosevich, M., Zhao, F., Zhang, Y., Han, S., Zhang, Y., 2017. Anaerobic lipopeptide biosurfactant production by an engineered bacterial strain for in situ microbial enhanced oil recovery. RSC Adv. 7, 20667-20676.

Liang, Y., Bradford, S.A., Simunek, J., Vereecken, H., Klumpp, E., 2013. Sensitivity of the transport and retention of stabilized silver nanoparticles to physicochemical factors. Water Res. 47, 2572-2582.

Loffler, F.E., Sanford, R.A., Tiedje, J.M., 1996. Initial Characterization of a Reductive Dehalogenase from Desulfitobacterium chlororespirans Co23. Appl. Environ. Microbiol. 62, 3809-3813.

Lovley, D.R., 2003. Cleaning up with genomics: applying molecular biology to bioremediation. Nat. Rev. Microbiol. 1, 35-44.

Maurice, P.A., Hochella, M.F., 2008. Nanoscale particles and processes: a new dimension in soil science. Adv. Agron. 100, 123-153.

Mayes, M.A., Jardine, P.M., Mehlhorn, T.L., Bjornstad, B.N., Ladd, J.L., Zachara, J.M., 2003. Hydrologic processes controlling the transport of contaminants in humid region structured soils and semi-arid laminated sediments. J. Hydrol. 275, 141-161.

McCarthy, J.F., McKay, L.D., 2004. Colloid transport in the subsurface: past, present and future challenges. Vadose Zone J. 3, 326-337.

McKay, L.D., Sanford, W.E., Strong, J.M., 2000. Field-scale migration of colloidal tracers in a fractured shale saprolite. Ground Water 38, 139-147.

Mehra, O.P., Jackson, M.L, 1960. Iron oxide removal from soils and clays by dithionite-citrate system buffered with sodium bicarbonate. Clay. Clay Miner. 7, 317-327.

Mejia, J., Roden, E.E., Ginder-Vogel, M., 2016. Influence of oxygen and nitrate on Fe (hydr) oxide mineral transformation and soil microbial communities during redox cycling. Environ. Sci. Technol. 50, 3580-3588.

Mohanty, S.K., Saiers, J.E., Ryan, J.N., 2016. Colloid mobilization in a fractured soil: effect of pore-water exchange between preferential flow paths and soil matrix. Environ. Sci. Technol. 50, 2310-2317.

Moon, H.S., Kim, B.A., Hyun, S.P., Lee, Y.H., Shin, D., 2017. Effect of the redox dynamics on microbial-mediated As transformation coupled with Fe and S in flow-through sediment columns. J. Hazard. Mater. 329, 280-289.

Pachapur, V.L., Larios, A.D., Cledon, M., Brar, S.K., Verma, M., Surampalli, R.Y., 2016. Behavior and characterization of titanium dioxide and silver nanoparticles in soils. Sci. Total Environ. 563, 933-943.

Pedersen, H.D., Postma, D., Jakobsen, R., 2006. Release of arsenic associated with the reduction and transformation of iron oxides. Geochim. Cosmochim. Acta 70, 4116–4129.

Qin, Q., Chen, X.J., Zhuang, J., 2017. The surface-pore integrated effect of soil organic matter on retention and transport of pharmaceuticals and personal care products in soils. Sci. Total Environ. 599, 42-49.

Ryan, J.N., Elimelech, M., Ard, R.A., Harvey, R.W., Johnson, P.R., 1999. Bacteriophage PRD1 and silica colloid transport and recovery in an iron oxide-coated sand aquifer. Environ. Sci. Technol. 33, 63-73.

Sagee, O., Dror, I., Berkowitz, B., 2012. Transport of silver nanoparticles (AgNPs) in soil. Chemosphere 88, 670-675.

Schaider, L.A., Senn, D.B., Estes, E.R., Brabander, D.J., Shine, J.P., 2014. Sources and fates of heavy metals in a mining-impacted stream: temporal variability and the role of iron oxides. Sci. Total Environ. 490, 456-466.

Shi, B., Liu, K., Wu, L., Li, W., Smeaton, C.M., Beard, B.L., Johnson, C.M., Roden, E.E., Van Cappellen, P., 2016. Iron isotope fractionations reveal a finite bioavailable Fe pool for structural Fe (III) reduction in nontronite. Environ. Sci. Technol. 50, 8661-8669.

Si, Y., Zou, Y., Liu, X., Si, X., Mao, J., 2015. Mercury methylation coupled to iron reduction by dissimilatory iron-reducing bacteria. Chemosphere 122, 206-212.

Šimůnek, J., van Genuchten, M.T. and Šejna, M., 2008. Development and applications of the HYDRUS and STANMOD software packages and related codes. Vadose Zone J. 7, 587-600.

Song, B., Zeng, G., Gong, J., Liang, J., Xu, P., Liu, Z., Zhang, Y., Zhang, C., Cheng, M., Liu, Y., Ye, S., 2017. Evaluation methods for assessing effectiveness of in situ remediation of soil and sediment contaminated with organic pollutants and heavy metals. Environ. Int. 105, 43-55.

Stookey, L.L., 1970. Ferrozine—a new spectrophotometric reagent for iron. Anal. Chem. 42, 779-781.

Thompson, A., Chadwick, O.A., Boman, S., Chorover, J., 2006. Colloid mobilization during soil iron redox oscillations. Environ. Sci. Technol. 40, 5743–5749.

Vink, J.P., van Zomeren, A., Dijkstra, J.J., Comans, R.N., 2017. When soils become sediments: Large-scale storage of soils in sandpits and lakes and the impact of reduction kinetics on heavy metals and arsenic release to groundwater. Environ. Pollut. 227, 146-156.

Viollier, E., Inglett, P.W., Hunter, K., Roychoudhury, A.N., van Cappellen, P., 2000. The ferrozine method revisited: Fe(II)/Fe(III) determination in natural waters. Appl. Geochem. 15, 785-790.

Weber, K.A., Achenbach, L.A., Coates, J.D., 2006. Microorganisms pumping iron: anaerobic microbial iron oxidation and reduction. Nat. Rev. Microbiol. 4, 752-764.

Wolin, F.A., Wolin, M.J., Wolfe, R.S., 1963. Formation of methane by bacterial extracts. J. Biol. Chem. 238, 2882-2886.

Xiao, W., Jones, A.M., Li, X., Collins, R.N., Waite, T.D., 2018. Effect of Shewanella oneidensis on the kinetics of Fe (II)-catalyzed transformation of ferrihydrite to crystalline iron oxides. Environ. Sci. Technol. 52, 114-123.

Zhang, D., Guo, H., Xiu, W., Ni, P., Zheng, H., Wei, C., 2017. In-situ mobilization and transformation of iron oxides-adsorbed arsenate in natural groundwater. J. Hazard. Mater. 321, 228-237.

Zhuang, J., Jin, Y., Flury, M., 2003. Colloid-facilitated cesium transport through water-saturated Hanford sediment and Ottawa sand. Environ. Sci. Technol. 37, 4905-4911.

Zhuang, J., Qi, J., Jin, Y., 2005. Retention and transport of amphiphilic colloids under unsaturated flow conditions: effect of particle size and surface properties. Environ. Sci. Technol. 39, 7853-7859.

Zhuang, J., McCarthy, J.F., Perfect E., Tyner, J., Flury, M., 2007. In-situ colloid mobilization in Hanford sediments under unsaturated transient flow condition: Effect of irrigation pattern. Environ. Sci. Technol. 41, 3199-3204.

Zhuang, J., Jin, Y., 2008. Interactions between virus and goethite during saturated flow: effects of solution pH, carbonate, and phosphate. J. Contam. Hydrol. 98, 15-21.

Zhuang, J., Tyner, J.S., Perfect, E., 2009. Colloid transport and remobilization in unsaturated porous media during transient flow. J. Hydrol. 377, 112-119.

Zhuang, J., Goeppert, N., Tu, C., McCarthy, J.F., Perfect, E., McKay, L.D., 2010. Colloid transport with wetting fronts: Interactive effects of solution surface tension and ionic strength. Water Res. 44, 1270-1278.

Chapter II Appendix

Table 2.3: Experimental protocols of transport tests in columns.

Experiments	Column #	Soil	Procedures
Effects of iron oxide on the transport of three tracers	1	Goethite-coated silica	1. Two columns were wet-packed with uncoated and goethite-coated sands, respectively. 2. The sand columns were flushed with KCl solution (0.67 mM, pH 6.5) prior to the tracer experiments. 3. The input solution for the sand columns contained Br- (50 mg/L KBr), 2,6-DFBA (40 mg/L), and SSSNP (40 µg/L) in the KCl solution. 4. Breakthrough and elution data of three tracers were collected.
	2	Uncoated silica	
Effect of Fe(III)-bioreduction on the transport of tracers (bioreduction duration of 20 days and 60 days, seperately)	3	Macroaggregates (250-2000 µm)	**1.** Five columns were dry-packed with *Geobactor*-inoculated soil macroaggregates under anoxic conditions. **2.** The soil aggregate columns were flushed with carbon dioxide to replace the air in soil pores, followed by flushing with KCl solution (0.67 mM, pH 6.5) to achieve fully saturated conditions without remaining gas pockets. **3.** Each column experiment consisted of three phases with constant total ionic strength of solutions (2 mM): **Phase 1:** Tracer transport experiments with the KCl input solution containing Br- (85 mg/L KBr), 2,6-DFBA (50 mg/L), and SSSNP (40 µg/L).Breakthrough and elution data of three tracers were collected. **Phase 2:** Columns were flushed with artificial groundwater solution (AGW), which had a total ionic strength of 2 mM and a pH value of 7.5, consisting of $CaCl_2$ (0.075 mM), $MgCl_2$ (0.082 mM), KCl (0.051 mM), $NaHCO_3$ (1.5 mM), trace elements, and vitamins. The AGW for bioreduction-stimulated column contained acetate, while the AGW for two control columns was prepared without acetate. The bioreducgtion phase lasted for 20 days in two columns (one acetate-treated column and one control column); while the other three columns (two acetate-treated columns and one control column) experienced 60 days of bioreduction. Phase 3: The same tracer transport experiments with Phase 1 were performed at the conclusion of bioreduction phase. **Phase 3:** The same tracer transport experiments with Phase 1 were performed at the conclusion of bioreduction phase.
	4	Macroaggregates (250-2000 µm)	
	A	Macroaggregates (250-2000 µm)	
	B	Macroaggregates (250-2000 µm)	
	C	Macroaggregates (250-2000 µm)	
Effects of aggregate size fractions on the transport of three tracers	5	Macroaggregates (250-2000 µm)	1. Two columns were dry packed with microaggregates and macroaggregates, respectively. 2. The soil aggregate columns were flushed with carbon dioxide, followed by flushing with KCl solution (0.67 mM, pH 6.5) to achieve fully saturated conditions without remaining gas pockets. 3. Tracer experiments withBr- (50 mg/L KBr), 2,6-DFBA (40 mg/L), and SSSNP (40 µg/L) in the KCl solution were performed in each column. 4. Breakthrough and elution data of three tracers were collected.
	6	Microaggregates (53-250 µm)	

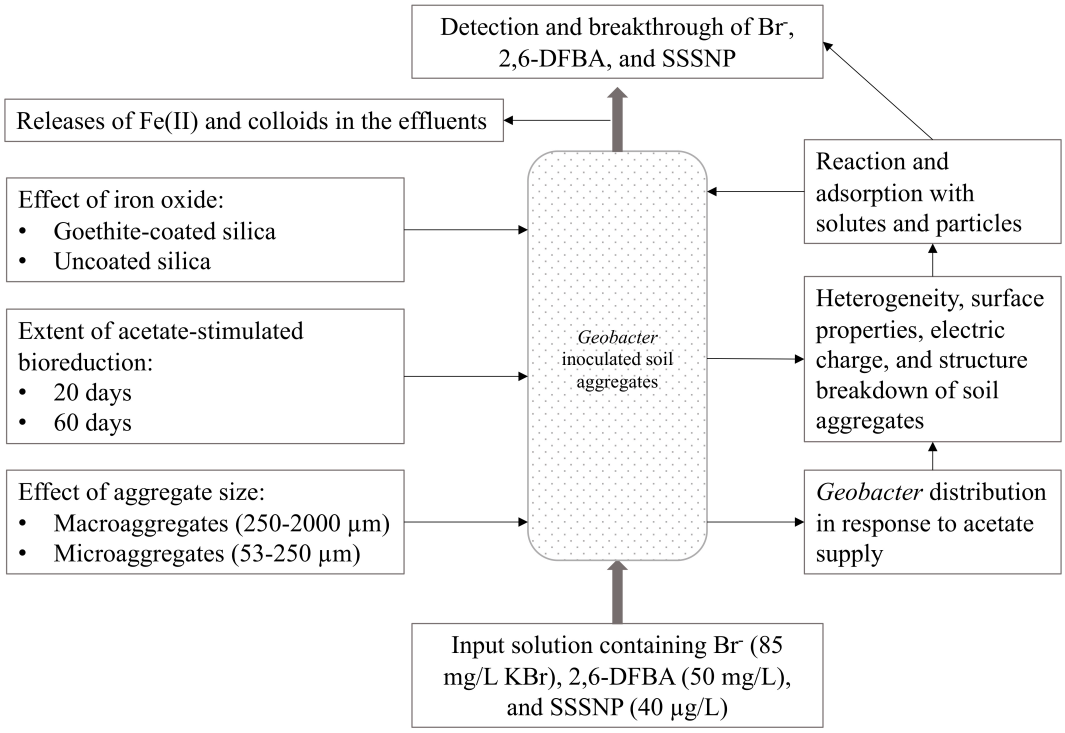

Figure 2.10: The schematic diagram of column experiments.

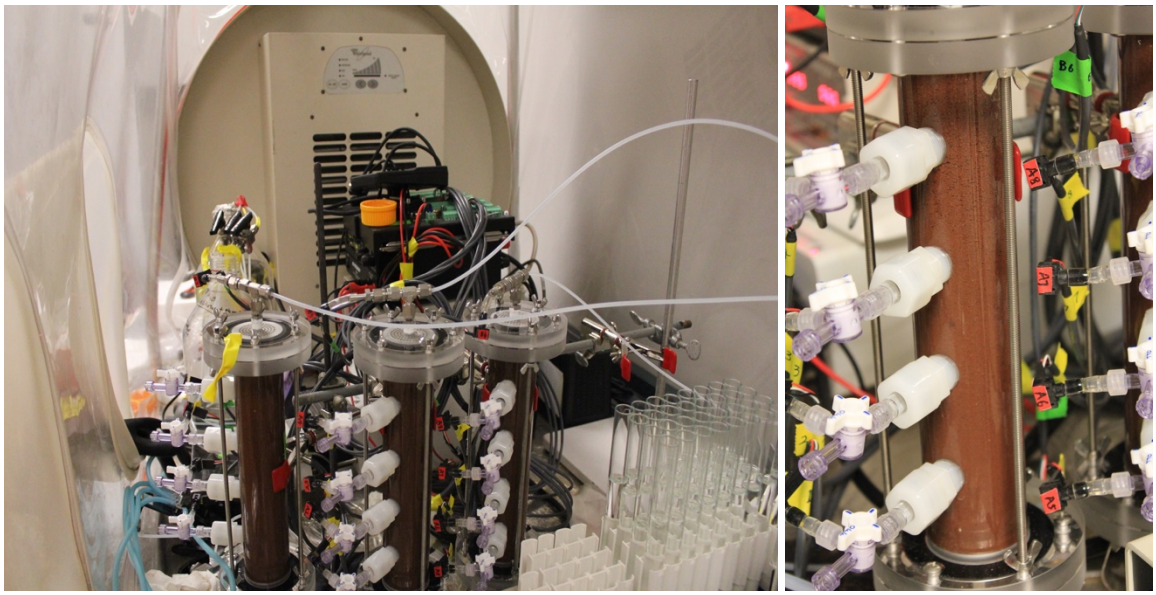

Figure 2.11: Pictures of column experiment system in the anoxic chamber. Columns were put into anoxic chamber to guarantee anaerobic bio-reduction. Acetate was used as electron donor for Fe(III)-bioreduction in this system. Artificial ground water with/without acetate was injected into the columns and effluent fractions were collected and analyzed.

CHAPTER III

Viral and bacterial community responses to stimulated Fe(III)-bioreduction during simulated subsurface bioremediation

Publication Note

This chapter was originally published as a peer-reviewed article by Xiaolong Liang, Jie Zhuang, Frank Löffler, Yingyue Zhang, Jennifer M. DeBruyn, Steven W. Wilhelm, Sean M. Schaeffer, and Mark Radosevich in *Environmental Microbiology*.

My contribution to this work includes conceiving and designing the experiments, setting up column experiments, sample collection and processing, statistical analyses, and composing the manuscript.

Citation

Liang, X., Zhuang, J., Löffler, F.E., Zhang, Y., DeBruyn, J.M., Wilhelm, S.W., Schaeffer, S.M. and Radosevich, M., 2019. Viral and bacterial community responses to stimulated Fe (III) - bioreduction during simulated subsurface bioremediation. Environmental Microbiology, 21, 2043-2055.

Abstract

The delivery of fermentable substrate(s) to subsurface environments stimulates Fe(III)-bioreduction and achieves detoxification of organic/inorganic contaminants. Though much research has been conducted on the microbiology of such engineered systems at lab and field scales, little attention has been given to the phage-host interactions and virus community dynamics in these environments. The objective was to determine the responses of soil bacterial communities and viral assemblages to stimulated anaerobic Fe(III)-bioreduction following electron donor (*e.g.*, acetate) addition. Microbial communities, including viral assemblages, were investigated after 60 days of Fe(III)-bioreduction in laboratory-scale columns continuously fed with acetate-amended artificial groundwater. Viral abundances were greatest in the influent section and decreased along the flow path. Acetate availability was important in influencing bacterial diversity, microbial interactions, and viral abundance and community composition. The impact of acetate addition was most evident in the influent section of the columns. The increased relative abundance of Fe(III)-reducing bacteria coincided with an increase in viral abundance in areas of the columns exhibiting the most Fe(III) reduction. The genetic composition of viruses in these column sections also differed from the control column and distal sections of acetate-treated columns suggesting viral communities responded to biostimulated Fe(III)-bioreduction.

Introduction

Anaerobic bioremediation has been widely applied for the *in situ* mitigation of subsurface contamination (Zhang et al., 2013; Höhener et al., 2014; Liang et al., 2017). Biostimulation is a common approach to enhance microbial reductive processes (*i.e.,* the contaminants are reduced to less toxic products) under anoxic subsurface conditions by addition of nutrients (*i.e.,* electron donors; usually organic) that are usually limiting factors for microbial functions in the subsurface environment. Many studies have revealed the dynamics of coupled physical, chemical, and biological processes in similarly manipulated environments, including impacts on the structure and function of microbial communities before, during, and after the application of anaerobic bioremediation technology (Williams et al., 2013; Höhener et al., 2014; Hansel et al., 2015).

Anoxic conditions established during bioremediation and stimulated microbially-mediated reduction of Fe(III)-(oxyhydr)oxides minerals produce soluble Fe(II), leading to aggregate dispersion and potential precipitation of secondary mineral phases (Byrne et al., 2015; Rawson et al., 2016; Garland et al., 2017). Fe(III)- (oxyhydr)oxides widely exist in the subsurface and are important components that facilitate mineral aggregation and pollutant adsorption (Navrotsky et al., 2008; Braunschweig et al., 2013). Microbial reduction of Fe(III)- (oxyhydr)oxides may exert secondary impacts on groundwater quality, pore structure, hydraulic conductivity, and in turn shape the fate and transport of contaminants and the functions of microbial communities (Wu et al., 2010; Gupta et al., 2015; Ni et al., 2018). Specific microorganisms often have a major role in driving overall community composition and function (Fuhrman, 2009; Nemergut et al., 2013; Fierer, 2017; Banerjee et al., 2018). For example, *Geobacter* species and other Fe(III)-reducing bacteria function effectively in anaerobic bioremediation (Caccavo et al., 1994; Anderson et al., 2003; Weber et al., 2006; Wu et al., 2010; Liu et al., 2014; Melton et al., 2014), since they are ubiquitous in subsurface environments and can couple the transformation of organic compounds, radionuclides, and heavy metals into less mobile and/or less toxic chemical species with Fe(III)-reduction when supplied with adequate electron donors (Holmes et al., 2015). Thus, understanding microbial iron redox processes is important for predicting

environmental health and providing opportunities of innovative remediation strategies (Borch et al., 2009; Shi et al., 2016).

A variety of environmental factors, e.g., pH, nutrient availability, and electron donor/acceptor gradients, that can shape bacterial community structure and activities, have been reported in previous research (Fierer et al., 2007; Cardenas et al., 2008; Hansel et al., 2015). However, little is known about biotic interactions, including microbe-microbe and microbe-virus interactions, that impact bacterial communities; particularly in systems undergoing stimulated bioremediation. Bacteriophages, or "phages", are obligate viral predators of bacteria and depend on host cells for replication, are abundant across a wide range of habitats (Suttle, 2007; Koskella and Brockhurst, 2014). Extracellular phages are metabolically inactive and passively disperse with water or air in the environment. Phage infection is dependent on encountering a suitable bacterial cell after which the phage genome is injected into the host cell entering an intracellular stage. As obligate predators of prokaryotes, lytic phages may reproduce through a lytic life cycle resulting in the destruction of the host cell following production of progeny phage (Williamson et al., 2017; Daly et al., 2019). Alternatively, temperate phages may reproduce lytically or via a lysogenic life cycle in which the phage genome is stably integrated into the host genome and replicated as the host cell grows and divides. These "prophage" as they are known can subsequently enter a lytic cycle of reproduction upon certain signals, ultimately killing the host cell (Ghosh et al., 2009; Slip and Bassler, 2019). In the lytic cycle, intracellular phage hijacks the host's transcription and translation systems to serve virion production ultimately ending in cell lysis and release of new phage particles.

The two life strategies of phages above have distinct effects on the hosts and hosts' behaviors (Breitbart et al., 2018). Likewise, phages that are more mobile with pore water in porous media likely experience greater host-cell contact rates leading to higher infection frequencies and greater impact on host community structure and activity (Williamson et al., 2017; Kuzyakov and Mason-Jones, 2018). For example, viruses may play a pivotal role in controlling bacterial populations, and virus-mediated cell lysis impacts biogeochemical cycles and influences the metabolism and behavior of infected host microbes, resulting in pronounced impacts on ecological processes (Wilhelm and Suttle, 1999; Weitz and

Wilhelm, 2012; Sullivan et al., 2017). Phages can also exert direct influences on host diversity and function through the incorporation and expression of phages' auxiliary metabolic genes (Breitbart et al., 2018). Auxiliary metabolic genes are genes and transcriptional regulators within bacteriophage genomes that have been acquired and maintained from bacterial host genomes. Once introduced into newly infected cells, they can modulate host metabolism and behavior; potentially influencing microbial mediated processes such as biogeochemical transformations, motility, surfactant production and other activities (Emerson et al., 2018; Trubl et al., 2018).

Viral population patterns and the potential roles that viruses play in modulating the population dynamics and activity of their hosts, especially Fe(III)-reducing bacteria, have not been investigated in terrestrial aquifer subsurface environments. A previous report regarding viruses in subsurface systems presented evidence for *Geobacter*-associated phages in a uranium-contaminated aquifer via metagenomic data analysis (Holmes et al., 2015). Viral population dynamics and their ecological correlations with biotic and environmental processes in terrestrial subsurface are under-investigated relative to freshwater, marine and aquatic sedimentary environments. However, several notable studies suggest that viruses are abundant, diverse, and active members of aquatic and terrestrial ecosystems (Williamson et al., 2005; 2017; Narr et al., 2017; Pratama and van Elsas, 2018; Daly et al., 2019). The purpose of this study was to determine the response of bacterial communities and their associated viral assemblages to stimulated anaerobic Fe(III)-bioreduction during electron donor addition in laboratory-scale bioremediation column experiments.

Experimental Procedures

In situ bioremediation experiments

Water-stable (*i.e.,* ability to resist disruption from water-associated forces) soil aggregates were fractionated from an iron oxide rich soil, Decatur silty clay loam (18% sand, 16% silt, and 66% clay with a soil pH of 5.9), as previously described in Liang et al. (2019). The fractionated soil aggregates (250-2000 μm) were sent to Midwest Laboratories

(Omaha, NE) for physicochemical analyses. The non-sterile, air-dried soil aggregates were inoculated with a stationary phase culture of *Geobacter sulfurreducens* strain PCA (ATCC 51573), a metal-reducing microorganism, which was isolated from hydrocarbon-contaminated sediments (Caccavo et al., 1994) prior to packing the plexiglass columns (25 cm in length and 3.8 cm inside diameter, with 4 side ports separated by 5-cm intervals) as previously described (Liang et al., 2019). For inoculation, 200 ml of *G. sulfureducens* culture in stationary growth phase (approximately 1×10^8 cells per milliliter) was centrifuged at 4,248 × *g*. The bacterial cells were resuspended in 20 ml of artificial groundwater (AGW) and uniformly sprayed onto 600 g of soil macroaggregates in the anaerobic chamber with an N_2/CO_2 (80/20, v/v) atmosphere. The inoculum was added to ensure significant Fe(III)-bioreduction would occur during the course of the experiment since it was necessary to air dry the soil aggregates to adequately pack the columns for tracer and particle transport studies reported elsewhere (Liang et al., 2019).

To stimulate Fe(III)-bioreduction, artificial groundwater (AGW; Ferris et al., 2004) containing 0.2 mM acetate as an electron donor was injected into replicate soil columns labeled A_1 and A_2, while AGW without acetate was injected into the control column labeled C. The experimental design was limited to two replicated treated columns and one control column due to the need to collect effluent fractions using fraction collectors for the tracer transport studies reported elsewhere (Liang et al., 2019). The limited space inside the anaerobic chamber would not accommodate additional replicate columns and accessory equipment. Analytical replication was included upon sectioning the columns for chemical and biological analyses as described below. The solutions were introduced into the columns continuously with a peristaltic pump at pore velocity of 3.4 cm/h for 60 d inside the anaerobic chamber with N_2/CO_2 (80/20). At the conclusion of the biostimulation phase of the experiment and a brief post-treatment tracer test (Liang et al., 2019), the columns were sectioned into five 5-cm segments from the top of the column (effluent end) to the bottom of the column (influent end). Sections were labeled 1 to 5 from influent to effluent end of the columns following the column label, A_1, A_2, (A for "acetate amended") or C (C for control column without acetate) (Appendix Fig. 3.7). Three sub-samples were taken

from each homogenized soil section to provide analytical replication. The replicate sub-samples were snap-frozen in liquid nitrogen and stored at -80°C for later analyses.

Enumeration of viruses and bacteria in soil aggregates

After 60 days of simulated subsurface bioremediation, soil samples from the acetate-treated and control columns were collected for analysis of viral and bacterial abundances. No corresponding measurements were made prior to acetate injection. Viruses and bacterial cells were extracted from triplicate samples of each section of the soil columns using a method modified from Williamson et al. (2005; 2007). Five grams of soil per sample were distributed into precooled (4 °C) glass jars (Ball Corp., Broomfield, CO) with 40 mL of cold extraction buffer (consisting of 1% w/v potassium citrate, 1.44 g L^{-1} $Na_2HPO_4 \cdot 7H_2O$, 0.24 g L^{-1} KH_2PO_4, pH 7). All jars were blended at the highest speed (*e.g.,* grind setting) with a kitchen blender (Oster, Sunbeam products, Inc., Boca Raton, FL) for 3 min. The slurries were transferred to 50-mL polypropylene centrifuge tubes (Corning Inc., Corning, NY) for centrifugation at 4,000 × *g* for 30 min at 4 °C. Supernatants were filtered through 0.22 μm syringe filters (low protein binding Durapore membrane; Merck Millipore Ltd., Cork, Ireland) to remove bacterial cells and soil colloids. Filtrates containing virus-like particles (VLPs) were transferred into 5 mL cryogenic vials (Fisher Scientific) and frozen in liquid nitrogen for storage at -80 °C. For bacterial extraction, 10 grams of soil were added to jars seated on ice, containing 100 mL of extraction buffer as used above. Slurries were blended for 3 min, and 9 mL of the blended slurries were slowly transferred into 2 mL of 60% (w/v) nycodenz solution (Accurate Chemical & Scientific, Westbury, NY) in a 15-mL centrifuge tube. The slurries on nycodenz were centrifuged at 5,000 x g for 30 min, and aliquots of the supernatants with nycodenz gradient were transferred into 5 mL cryogenic vials and stored at -80 °C after being frozen in liquid nitrogen.

Viral and bacterial enumerations with epifluoresence microscopy were performed as previously described by Williamson et al. (2007; 2008). Viral and bacterial extractions were treated with DNase I (10 units DNase I/100 μL) for epifluoresence microscopy observation. Each viral sample was filtered through a 0.02-μm Anodisc filter on a

microfiber filter, while bacterial cells in each bacterial extraction were captured by a 0.22-μm polycarbonate filter (Marine manufacturing, Long Beach, CA) on a glass microfiber filter. Viruses and bacterial cells on separate filters were stained by SYBR gold (in a final 2 x concentrate). The prepared filters were mounted onto glass microscope slides for immediate analysis using a Nikon Eclipse E600 epifluorescence microscope with FITC excitation and emission filter set. Ten to 20 fields per sample were digitally photographed at 1000-fold magnification by Retiga EX-i CCD camera (Qimaging, BC, Canada).

DNA extraction and sequencing

Whole soil DNA was obtained by extracting both soil aggregates and associated pore water (Cápiro et al., 2014) using PowerLyser PowerSoil DNA isolation kit (MoBio Laboratories Inv. Carlsbad, CA) following the manufacturer's instructions. The extracted DNA in each sample was quantified with the PicoGreen Assay Kit (Invitrogen, Carlsbad, CA) according to the manufacturer's instructions and sent to Genomic Services Lab at HudsonAlpha Institute for Biotechnology for sequencing. Primer set (341F_CCTACG GGNGGCWGCAG, 785R_GACTACHVGGGTATCTAATCC) was used to amplify the V3-V4 region of 16S rRNA gene by PCR to construct libraries. The pooled library was sequenced using 300PE (paired-end) on the Illumina MiSeq platform (Illumina, USA) at HudsonAlpha Institute for Biotechnology, Huntsville, AL.

Bacterial community analysis

Raw sequence files were analyzed by MOTHUR v.1.40.0 following the Mothur MiSeq SOP (Mothur code in supplementary file; Kozich et al., 2013). Sequence data was demultiplexed, trimmed of primers and reads containing ambiguous bases and long polymers, and merged to contigs. Unique sequences were sorted by abundance and all quality-filtered sequences were aligned to the generated SILVA non-redundant (NR99) 16S reference database (release 128; using TestPrime version 1.0; Quast et al., 2012) and pre-clustered by 99% similarity to de-noise the sequences, followed by removal of chimeric sequences using the VSEARCH algorithm. The clustered sequences were classified using the Bayesian classifier into OTUs (operational taxonomic unit) at 97% similarity cutoff.

The raw sequences before Mothur processing were deposited into National Center for Biotechnology Information Databases (Sequence Read Archive) under the accession number SRP156275.

The census at each taxonomic level and further analyses were investigated using R version 3.2.3 (R Core Team, 2015) packages phyloseq (McMurdie and Holmes, 2014), vegan (version 2.5-2; Oksanen et al., 2016), and ggplot2 (Wickham, 2016). Nonmetric multidimensional scaling (NMDS) with ordination were built based on Bray-Curtis dissimilarity matrix to represent variations in bacterial community composition. Further visualization of phylogenic and taxonomic data was performed with GraPhlAn (Asnicar et al., 2015) to show the overall distribution of bacterial communities within column soils. Bacterial taxonomic groups identified by Mothur were used for generation of a circular cladogram representing unique bacterial taxonomic compositions using R. Further analysis with GraPhlAn was implemented in Python with source code, manual, and tutorials at http://segatalab.cibio.unitn.it/tools/graphlan/. Stacked bar-plots, boxplots, and heatmaps were built in R to show the distribution of bacterial communities in column soils. The co-occurrence correlation networks of bacterial taxa were generated by SparCC (Friedman and Alm, 2012). The OTU data set of each sample was rarefied to the same number of OTUs per sample (37944, the minimum among all samples), and OTU tables were then filtered to capture the OTUs with a sum of more than 50 occurrences across all samples. The mean correlation scores were calculated based on 20 inference interactions, and the *P* value matrices were calculated with 200 bootstrapping processes. Significant edges ($P < 0.05$) and nodes with more than 1 adjacent significant edge were selected for visualization of networks.

Randomly amplified polymorphic DNA-polymerase chain reaction (RAPD-PCR) for assessment of viral genetic fingerprints

Viral filtrates were treated with DNase I (10 units DNase I/100 µl), and PCR amplification of the 16S RNA gene with primers 27F/1492R was performed to confirm the absence of bacterial DNA contamination. These reactions were negative suggesting the absence of bacterial DNA. Fifteen mL of the original DNase I-treated viral filtrates,

roughly equivalent to viruses contained within 2 g of soil, were concentrated to a final volume of 250 µL using Amicon centrifugal filters (30 K, Merck Millipore Ltd., Tullagreen, Ireland). The viral DNA was extracted using PowerViral Environmental RNA/DNA Isolation Kit (Mo BIO Laboratories, Carlsbad, CA) using 250 µl of viral concentrates. The concentration of viral DNA extractions was determined using PicoGreen DNA assay kit (Invitrogen, Carlsbad, CA, USA), and all viral DNA extractions were diluted to 5 ng mL^{-1} as templates for RAPD-PCR so that all samples for RAPD-PCR contained equivalent amounts of viral DNA. Each RAPD-PCR assay mixture (25 µL) contained 2.5 µL of 10 x Ex Taq buffer (Mg^{2+} plus), 2 µL of dNTPs mixture, 2 µL of 50 pmol/µL primer stock, 0.5 µL of TaKaRa Hot-Start DNA polymerase (5 units/µL; TaKaRa Bio Inc., Otsu, Shiga, Japan) and 2 µL of viral DNA. The primer HCB-1 (5'-CCAGCAGCAG-3') serving as both forward and reverse primer in the PCR amplification was used in the RAPD-PCR, as HCB-1 produced more bands with lower template concentrations (Srinivasiah et al., 2013). This primer also was determined to occur in the highest frequency in blast searches of soil viral metagenomes (Srinivasiah et al., 2013). Thermocycler conditions were set as reported elsewhere (Srinivasiah et al., 2013).

RAPD-PCR products were separated by gel electrophoresis on 1.8% high resolution agarose (Agarose-Hi-Res separation ≤ 1000 bp [USB Corp. Cleveland, OH]) prepared in 1 × TBE (89 mM Tris-Base, 89 mM boric acid, 2 mM EDTA, pH 8.3) and run in 0.5 × TBE at 4 V/cm and visualized by SYBR gold staining (Molecular Probes) according to manufacturer's instructions. Stained gels were imaged using Kodak Gel Logic 100 imaging system (Eastman Kodak Inc., Rochester, NY). GelCompar II (version 4.5; Applied Maths, Sint-Martens-Latem, Belgium) was used to analyze the banding patterns on gel images.

Results

Evidence of biological Fe(III) oxide reduction

The physicochemical characterization of the water-stable soil aggregates (250-2,000 µm) fractionated from an iron oxide rich soil were performed by Midwest

Laboratories (Omaha, NE). The fractionated soil aggregates (250-2000 μm) contained 5.2% (w/w) citrate-bicarbonate-dithionite extractable iron, 2.5% (w/w) organic matter, and 21 mg kg^{-1} sulfur prior to the start of the experiment (Appendix Table 3.1). Three columns were packed with the above soil aggregates, and artificial groundwater (AGW) containing 0.2 mM acetate as an electron donor was injected into duplicate soil columns labeled A_1 and A_2 for Fe(III)-bioreduction stimulation. Meanwhile, AGW without acetate was injected into the control column labeled C. This experimental design was limited to just two replicated treated columns and one control due to limited space in the anaerobic chamber, extended duration of the experiment, and a limited capacity to collect effluent samples necessary for tracer studies presented elsewhere (Liang et al., 2019; see Methods section). During acetate introduction, soluble Fe(II) was continuously released in the effluent from the columns treated with acetate as presented in Liang et al. (2019) where aggregate structural breakdown and Fe(III)-bioreduction were reported. All the injected acetate (0.2 mM in AGW) was consumed by bacterial metabolism and no acetate was detected in the effluent. The amount of reduced iron was also quantified and reported in Liang et al. (2019) in which a steady increase of Fe(II) concentration in the effluent during the 60-d stimulated bioreduction was observed and the effluent concentration of soluble Fe(II) reached 300 μM.

Viral and bacterial abundances

After 60 days of treatment, viral and bacterial abundances, and virus-to-bacteria ratios measured in this study exhibited significant differences between acetate-treated columns and the control column (one-tailed t-test, $P < 0.05$) and also showed significant variations along the flow path in the columns (linear regression, $P < 0.001$; Fig. 3.1A). The acetate-treated columns contained more bacteria and viruses than the control column, and the linear regression modeling showed that viral abundances and bacterial abundances decreased from the influent to the effluent sections of the columns. Bacterial cell counts in the acetate-treated columns varied from 5.12×10^7 g^{-1} soil to 5.51×10^6 g^{-1} soil, and from 1.90×10^7 g^{-1} soil to 3.70×10^6 g^{-1} soil in control column. Viral counts in the acetate-treated columns ranged from 1.13×10^9 to 2.54×10^8 g^{-1} soil (dry weight), while those in

Figure 3.1: A) Viral and bacterial abundance, and virus-to-bacteria ratio in soil sampled from the five sections of each aggregate-packed column. Columns A_1 and A_2 received acetate in the feed solution and column C served as the control column and did not receive any acetate over the 60 d biostimulation period. The numbers one through five denote soil sections from near the influent (section 1) to the effluent ends (section 5) of each column. Error bars (standard deviation) are based on three technical replicate sub-samples analyzed from each column section. B) The correlations between viral abundance and bacterial abundance. The equations with R^2 values describe linear regression testing against a slope of 0. Filled symbols indicate the acetate-treated columns, and the open circles indicate the soils from the control column without acetate.

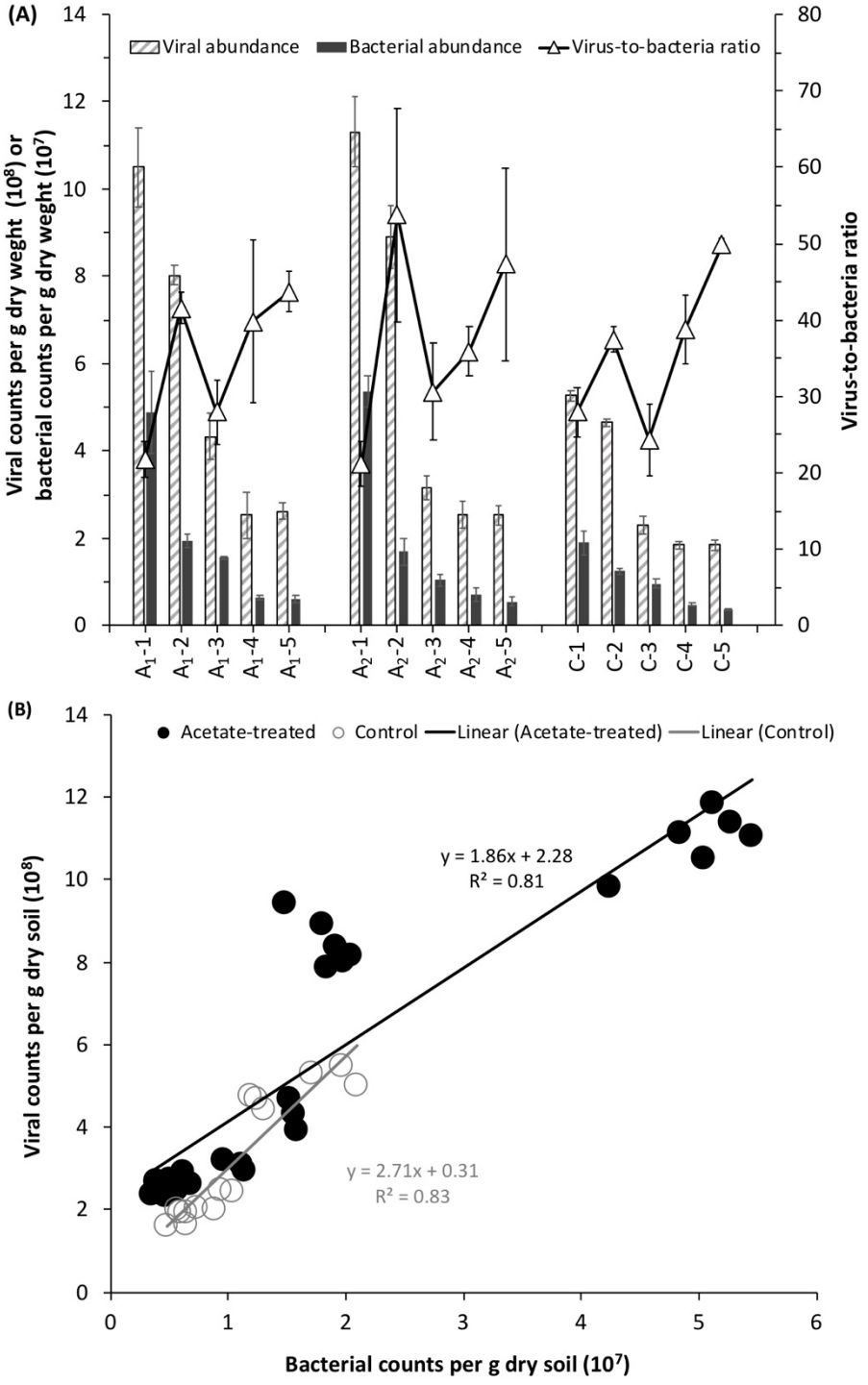

Figure 3.1 Continued

the control column ranged from 5.26×10^8 to 1.15×10^7 g^{-1} soil. The highest virus-to-bacteria ratios were observed in the effluent section of the acetate-treated columns and in the second section nearest to the influent of the control column (Fig. 3.1A). The best-fit linear relationship between viral and bacterial abundances had a slope of 18.7 ($R^2 = 0.8$, $P < 3.5 \times 10^{-6}$, linear regression, Fig. 3.1B), indicating a strong positive relationship between viral abundance and bacterial abundance.

Bacterial diversity along the column flow path

Alpha diversity of the bacterial communities was assessed based on the 16S rRNA gene sequences (Appendix Fig. 3.8). The abundance-based coverage estimators of bacterial species richness had no discernable trends among different sections in each column and showed no significant difference between the acetate-treated columns and the control column. Unlike the pattern of abundance-based coverage estimators, the control column had a significantly higher overall diversity (Shannon and Inverse Simpson indices) than the acetate-treated columns (t-test, $P < 0.01$). Bacterial diversity increased along the flow path in the acetate-treated columns (linear regression, $P < 0.05$); however, the bacterial diversity in section 2 was as high as that in the effluent section of the acetate-treated columns.

Nonmetric multidimensional scaling (NMDS) with vectors for significantly correlated parameters was constructed to explore the factors that impacted the shifts of bacterial communities. Factors affecting the community composition most were virus abundance, depth in the column, acetate addition, and virus-to-bacteria ratio (Fig. 3.2). Differences of bacterial communities were observed in different sections and in acetate-treated versus control columns. PERMANOVA analysis demonstrated a significant relationship between the bacterial community composition and the abiotic (acetate addition) and biotic factors (viral abundance). Acetate addition and virus abundance were strongly correlated with bacterial community structure across all sections ($P < 0.05$), however their influences were more significant in the influent sections than at the effluent sections. Bacterial community composition was most correlated to virus abundance at the central section of each column ($P < 0.01$; Adonis test).

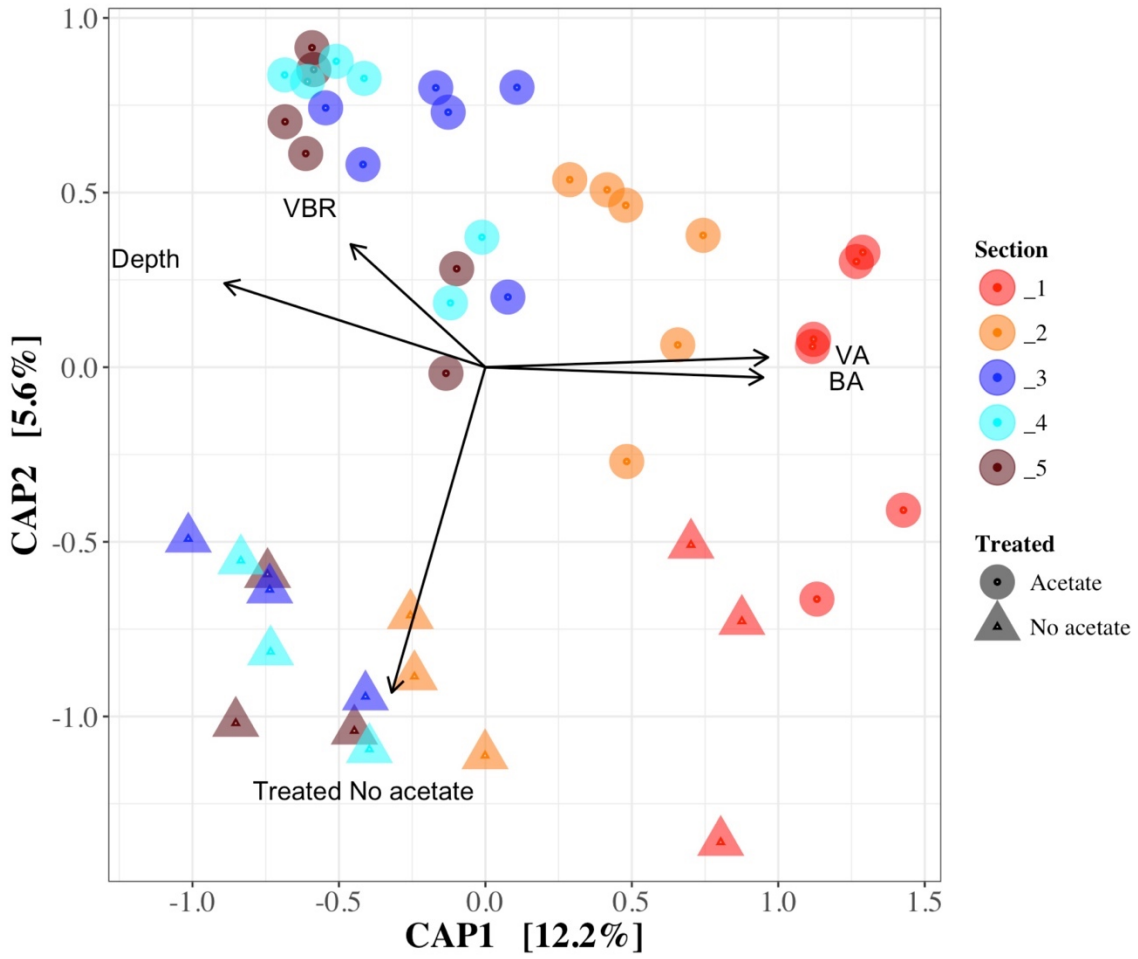

Figure 3.2: Nonmetric multidimensional scaling (NMDS) of bacterial communities. The vectors in the graph include: VA (viral abundance), BA (bacterial abundance), VBR (virus-to-bacteria ratio), Depth (distance from the column inlet), and Treatment (with acetate or no acetate). The NMDS represents a constrained ordination showing how the examined factors are associated with the changes in community composition. Each point corresponds to a sub-sample taken from one homogenized column section. The color-coded symbols represent the column section. Circles represent samples taken from columns supplemented with acetate while triangles represent samples taken from the acetate-free control column. Arrows (vectors) indicate significant factors accounting for the separation of communities and the length of the arrow indicates the strength of the effect the factor has on the community composition.

Fourteen bacterial phyla (relative abundance > 0.5%) in three columns were observed, and the most dominant phyla included Firmicutes (relative abundance across all samples of 25.1%), Proteobacteria (20.3%), Actinobacteria (11.6%), Planctomycetes (5.0%), Acidobacteria (4.0%), Chloroflexi (3.98%), Deinococcus-Thermus (3.8%), Bacteroidetes (2.7%), Verrucomicrobia (2.4%), Armatimonadetes (0.39%), and Gemmatimonadetes (0.13%) (Appendix Fig. 3.9). Delta- and Beta-Proteobacteria were most abundant in the influent sections of all columns, and their relative abundances decreased from the influent to the effluent sections of the acetate-treated columns (linear regression, $P < 0.001$), yet relatively evenly distributed across sections of the control column (Appendix Fig. 3.9). Delta- and Beta-Proteobacteria were significantly more abundant in the acetate-treated columns than in the control column (t-test, $P < 0.001$). By contrast, Alpha-Proteobacteria showed an indiscernible trend in all columns, and the relative abundance of Alpha-Proteobacteria was higher in the control column than in the acetate-treated columns. The relative abundance of Firmicutes in the control column decreased notably with distance from the AGW injection point (linear regression, $P < 0.01$). Contrastingly, the relative abundances of Deinococcus-Thermus increased from the influent to the effluent ends in all columns (linear regression, $P < 0.01$). The distribution patterns of bacterial classes in the columns were shown in Appendix Fig. 3.10.

On the genus level, *Geobacter* and *Anaeromyxobacter* were eight- and two-fold more abundant in the acetate-amended columns than in the control column, respectively (Fig. 3.3). Higher abundances of *Geobacter* and *Anaeromyxobacter* were consistent with the higher level of Fe(III)-bioreduction observed based on the release of ferrous iron in the column effluent. Acetate-treated columns also had notably higher abundances of *Desulfosporosinus* (three-fold higher), *Ralstonia* (three-fold), *Bacillus* (two-fold), and *Sporomusa* (five-fold) within Firmicutes compared to the control column (t-test, $P < 0.05$). The relative abundances of *Sporomusa*, *Bacillus*, *Desulfotomaculum*, *Desulfosporosinus*, *Geobacter*, and *Ralstonia* were negatively related to the distance from the column influent (linear regression, $P < 0.01$). In contrast, the control column had a higher relative abundance of *Flavisolibacter*, *Bradyrhizobium*, *Singulisphaera* and *Zavarzinella*.

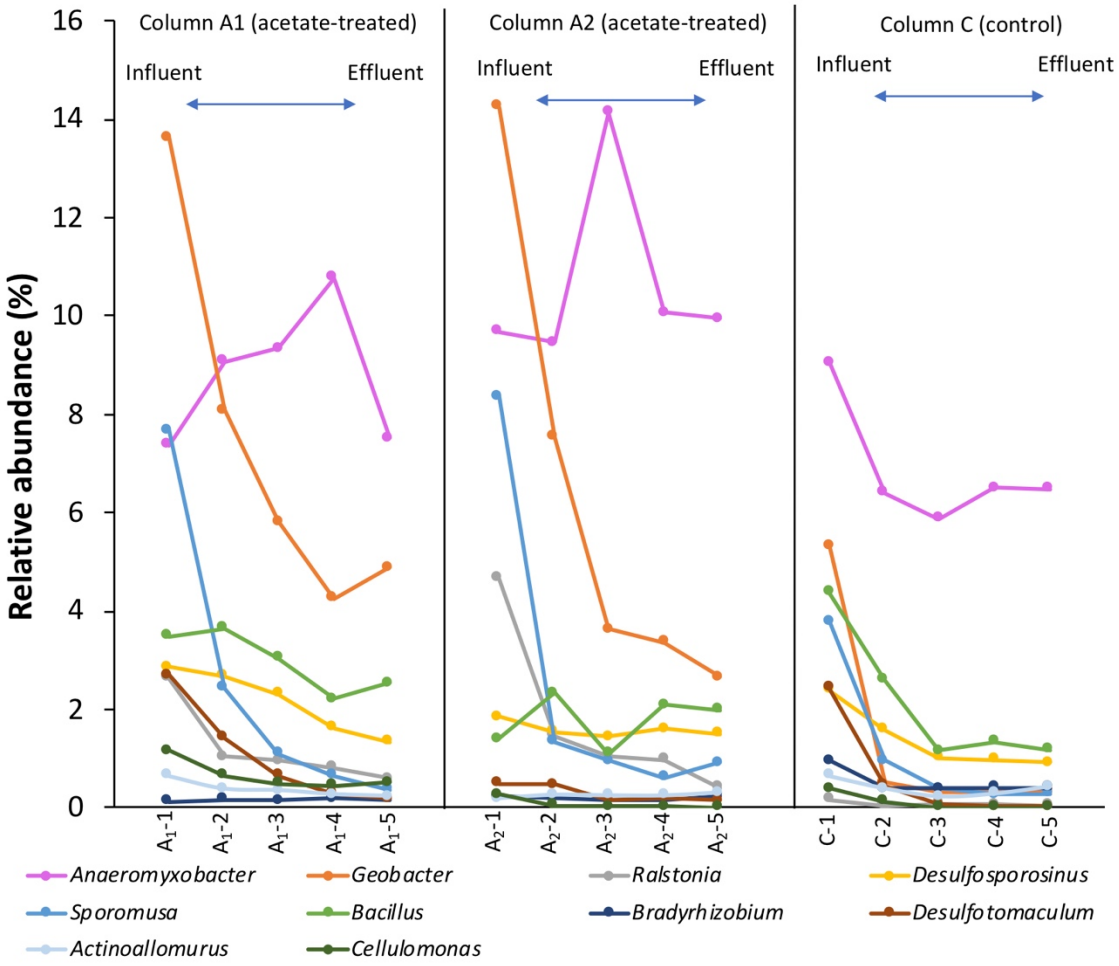

Figure 3.3: The distribution of major bacterial genera in the soil columns. Each data point represents the mean value of three sub-samples taken from of homogenized column sections. The x-axes show the five column sections from influent section towards effluent ends of the column as you move from left (section 1) to right (section 5).

Hierarchical clustering analysis was performed to examine the population shifts of the bacterial community. The samples clustered into two main groups where the influent sections of acetate-treated columns (A_1-1 and A_2-1) clustered into one group, while all other sections clustered together based on distance from the influent end of the column, indicating distinct taxonomic compositions along the flow path of acetate injection (Appendix Fig. 3.11). Sections 2-5 in the control column also clustered together. The clustered OTU groups *Desulfosporosinus*, *Bacillus*, *Streptomyces*, *Sporomusa*, and *Ralstonia* were most abundant in the influent sections. *Geobacter* and *Anaeromyxobacter* were more abundant in acetate-treated columns and showed different distribution patterns from all other taxonomic groups. The *Rhizobiales*, *Spartobacteria*, *Ktedonobacteriales*, and *Flavisolibacter* were clustered together due to their higher relative abundances in the control column than in the acetate-treated columns. Twenty-one of the top 26 genus-level groups showed significant correlations with the bacterial community composition implying contributions to the changes of bacterial composition across different samples ($P < 0.05$; Adonis test; Appendix Fig. 3.11).

Six genus-level correlation networks were constructed to explore the dynamics of bacterial interaction. The effluent section of an acetate-treated column had 64 nodes and 596 edges, more than any other section (Appendix Fig. 3.12). Section A_1-3 had 49 nodes and 355 edges, and section A_1-1 (the influent section) had just 23 nodes and 111 edges. The sections throughout the control column had similar correlation networks, in which C-5 had 23 nodes and 49 edges, and C3 had 20 nodes and 38 edges, and C-1 had 19 nodes and 43 edges. In terms of centrality of the networks, Firmicutes and Proteobacteria were dominant in all networks, but mainly in the influent section networks, indicative of spread and influence over other nodes in the networks. Other abundant phyla having more correlations with other groups in the effluent sections included Actinobacteria, Chloroflexi, Planctomycetes, and Acidobacteria. The effluent section in the acetate-treated column had the most Actinobacteria and Cloroflexi correlations compared with other sections. *Arthrobacter*, *Thermosporothrix*, and subgroup *Gp16* Acidobacteria were the most connected nodes in the A_1-5 network, while Ruminococcaceae, Oxalobacteraceae, *Gp4*,

Planococcaceae, and Nitrospira were the most connected nodes in A_1-3 network, and *Gracilibacter*, *Gp3*, and *Paenibacillus* were the most connected nodes in A_1-1 network.

Viral community responses

Viral DNA from extracted and purified virus extracts was used as template for RAPD-PCR genetic fingerprinting to examine the viral community composition. Unique virus diversity patterns with visible bands were obtained with extracts from the influent sections of the acetate-treated columns, which showed a clear separation from the viral community fingerprints in all other sections (Fig. 3.4). The viral communities generally clustered based on depth with viral communities in the control column separated from those in the acetate-treated columns. Consistent with bacterial community patterns, the viral communities in A_1-1 and A_2-1 sections were also distinct from other sections. The correlation network analysis showed that virus abundance was positively correlated with Delta-proteobacteria, Clostridia, Bacilli, Negativicutes, and Beta-Proteobacteria, which were relatively abundant in the columns (Fig. 3.5). The presence of viruses also showed a strong positive correlation with the amount of reduced iron, quantified and reported in Liang et al. (2019) The extent of Fe(III)-bioreduction based on the reduced iron eluted from the columns showed strong positive correlations with virus and microbe abundance in soil aggregates (R^2 = 0.89 and 0.66, respectively, $P < 0.001$, linear regression, Fig. 3.6).

Discussion

The current study explored the responses of viral and bacterial communities to acetate-based biostimulation of Fe(III) reduction in continuous flow soil column systems that simulated subsurface anaerobic bioremediation. The abundance of viruses and bacterial cells were strongly correlated (Fig. 3.1B), consistent with previous studies of virus-host abundance in aquatic and sedimentary environments (Säwström and Pollard, 2012; Chow et al., 2014; Pan et al., 2017; Finke et al., 2017). Viruses were more abundant in the influent sections presumably where bacterial production was stimulated by constant acetate supply. Higher host abundance and increasing bacterial production may increase the probability of virus-host contact and sustain more viral production in the environment

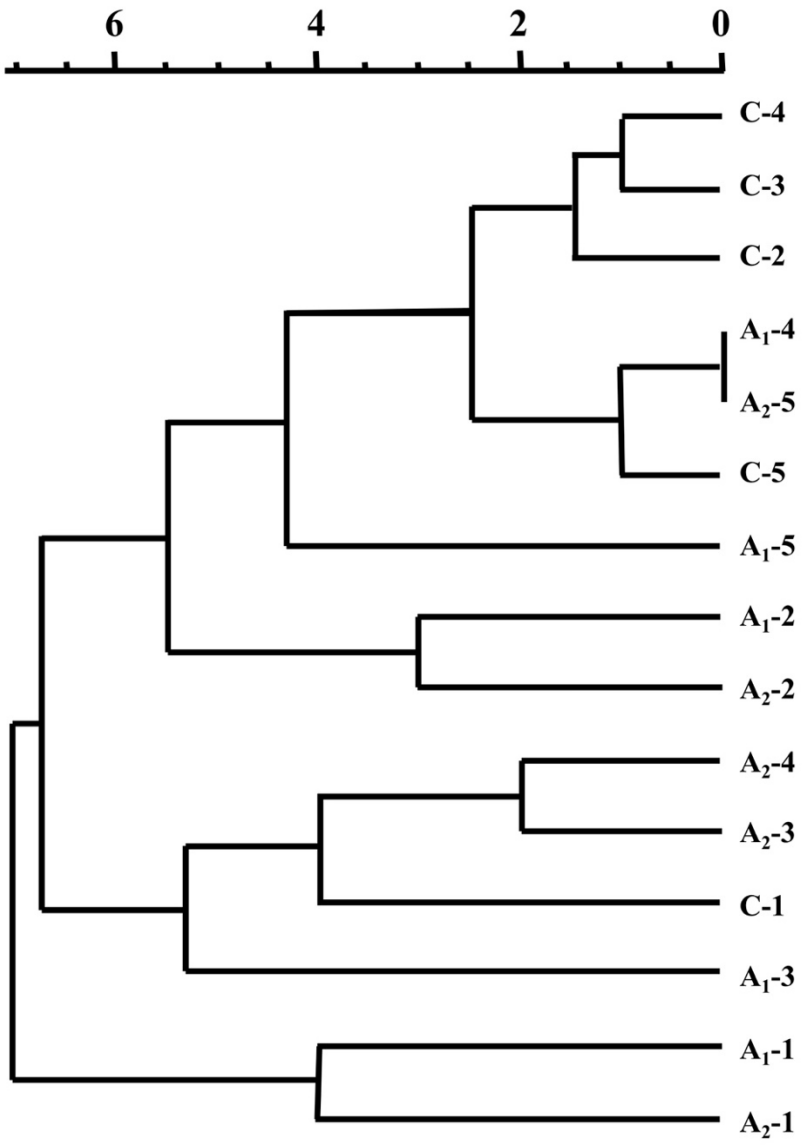

Figure 3.4: Dendrogram of viral randomly amplified polymorphic DNA-polymerase chain reaction (RAPD-PCR) fingerprints. The scale at the upper top right is the similarity distance of RAPD-PCR fingerprints. A_1 and A_2 represent the duplicate columns that received acetate in the feed solution, and C denotes the control column receiving no acetate over the 60 d biostimulation period. The numbers (1-5) following the column labels denote soil sections from near the influent (section 1) to the effluent ends (section 5) of each column.

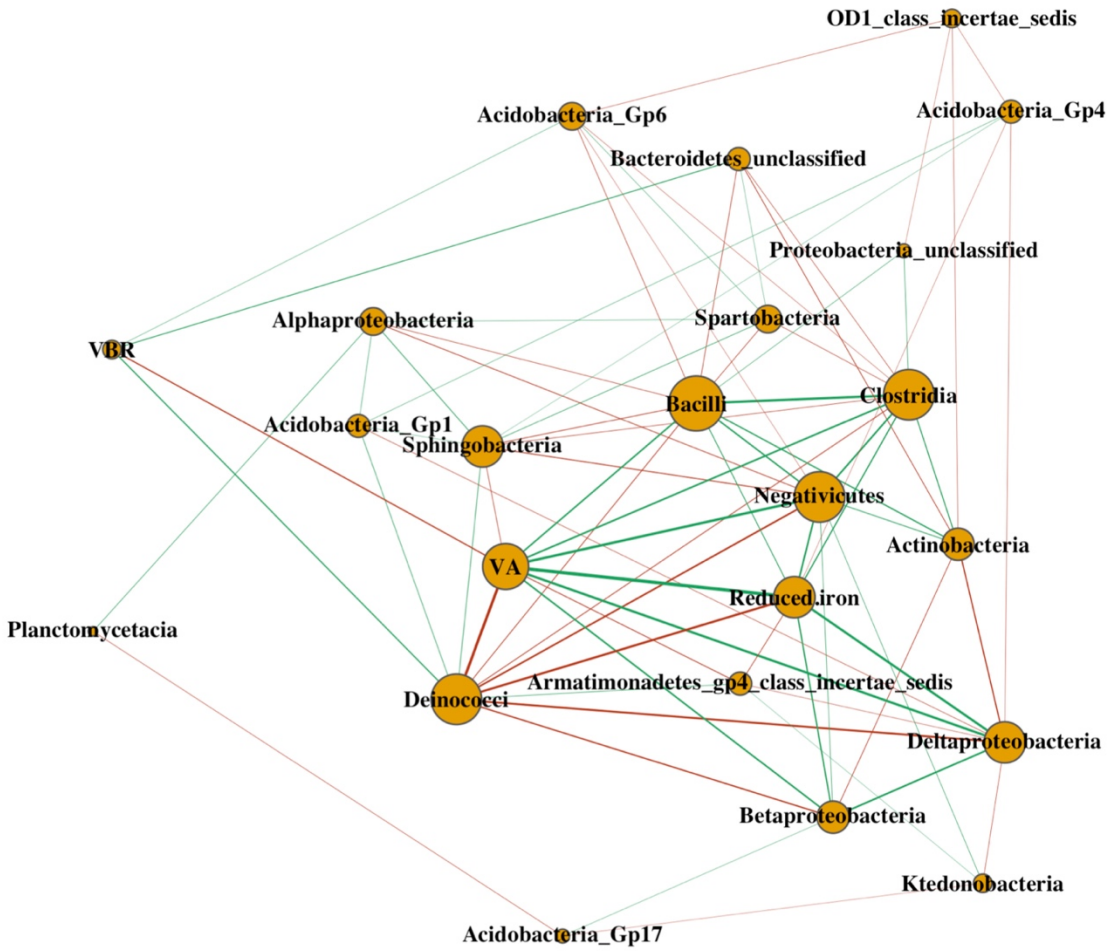

Figure 3.5: Correlation network among bacterial classes, virus abundance (VA), virus-to-bacteria ratio (VBR), and reduced iron (i.e. Fe(II)). The linkages in the correlation networks are edges (lines connecting the nodes) with *P* values calculated with 200 bootstrapping processes smaller than 0.05. Negative correlations are shown in red and positive correlations in green. The thickness of the lines represents the strength of the correlations.

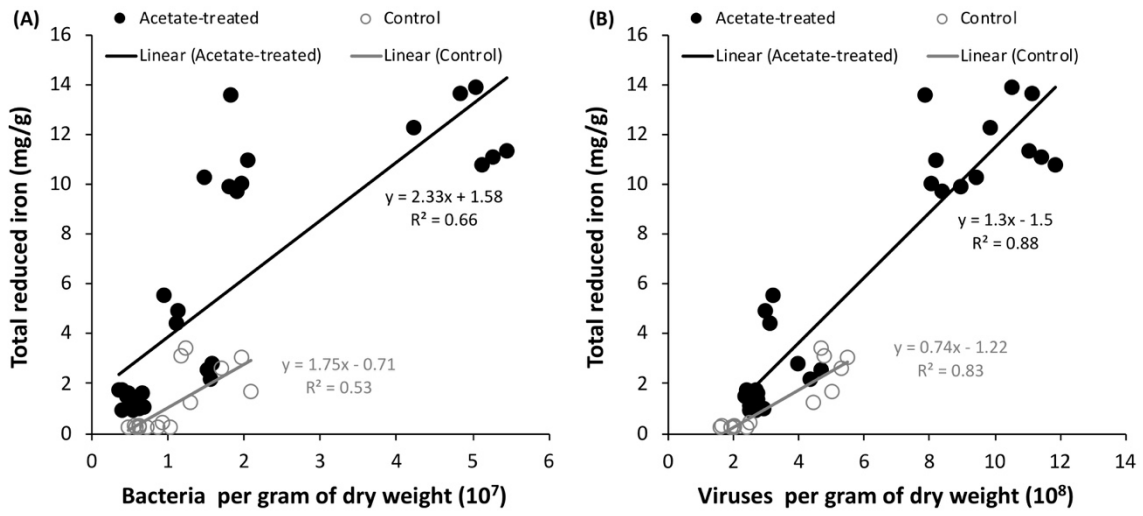

Figure 3.6: The relationships between Fe(II) concentration (as reported in Liang et al., 2019) with bacterial (A) and viral abundance (B) in soil samples. All equations with R^2 values describe linear regressions testing against a slope of 0. Solid circles indicate soils sampled from the acetate-treated columns, and hollow circles denote soils taken from the control column.

(Brum et al., 2016). Våge et al. (2016) proposed a framework through integration of a nested virus-host interaction model into the microbial food web model, and the framework indicated that virus abundance increases with increasing host growth rate. Virus-to-bacteria ratio was reported to be inversely related with bacterial abundance and production, but positively related with virus abundance, frequency of visibly infected cells, burst size, and frequency of lysogenic cells (Parikka et al., 2017). The propagation of phages is based on contacting and infecting their host cells, therefore the reproduction strategy decisions (i.e., lytic and lysogenic cycles) of viral community can be influenced by microbial host abundances (Brum et al., 2016; Wigington et al., 2016). Since lytic life cycles of phages lead to decreases in the host cell density and increased production of progeny phages, virus-to-bacteria ratio is positively related to lytic production of phages. In comparison, the temperate phages may reproduce via lysogenic life cycles in which the prophages in the host genome replicate as the host cell grows and divides (Williamson et al., 2017). The virus-to-bacteria ratio is usually low when the phage community reproduce mostly by lysogenic cycles.

In the present study, the extent of Fe(III) reduced (i.e. production of Fe(II)) was positively related with virus and host cell abundance in soil aggregates within the columns (Fig. 3.6). A high concentration of Fe(II) was detected in the effluents from the acetate-treated columns which was presumably generated by Fe(III) bioreduction and might also derive from virus-induced mortality of bacterial cells. It was reported that naturally occurring viral infection can mediate lysis of bacteria regenerating a large quantity of dissolved organically complexed Fe (Poorvin et al., 2004; Mioni et al., 2005). Virus-to-bacteria ratio generally increased from the influent to the effluent sections of the columns, possibly due to transport of viruses through the columns and lower bacterial abundance in the effluent sections (Park et al., 2017). Previous investigations in packed porous media suggested that bacteriophages pass through porous media more easily with greater recovery than bacteria (Park et al., 2017). It is noteworthy that the VBRs in the soil columns fell within the reported value range in soils and sediments (Williamson et al., 2005; 2007; Parikka et al., 2017).

Although previous studies have shown that environmental factors led to great variation in bacterial community diversity and composition (Campbell and Kirchman, 2013; Shen et al., 2013; Zhang et al., 2017; Borer et al., 2018), few studies have investigated the impacts of viruses on microbial-mediated processes in soil ecosystems. This work showed that acetate addition and the distance from the point of acetate injection were major abiotic drivers of bacterial community composition, and that virus production and presumably composition were related to the bacterial community responses observed in the columns. Our data indicated that bacterial communities were least diverse in the influent section of the acetate-treated columns and in the middle section of the control column. This observation is consistent with the enrichment of Delta-Proteobacteria and particularly *Geobacter* given the stimulation of Fe(III)-bioreduction. Acetate addition as selective electron donor undoubtedly contributed to the shifts in bacterial community structure (Bardgett and van der Putten, et al., 2014; Hansel et al., 2015). Our results are consistent with acetate selective growth of Fe(III) reducers, thereby favoring some specific bacterial groups and lowering the overall diversity in the influent section of the acetate-treated columns. However, as reported in previous studies, significant bacterial community shifts could also be attributed to viral-mediated cell lysis or "top-down" controls (Gómez and Buckling 2011; Koskella et al., 2014; Våge et al., 2016; Scanlan, 2017). Though some influence was evident through the correlation network analysis, the extent to which viral infection contributed to structuring bacterial communities was not discernable with the data collected in this study.

This study revealed enrichment of diverse bacterial taxa (Fig. 3.3), previously reported to contribute to metal redox processes. In a previous report using the identical soil columns, we showed a significant and consistent release of Fe(II) in response to acetate input, suggesting the stimulation of Fe(III)-oxide reducing microorganisms, i.e. *Geobacter* (Liang et al., 2019). The acetate-stimulated Fe(III) bioreduction was also supported by the increase in the relative abundance of Fe(III)-reducers (i.e. *Geobacter*, *Anaeromyxobacter*, *Sporomusa*, *Desulfosporosinus*, and *Desulfotomaculum*) in the acetate-treated columns within the influent sections. Flexible metabolisms have been observed in many Fe(III)-reducing bacteria, which consolidates adaptation to environmental fluctuations of electron

donors and acceptors (Melton et al., 2014) and the bacterial community patterns in Fe(III)-bioreduction environments have been well documented (Weber et al., 2006; Cardenas et al., 2008; Kwon et al., 2016). In a recent study, acetate addition as electron donor specifically promoted Proteobacteria and Firmicutes as Fe(III) reducers in the system (Kwon et al., 2016). Cardenas et al. (Cardenas et al., 2008) observed more Delta- and Beta-Proteobacteria in the acetate-treated zones than in the background area. Here *Geobacter*, *Anaeromyxobacter*, *Acidovorax*, and *Desulfosporosinus* were the most well represented Fe(III) reducing taxa. Among the observed phyla, Acidobacteria as a well-defined oligotrophic phylum (Fierer et al., 2007; Cardenas et al., 2008; Hansel et al., 2008) had a greater relative abundance in the control column and effluent sections of acetate-treated columns (Appendix Fig. 3.9); environments that were relatively nutrient-deficient and perhaps supplied with low levels of organic compounds from viral-mediated cell lysis in the influent sections of the acetate-supplied columns. Though every effort was made to homogenize each column section prior to bulk sub-sampling, we can not exclude the possibility that the heterogeneous soil aggregate structure within the columns may have also contributed to spatially structuring bacterial communities and viruses (i.e., aggregate structure contributes to "microenvironments", surface adsorption and lower mobility likely contribute to more limited spread within the column). Consistent with this notion, the bacterial-mediated Fe(III)-bioreduction caused varying-degrees of aggregate structural breakdown along the flow path making the soil structure an important factor to consider (Liang et al., 2019).

Hierarchical clustering analysis showed that *Anaeromyxobacter* and *Geobacter*, with higher relative abundances in the influent section of the acetate-treated columns, contributed to the separation of microbial communities in the influent section of acetate-treated columns from those in distal sections and the control column. High abundances of *Veillonellaceae*, *Desulfosporosinus*, *Bacillus*, *Clostridium*, and *Bacillales*, which contain notable Fe(III) reducers (Weber et al., 2006; Hansel et al., 2008), were observed in the acetate-treated columns, particularly in the influent sections (Appendix Fig. 3.11). Bacterial co-occurrence revealed by network analysis has shed light on the bacterial community structure and assembly patterns from various environments (Banerjee et al.,

2018). *Arthrobacter*, *Ruminococcus*, and *Gracilibacter*, known as metal reducers and contaminant degraders, were keystone taxa (i.e. nodes with the greatest numbers of connections) and were most correlated with other taxa in the effluent, central, and influent sections, respectively. The Acidobacteria, even with a somewhat lower relative abundance, also exhibited strong correlations with other bacterial groups. Interestingly, *Geobacter* as the most notable Fe(III) reducers were remarkably underrepresented in the networks despite their high relative abundance in the systems, which was unexpected.

Clustering based on viral genetic fingerprints showed viral community responses presumably due to the direct impact of acetate injection on bacterial communities leading to subsequent changes in viral community composition. The viral communities in the influent sections of the acetate-treated columns were different from those in other sections, and the distance-based clusters (i.e. distance from the point of acetate injection) of viral communities were consistent with the bacterial community patterns. The physico-chemical interactions between phages and soils, which are important in influencing phage dissemination, propagation and distribution and eventually shaping phage population patterns, are still underexplored. Kuzyakov et al. (2018) speculated that phages can passively diffuse with water more easily than bacteria which implies the widespread presence of phages in pores larger than nanopores. The differences of viral community patterns along the column length showed the unevenness of viral dispersion and reproduction which might be caused by the highly stimulated infection rates and subsequent lysis in bacterial populations most active in the sections with the highest acetate concentration. Viral abundance also corresponded to bacterial density along the flow path. Based on the co-occurrence correlation network analysis, viral abundances were positively correlated with five dominant bacterial classes (Delta-Proteobacteria, Clostridia, Bacilli, Negativicutes, and Betaproteobacteria), most of which include Fe(III) reducers. A recent study showed that viral and bacterial communities were highly interconnected, and phages were a major biotic factor in shaping the bacterial community dynamics in an anaerobic digester system (Zhang et al., 2017). For future work, sampling with a time series will be helpful in determining the mechanism of virus-host interactions in the systems combined with metagenomic, metaviromic and metatranscriptomic analyses. Virus abundance also

showed strong positive correlations with Fe(III)-bioreduction, indicating central roles that viruses may play in biogeochemical cycling. Ecosystems with viruses may increase the total abundance of heterotrophic bacteria and increase organic and inorganic nutrients as a result of viral-mediated cell lysis induced nutrient recycling (Weitz et al., 2015).

One notable gap in our understanding of the engineered anaerobic subsurface systems is the potential top-down control exerted by viral infection on host community structure and function. The present study investigated interactions of bacterial and viral communities under simulated anaerobic bioremediation conditions involving the stimulation of Fe(III)-oxide bioreduction. We observed that electron donor (acetate) addition and virus abundance were the two factors in structuring bacterial community composition in column-scale experiments with water-stable soil aggregates. Though viral metagenomic analyses were not performed, RAPD-PCR fingerprinting revealed a change in the genetic composition of viruses in response to acetate-stimulated Fe(III)-bioreduction. Despite the absence of viral metagenomic data, this is the first report to demonstrate viral community responses during simulated anaerobic bioremediation. In moving forward, viral community diversity and ecological functions at different spatiotemporal scales utilizing metagenomic approaches should be employed to better understand bacteria-virus dynamics and interactions in soils and subsurface ecosystems.

Acknowledgements

The authors acknowledge with tremendous respect, the contributions of Dr. Phillip Jardine (posthumously) and his collaborators (Drs. Colleen Hansel, Jack Parker, Ungtae Kim, and Kirk Scheckel) for conceiving and securing the original funding that ultimately led to the current work. This work was supported by the Strategic Environmental Research and Development Program (SERDP) under project number ER-2130. X.L. received support from China Scholarship Council with the University of Tennessee.

Conflict of Interest

The authors declare no competing interests.

List of References

Anderson, R.T., Vrionis, H.A., Ortiz-Bernad, I., Resch, C.T., Long, P.E., Dayvault, R., et al. (2003) Stimulating the in situ activity of *Geobacter* species to remove uranium from the groundwater of a uranium-contaminated aquifer. Appl Environ Microbiol 69: 5884-5891.

Asnicar, F., Weingart, G., Tickle, T.L., Huttenhower, C., and Segata, N. (2015) Compact graphical representation of phylogenetic data and metadata with GraPhlAn. Peer J 3: e1029.

Banerjee, S., Schlaeppi, K., and Heijden, M.G. (2018) Keystone taxa as drivers of microbiome structure and functioning. Nat Rev Microbiol 16: 567–576.

Bardgett, R.D., van der Putten, W.H. (2014) Belowground biodiversity and ecosystem functioning. Nature 515: 505-511.

Borch, T., Kretzschmar, R., Kappler, A., Cappellen, P.V., Ginder-Vogel, M., Voegelin, A., and Campbell, K. (2009) Biogeochemical redox processes and their impact on contaminant dynamics. Environ Sci Technol 44: 15-23.

Borer, B., Tecon, R., and Or, D. (2018) Spatial organization of bacterial populations in response to oxygen and carbon counter-gradients in pore networks. Nat Commun 9: 769.

Braunschweig, J., Bosch, J., and Meckenstock, R.U. (2013) Iron oxide nanoparticles in geomicrobiology: from biogeochemistry to bioremediation. New Biotechno 30: 793-802.

Breitbart, M., Bonnain, C., Malki, K., and Sawaya, N.A. (2018) Phage puppet masters of the marine microbial realm. Nat Microbiol 3: 754-766.

Brum, J.R., Ignacio-Espinoza, J.C., Roux, S., Doulcier, G., Acinas, S.G., Alberti, A., et al. (2015) Patterns and ecological drivers of ocean viral communities. Science 348: 1261498.

Brum, J.R., Hurwitz, B.L., Schofield, O., Ducklow, H.W., and Sullivan, M.B. (2016) Seasonal time bombs: dominant temperate viruses affect Southern Ocean microbial dynamics. ISME J 10: 437-449.

Byrne, J.M., Klueglein, N., Pearce, C., Rosso, K.M., Appel, E., and Kappler, A. (2015) Redox cycling of Fe (II) and Fe (III) in magnetite by Fe-metabolizing bacteria. Science 347: 1473-6.

Caccavo, F., Lonergan, D.J., Lovley, D.R., Davis, M., Stolz, J.F., and McInerney, M.J. (1994) *Geobacter sulfurreducens sp. nov.*, a hydrogen-and acetate-oxidizing dissimilatory metal-reducing microorganism. Appl Environ Microbiol 60: 3752-3759.

Campbell, B.J., and Kirchman, D.L. Bacterial diversity, community structure and potential growth rates along an estuarine salinity gradient. ISME J 7: 210-220.

Cápiro, N.L., Wang, Y., Hatt, J.K., Lebrón, C.A., Pennell, K.D., and Löffler, F.E. (2014) Distribution of organohalide-respiring bacteria between solid and aqueous phases. Environ Sci Technol 48: 10878-10887.

Cardenas, E., Wu, W.M., Leigh, M.B., Carley, J., Carroll, S., Gentry, T., et al. (2008) Microbial communities in contaminated sediments, associated with bioremediation of uranium to submicromolar levels. Appl Environ Microbiol 74: 3718-3729.

Chow, C.E., Kim, D.Y., Sachdeva, R., Caron, D.A., and Fuhrman, J.A. (2014) Top-down controls on bacterial community structure: microbial network analysis of bacteria, T4-like viruses and protists. ISME J 8: 816-829.

Daly, R.A., Roux, S., Borton, M.A., Morgan, D.M., Johnston, M.D., Booker, A.E., et al. (2019) Viruses control dominant bacteria colonizing the terrestrial deep biosphere after hydraulic fracturing. Nat Microbiol 4: 352-361.

Emerson, J.B., Roux, S., Brum, J.R., Bolduc, B., Woodcroft, B.J., Jang, H.B., et al. (2018) Host-linked soil viral ecology along a permafrost thaw gradient. Nat Microbiol 3: 870-880.

Ferris, F.G., Phoenix, V., Fujita, Y., and Smith, R.W. (2004) Kinetics of calcite precipitation induced by ureolytic bacteria at 10 to 20 C in artificial groundwater. Geochim Cosmochim Acta 68: 1701-1710.

Fierer, N., Bradford, M.A., and Jackson, R.B. (2007) Toward an ecological classification of soil bacteria. Ecology 88: 1354-1364.

Fierer, N. (2017) Embracing the unknown: disentangling the complexities of the soil microbiome. Nat Rev Microbiol 15: 579-590.

Finke, J.F., Hunt, B.P., Winter, C., Carmack, E.C., and Suttle, C.A. (2017) Nutrients and other environmental factors influence virus abundances across oxic and hypoxic marine environments. Viruses 9: 152.

Friedman, J., and Alm, E.J. (2012) Inferring correlation networks from genomic survey data. PLoS Comput Biol 8: e1002687.

Fuhrman, J.A. (2009) Microbial community structure and its functional implications. Nature 459: 193-199.

Garland, G., Bünemann, E.K., and Six, J. (2017) New methodology for soil aggregate fractionation to investigate phosphorus transformations in iron oxide-rich tropical agricultural soil. Eur J Soil Sci 68: 115-125.

Ghosh, D., Roy, K., Williamson, K.E., Srinivasiah, S., Wommack, K.E. and Radosevich, M., 2009. Acyl-homoserine lactones can induce virus production in lysogenic bacteria: an alternative paradigm for prophage induction. Appl Environ Microbiol 75: 7142-7152.

Gómez, P., and Buckling, A. (2011) Bacteria-phage antagonistic coevolution in soil. Science 332: 106-109.

Gupta, V.V., and Germida, J.J. (2015) Soil aggregation: Influence on microbial biomass and implications for biological processes. Soil Biol Biochem 80: A3-A9.

Hansel, C.M., Fendorf, S., Jardine, P.M., and Francis, C.A. (2008) Changes in bacterial and archaeal community structure and functional diversity along a geochemically variable soil profile. Appl Environ Microbiol 74: 1620-1633.

Hansel, C.M., Lentini, C.J., Tang, Y., Johnston, D.T., Wankel, S.D., and Jardine, P.M. (2015) Dominance of sulfur-fueled iron oxide reduction in low-sulfate freshwater sediments. ISME J 9: 2400-2412.

Höhener, P., and Ponsin, V. (2014) In situ vadose zone bioremediation. Curr Opin Biotechnol 27: 1-7.

Holmes, D.E., Giloteaux, L., Chaurasia, A.K., Williams, K.H., Luef, B., Wilkins, M.J., et al. (2015) Evidence of *Geobacter*-associated phage in a uranium-contaminated aquifer. ISME J 9: 333-346.

Koskella, B., and Brockhurst, M.A. (2015) Bacteria–phage coevolution as a driver of ecological and evolutionary processes in microbial communities. FEMS Microbiol Rev 38: 916-931.

Kozich, J.J., Westcott, S.L., Baxter, N.T., Highlander, S.K., and Schloss, P.D. (2013) Development of a dual-index sequencing strategy and curation pipeline for analyzing amplicon sequence data on the MiSeq Illumina sequencing platform. Appl Environ Microbiol 79: 5112-5120.

Kuzyakov, Y., and Mason-Jones, K. (2018) Nano-scale undead drivers of microbial life, biogeochemical turnover and ecosystem functions. Soil Biol Biochem 127: 305-317.

Kwon, M.J., O'Loughlin, E.J., Boyanov, M.I., Brulc, J.M., Johnston, E.R., Kemner, K.M., and Antonopoulos, D.A., (2016) Impact of organic carbon electron donors on microbial community development under iron-and sulfate-reducing conditions. PloS One 11: e0146689.

Liang, X., Radosevich, M., Löffler, F.E., Schaeffer, S., and Zhuang, J. (2019) Impact of microbial iron oxide reduction on the transport of diffusible tracers and non-diffusible nanoparticles in soils. Chemosphere 220: 391-402.

Liang, X., Shi, R., Radosevich, M., Zhao, F., Zhang, Y., Han, S., and Zhang, Y. (2017) Anaerobic lipopeptide biosurfactant production by an engineered bacterial strain for in situ microbial enhanced oil recovery. RSC Adv 7: 20667-20676.

Liu, H., Bruton, T.A., Doyle, F.M., and Sedlak, D.L. (2014) In situ chemical oxidation of contaminated groundwater by persulfate: decomposition by Fe (III)-and Mn (IV)-containing oxides and aquifer materials. Environ Sci Technol 48: 10330-10336.

McMurdie, P.J., and Holmes, S. Waste not, want not: why rarefying microbiome data is inadmissible. PLoS Comput Biol 10: e1003531.

Melton, E.D., Swanner, E.D., Behrens, S., Schmidt, C., and Kappler, A. (2014) The interplay of microbially mediated and abiotic reactions in the biogeochemical Fe cycle. Nat Rev Microbiol 12: 797-808.

Mioni, C.E., Poorvin, L., and Wilhelm, S.W. (2005) Virus and siderophore-mediated transfer of available Fe between heterotrophic bacteria: characterization using an Fe-specific bioreporter. Aquat Microb Ecol 41: 233-245.

Narr, A., Nawaz, A., Wick, L.Y., Harms, H., and Chatzinotas, A. (2017) Soil viral communities vary temporally and along a land use transect as revealed by virus-like particle counting and a modified community fingerprinting approach (fRAPD). Front Microbiol 8: 1975.

Navrotsky, A., Mazeina, L., and Majzlan, J. (2008) Size-driven structural and thermodynamic complexity in iron oxides. Science 319: 1635-1638.

Nemergut, D.R., Schmidt, S.K., Fukami, T., O'Neill, S.P., Bilinski, T.M., Stanish, L.F., et al. (2013) Patterns and processes of microbial community assembly. Microbiol Mol Biol Rev 77: 342-356.

Ni, Z., van Gaans, P., Rijnaarts, H., and Grotenhuis, T. (2018) Combination of aquifer thermal energy storage and enhanced bioremediation: Biological and chemical clogging. Sci Total Environ 613: 707-713.

Oksanen, F.G.B., Friendly, M., Kindt, R., Legendre, P., McGlinn, D., Minchin, P.R., et al. (2016) vegan: Community Ecology Package.

Pan, D., Nolan, J., Williams, K.H., Robbins, M.J., and Weber, K.A. (2017) Abundance and Distribution of Microbial Cells and Viruses in an Alluvial Aquifer. Front Microbiol 8: 1199.

Parikka, K.J., Le Romancer, M., Wauters, N., and Jacquet, S. (2017) Deciphering the virus-to-prokaryote ratio (VPR): insights into virus–host relationships in a variety of ecosystems. Biol Rev 92: 1081-1100.

Park, J.A., Kang, J.K., and Kim, S.B. (2017) Comparative analysis of bacteriophages and bacteria removal in soils and pyrophyllite-amended soils: column experiments. Water Air Soil Pollut 228: 103.

Poorvin, L., Rinta-Kanto, J.M., Hutchins, D.A., and Wilhelm S.W. (2004) Viral release of iron and its bioavailability to marine plankton. Limnol Oceanogr 49: 1734-1741.

Pratama, A.A., and van Elsas, J.D. (2018) The 'neglected' soil virome – potential role and impact. Trends Microbiol 8: 649-662.

Quast, C., Pruesse, E., Yilmaz, P., Gerken, J., Schweer, T., Yarza, P., et al. (2012) The SILVA ribosomal RNA gene database project: improved data processing and web-based tools. Nucleic Acids Res 41: D590-D596.

R Core Team. (2015) R: A Language and Environment for Statistical Computing. http://www.r-project.org/.

Rawson, J., Prommer, H., Siade, A., Carr, J., Berg, M., Davis, J.A., and Fendorf, S. (2016) Numerical modeling of arsenic mobility during reductive iron-mineral transformations. Environ Sci Technol 50: 2459-2467.

Säwström, C., and Pollard, P. (2012) Environmental influences on virus–host interactions in an Australian subtropical reservoir. Environ Microbiol Rep 4: 72-81.

Scanlan, P.D. (2017) Bacteria–Bacteriophage Coevolution in the Human Gut: Implications for Microbial Diversity and Functionality. Trends Microbiol 25: 614-623.

Shen, C., Xiong, J., Zhang, H., Feng, Y., Lin, X., Li, X., et al. (2013) Soil pH drives the spatial distribution of bacterial communities along elevation on Changbai Mountain. Soil Biol Biochem 57: 204-211.

Shi, L., Dong, H., Reguera, G., Beyenal, H., Lu, A., Liu, J., et al. (2016) Extracellular electron transfer mechanisms between microorganisms and minerals. Nat Rev Microbiol 14: 651-662.

Silpe, J.E. and Bassler, B.L. (2019) A Host-Produced Quorum-Sensing Autoinducer Controls a Phage Lysis-Lysogeny Decision. Cell 176: 268-280.

Srinivasiah, S., Lovett, J., Polson, S., Bhavsar, J., Ghosh, D., Roy, K., et al. (2013) Direct assessment of viral diversity in soils using RAPD-PCR. Appl Environ Microbiol 79: 5450-5457.

Suttle, C.A. (2007) Marine viruses—major players in the global ecosystem. Nat Rev Microbiol 5: 801-812.

Sullivan, M.B., Weitz, J.S., and Wilhelm, S. (2017) Viral ecology comes of age. Environ Microbiol Rep 9: 33-35.

Våge, S., Pree, B., and Thingstad, T.F. (2016) Linking internal and external bacterial community control gives mechanistic framework for pelagic virus-to-bacteria ratios. Environ Microbiol 18: 3932-3948.

Weber, K.A., Achenbach, L.A., and Coates, J.D. (2006) Microorganisms pumping iron: anaerobic microbial iron oxidation and reduction. Nat Rev Microbiol 4: 752-764.

Weitz, J.S., and Wilhelm, S.W. (2012) Ocean viruses and their effects on microbial communities and biogeochemical cycles. F1000 Biol Rep 4: 17.

Weitz, J.S., Stock, C.A., Wilhelm, S.W., Bourouiba, L., Coleman, M.L., Buchan, A., et al. (2015) A multitrophic model to quantify the effects of marine viruses on microbial food webs and ecosystem processes. ISME J 9: 1352-1364.

Wickham, H. (2016) ggplot2: elegant graphics for data analysis. Springer.

Wigington, C.H., Sonderegger, D., Brussaard, C.P., Buchan, A., Finke, J.F., Fuhrman, J.A., et al. (2016) Re-examination of the relationship between marine virus and microbial cell abundances. Nat Microbiol 1: 15024.

Wilhelm, S.W., and Suttle, C.A. (1999) Viruses and nutrient cycles in the sea: viruses play critical roles in the structure and function of aquatic food webs. Bioscience 49: 781-788.

Williams, K.H., Bargar, J.R., Lloyd, J.R., and Lovley, D.R. (2013) Bioremediation of uranium-contaminated groundwater: a systems approach to subsurface biogeochemistry. Curr Opin Biotechnol 24: 489-497.

Williamson, K.E., Radosevich, M., and Wommack, K.E. (2005) Abundance and diversity of viruses in six Delaware soils. Appl Environ Microbiol 71: 3119-3125.

Williamson, K.E., Radosevich, M., Smith, D.W., and Wommack, K.E. (2007) Incidence of lysogeny within temperate and extreme soil environments. Environ Microbiol 9: 2563-2574.

Williamson, K.E., Schnitker, J.B., Radosevich, M., Smith, D.W., and Wommack, K.E. (2008) Cultivation-based assessment of lysogeny among soil bacteria. Microb Ecol 56: 437-447.

Wu, W.M., Carley, J., Green, S.J., Luo, J., Kelly, S.D., Nostrand, J.V, et al. (2010) Effects of nitrate on the stability of uranium in a bioreduced region of the subsurface. Environ Sci Technol. 44: 5104-5111.

Williamson, K.E., Fuhrmann, J.J., Wommack, K.E., and Radosevich, M. (2017) Viruses in soil ecosystems: an unknown quantity within an unexplored territory. Annu Rev Virol 4: 201-219.

Zhang, J., Gao, Q., Zhang, Q., Wang, T., Yue, H., Wu, L., et al., (2017) Bacteriophage–prokaryote dynamics and interaction within anaerobic digestion processes across time and space. Microbiome 5: 57.

Chapter III Appendix

Table 3.1: Physicochemical properties of soil aggregates (250-2,000 μm).

Organic matter (%)	Weak bray phosphorus (ppm)	Strong bray phosphorus (ppm)	Potassium (ppm)	Magnesium (ppm)	Calcium (ppm)	Soil pH
2.5	8	10	90	192	1,419	5.9
Cation exchange capacity (meq/100g)	Sulfur (ppm)	Zinc (ppm)	Manganese (ppm)	Iron (ppm)	Copper (ppm)	Boron (ppm)
10.7	21	1.3	7	34	0.8	0.4

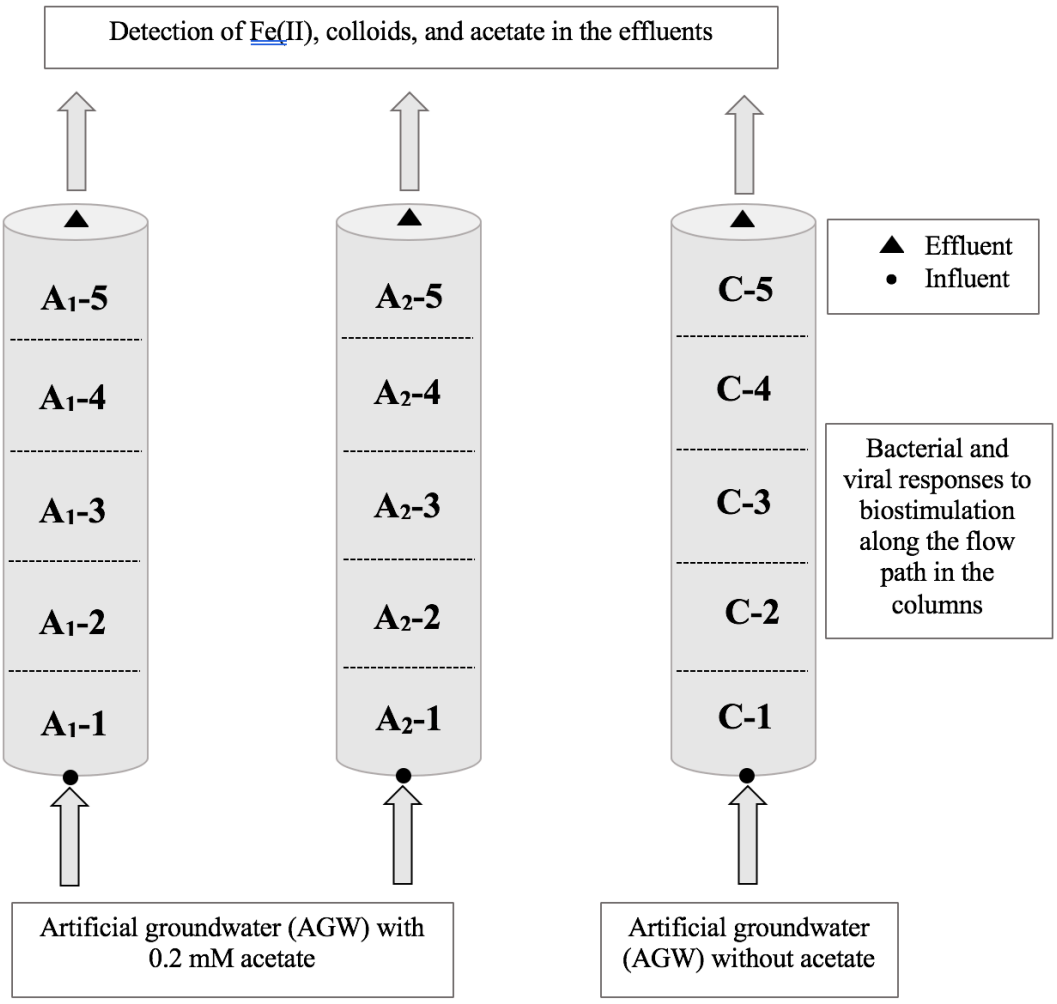

Figure 3.7: Experimental design for water-stable soil aggregate column experiment. Duplicate soil columns (A_1 and A_2) were flushed with artificial ground water (AGW) containing 0.2 mM acetate as an electron donor in columns, while the control column (C) was flushed with AGW without acetate. The solutions were introduced into the columns continuously at a pore velocity of 3.4 cm/h for 60 d within the anoxic chamber. At the conclusion of the acetate biostimulation phase, the columns were sectioned into 5 cm segments from the influent to the effluent ends (sections were labeled 1 to 5).

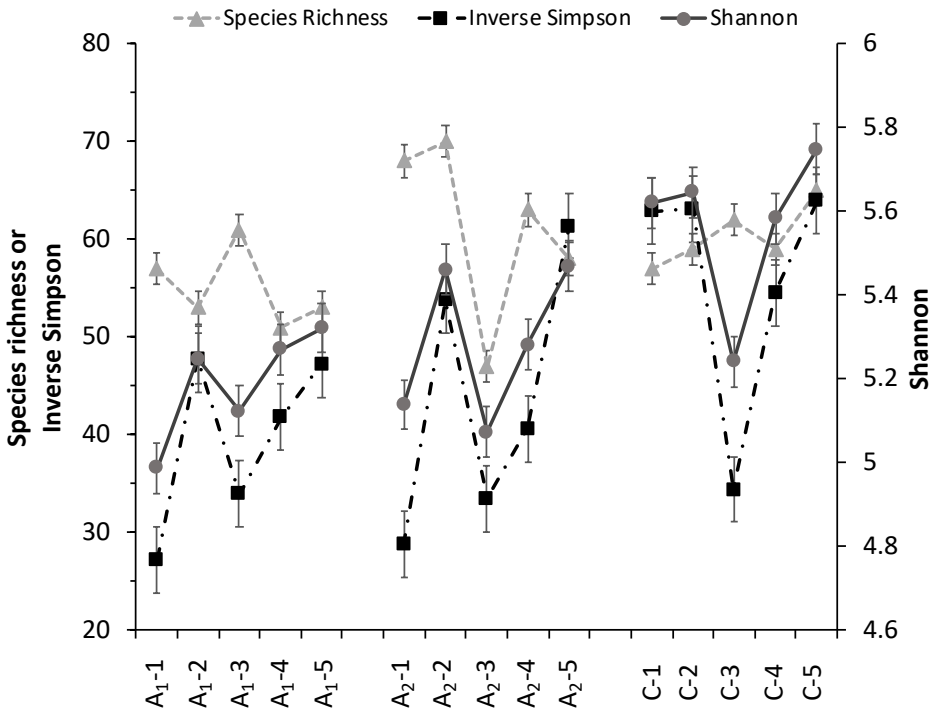

Figure 3.8: Alpha diversity of bacterial communities along the hydrologic flow path of the soil aggregate columns. Operational Taxonomic Units (OTUs) were determined at 97% similarity level. Columns A_1 and A_2 were duplicate columns treated with acetate and column C was the control column without acetate. Numbers 1 to 5 represent sections of collected soil from the columns with section 1 closest to the influent end and section 5 at the effluent end.

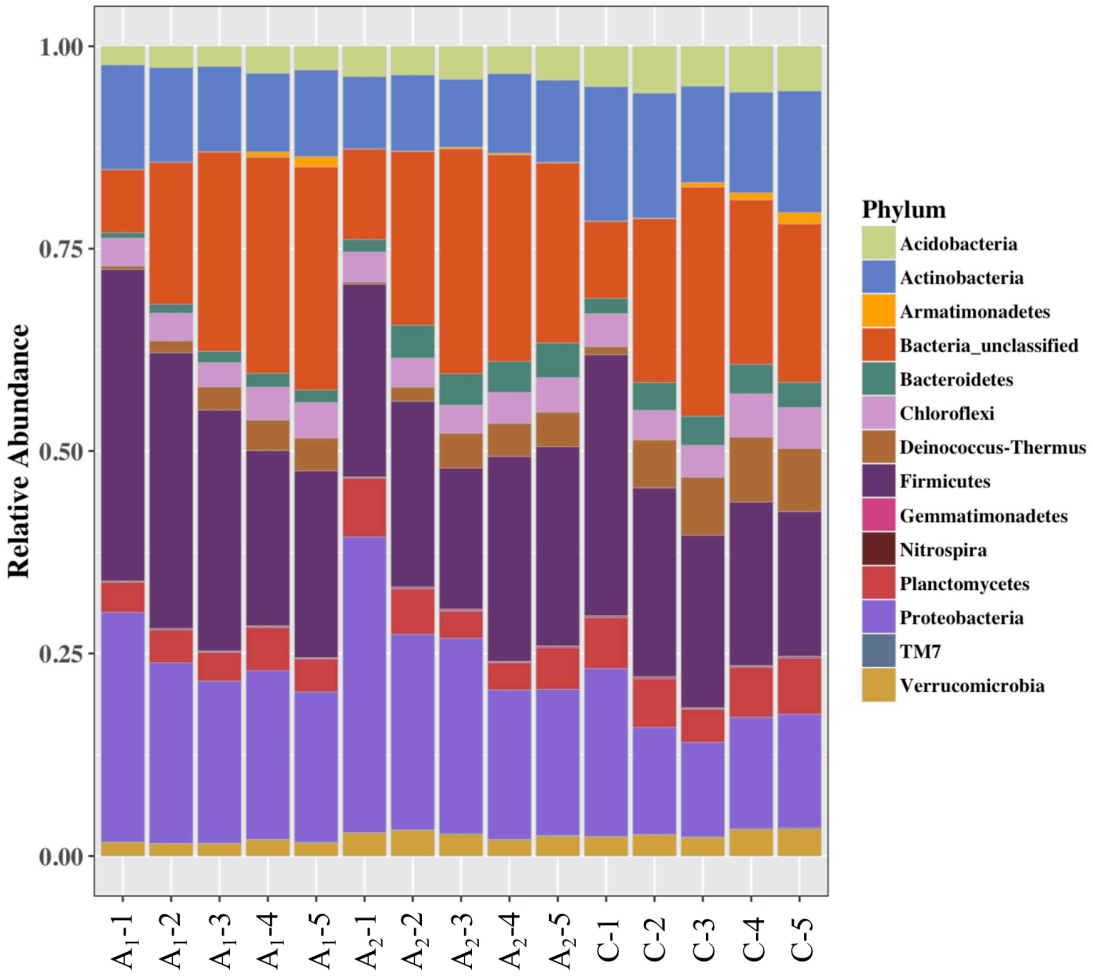

Figure 3.9: Relative abundances of the major bacterial phyla in the soil aggregate columns. Two columns (A_1 and A_2) were treated with acetate and the column C was the control column without acetate. Numbers 1 to 5 following the column labels (A_1, A_2, and C) represent sampled soil sections from influent (section 1) to effluent ends (section 5) in each column.

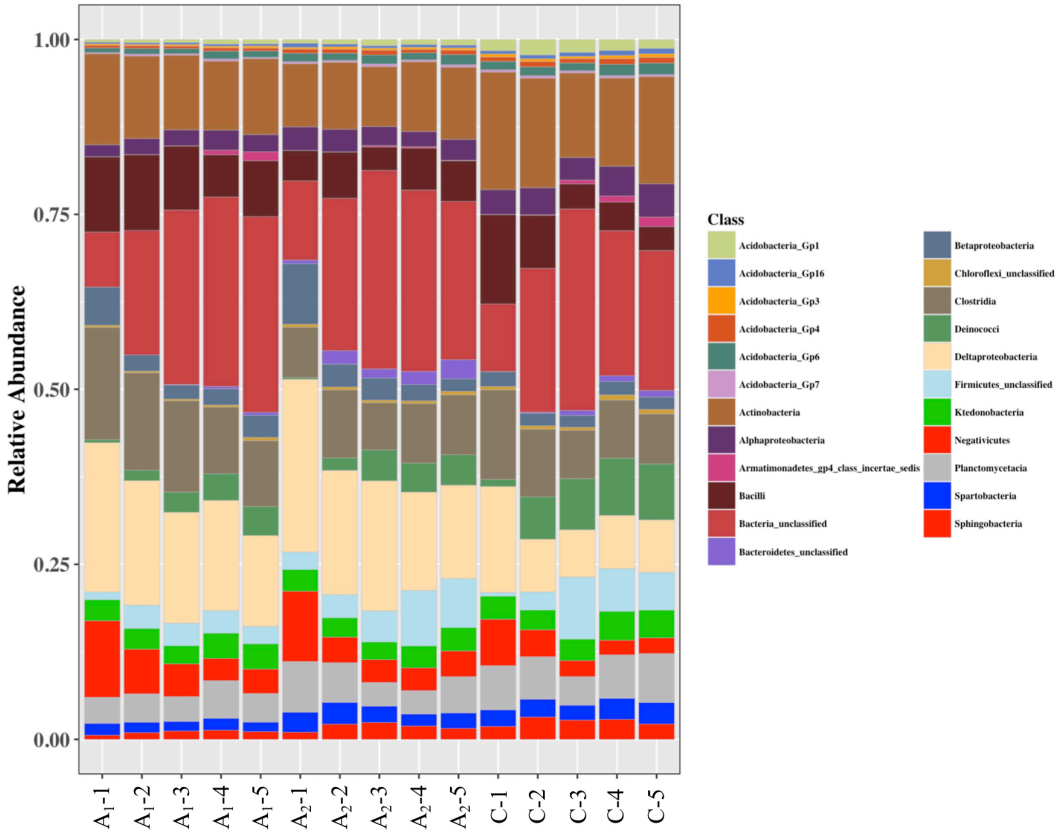

Figure 3.10: Relative abundances of the major bacterial classes in the soils. During 60-d treatment, soils in columns A_1 and A_2 received acetate, while soils in the column C received no acetate. Five sections in each column were numbers 1 to 5 following the column labels (A_1, A_2, and C). Deltaproteobacteria, Actinobacteria, Clostridia, Bacilli, Planctomycetes, Negativicutes, Deinococci, Ktedonobacteria, and Alphaproteobacteria were the nine most abundant classes in the three columns. The relative abundances of Delta-, Beta-Proteobacteria, Clostridia, Bacilli, and Negativicutes in the acetate-treated columns were greater than those in the control column and decreased along the acetate flow path.

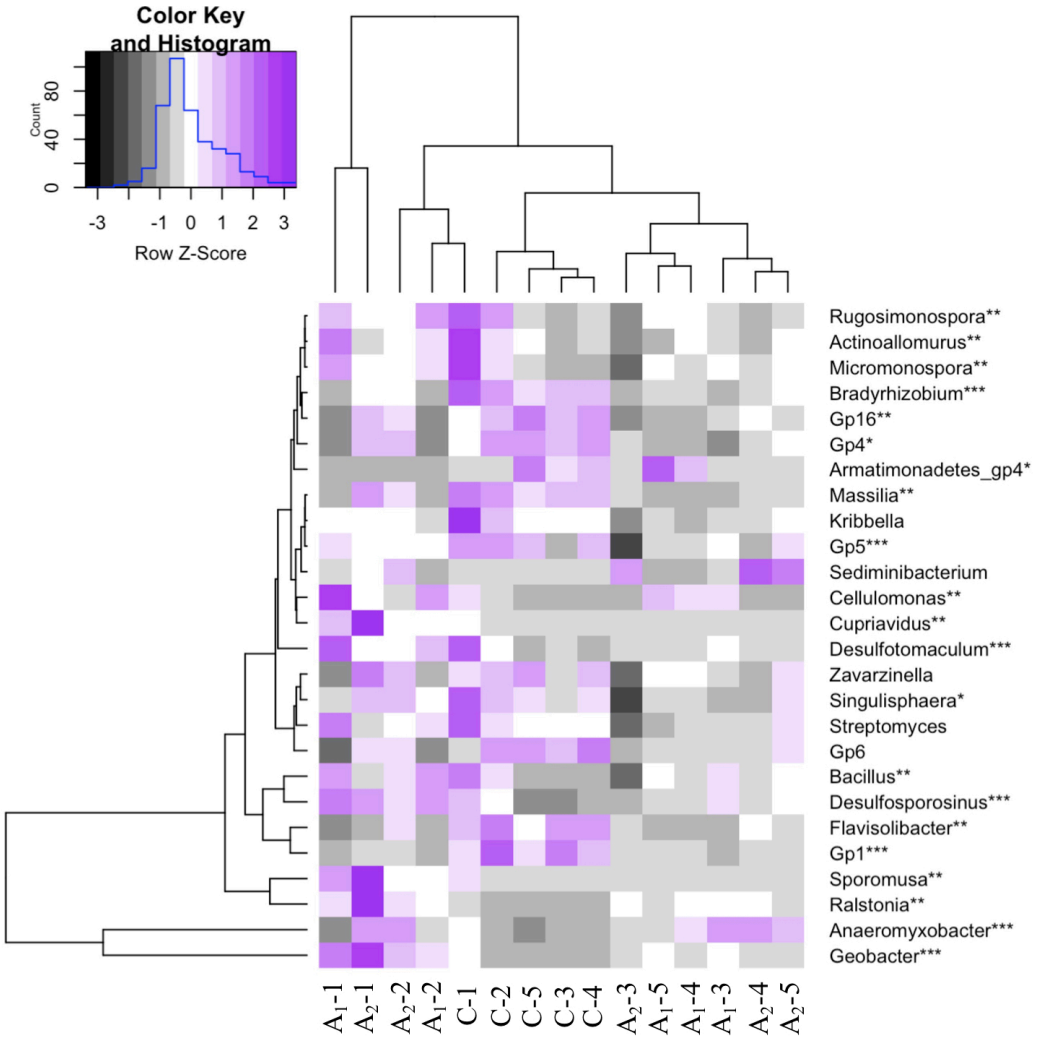

Figure 3.11: Heatmap showing the distribution patterns of 26 most abundant OTU groups at genus level (map rows). The color intensity in each panel indicates the relative abundance per sample (map columns). The samples and OTU groups were clustered based on Non-metric multidimensional scaling and Bray-Curtis distances. The significance of bacterial taxa in structuring the microbial communities was examined using Adonis test. Significance codes are:

'***': $0 < P < 0.001$; '**': $0.001 < P < 0.01$; '*': $0.01 < P < 0.05$; no label for $P > 0.05$.

Figure 3.12: Correlation networks of bacterial groups in section A_1-1, A_1-3, and A_1-5 from acetate-treated column, and C-1, C-3, and C-5 from the control column. Each node represents one OTU group on genus or family (in cases where no genera are recognized) level classification. The color/number of the nodes indicates a phylum as shown in the legend. The linkages in the correlation networks are edges with *P* value smaller than 0.05 (calculated with 200 bootstrapping processes). Negative and positive correlations are shown in red and green, respectively.

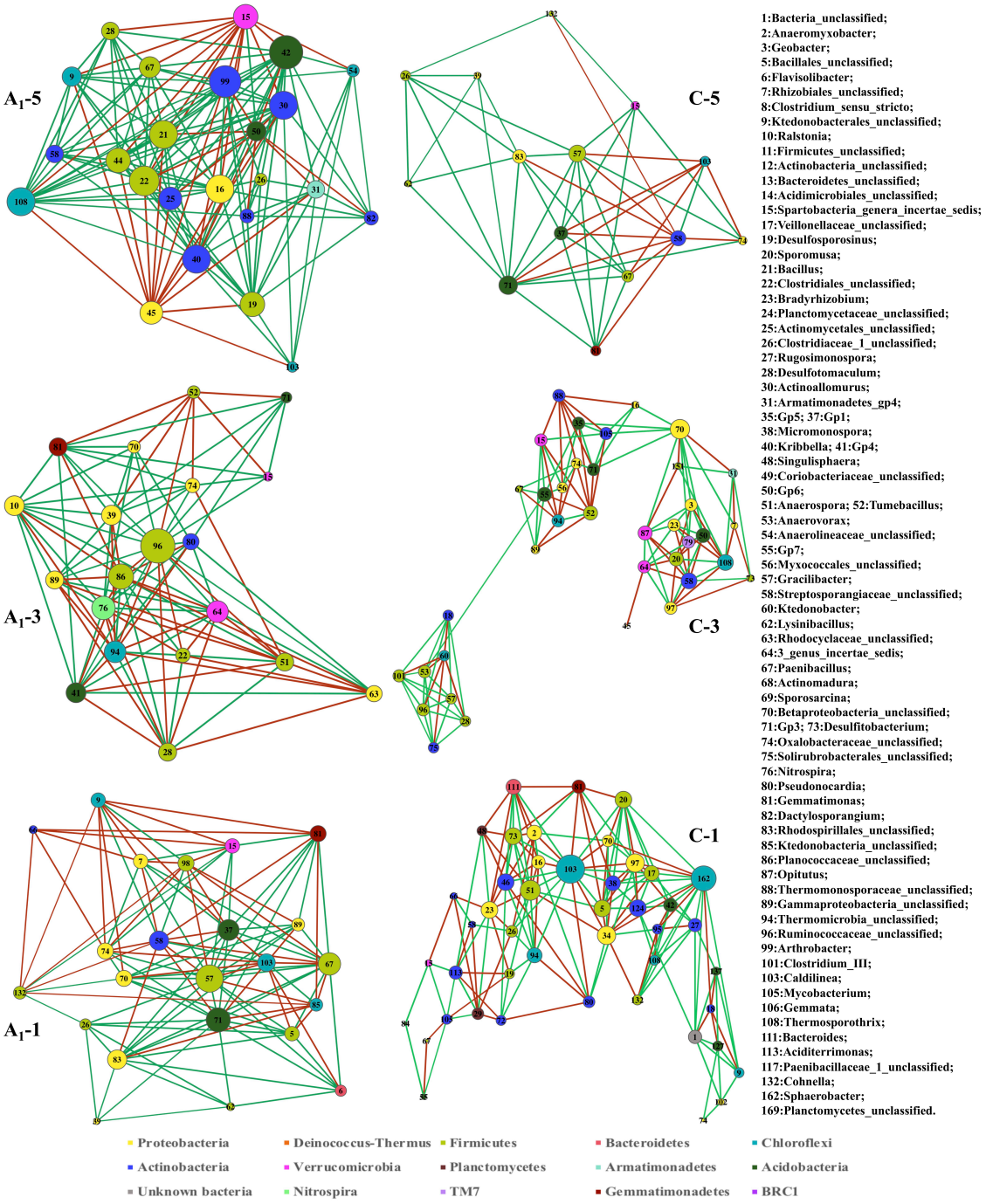

Figure 3.12 continued.

CHAPTER IV

Viral abundance and diversity vary with depth in a southeastern United States agricultural Ultisol

Publication Note

This chapter was originally published as a peer-reviewed article by Xiaolong Liang, Regan E. Wagnera, Jie Zhuang, Jennifer M. DeBruyn, Steven W. Wilhelm, Fang Liu, Lu Yang, Margaret E. Staton, Andrew C. Sherfy, and Mark Radosevich in *Soil Biology and Biochemistry*.

My contribution to this work was conceiving and designing the experiments, processing the samples, extraction and numeration of viruses, bioinformatics and statistical analyses, and drafting the manuscript.

Citation

Liang, X., Wagner, R.E., Zhuang, J., DeBruyn, J.M., Wilhelm, S.W., Liu, F., Yang, L., Staton, M.E., Sherfy, A.C. and Radosevich, M., 2019. Viral abundance and diversity vary with depth in a southeastern United States agricultural ultisol. Soil Biology and Biochemistry, 107546. https://doi.org/10.1016/j.soilbio.2019.107546

Abstract

Viruses shape microbial communities and associated processes across ecosystems. However, soil viral ecology remains poorly understood, and in particular, the vertical distribution and diversity of viruses and virus-host interactions in soils remain underexplored. In this study, 16S rRNA gene amplicon and virome sequencing were applied to investigate bacterial and viral diversity and provide insight on virus-bacterium interactions in different depths of soil profiles. The results show that bacterial community composition varied with soil depth, driven by an increase in the relative abundance of Chloroflexi and a decline in the relative abundance of Planctomycetes, Proteobacteria, Verrucomicrobia, Actinobacteria, and Acidobacteria. Additionally, landscape position, depth, and virus abundance had the strongest correlation with the bacterial community structure. Virus abundance decreased with soil depth, and bacterial community diversity correlated positively with viral abundance ($P < 0.001$). Viruses of prokaryotes were most prevalent in the viromes of both surface and subsurface soils relative to the total viruses detected, however the relative abundance of bacteriophages was greater in the subsurface than in the surface soil. Viral abundances showed significant correlations (negative/positive) with many bacterial taxa in soil, suggesting possible ecological interactions between viruses and specific bacterial taxa. Auxiliary metabolic genes (AMGs, e.g., genes of oxidative phosphorylation, cell signaling, and nucleotide, amino acids, and carbohydrates metabolisms) were detected in viromes (surface: 2,359 AMGs with 35.7% coding percentage; subsurface: 8,150 AMGs with 87.1% coding percentage). The abundances of AMGs were up to 16-fold higher in subsurface than in the surface viromes. The results showed that soil viruses are diverse and have potential to modulate host metabolism and community structure.

Introduction

Soil properties and conditions (*e.g.,* pH, carbon quantity, moisture content, particle size, oxygen level) vary with depth, and heterogeneity in physicochemical and structural properties may shape the distribution of microbial populations in soils (Hansel et al., 2008; Eilers et al., 2012; Jiao et al., 2018). Virus-mediated processes are increasingly recognized as key drivers in controlling microbial diversity and ecosystem function particularly in aquatic ecosystems (Weitz and Wilhelm, 2012; Williamson et al., 2017; Pratama and van Elsas, 2018). Viruses, especially those that infect prokaryotes, are abundant in soils but there is a dearth of information about viruses and virus-host dynamics in soil habitats compared to aquatic ecosystems. The relationship between viral infection and microbial host abundance and diversity has been explored through microscopic direct counting (Williamson et al., 2005; 2017; Liang et al., 2019b) and viromic analyses (Edwards at al., 2016; Paez-Espino et al., 2016). Previous investigations have established that viruses contribute significantly to the structure and evolution of microbial communities (Chow et al., 2014; Koskella and Brockhurst, 2014; Storesund et al., 2015; Williamson et al., 2017) and influence biogeochemical cycles in various ecosystems (Sullivan et al., 2017; Emerson et al., 2018). For example, Zhang et al. (2017) showed that bacteriophages (viruses that infect bacteria) accounted for a much higher rate (40.6%) of total variations of the prokaryotic community composition than abiotic factors (14.5%) and were significantly linked to microbial processes, such as biogas production. While the complexities of microbial ecology have been consistently re-evaluated with innovative methods and theories, the impacts of viruses on bacterial communities remain under studied especially in soil ecosystems.

Compared with the efforts in soil virus research, the functions of environmental conditions in soil microbial community development and activity have been studied extensively (Schütz et al., 2010; van Leeuwen et al., 2017; Taş et al., 2018). As previously reported, a wide range of environmental factors, either naturally occurring or brought about by human imposed management practices, can structure soil microbial communities and processes (Militon et al., 2010; Jiao et al., 2018; Kuzyakov and Mason-Jones., 2018; Liang et al., 2019a). Different horizons or layers throughout a soil profile possess varying

chemical and physical properties, leading to unique microbial community composition within each horizon (Stone et al., 2014; Jiao et al., 2018). The microbial biomass, community composition, diversity, and metabolic functions vary notably with soil depth (Eilers et al., 2012; Marinari et al., 2013). Furthermore, the microbial communities at different soil depths respond differently to oscillating environmental conditions (Schütz et al., 2010; Bai et al., 2017; Durán et al., 2017). Although microbial biomass and metabolic activity decrease with soil depth, considerable numbers of microbial cells, with varying levels of activity, are still present in deep soils (Schutz et al., 2010; Chen et al., 2016; Jiao et al., 2018). Subsurface soil horizons contain over half of the total soil organic carbon (SOC) (Jobbágy and Jackson 2000; Durán et al., 2017), and the organic matter in deep soil layers is more persistent than that in the upper horizons (Fontaine et al., 2007; Stone et al., 2014). Moreover, the subsurface microbes may play a critical role in soil carbon sequestration considering substantial quantities of microbial-derived organic matter are contained in deep soil horizons (Rumpel and Kögel-Knabner 2011).

While we now have knowledge of sub-surface microbial communities and their importance in ecological functions, studies of viruses in soil remain rare, and most have focused exclusively on viruses in near-surface soils (0–15 cm depth) with no comparison of depths. We have very little knowledge of the distribution of viruses or the interplay between bacteria and viruses with soil depth (Kuzyakov and Mason-Jones, 2018; Pratama and van Elsas, 2018; Liang et al., 2019b). Viral metagenomics (viromics) has enabled surveys of viral diversity and their potential impacts on ecosystem function, yet only a very limited number of soil viromes have been reported relative to other environments (Williamson et al., 2017; Segobola et al., 2018; Trubl et al., 2018). This study aimed to determine bacterial and viral distribution, their community structure, and bacteria-virus interactions in soil profiles. Based on the previous research, we expected that virus abundance would follow bacterial abundance and decrease with depth in soil. Additionally, we expected the genetic composition of the viral communities, as revealed by virome sequencing, would differ with depth, with a greater relative abundance of functional genes consistent with temperate phage in the subsurface.

Material and Methods

Site description and sample collection

The soils used for this study were Ultisols (United States Department of Agriculture (USDA) Soil Taxonomy). Samples were collected at four agriculturally plowed sites, two foot-slope landscape positions (FS1, FS2) and two upland soil positions (UP1, UP2) near Auburn, Alabama. A pit at each site was excavated to expose all of the master horizons in the profile. The profiles were field described and classified (Appendix Table 4.2) according the Keys to Soil Taxonomy. Three replicate core samples were randomly taken from each described horizon by inserting the coring device horizontally into the pit face from each depth (Appendix Table 4.2). The coring device was cleaned with ethanol (70%, v/v) after each sample was taken to prevent cross sample contamination. Each of the soil samples was placed into a zip-lock plastic bag and immediately shipped overnight back to the laboratory on ice for further analyses that was initiated upon receipt of the samples (less than 24 h). Before analysis, each soil sample was thoroughly mixed separately with sterile glass rods.

DNA extraction and sequencing

Whole soil DNA was extracted from 250 mg of moist soil samples taken from each independent, well-homogenized soil core sample with the PowerLyser PowerSoil DNA isolation kit (Qiagen, Hilden, Germany), and quantified using PicoGreen Assay Kit (Invitrogen, Carlsbad, CA). These three DNA samples taken from each horizon were considered triplicates of each soil depth sample. The DNA samples were sent to the Genomic Services Lab at Hudson Alpha Institute for Biotechnology (Huntsville, AL, USA) for 16S rRNA gene amplicon library preparation and sequencing. The V3-V4 region of 16S rRNA genes were amplified with adaptor-labeled primers of 341F (5'-CCTACG GGNGGCWGCAG-3') and 785R (5'-GACTACHVGGGTATCTAATCC-3') in PCR (Muyzer et al., 1993). The V3-V4 gene libraries generated from PCR amplifications were pooled and sequenced with 300PE (paired-end) on the Illumina MiSeq™ platform (Illumina, USA).

Bacterial community analysis

The amplicon sequence data, containing in total 8,615,538 sequences, was processed using the MOTHUR pipeline according to the standard operating procedure (Kozich et al., 2013). In total, 87,280 operational taxonomic units (OTUs) were classified at a 0.03 distance with Bayesian classifier. Further statistical analyses on the sequence files was performed using the statistical analysis software R packages (https://www.rstudio.com/products/rpackages/). Microbial taxonomic community composition, and alpha-, and beta-diversity were determined. The raw sequence files were archived at the National Center for Biotechnology Information Databases (Sequence Read Archive) under accession number SRP158131.

The microbial community composition of all soil samples was analyzed and displayed in a circular annotated phylogenic tree which was generated and visualized with GraPhlAn (Python source code, manual, and tutorials at http://segatalab.cibio.unitn.it/tools/graphlan/; Asnicar et al., 2015). Analysis of microbial taxa co-occurrence was performed with the SparCC method (Friedman and Alm, 2012). The OTU dataset from each soil sample was rarefied to the same level of 29,867 OTUs (the minimum among all samples), and OTU groups with a sum of less than 50 were filtered out. For visualization of networks, the average correlation was calculated in 20 inference interactions, and the *P* value matrix for the correlations was calculated with 200 bootstrapping processes. The strength of an associative relationship between the correlated entities was determined based on the frequency of co-occurrence of them. Each node represented one bacterial taxon, and edges connecting the nodes represented significant correlations ($P < 0.05$) between two specific taxa.

Epifluorescence microscopy

Viruses and bacteria were extracted from soil samples and enumerated using epifluorescence microscopy according to the method described by Williamson et al. (2005). Briefly, 30 g of soil samples were suspended with 100 ml cold extraction buffer (in 50 mM phosphate buffer containing 1% potassium citrate, w/v, pH 7) and blended for three minutes. The slurries were centrifuged at 4,000 g for 20 min at 4 °C, and supernatants were

filtered through 0.22-µm Millex syringe filters (Merck Millipore Ltd., Tullagreen, Co. Cork, Ireland). These viral extracts were flash frozen using liquid nitrogen and stored at -80 °C until further processing. Thawed viral extracts were treated with Deoxyribonuclease (DNase) I enzyme to digest extracellular DNA. After DNase treatment, each viral extract was then vacuum filtered through a 0.02-µm-pore-size Whatman Anodisc filter thereby capturing viruses between 20 to 220 nm in diameter. The viruses trapped on the Anodisc filters were stained with SYBR gold (at final concentration of 2 X, 1:5000 dilution of original stock, Molecular probes). The filters were counted immediately using a Nikon Eclipse E600 epifluorescence microscopy with FITC excitation (467–498 nm wavelength) and emission (513–556 nm) filter set. Images of viruses and bacteria on the filters were taken using Retiga Ex-i CCD camera (Qimaging, BC, Canada) and enumerated using IPlab software (Scanalytics Inc., Fairfax, VA).

Virome extraction, sequencing and analysis

The viral extracts (extracted from 30 g soil each sample) from FS2 surface (0–16 cm) and subsurface (55–92 cm) soil samples were concentrated (approx. 250-fold) by centrifugation at 5,000 g for 20 min (F13S-14x50cy rotor, Sorval RC-6 plus, Thermo Scientific) through centrifugal filter units (30 KDa cutoff, Amicon Ultra-15, Millipore). The concentrated virus solution was treated with DNase I enzyme (catalog no. EN0525; Thermo Scientific) to remove extracellular DNA (Adriaenssens et al., 2017), and PCR reactions with primers 27F/1492R were performed to ensure that the extracts were free of bacterial DNA contamination. Nucleic acids from viruses were purified with the Power Viral Environmental RNA/DNA Isolation Kit (catalog no. 28000-50; Qiagen, Hilden, Germany) and sent to Lucigen Corporation for library preparation and Illumina Miseq™ sequencing as briefly described as follows. Viral DNA samples were amplified with Sygnis TruePrime whole genome amplification (WGA) kit (Expedeon Ltd, Cambridge, United Kingdom) in which multiple displacement amplification (MDA) method based on high fidelity Phi29 DNA polymerase was used to amplify total genomic DNA uniformly. Amplified DNA was purified with a Zymo Research genomic DNA purification and concentration kit (catalog number D4010) following the manufacturer's protocol. MiSeq

Reagent Nano Kit v2 (300-cycles) was used to verify library integrity and optimize clustering. Libraries proceeded to full 300C Miseq™ sequencing.

Raw virome reads were demultiplexed, and paired sequences were quality filtered using Trimmomatic v0.36 to remove adapter sequences and low-quality reads (Bolger et al., 2014). The virome reads were de novo assembled into contigs using Megahit (Li et al., 2015). Viral taxonomic affiliation was performed using protein-level sequence classification based on the Burrows-Wheeler transform algorithm in the Kaiju taxonomy classifier (version 1.6.2) with RefSeq viral genomes from NCBI as references (Menzel et al., 2016). The threshold of viral taxonomic assignment was 10^{-10} on *E*-value. Classification of predicted open reading frames (ORFs) were performed through the VIROME pipeline (Wommack et al., 2012). The predicted ORFs were compared to RefSeq complete viral database (using the following databases: ACLAME (Leplae et al., 2010), Clusters of Orthologous Groups of proteins (Tatusov et al., 2000), Gene Ontology Consortium (Ashburner et al., 2000), Kyoto Encyclopedia of Genes and Genomes (Ogata et al., 1999), and SEED for functional annotations.

Results

Bacterial diversity

In total 15,767,219 paired-end 16S rRNA gene amplicon sequences from nineteen samples revealed 87,280 OTUs at a 0.03 distance threshold. The rarefaction curves indicated sufficient sequencing depth for representative coverage of the community diversity in each sample (Appendix Fig. 4.7). Specifically, the deep subsurface soil samples had lower slopes for the rarefaction curves than the surface soil samples. The diversity and richness of bacterial communities generally decreased with depth in the soil profiles and varied across soil sites (Fig. 4.1). While all soil samples included a similar number of sequences, significantly more OTUs were detected in the surface soils across all soil profiles. Estimates of species richness based on the bias-corrected Chao1 estimator and the abundance-based coverage estimate (ACE) showed that the bacterial species richness was highest in surface soils and declined with depth in the soil profiles. Shannon and Fisher

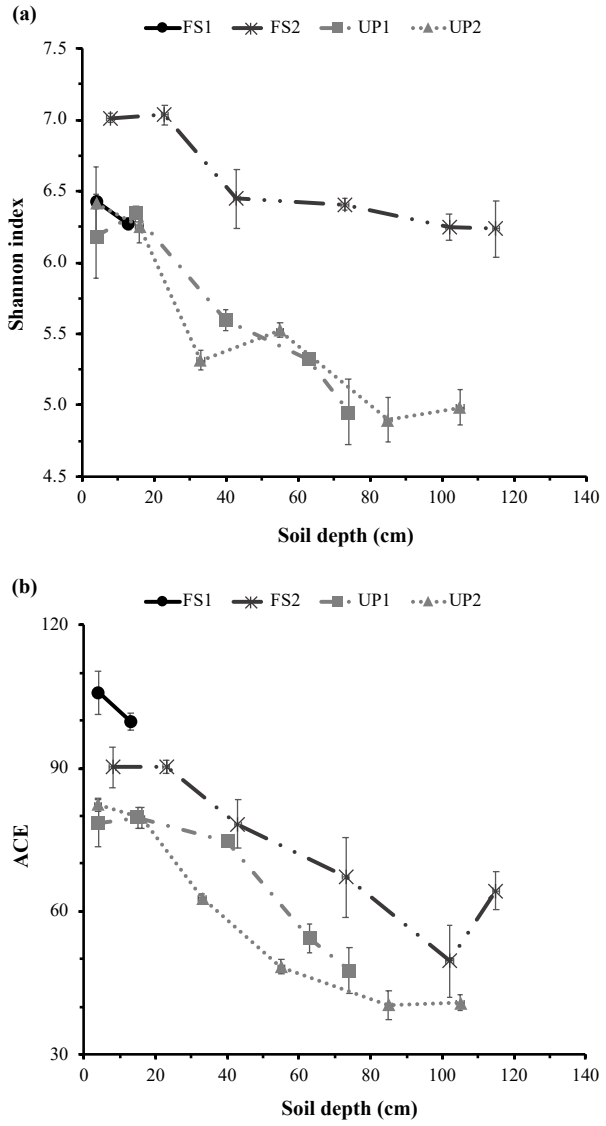

Figure 4.1: Alpha-diversity of bacterial communities versus soil depth. OTUs were determined at 3% dissimilarity level. Estimates of species richness were based on the abundance-based coverage estimate (ACE), and community diversity was estimated based on Shannon index. Each data point represents the mean value (n=3), and the error bars show standard deviation.

indices based on species richness and evenness were significantly negatively correlated with soil depth (Shannon index: r = -0.51, $P < 0.05$; Fisher index: r = -0.68, $P < 0.01$; Appendix Fig. 4.8).

Bacterial community structure

The constrained analysis of the principal coordinates (CAP) based on Bray–Curtis dissimilarity was used to visualize the similarities of bacterial communities from different soil horizons at the four sampling sites. The bacterial community composition separated according to soil depths (Adonis, $P < 0.01$); in particular, the bacterial communities in A horizon samples clustered away from the others. Samples from the foot-slope sites (FS1 and FS2) were clustered together, while samples from the upland sites (UP1 and UP2) were clustered based on their similar bacterial community composition (Fig. 4.2). The constrained CAP showed that landscape position, and depth (horizon) were the most significant factors accounting for the difference in community composition with viral abundance also contributing to differences in bacterial communities in the soil profiles (Fig. 4.2). Four major groupings were revealed based on Bray-Curtis distances: (1) subsurface soil samples (23–110 cm) from two upland sites, (2) subsurface soil samples (30–120 cm) from site FS2, (3) surface soil samples (0–30 cm) from the foot-slope landscape positions, and (4) surface soil samples (0–25 cm) from the upland sites UP1 and UP2 (Fig. 4.3).

In all soil samples, the bacterial community was composed of 14 different bacterial phyla, as well as unclassified bacterial members (Appendix Fig. 4.9). Deep soil samples contained relatively more sequences (ranging from 8.3% to 41.7%) that could not be identified than surface soil samples, indicating a higher proportion of the bacterial communities were unclassified in deeper soils. The dominant phyla included Chloroflexi, Planctomycetes, Proteobacteria, Verrucomicrobia, Actinobacteria, Acidobacteria, and Firmicutes, representing more than 80% of sequences in all soil profiles collectively (Appendix Fig. 4.9). Some of these bacterial taxa showed distinct distribution patterns in response to sampling site and depth. The relative abundance of Chloroflexi, the most dominant phylum in the upland (UP1 and UP2) subsurface soils, generally increased with

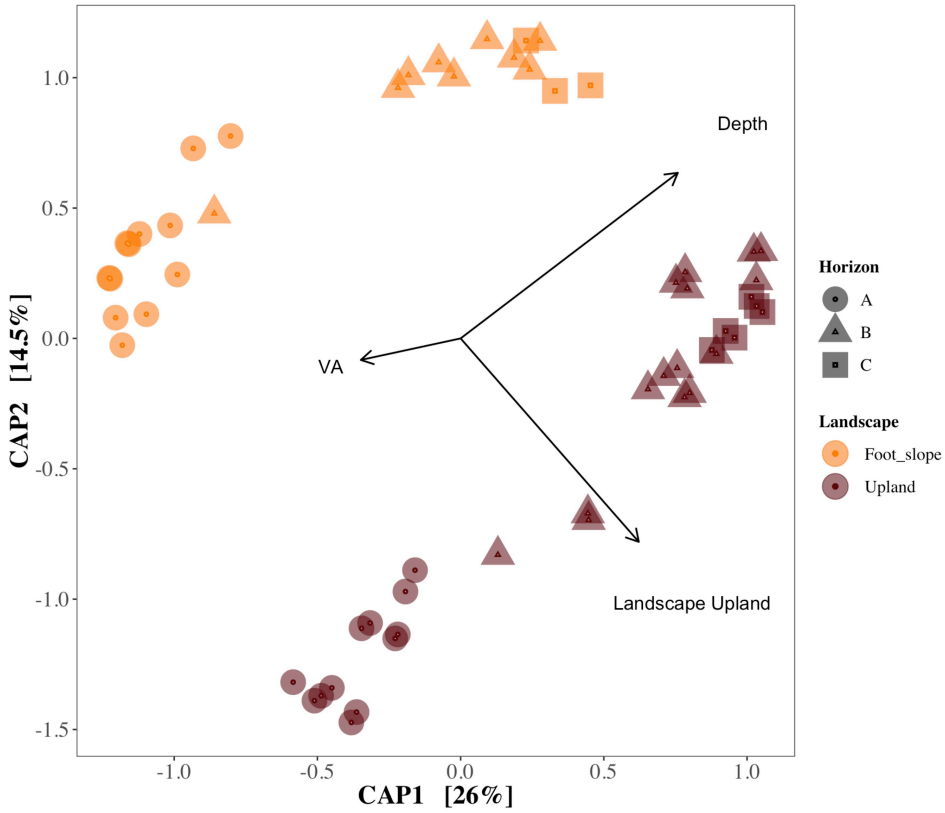

Figure 4.2: Constrained analysis of the principal coordinates (CAP) of bacterial community composition. Samples are color-coded base on sampling site and shape-coded by horizon. Foot-slope landscape sites include FS1 and FS2, and upland sites are UP1 and UP2. Different shapes represent the soil horizon that each sample was collected in each soil pit. Arrows represent notably correlated factors influencing the composition of microbial communities, and the length of the arrow indicates the effect size of the factor on the community composition. VA is viral abundance.

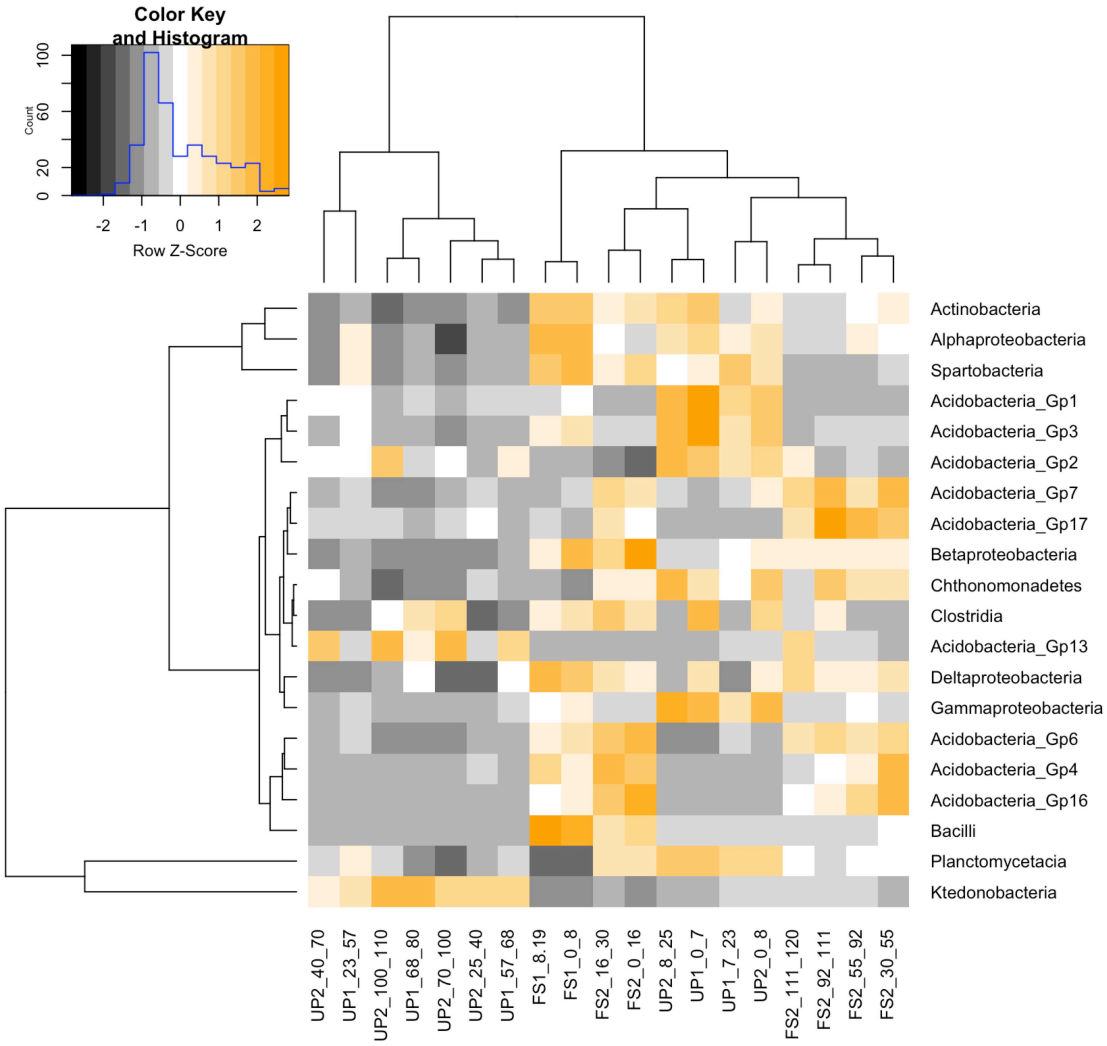

Figure 4.3: Heatmap showing the distribution patterns of 20 most abundant OTU groups at class level. The color intensity in each panel indicates the relative abundance per sample. The samples and OTU groups were clustered based on Bray-Curtis dissimilarity. FS1 and FS2 represent two foot-slope sites, and UP1 and UP2 are two upland sites. The depths that samples were collected from the soil profiles are 0–8 and 8–19 cm in FS1; 0–16, 16–30, 30–55, 55–92, 92–111, and 111–120 cm in FS2; 0–7, 7–23, 23–57, 57–68, and 68–80 cm in UP1; 0–8, 8–25, 25–40, 40–70, 70–100, and 100–110 cm in UP2.

depth in the profile (with relative abundances of 2.1–44.8%). Planctomycetes was the most dominant phylum in the surface soil of FS2, UP1, and UP2, and Proteobacteria was the most dominant phylum in the surface soil of FS1. The relative abundance of Proteobacteria (2.9–19.5%), Planctomycetes (11.3–25.6%), Verrucomicrobia (0.6–18.4%), Actinobacteria (2.2–16.6%), and Acidobacteria (4.4–18.2%) decreased with depth.

Notable differences in community composition were observed within soil profiles and across sites. Ktedonobacteria (with relative abundances of 3.1–44.0% in different samples) and Planctomycetacia (11.4–25.9%) were widely distributed; and Ktedonobacteria showed higher relative abundance in subsurface soil horizons, whereas Planctomycetacia showed higher abundance in surface horizons (Fig. 3). Actinobacteria (2.2–17.1%), Alphaproteobacteria (2.1–15.1%), and Spartobacteria (0.6–17.9%) had similar distribution patterns across samples. Acidobacteria Gp1 (0.7–6.0%), Gp2 (0.3–3.8%), and Gp3 (0.1–3.8%) all had higher relative abundance in upland soils than in foot-slope landscape positions. The relative abundances of Acidobacteria Gp4 (0.004–1.0%), Gp6 (0.4–4.5%), Gp16 (0.0004–3.8%), and Bacilli (0.07–7.8%) were higher in foot-slope soils than in upland soils.

Planctomycetacia were the most abundant class accounting for 6.1% of sequences followed by Ktedonobacteria (4.6%), Actinobacteria (3.6%), Alphaproteobacteria (3.3%), and Spartobacteria (2.6%). The relative abundance of Alphaproteobacteria was highest in surface soils of the upland soil profiles but showed a mid-profile peak in foot-slope soils (Appendix Fig. 4.10). Twelve Acidobacteria classes were detected in the four soil profiles. The relative abundances of Acidobacteria Gp1, Gp2, and Gp3 generally decreased with depth in upland soils (Appendix Fig. 4.10). Specifically, the relative abundance of Acidobacteria Gp13 (0.003–0.7%) increased with depth in all profiles despite its relatively low total abundance.

Overall, genus could be assigned to 26.1% of the total sequences, and the percentage of sequences that could be assigned to genus level decreased with depth ranging from 42.1% in surface soils to 8.8% in subsurface soils. There were 175 (out of 436) identified genera having relative abundances of more than 0.001%. *Singulisphaera* was the most abundant genus, constituting 2.7% of total sequences, followed by Acidobacteria *Gp1*

(2.6%), *Gp2* (2.1%), *Gp3* (1.9%), *Gp6* (1.8%), *Gp4* (1.6%), and *Ktedonobacter* (1.1%). The relative abundances of *Singulisphaera*, *Gemmata*, *Bradyrhizobium*, *Bacillus*, and *Ktedonobacter* were negatively correlated with soil depth (Pearson correlation, r = -0.62, r = -0.57, r = -0.79, r = -0.48, r = -0.59, $P < 0.05$). In contrast, the relative abundance of *Thermosporothrix* increased with soil depth (Pearson correlation, r = 0.52, $P < 0.05$). Meanwhile, upland soils contained relatively more *Rhizobiales*, *Gemmata*, *Bradyrhizobium*, and *Bacillus* compared with foot-slope soils ($P < 0.05$; Appendix Fig. 4.11).

Interactions among bacterial OTUs in the various horizons were investigated using co-occurrence network analysis. The complexity of the networks decreased with depth, exhibited by more nodes and edges in networks in upper soil horizon (Appendix Fig. 4.12). The ratio of negative to positive correlations increased with depth in FS2 and UP2 profiles (ranging from 1.09 to 1.33 at FS2 and from 1.21 to 1.62 at UP2). Four bacterial phyla, including Proteobacteria, Acidobacteria, Actinobacteria, and Firmicutes, were the most well represented in all soil samples.

Viral abundance decreased with soil depth

Viruses were extracted from soil samples, and epifluorescence microscopy was used to count the virus-like particles (VLPs) in all samples. The abundance of VLPs was greatest in the surface soils (0-16 cm) and decreased remarkably with soil depth in all profiles (Pearson correlation, r = -0.54, $P < 0.01$, Fig. 4.4a). The abundance of VLPs decreased by three-orders of magnitude from 1.14×10^{10} at the surface to 1.31×10^{7} g^{-1} soil (dry weight) with soil depth. Both the bacterial community diversity (based on Fisher index) and species richness (based on ACE) were positively correlated with the abundance of VLPs (r = 0.54 and r = 0.53, separately, $P < 0.05$; Fig. 4.4b, c).

Viral diversity and functional composition

A total of 8,382,050 sequences (length ranging from 142 to 154 bp, GC content of 32–41%) of viral metagenomic DNA (libraries derived from MDA method) from surface (0–16 cm) and subsurface (55–92 cm) soil samples of FS2 were analyzed (Table 4.1).

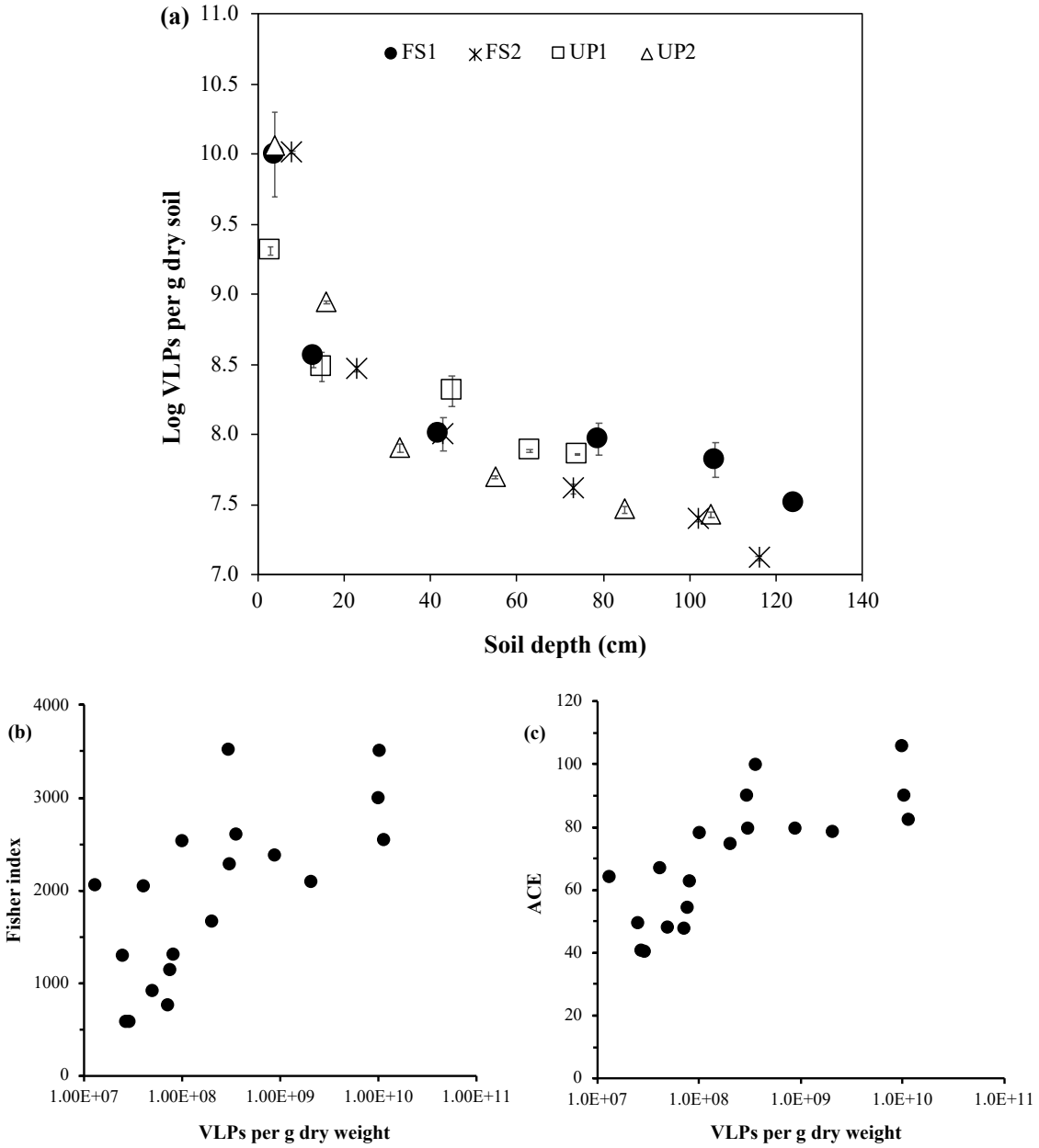

Figure 4.4: Virus-like particle abundance (VLPs) and its relationship with bacterial community diversity and species richness in soil. (a) The VLPs variation with depth in the soil profiles. Each data point is based on the mean of triplicate samples, (n=3), and the error bars show standard deviation. Fisher index (b) represents bacterial community diversity. Species richness (c) is based on abundance-based coverage estimate (ACE).

Table 4.1: Metavirome sequence analysis in surface (0-16 cm) and subsurface (55-92 cm) soil samples in Ala8 soil profile. % total abundance = $\frac{A}{T} \times 100$. A represents the number of sequences assigned into the category (annotated as virus or unclassified); T means the total number of raw sequences reads.

Sample	Number of reads	Total Number of Bases	GC content (%)	Number of contigs generated	Longest contig (bp)	Shortest contig (bp)	% total abundance	
							Annotated as viral	Unclassified
Ala8-surface	4,056,970	602,055,858	32.17	1,382	13,335	306	6.8	93.2
Ala8-subsurface	4,325,080	642,468,744	40.97	3,171	23,973	302	32.67	67.33

Assembly with Megahit generated 1,382 and 3,171contigs in surface and subsurface viromes respectively, which were used for further taxonomic analysis on the Kaiju taxonomic classifier. BLASTn searches of the Kaiju taxonomic classifier suggested 6.8% of the total contigs were viral in surface soil and 32.7% in subsurface. Among the total number of sequences that could be identified as viral, viruses of prokaryotes (bacteriophage) were most dominant, and the relative abundance of prokaryote viruses was notably higher in the subsurface sample (representing 86.8% of taxonomically assignable viral contigs in the virome) than in surface sample (31.1%; Fig. 4.5). Bacteriophage sequences were consistent with tailed double-stranded DNA (dsDNA) viruses (*Myoviridae*, *Siphoviridae*, and *Podoviridae*) in the order *Caudovirales* and small single-stranded DNA (ssDNA) *Microviridae*. Amoeba-and eukaryotic-infecting *Mimiviridae* (relative abundance of 11%) and *Phycodnaviridae* (7.2%) were also highly represented virus families in surface soil. Eukarya dsDNA viruses belonging to *Herpesviridae*, *Baculoviridae*, and *Polydnaviridae* were also detected in the surface soil sample.

The annotated ORFs on the assembled contigs were analyzed using VIROME for putative structural/functional genes in the surface and subsurface viromes. Many of the virome sequences were annotated as “unknown”, with 50.3% of predicted proteins having no significant homologs in the examined databases. Twenty-nine functional categories were annotated by VIROME (Fig. 4.6). The “Phage” category was the most abundant assigned functions, and the highest functional categories included oxidative phosphorylation, genetic information processing, cell signaling, and metabolic pathways of nucleotide, amino acids, and carbohydrates. The functional categories of membrane transport, phosphorous metabolism, lipid metabolism, protein metabolism and metal acquisition and metabolism were also abundant. Higher (up to 16-fold) abundances of the annotated functional protein-coding genes (except proteins involved in oxidative phosphorylation) were detected in the virome of subsurface soil compared with the virome of surface soil. The normalized abundances of proteins associated with phage infectious cycles (i.e., phage lysogeny, lytic cycle, and prophage induction) and phage structural components (e.g., phage capsid, tail, and neck fiber) were also more prevalent in the subsurface soil virome consistent with the apparent prevalence of tailed dsDNA phages in

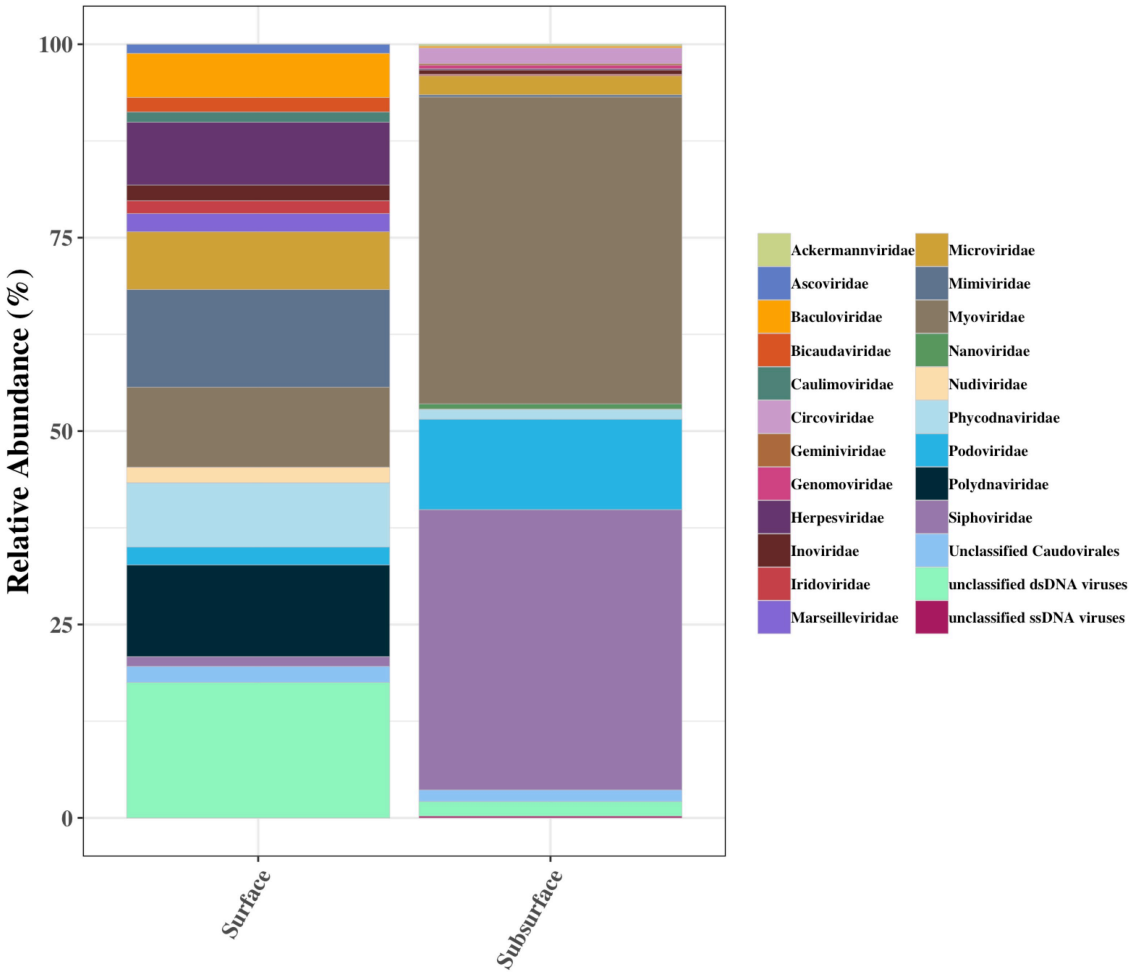

Figure 4.5: Taxonomic composition of virome in surface (0–16 cm) and subsurface (55–92 cm) soil samples in FS2 soil profile. The libraries for virome sequencing were constructed using multiple-displacement amplification (MDA) method. Megahit-assembled contigs were used for protein-level sequence classification based on the Burrows-Wheeler transform algorithm in Kaiju server (E-value=1e-10).

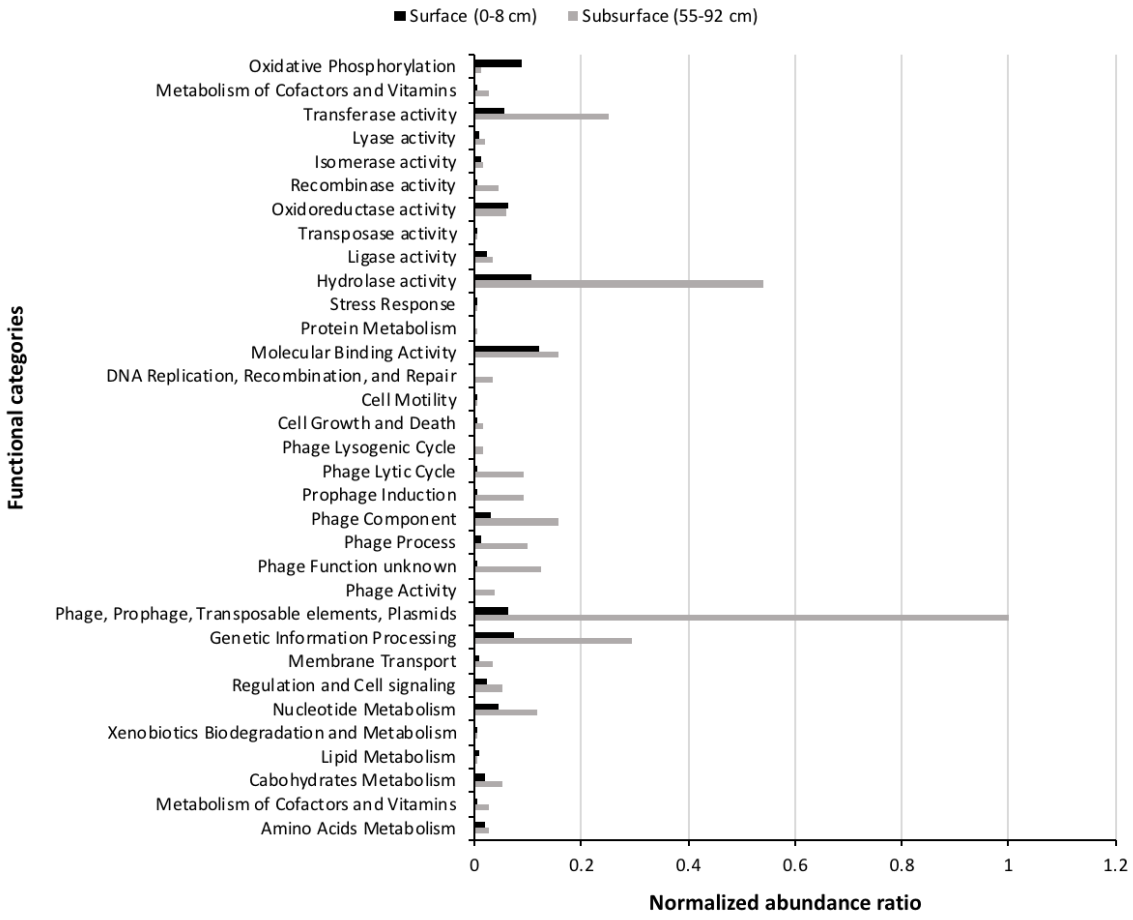

Figure 4.6: Relative abundance of functional genes in viromic sequences. The predicted ORFs were identified and functionally annotated by VIROME server (compared to the following databases: ACLAME, Clusters of Orthologous Groups of proteins, Gene Ontology Consortium, Kyoto Encyclopedia of Genes and Genomes, SEED) using an E value cutoff of 10^{-5}. Normalized abundance ratio is the abundance of a definite function category divided by the abundance of Phage, Prophage, Transposable elements, Plasmids category (having the most amounts of prediction ORFs).

the oligotrophic sub-surface soil environment. In contrast, the proteins involved in metabolic pathway of oxidative phosphorylation, with which cells oxidize nutrients for energy, were more abundant in the surface soil virome.

Discussion

Our understanding of how viruses shape microbial processes in soil ecosystems lags well behind that of aquatic ecosystems. Soil profiles exhibit heterogeneous environmental factors that change with depth (Eilers et al., 2012; Williamson et al., 2017). One very clear finding in the present study was the significant decrease in viral abundance and decreased bacterial diversity with depth. Previous studies reported viral abundance ranging from 2.2×10^3 in desert sands (Gonzalez-Martin et al., 2013) to 1.5×10^{10} gdw^{-1} in upland soil (Han et al., 2017). Published studies have indicated that viral abundance was significantly correlated with soil type, and tended to be higher in forest and wetlands compared with agricultural fields (Williamson et al., 2017). Narr et al. (2017) suggested that soil pH, total nitrogen content, and sampling site were key factors influencing the abundance of soil viruses. That study revealed a significant positive correlation of viral abundance with soil pH, total nitrogen, and total organic carbon, yet a significant negative correlation between viral abundance and carbon-to-nitrogen ratio.

Assignable taxonomic distribution of viral contigs from soil viromes revealed that viruses of prokaryotes were most dominant. Among these, tailed bacteriophages, including *Myoviridae*, *Siphoviridae*, and *Podoviridae*, were abundant in soil, consistent with previous studies (Adriaenssens et al., 2017). *Microvirodae* and *Inoviridae*, spherical viruses with ssDNA genomes, have been shown to be sometimes more abundant than dsDNA viruses in many habitats (Reavy et al., 2015). In the present study, dsDNA tailed phages were relatively more abundant than ssDNA spherical phages despite the use of multiple displacement amplification (MDA) using the phi29 DNA polymerase system for library preparation prior to sequencing (Binga et al., 2008). Previous comparison studies have suggested that this amplification method exhibits bias towards ssDNA viruses thus favoring their amplification and skewing their relative abundance (Kim and Bae, 2011; Marine et al., 2014; Reavy et al., 2015; Roux et al., 2016). It should also be noted however

that less is known about ssDNA viruses, especially from soils, and consequently they are under-represented in public sequence databases. Therefore, our observation that the relative abundance of dsDNA exceeded that of ssDNA may have also resulted from an inability to detect ssDNA viruses in the samples. Amoeba- and Eukarya-infecting viruses (*e.g., Mimiviridae*, *Baculoviridae*, *Polydnavirida*, and *Herpesviridae*) were also present in the surface soil virome. Giant viruses were rarely detected in soil habitats, however a most recent study by Schulz et al. (2018) revealed the diversity and coding potential of giant viruses in a forest soil ecosystem. These families were members of nucleocytoplasmic large DNA viruses (NCLDVs) and also reported to be common in other environments (Adriaenssens et al., 2017; Wilhelm et al., 2017).

The soil microbiome is a critical component of soil ecosystem health and agricultural production, and bacterial diversity has exhibited strong correlations with sustainable ecosystem functions and susceptibility to disturbance (Hartmann et al., 2015; van Leeuwen et al., 2017). Our results showed that bacterial diversity and richness decreased with soil depth. Two-dimensional constrained CAP analysis revealed that the structural dissimilarities between bacterial communities were related with soil depth, and landscape position, horizon, and viral abundance were major factors separating the bacterial communities. Hansel et al. (2008) investigated the variations of bacterial communities in soil profiles and found that the bacterial community varied with soil depth which was potentially induced by water content, pH, soil texture, and nutrient and water availability. Eilers et al. (2012) also reported that soil depth significantly affected bacterial community composition and diversity. Taş et al. (2018) showed that microbial diversity and composition with functional potential changed horizontally across landscape topography and vertically with depth.

The surface soil had the greatest bacterial diversity in the soil profile, likely driven by a combination of factors such as nutrients, moisture, pH, viral predation, and others (Sandaa et al., 2017). Trophic conditions impose bottom-up regulation of bacterial diversity (competition for limiting nutrients), while viruses exert negative frequency-dependent control over bacterial population and community evenness (Storesund et al., 2015; Maslov and Sneppen, 2017; Liang and Radosevich, 2019). Viruses might contribute

to host community diversity as viruses can mediate horizontal gene transfer among host cells and moderate the host population via 'killing the winner' population dynamics (Thingstad and Lignell, 1997; Weinbauer and Rassoulzadegan, 2004). Maslov and Sneppen (2017) proposed interpretations of population cycles and species diversity in the Kill-the-Winner (KtW) model and described the dynamics of bacterial diversity with respect to viral infections. They suggested that viral infections arouse cyclic dynamics of abrupt and acute declines following exponential growth in each bacterial population. The population cycles predict that the more severe perturbations will generate higher diversity in bacterial community. The high viral abundance indicated high levels of virus-mediated mortality of host bacteria (Storesund et al., 2015), therefore higher viral abundance in near-surface soil might have provoked more violent disruption to bacterial communities leading to higher diversity in accordance with the KtW model. Sandaa et al. (2017) reported that viruses as a central component in food chains were also strongly associated with predation and nutrient availability. All these results suggest that viral predation is a key factor in shaping and maintaining bacterial diversity. However, it should be noted that the presented studies are insufficient to conclude that viral-mediated cell lysis is a primary driver of microbial diversity in soil ecosystems. Further investigation with more extensive examination of viromes is needed.

The bacterial communities in the soil profiles were dominated by Chloroflexi, Planctomycetes, Acidobacteria, Proteobacteria, Actinobacteria, Verrucomicrobia, and Firmicutes. The microbial community composition was common and similar to other reports, but the deeper soil horizons harbored more unidentified/uncharacterized microbes than previous studies (Eilers et al., 2012; Bai et al., 2017). The distribution of Choloflexi in soil profiles was striking, as members of this phylum were more abundant in deeper soil horizons than in upper horizons, which was opposite to the distribution patterns of all other phyla. Increasing relative abundance of Chloroflexi with depth was also observed in previous studies (Hansel et al., 2008; Bai et al., 2016). Costello and Schmidt (2006) also reported Chloroflexi as the most abundant taxa and might play active biogeochemical role in cold, anoxic soils.

Proteobacteria possess exceedingly diverse members with distinct morphology, physiology and metabolism, and are of vital importance to biogeochemical cycles and in bioremediation processes (Militon et al., 2010; Liang et al., 2019b). The most abundant class within Proteobacteria was Alphaproteobacteria (representing 63–86% of Proteobacterial sequences across all soil samples), followed by the Delta- (6–18%), Gama- (2–14%) and Beta-Proteobacteria (2–16%). These findings are in agreement with the results of the survey in abundance, composition, and novelty of soil Proteobacteria (Spain et al., 2009). The bacterial groups such as Alpha-, Delta-, Gamma-proteobacteria, Acidobacteria_Gp1 and Gp3 were relatively evenly distributed in each horizon in foot-slope soil profiles but showed a preference for upper soil layers in upland soils. Betaproteobacteria, Bacilli, Spartobacteria, and Planctomycetia tended to have higher relative abundance in upper soil horizons, suggesting preference for an aerobic habitat. Many soil Verrucomicrobia have been described as oligotrophs that can grow with low carbon availability. Eilers et al. (2012) reported a mid-profile peak (10–50 cm) in the relative abundance of Verrucomicrobia, which is similar to the results in this study. Members of Acidobacteria have been reported to have capacity of growing under fluctuating oxygen concentrations and using diverse carbohydrates and organic/inorganic nitrogen sources, thus can be abundant and ubiquitous in soils (Eichorst et al., 2018). Actinobacteria are suggested to be copiotrophs which are inclined to thrive in environments with abundant carbon and nutrient availability (Ramirez et al., 2012), which can partly explain why the highest relative abundance of Actinobacteria is in the top soil horizons across all soil profile samples in this study. In contrast to this pattern, Taş et al. (2018) showed an increasing relative abundance of Actinobacteria with soil depth in permafrost soil profiles, correlated with a decrease in organic carbon and nutrients. These inconsistent results suggest that the functions of depth in structuring soil microbiome are, to some extent, subject to specific environmental conditions and soil characteristics. Co-occurrence network analysis may imply novel relationships between ecological components due to interactive responses (Edwards et al., 2016; Trubl et al., 2018). More complex association network in the upper soil horizons suggested more interactions between bacterial taxa. The networks in the B and C horizons contained higher ratios of negative-to-positive

correlations, suggesting that interactions in the bacterial communities were mostly competitive. The growth substrates tend to be more limited in deeper soil horizons, and the relationships between bacterial taxa are mostly antagonistic with harsher competition.

Viruses are major drivers, as well as critical regulators of host diversity and biogeochemical functions in different environments (Storesund et al., 2015; Sandaa et al., 2017). A recent study by Trubl et al. (2018) showed that the viruses in a thawing permafrost peatland were linked to abundant lineages from Acidobacteria, Verrucomicrobia, and Deltaproteobacteria, suggesting important roles of these viruses in mediating key biogeochemical functions. The virome in subsurface soil contained notably higher relative abundance of tailed dsDNA bacteriophages (*Myoviridae*, *Siphoviridae*, and *Podoviridae*) than the virome in surface soil, which might result from the dominance of bacterial communities in deeper soil horizons.

Viruses can acquire host genes through infection, and the acquired genes become auxiliary metabolic genes (AMGs) in viruses and may contribute to host fitness (Adriaenssens et al., 2017; Emerson et al., 2018). Viruses may influence ecosystem function through significant association (e.g., lytic and lysogenic infections) with host microorganisms that play key roles in biogeochemical cycles (Emerson et al., 2018). In our study, 35.4–38.7% of predicted ORFs were identified as putative functional proteins, which were related to host metabolic pathways (e.g., cell signaling, oxidative phosphorylation, genetic information processing, and metabolisms of phosphorous, protein, and carbohydrates) and might suggest the potential importance of viruses in ecosystem functions. These functions have also been reported in previous viromics studies (Reavy et al., 2015; Emerson et al., 2018). For example, auxiliary carbohydrate-degrading genes were reported to be abundant in mangrove soils (Jin et al., 2019) and permafrost peatland soils (Trubl et al., 2018). In our study, high abundance of putative viral carbohydrate metabolism genes was observed in both surface and subsurface viromes suggesting carbohydrate-degrading AMGs are widespread in soil viruses and may contribute to modulation of carbon cycling. Interestingly, our results revealed that the virome in subsurface soil had up to 16-fold higher abundances of the annotated functional protein-coding genes (except proteins involved in oxidative phosphorylation) than the surface soil virome, indicating the

viruses in the subsurface, though lower in density, might be highly involved in microbial-mediated processes. The relative abundances of proteins associated with phage infectious cycle (phage lysogeny, lytic cycle, and prophage induction) were also higher in the subsurface soil virome, which may be related to virus-host co-evolution in response to the environments with low resource availability (Koskella et al., 2014).

This study presented a detailed survey of bacterial community composition and diversity with soil depth and provided the first insight into viral abundance distribution, composition, and host-virus interactions in soil with depth. Pronounced shifts in bacterial and viral composition were observed with soil depth. Viruses affect the host communities that drive ecological cycles in soil and further contribute to microbial-mediated processes, and viral abundances may be significant predictors of specific biogeochemical processes. Although this study revealed the potential top-down control that viruses exert on bacterial community composition and diversity, other ecological factors also impact the community structure. Landscape position and depth imposed the strongest influence in the bacterial community structure and should be carefully considered when relating microbial community structure to soil ecosystem processes at larger spatial scales. A definitive understanding of the influence of viral infection on the distributions and structure of microbial communities in soil profiles has yet to be drawn, thus further investigations are clearly needed to reveal the ecology and function of viruses in soil ecosystems especially in the sub-surface. Our survey suggested that metagenomic characterization of viral and bacterial communities can potentially enlighten the understanding of the influence of viruses on microbial host community structure at a higher resolution scale.

Acknowledgements

This work was supported in part by a United States Department of Agriculture project grant to MR (award number: 2018-67019-27792). X.L., F.L., and L.Y. received financial support from China Scholarship Council. The authors would like to thank Dr. Joey N. Shaw, Crop, Soil and Environmental Sciences at Auburn University the host of the 2016 Southeast Regional Soil Judging Contest (in Auburn, Alabama, USA) for their assistance with soil

sampling. The authors also wish to thank the reviewers for their constructive suggestions for improving the manuscript.

Conflict of Interest

No conflicts of interest are declared.

List of References

Adriaenssens, E.M., Kramer, R., Van Goethem, M.W., Makhalanyane, T.P., Hogg, I., Cowan, D.A., 2017. Environmental drivers of viral community composition in Antarctic soils identified by viromics. Microbiome 5, 83.

Ashburner, M., Ball, C.A., Blake, J.A., Botstein, D., Butler, H., Cherry, J.M., Davis, A.P., Dolinski, K., Dwight, S.S., Eppig, J.T., Harris, M.A., 2000. Gene ontology: tool for the unification of biology. Nature Genetics 25, 25-29.

Asnicar, F., Weingart, G., Tickle, T.L., Huttenhower, C., Segata, N., 2015. Compact graphical representation of phylogenetic data and metadata with GraPhlAn. PeerJ 3, e1029.

Bai, R., Wang, J.T., Deng, Y., He, J.Z., Feng, K., Zhang, L.M., 2017. Microbial community and functional structure significantly varied among distinct types of paddy soils but responded differently along gradients of soil depth layers. Frontiers in Microbiology 8, 945.

Binga, E.K., Lasken, R.S., Neufeld, J.D., 2008. Something from (almost) nothing: the impact of multiple displacement amplification on microbial ecology. The ISME Journal 2, 233-241.

Bolger, A.M., Lohse, M., Usadel, B., 2014. Trimmomatic: a flexible trimmer for Illumina sequence data. Bioinformatics 30, 2114-2120.

Chen, Y., Chen, G., Robinson, D., Yang, Z., Guo, J., Xie, J., Fu, S., Zhou, L., Yang, Y., 2016. Large amounts of easily decomposable carbon stored in subtropical forest subsoil are associated with r-strategy-dominated soil microbes. Soil Biology & Biochemistry 95, 233-242.

Chow, C.E.T., Kim, D.Y., Sachdeva, R., Caron, D.A., Fuhrman, J.A., 2014. Top-down controls on bacterial community structure: microbial network analysis of bacteria, T4-like viruses and protists. The ISME Journal 8, 816-829.

Costello, E.K., Schmidt, S.K., 2006. Microbial diversity in alpine tundra wet meadow soil: novel Chloroflexi from a cold, water-saturated environment. Environmental Microbiology 8, 1471-1486.

Durán, J., Morse, J.L., Rodríguez, A., Campbell, J.L., Christenson, L.M., Driscoll, C.T., et al. (2017) Differential sensitivity to climate change of C and N cycling processes across soil horizons in a northern hardwood forest. Soil Biology & Biochemistry 107, 77-84.

Edwards, R.A., McNair, K., Faust, K., Raes, J., Dutilh, B.E., 2016. Computational approaches to predict bacteriophage–host relationships. FEMS Microbiology Reviews 40, 258-272.

Eichorst, S.A., Trojan, D., Roux, S., Herbold, C., Rattei, T., Woebken, D., 2018. Genomic insights into the Acidobacteria reveal strategies for their success in terrestrial environments. Environmental Microbiology 20, 1041-1063.

Eilers, K.G., Debenport, S., Anderson, S., Fierer, N., 2012. Digging deeper to find unique microbial communities: the strong effect of depth on the structure of bacterial and archaeal communities in soil. Soil Biology & Biochemistry 50, 58-65.

Emerson, J.B., Roux, S., Brum, J.R., Bolduc, B., Woodcroft, B.J., Jang, H.B., Singleton, C.M., Solden, L.M., Naas, A.E., Boyd, J.A., Hodgkins, S.B., 2018. Host-linked soil viral ecology along a permafrost thaw gradient. Nature Microbiology 3, 870-880.

Fontaine, S., Barot, S., Barré, P., Bdioui, N., Mary, B., Rumpel, C., 2007. Stability of organic carbon in deep soil layers controlled by fresh carbon supply. Nature 450, 277-280.

Friedman, J., Alm, E.J., 2012. Inferring correlation networks from genomic survey data. PLOS Computational Biology 8,e1002687.

Gonzalez-Martin, C., Teigell-Perez, N., Lyles, M., Valladares, B., Griffin, D.W., 2013. Epifluorescent direct counts of bacteria and viruses from topsoil of various desert dust storm regions. Research in Microbiology 164, 17-21.

Han, L.L., Yu, D.T., Zhang, L.M., Shen, J.P., He, J.Z., 2017. Genetic and functional diversity of ubiquitous DNA viruses in selected Chinese agricultural soils. Scientific Reports, 7, 45142.

Hansel, C.M., Fendorf, S., Jardine, P.M., Francis, C.A., 2008. Changes in bacterial and archaeal community structure and functional diversity along a geochemically variable soil profile. Applied & Environmental Microbiology 74, 1620-1633.

Hartmann, M., Frey, B., Mayer, J., Mäder, P., Widmer, F., 2015. Distinct soil microbial diversity under long-term organic and conventional farming. The ISME Journal 9, 1177 – 1194.

Jiao, S., Chen, W., Wang, J., Du, N., Li, Q., Wei, G., 2018. Soil microbiomes with distinct assemblies through vertical soil profiles drive the cycling of multiple nutrients in reforested ecosystems. Microbiome 6, 146.

Jin, M., Guo, X., Zhang, R., Qu, W., Gao, B., Zeng, R., 2019. Diversities and potential biogeochemical impacts of mangrove soil viruses. Microbiome 7, 58.

Jobbágy, E.G., Jackson, R.B., 2000. The vertical distribution of soil organic carbon and its relation to climate and vegetation. Ecological Applications 10, 423-436.

Kim, K.H., Bae, J.W., 2011. Amplification methods bias metagenomic libraries of uncultured single-stranded and double-stranded DNA viruses. Applied & Environmental Microbiology 77, 7663-7668.

Koskella, B., Brockhurst, M.A., 2014. Bacteria–phage coevolution as a driver of ecological and evolutionary processes in microbial communities. FEMS Microbiology Reviews 38, 916-931.

Kozich, J.J., Westcott, S.L., Baxter, N.T., Highlander, S.K., Schloss, P.D., 2013. Development of a dual-index sequencing strategy and curation pipeline for analyzing amplicon sequence data on the MiSeq Illumina sequencing platform. Applied & Environmental Microbiology 79, 5112-5120.

Kuzyakov, Y., Mason-Jones, K., 2018. Viruses in soil: nano-scale undead drivers of microbial life, biogeochemical turnover and ecosystem functions. Soil Biology & Biochemistry 127, 305-317.

Leplae, R., Lima-Mendez, G., Toussaint, A., 2010. ACLAME: a CLAssification of Mobile genetic Elements, update 2010. Nucleic Acids Research 38, D57-D61.

Li, D., Liu, C.M., Luo, R., Sadakane, K., Lam, T.W., 2015. MEGAHIT: an ultra-fast single-node solution for large and complex metagenomics assembly via succinct de Bruijn graph. Bioinformatics 31, 1674-1676.

Liang, X., Radosevich, M., 2019. Commentary: A Host-Produced Quorum-Sensing Autoinducer Controls a Phage Lysis-Lysogeny Decision. Frontiers in Microbiology 10, 1201.

Liang, X., Radosevich, M., Löffler, F.E., Schaeffer, S., Zhuang, J., 2019a. Impact of microbial iron oxide reduction on the transport of diffusible tracers and non-diffusible nanoparticles in soils. Chemosphere 220, 391-402.

Liang, X., Zhuang, J., Löffler, F.E., Zhang, Y., DeBruyn, J., Wilhelm, S., Schaeffer, S.M., Radosevich, M., 2019b. Viral and bacterial community responses to stimulated Fe(III)-bioreduction during simulated subsurface bioremediation. Environmental Microbiology 21, 2043-2055.

Marine, R., McCarren, C., Vorrasane, V., Nasko, D., Crowgey, E., Polson, S.W., Wommack, K.E., 2014. Caught in the middle with multiple displacement amplification: the myth of pooling for avoiding multiple displacement amplification bias in a metagenome. Microbiome 2, 3.

Maslov, S., Sneppen, K., 2017. Population cycles and species diversity in dynamic Kill-the-Winner model of microbial ecosystems. Scientific Reports 7, 39642.

Marinari, S., Bonifacio, E., Moscatelli, M.C., Falsone, G., Antisari, L.V., Vianello, G., 2013. Soil development and microbial functional diversity: proposal for a methodological approach. Geoderma 192, 437-445.

Menzel, P., Ng, K.L., Krogh, A., 2016. Fast and sensitive taxonomic classification for metagenomics with Kaiju. Nature Communications 7, 11257.

Militon, C., Boucher, D., Vachelard, C., Perchet, G., Barra, V., Troquet, J., Peyretaillade, E., Peyret, P., 2010. Bacterial community changes during bioremediation of aliphatic hydrocarbon-contaminated soil. FEMS Microbiology Ecology 74, 669-681.

Muyzer, G., De Waal, E.C., Uitterlinden, A.G., 1993. Profiling of complex microbial populations by denaturing gradient gel electrophoresis analysis of polymerase chain

reaction-amplified genes coding for 16S rRNA. Applied & Environmental Microbiology 59, 695-700.

Narr, A., Nawaz, A., Wick, L.Y., Harms, H., Chatzinotas, A., 2017. Soil Viral Communities Vary Temporally and along a Land Use Transect as Revealed by Virus-Like Particle Counting and a Modified Community Fingerprinting Approach (fRAPD). Frontiers in Microbiology 8, 1975.

Ogata, H., Goto, S., Sato, K., Fujibuchi, W., Bono, H., Kanehisa, M., 1999. KEGG: Kyoto Encyclopedia of Genes and Genomes. Nucleic Acids Research 27, 29-34

Paez-Espino, D., Eloe-Fadrosh, E.A., Pavlopoulos, G.A., Thomas, A.D., Huntemann, M., Mikhailova, N., Rubin, E., Ivanova, N.N., Kyrpides, N.C., 2016. Uncovering Earth's virome. Nature 536: 425-430.

Pratama, A.A., van Elsas, J.D., 2018. The 'neglected' soil virome – potential role and impact. Trends in Microbiology 8, 649-662.

Ramirez, K.S., Craine, J.M., Fierer, N., 2012. Consistent effects of nitrogen amendments on soil microbial communities and processes across biomes. Global Change Biology 18, 1918-1927.

Reavy, B., Swanson, M.M., Cock, P.J., Dawson, L., Freitag, T.E., Singh, B.K., Torrance, L., Mushegian, A.R., Taliansky, M., 2015. Distinct circular ssDNA viruses exist in different soil types. Applied & Environmental Microbiology 81,3934–3945.

Roux, S., Solonenko, N.E., Dang, V.T., Poulos, B.T., Schwenck, S.M., Goldsmith, D.B., Coleman, M.L., Breitbart, M., Sullivan, M.B., 2016. Towards quantitative viromics for both double-stranded and single-stranded DNA viruses. PeerJ 4, e2777.

Rumpel, C., Kögel-Knabner, I., 2011. Deep soil organic matter—a key but poorly understood component of terrestrial C cycle. Plant & Soil 338, 143-158.

Sandaa, R.A., Pree, B., Larsen, A., Våge, S., Töpper, B., Töpper, J., Thyrhaug, R., Thingstad, T., 2017. The response of heterotrophic prokaryote and viral communities to labile organic carbon inputs is controlled by the predator food chain structure. Viruses 9, 238.

Schulz, F., Alteio, L., Goudeau, D., Ryan, E.M., Feiqiao, B.Y., Malmstrom, R.R., Blanchard, J., Woyke, T., 2018. Hidden diversity of soil giant viruses. Nature Communications 9, 4881.

Schütz, K., Kandeler, E., Nagel, P., Scheu, S., Ruess, L., 2010. Functional microbial community response to nutrient pulses by artificial groundwater recharge practice in surface soils and subsoils. FEMS Microbiology Ecology 72, 445-455.

Segobola, J., Adriaenssens, E., Tsekoa, T., Rashamuse, K., Cowan, D., 2018. Exploring viral diversity in a unique South African soil habitat. Scientific Reports 8, 111.

Spain, A.M., Krumholz, L.R., Elshahed, M.S., 2009. Abundance, composition, diversity and novelty of soil Proteobacteria. The ISME Journal 3, 992-1000.

Storesund, J.E., Erga, S.R., Ray, J.L., Thingstad, T.F., Sandaa, R.A., 2015. Top-down and bottom-up control on bacterial diversity in a western Norwegian deep-silled fjord. FEMS Microbiology Ecology 91, fiv076.

Stone, M.M., DeForest, J.L., Plante, A.F., 2014. Changes in extracellular enzyme activity and microbial community structure with soil depth at the Luquillo Critical Zone Observatory. Soil Biology & Biochemistry 75, 237-247.

Sullivan, M.B., Weitz, J.S., Wilhelm, S., 2017. Viral ecology comes of age. Environmental Microbiology Reports 9, 33-35.

Taş, N., Prestat, E., Wang, S., Wu, Y., Ulrich, C., Kneafsey, T., Tringe, S.G., Torn, M.S., Hubbard, S.S., Jansson, J.K., 2018. Landscape topography structures the soil microbiome in arctic polygonal tundra. Nature Communications 9, 777.

Tatusov, R.L., Galperin, M.Y., Natale, D.A., Koonin, E.V., 2000. The COG database: a tool for genome-scale analysis of protein functions and evolution. Nucleic Acids Research 28, 33-36.

Thingstad, T.F., Lignell, R., 1997. Theoretical models for the control of bacterial growth rate, abundance, diversity and carbon demand. Aquatic Microbial Ecology 13, 19-27.

Trubl, G., Jang, H.B., Roux, S., Emerson, J.B., Solonenko, N., Vik, D.R., Solden, L., Ellenbogen, J., Runyon, A.T., Bolduc, B., Woodcroft, B.J., 2018. Soil viruses are underexplored players in ecosystem carbon processing. mSystems 3, e00076-18.

van Leeuwen, J.P., Djukic, I., Bloem, J., Lehtinen, T., Hemerik, L., de Ruiter, P.C., Lair, G.J., 2017. Effects of land use on soil microbial biomass, activity and community structure at different soil depths in the Danube floodplain. European Journal of Soil Biology 79, 14-20.

Weinbauer, M.G., Rassoulzadegan, F., 2004. Are viruses driving microbial diversification and diversity?. Environmental Microbiology 6, 1-11.

Weitz, J.S., Wilhelm, S.W., 2012. Ocean viruses and their effects on microbial communities and biogeochemical cycles. F1000 Biological Reports 4, 17.

Wilhelm, S., Bird, J., Bonifer, K., Calfee, B., Chen, T., Coy, S., Gainer, P., Gann, E., Heatherly, H., Lee, J., Liang, X., 2017. A student's guide to giant viruses infecting small eukaryotes: From Acanthamoeba to Zooxanthellae. Viruses 9, 46.

Williamson, K.E., Radosevich, M., Wommack, K.E., 2005. Abundance and diversity of viruses in six Delaware soils. Applied & Environmental Microbiology 71, 3119-3125.
Williamson, K.E., Fuhrmann, J.J., Wommack, K.E., Radosevich, M., 2017. Viruses in soil ecosystems: an unknown quantity within an unexplored territory. Annual Review of Virology 4, 201-219.

Wommack, K.E., Bhavsar, J., Polson, S.W., Chen, J., Dumas, M., Srinivasiah, S., Furman, M., Jamindar, S., Nasko, D.J., 2012. VIROME: a standard operating procedure for analysis of viral metagenome sequences. Standards in Genomic Sciences 6, 421-433.

Zhang, J., Gao, Q., Zhang, Q., Wang, T., Yue, H., Wu, L., Shi, J., Qin, Z., Zhou, J., Zuo, J., Yang, Y., 2017. Bacteriophage–prokaryote dynamics and interaction within anaerobic digestion processes across time and space. Microbiome 5, 57.

Chapter IV Appendix

Table 4.2: Sampling scheme and description of sampling sites and soil profiles.

Landscape position	Pit	Depth	Horizon description
Upland	UP1	0–7 cm	A
		7–23 cm	AB
		23–57 cm	Bt1
		57–68 cm	Bt2
		68–80 cm	Bt3
	UP2	0–8 cm	A
		8–25 cm	AB
		25–40 cm	Bt1
		40–70 cm	Bt2
		70–100 cm	Bt3
		100–110 cm	C
Foot-slope	FS1	0–8 cm	A
		8–19 cm	AB
	FS2	0–16 cm	A
		16–30 cm	AB
		30–55 cm	Bt1
		55–92 cm	Bt2
		92–111 cm	Bt3
		111–120 cm	C

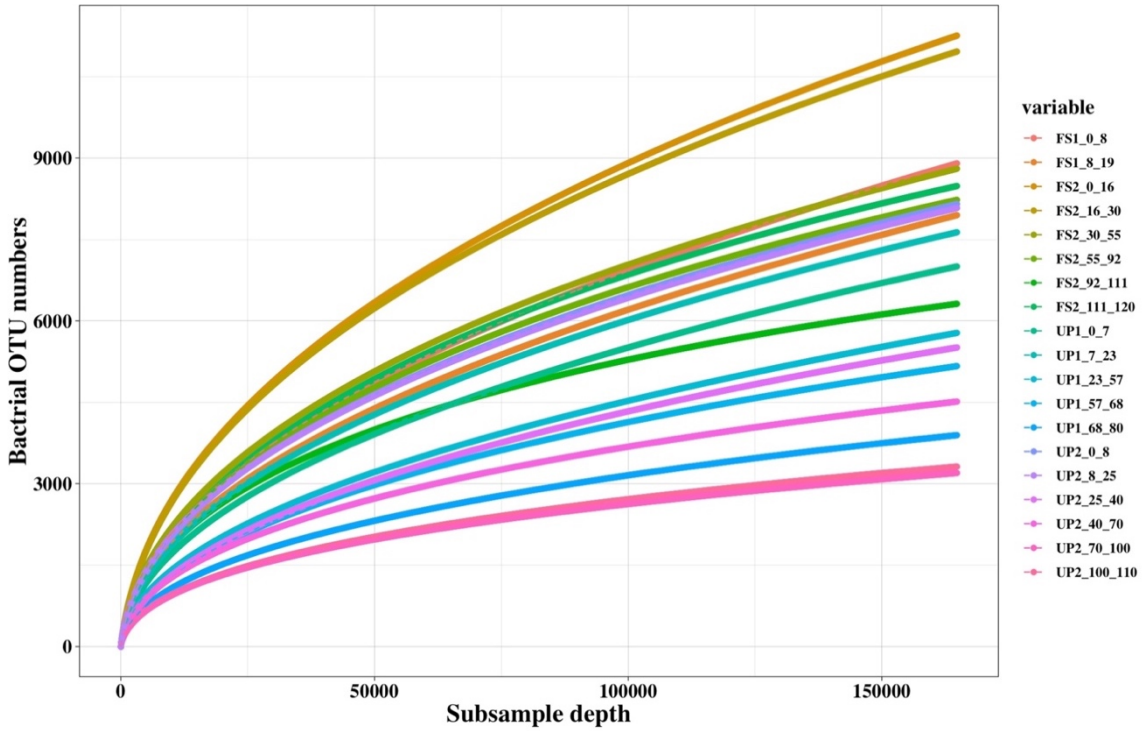

Figure 4.7: Refraction curve with maximum read depth. Sufficient sequencing depth was achieved for representative coverage of the community diversity in each sample. Soil samples were collected from different depths in each pit shown as following: 0–8 and 8–19 cm in FS1; 0–16, 16–30, 30–55, 55–92, 92–111, and 111–120 cm in FS2; 0–7, 7–23, 23–57, 57–68, and 68–80 cm in UP1; 0–8, 8–25, 25–40, 40–70, 70–100, and 100–110 cm in UP2.

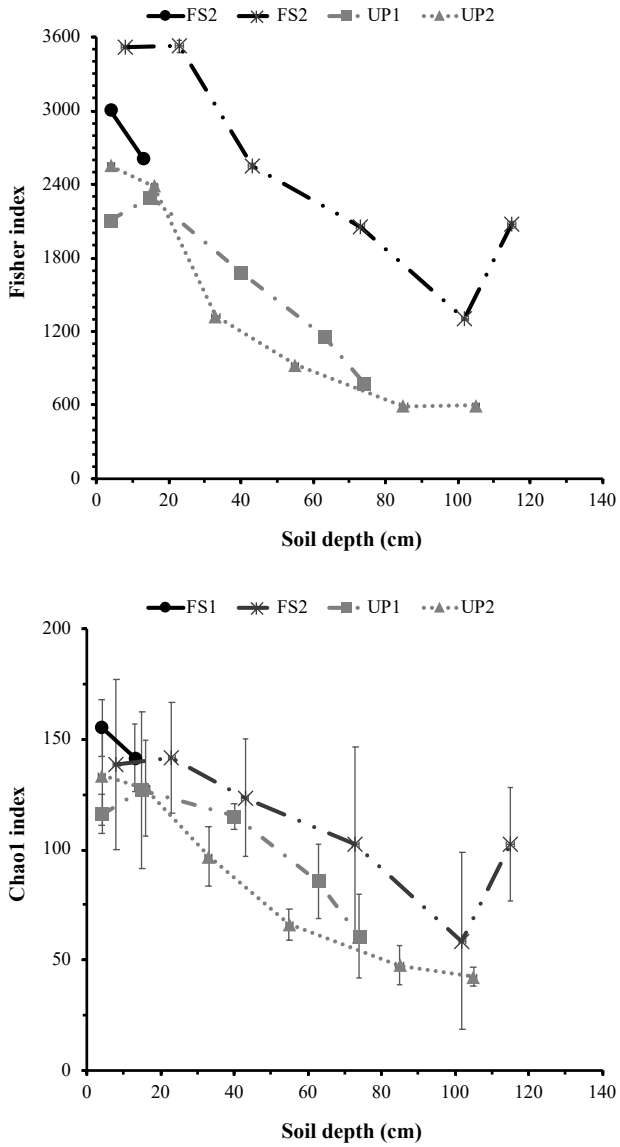

Figure 4.8: Alpha-diversity of bacterial communities versus soil depth. OTUs were determined at 3% dissimilarity level. Chao1 index was used to estimates the species richness, and inverse Simpson index was used for estimates of community diversity. Each data point represents the mean value (n=3), and the error bars show standard deviation.

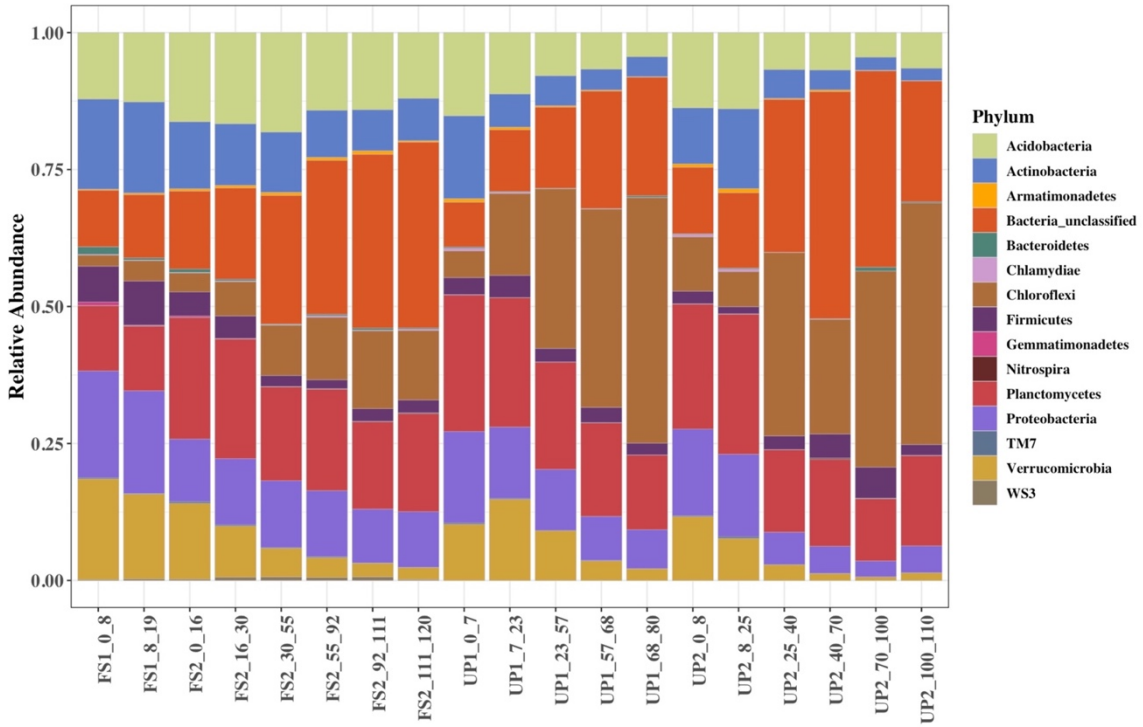

Figure 4.9: The distribution patterns of the relative abundances of major bacterial phyla. The soil depths in each pit are 0–8 and 8–19 cm in FS1; 0–16, 16–30, 30–55, 55–92, 92–111, and 111–120 cm in FS2; 0–7, 7–23, 23–57, 57–68, and 68–80 cm in UP1; 0–8, 8–25, 25–40, 40–70, 70–100, and 100–110 cm in UP2.

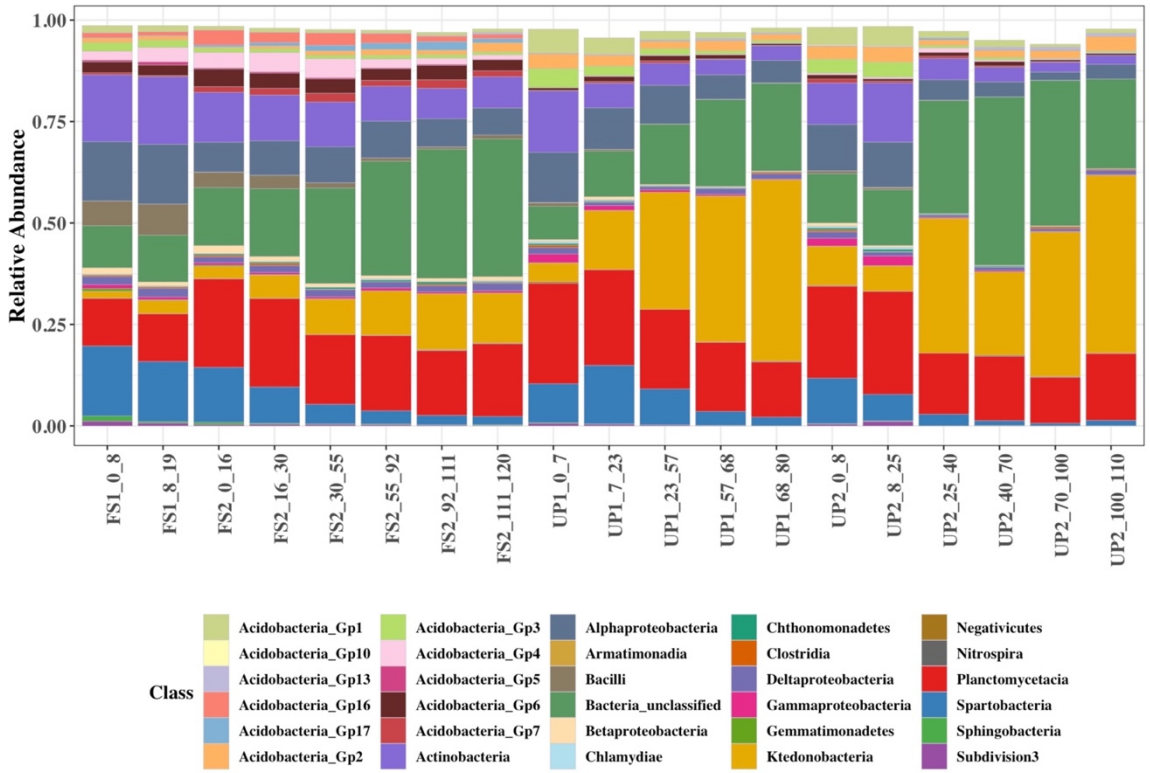

Figure 4.10: Taxonomic distribution of bacterial communities through four soil profiles. The soil depths in each pit are 0–8 and 8–19 cm in FS1; 0–16, 16–30, 30–55, 55–92, 92–111, and 111–120 cm in FS2; 0–7, 7–23, 23–57, 57–68, and 68–80 cm in UP1; 0–8, 8–25, 25–40, 40–70, 70–100, and 100–110 cm in UP2.

Figure 4.11: Circular annotated phylogenic and taxonomic tree showing variances in bacterial community composition along the soil profiles. The phylogenetic tree was generated and drawn with GraPhlAn. The size of nodes represents the relative abundance of the taxa. Each circle stands for one soil depth. FS1 and FS2 are two toe-slope sites, while UP1 and UP2 represent upland sites. The small numbers in the phylogenetic tree denote specified bacterial genera (as noted). The degree of red color in each ring shows the relative abundance of each taxonomic group. The node colors indicate specified bacterial phyla (as noted). The numbers represent specified bacterial genera noted as following. (1:Bradyrhizobium; 2:Gp3; 3:Bacillus; 4:Gp1; 5:Gp6; 6:Gp16; 7:Planctomyces; 8:Gp2; 9:Singulisphaera; 10:Gp7; 11:Conexibacter; 12:Streptomyces; 13:Mycobacterium; 14:Thermosporothrix; 15:Pedomicrobium; 16:Gp4; 17:Zavarzinella; 18:Gemmata; 19:Kitasatospora; 20:Gp17; 21:Gp5; 22:Actinoallomurus; 23:Rugosimonospora; 24:Ktedonobacter; 25:Aciditerrimonas; 26:Geobacter; 27:Solirubrobacter; 28:Burkholderia; 29:Iamia; 30:Sporosarcina; 31:Arthrobacter; 32:Massilia; 33:Anaeromyxobacter; 34:Gp10; 35:Pasteuria; 36:Dactylosporangium; 37:Nocardioides; 38:Catelliglobosispora; 39:Phenylobacterium; 40:Bacteroides; 41:Catenulispora; 42:Sphaerisporangium; 43:Gp20; 44:Paenibacillus; 45:Nitrospira; 46:Rhizomicrobium; 47:Kribbella; 48:Ilumatobacter; 49:Ralstonia; 50:Tumebacillus; 51:Rhodopila; 52:Gp13; 53:Gemmatimonas; 54:Cohnella; 55:Ammoniphilus; 56:Thermoleophilum; 57:Duganella; 58:Mesorhizobium; 59:Phycisphaera; 60:Skermanella; 61:Steroidobacter; 62:Labrys; 63:Nonomuraea; 64:Telmatospirillum; 65:Sphingomonas; 66:Ramlibacter; 67:Pseudonocardia; 68:Methylobacterium; 69:Gp11; 70:Amycolatopsis; 71:Acidocella; 72:Faecalibacterium; 73:Desulfosporosinus; 74:Nocardia; 75:Rhodomicrobium; 76:Hyphomicrobium; 77:Neochlamydia; 78:Streptosporangium; 79:Gp18; 80:Flavobacterium; 81:Caldilinea; 82:Phascolarctobacterium; 83:Sinomonas; 84:Syntrophobacter; 85:Mucilaginibacter; 86:Kofleria; 87:Actinospica; 88:Cupriavidus; 89:Rhizobium; 90:Actinomycetospora; 91:Brevibacillus; 92:Blastococcus; 93:Delftia; 94:Zymophilus; 95:Geminicoccus; 96:Bifidobacterium; 97:Legionella; 98:Terrimonas; 99:Parachlamydia.)

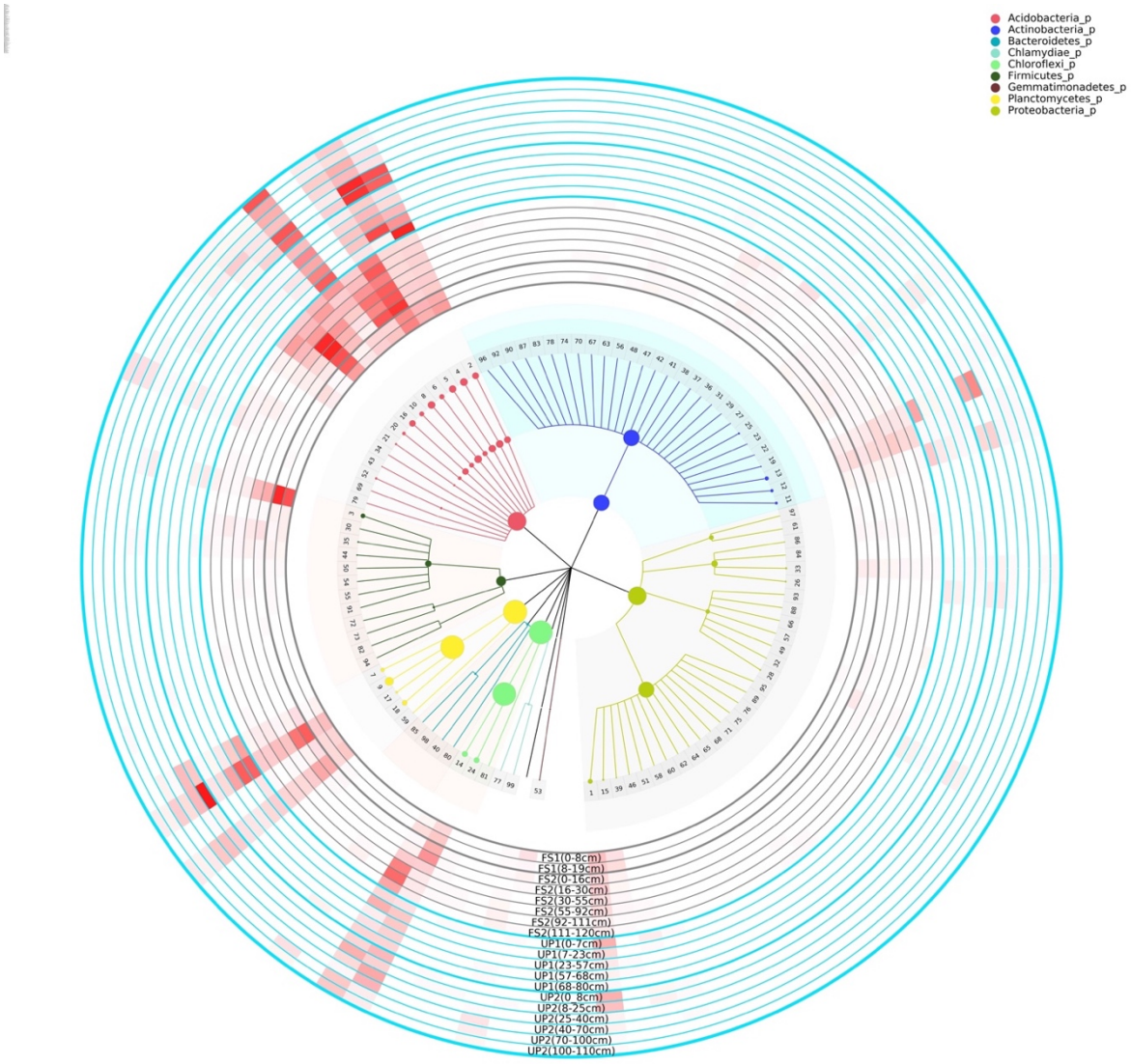

Figure 4.11 continued.

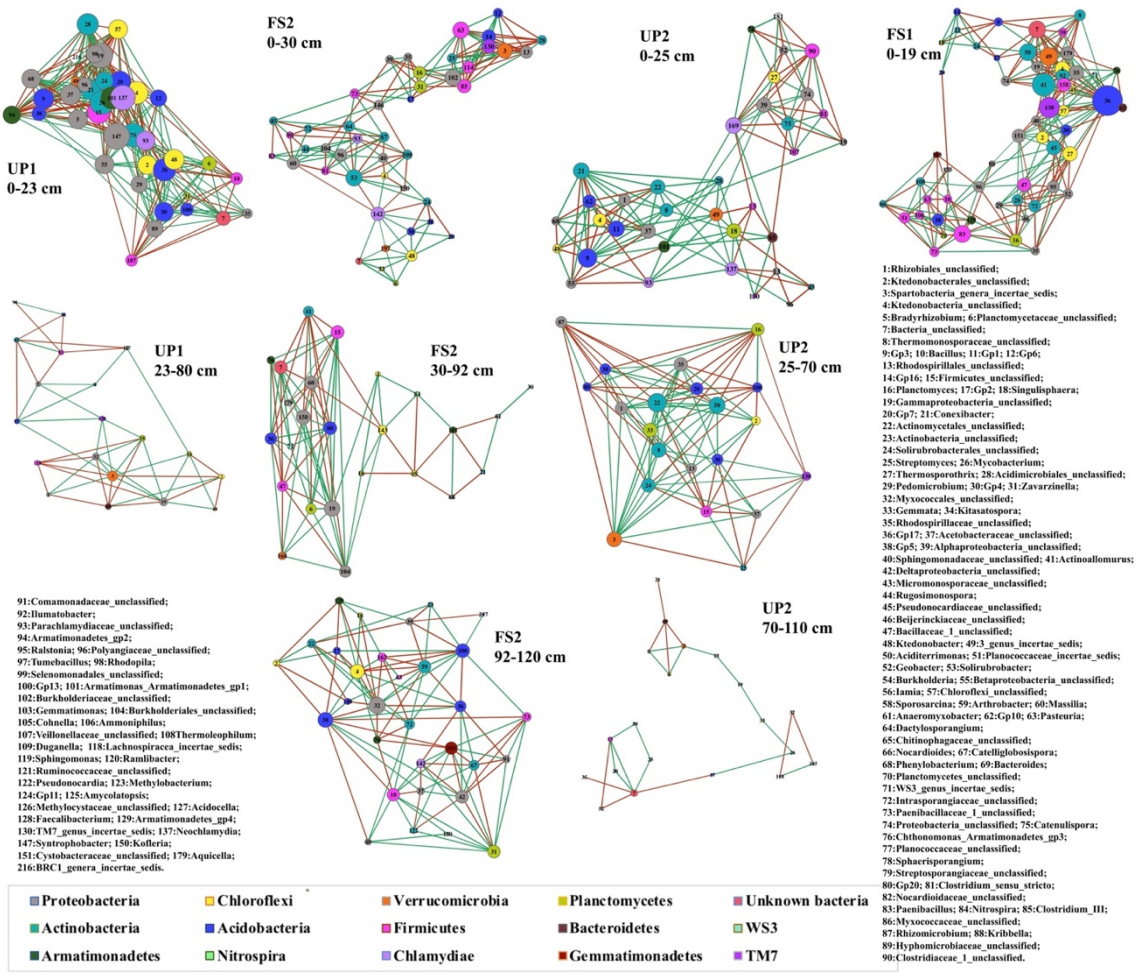

Figure 4.12: The co-occurrence network between bacterial taxa with depth in soil profile. The co-occurrence correlation along soil profiles were performed with SparCC method, and the edges in the network show correlations with *P* value calculated with 200 bootstrapping processes smaller than 0.01. Negative correlations are displayed in red and positive correlations in green. The thickness of the lines indicates the strength of the correlations.

CHAPTER V

Viral abundance, community structure and reproductive strategies at different soil depths

Publication Note

This chapter a version of article in preparation for submission to *Soil Biology & Biochemistry* by Xiaolong Liang, Yingyue Zhang, K. Eric Wommack, Steven W. Wilhelm, Jennifer M. DeBruyn, Jie Zhuang, and Mark Radosevich.

My contribution to this work was experimental design, samples processing, extraction and numeration of viruses and bacteria, bioinformatics and statistical analyses, and drafting the manuscript.

Abstract

Increased awareness of the abundance and diversity of viruses in soils has led to a soaring interest in soil virus ecology. The roles of virus-host relationships within soil ecosystems remain under-investigated relative to other environments. To explore the virus-host interactions in soil profiles, viral and bacterial community composition and structure, viral and bacterial abundances, and the lysogenic fractions (LF) of bacterial populations were assessed. Epifluorescence microscopy counting, mitomycin C-induction assays, viral metagenomics sequencing, bacterial 16S rRNA gene amplicons sequencing, and bioinformatics tools were used in this study. The abundances of both free viruses and bacterial cells decreased with soil depth, but viral abundances decreased more quickly than bacterial abundances leading to a decreasing virus-to-bacteria ratio with depth. In contrast, LF increased with soil depth, indicating lysogeny became the more dominant reproduction strategy for autochthonous soil bacteriophages in deeper soil. The virome composition differed between surface and subsurface soil samples. *Microviridae* (ssDNA virus) were the predominant viral taxonomic class in the surface soil virome, but had an extremely low relative abundance in the subsurface soil virome. Meanwhile, subsurface soil had higher relative abundances of dsDNA viruses, including *Myoviridae*, *Podoviridae*, and *Siphoviridae*, compared with surface soil. The subsurface soil virome contained higher abundances of auxiliary metabolic genes and genes potentially encoding proteins of bacteriophage structural components and replication machinery than the surface soil virome. Significant shifts in bacterial community composition and diversity with soil depth were closely correlated with viral abundance, virus-to-bacteria ratio, and LF. Together the results suggest that the viral community structure and life strategies are linked to microbial host cell composition and function in soil. The linkage is subject to environmental conditions.

Introduction

Microorganisms are the most abundant life forms in soils and play critical roles in Earth's biogeochemical cycling and overall ecosystem functioning. The substantial roles of viruses in influencing microbial community structure and functions have become increasingly evident (Wilhelm and Suttle 1999; Brum et al., 2016; Fierer, 2017; Emerson et al., 2018). Viruses are obligate parasites of bacteria and extremely abundant in nature, with numbers exceeding their co-occurring host cells by 10- to 1000-fold in soil (Wigington et al., 2016; Williamson et al., 2017). Although some interesting phenomena regarding virus spread from cell to cell, e.g., viruses exit from the intact host cell, were revealed, most viruses multiply at the expense of the cell through two distinct reproductive life cycles, lytic and lysogenic (Feiner et al., 2015; Liang and Radosevich, 2019). Obligate lytic infection of host cells involves hijacking the host metabolic machinery to produce progeny viruses leading ultimately to host cell lysis and release of viruses and microbial necromass to the environment. Temperate viruses may reproduce either lytically or lysogenically depending on host cell density and environmental conditions. During a lysogenic infection, the virus genome is integrated into the host genome and expression of the lytic functions and structural genes are repressed. In this state the virus is termed a prophage and the host a lysogen and the prophage is replicated as the lysogen grows and divides. A variety of agents and environmental variables have been shown to trigger excision of the prophage and initiate lytic cycle replication or it may occur spontaneously (Ghosh et al., 2008; Brum et al., 2016). This process is termed prophage induction.

Virus production rates and strategies exhibit highly divergent influences in host diversity and microbially-driven processes. Pioneering studies have shown that various factors contribute to viral abundance, production rates/strategies, and diversity, implicating complicated virus-host dynamics in response to environmental conditions (Brum et al., 2015; 2016; Liang et al., 2019). Though increased efforts have been made, the drivers of virus-host dynamics in soil are still unknown, leaving a critical gap in our understanding of microbial diversity and soil ecosystem function.

The importance of viruses in soils was initially suggested by epifluorescence microscopy direct counting that revealed the high abundance of autochthonous soil viruses

(Williamson et al., 2003; 2005). Many studies have shown that viral community patterns vary significantly in different soils suggesting that soil spatial and temporal heterogeneity may establish distinct viral communities (Srinivasiah et al., 2015; Han et al., 2017). Viral infection is known to impact evolution of microbial communities, modify the host community composition, and mediate nutrient cycling through various reproductive strategies in aquatic environments (Kimura et al., 2008; Roux et al., 2016; Pan et al., 2017). Many studies based on results from chemical-based prophage induction assays, have reported that lytic reproduction is more prevalent under conditions that favor high host cell densities and growth rates, while lysogenic reproduction becomes prevalent when host cell abundance is low and growth rates are slow or cells exhibit dormancy. (Maurice et al., 2010; Williamson, 2011). Interestingly, Knowles et al. (2016) reported relatively lower viral abundances and more prevalent temperate life cycles at high host cell densities, which led them to propose the piggyback-the-winner model of virus reproduction. Viral-mediated cell lysis neutralizes microbial production and shunts some critical nutrients back to soluble pools for heterotrophic bacterial growth, potentially increasing microbial metabolism (Wilhelm and Suttle, 1999; Weinbauer and Rassoulzadegan, 2004; Williamson, 2017). Lysogenic infection may confer enhanced fitness to the infected host cell *via* genetic elements contained within the virus genome (lysogenic conversion) and/or facilitate horizontal gene transfer (transduction). Together, virus infection plays a significant role in the genetic diversity and evolution of host microorganisms (Ghosh et al., 2008; Aminov, 2011; Williamson, 2017). Thus, virus-host interactions are the fundamentally part of soil microbial ecological functions and may vary according to the environmental conditions (Williamson et al., 2007; Holmfeldt et al., 2016; Parikka et al., 2017; Liang et al., 2019).

Soils are spatially and temporally heterogeneous in physical, chemical, and biological properties, providing complex and diverse habitats for microorganisms (O'Donnell et al., 2007; Hansel et al., 2008; Fierer, 2017). These characteristics can exert influences on virus-host dynamics. Here we investigated viral and microbial abundances, lysogenic fractions among microbial populations, viral diversity, potential functions of viromes, and correlation of viral assemblages with bacterial communities within two vertical soil profiles. Our objective was to determine the dependence of viral abundance,

diversity, genetic functional potential, and reproductive strategy on soil depth in two soils (*i.e.*, Alfisol vs. Mollisol) formed from contrasting parent materials (eolian sand and glacial outwash vs. loess plain, respectively).

Materials and Methods

Site description and sample collection

Two sites with soils, an Alfisol and a Mollisol, formed from contrasting parent materials were sampled near DeKalb, Illinois for this study. The Alfisol (ALF) was classified as a hapludalf with sandy loam texture in the surface horizon. This soil formed in a wind-blown loess parent material. The Mollisol (MOL) located nearby was classified as an argiudoll with a silt loam surface texture. This soil formed in glacial outwash parent material overlain by eolian sand. Soil samples from different horizons (including A, E, B, and C master horizons) from sites ALF and MOL, (both with backslope landscape positions) were collected. Soil pits were excavated at each site to expose the master horizons of each soil profile. Depths and boundaries of soil horizons were measured and characterized according to the Keys to Soil Taxonomy (ref). Three bulk soil samples were randomly obtained by inserting a soil coring probe horizontally into the pit face from each horizon. The soil coring device was cleaned with 70% ethanol (v/v) before each sample was taken to minimize cross-contamination of the soil and sub-soil samples. Each sample was packed into a zip-lock plastic bag and immediately stored on ice and shipped overnight to the laboratory in Knoxville, TN. Upon arrival, each soil sample was thoroughly mixed separately within their respective sample bags with sterile glass rods, and bacteria and viruses were immediately extracted with the following methods. For each soil sample collected, three sub-samples were taken and processed to provide technical replicates for viral and bacterial abundance, prophage induction assays, and bacterial community analyses by 16S rRNA gene sequencing. One surface and one subsurface sample from the ALF site were used for virome analyses.

Extraction of viruses and bacteria

Viruses and bacteria were extracted from separate subsamples as instructed by Williamson et al. (2003). Extractions of viruses and bacteria were performed with triplicate samples from each horizon to investigate the actual differences in the abundance of virus-like particles (VLPs) and bacteria. Thirty grams of soil were suspended in 100 ml of cold extraction buffer (one liter of buffer contained 10 g potassium citrate, 1.44 g $Na_2HPO_4 \cdot 7H_2O$, and 0.24 g KH_2PO_4, adjusted to pH 7). The mixture was transferred into an autoclaved clean blender vessel and blended at the maximum speed for 3 min. For virus extraction, slurries were transferred into 50 ml polypropylene conical tubes (Corning Science Mexico, Reynosa, Tamaulipas, Mexico) and centrifuged at 4,000 g for 20 min at 4 °C. Supernatants were sequentially filtered through 0.45-µm and 0.22-µm Millex syringe filters (Merck Millipore Ltd., Tullagreen, Co. Cork, Ireland). Filtrates with viruses were flash frozen in liquid nitrogen and stored at –80 °C until further processing. For bacterial extraction, nine ml of bacterial extracts (soil slurries) were gently transferred after blending into a 15-ml centrifuge tube containing 2 ml 60% (w/v) nycodenz solution (Accurate Chemical & Scientific, Westbury, NY) and centrifuged at 6,000 rpm for 20 min at 4 °C in SW 41 Ti swinging bucket rotor (Beckman Coulter Inc., Ashville, NC). Supernatant including the nycodenz phase was transferred to 4.5 ml cryovial with glycerol, flash frozen with liquid N2 and stored at -80ºC until further processing.

Prophage induction assays

Prophage induction assays were performed as previously reported (Ghosh et al.,add ref). To provide carbon, energy and other nutrient resources to support viral production during prophage induction assays, sterile water-soluble organic carbon (WSOC) solutions were prepared. Each soil sample was suspended in sterile deionized water and blended at the maximum speed for 3 min. The soil extractions were centrifuged at 5,000 g for 20 min and the supernatants were filtered through 0.22-µm Nalgene Rapid-Flow bottle-top filters (Thermo Scientific) and then autoclaved for use in induction assays.

The bacterial extracts prepared as described above of each sample were centrifuged at 5,000 g for 20 min to collect the bacterial pellets, and the bacterial pellets were

resuspended with the prepared sterile WSOC solutions. Each resuspended bacterial solution was divided into two equal aliquots. For whole-community prophage induction assays, one bacterial suspension was treated with 1 µg/ml (final concentration) mitomycin C (MC), while the other aliquot of bacterial suspension served as control samples and was not treated with MC. All suspensions were incubated in the dark for 18 h at room temperature (Williamson et al., 2007). The viruses and bacteria in the MC and control cell suspensions were enumerated with epifluorescence microscopy (Williamson et al., 2005). Burst size representing the number of produced viruses per lysed host cell (Williamson et al, 2007) was calculated as:

$$Bz = (V_i - V_c)/(B_c - B_i).$$

Where V_i is the VLP counts in the MC-induced sample, V_c is the VLP counts in the control sample, B_c and B_i are the bacteria direct counts in the control and the MC-induced samples, respectively. Lysogenic fraction (LF) among host microbial community was calculated as:

$$LF\ (\%) = [(V_i - V_c)/Bz]/B_c * 100.$$

Epifluorescence microscopy analysis

Viral and bacterial abundances in soils were estimated as described by Williamson et al. (2003). Aliquots of viral extracts (100 µl) were suspended in 900 µl of sterilized HPLC water, while aliquots of bacterial extracts (200 µl) were mixed with 800 µl of sterilized phosphate buffer. All suspensions were treated with Deoxyribonuclease I (DNase I, 2.5 units/µl, Thermo Scientific) to remove extracellular DNA and digestion was terminated after 20 min by addition of 35 µl of 0.5 M EDTA. Each DNase-treated viral suspension was vacuum (less than 62 kPa pressure) filtered through a 0.02-µm-pore-size Whatman Anodisc filter supported by a 0.22-µm Supor (Pall Corp., Ann Arbor, MI) and a glass microfiber filter (Whatman International Ltd., Maidstone, England) in Millipore vacuum manifold (Sigma-Aldrich Corporation). Bacterial solutions were filtered through 0.2-µm Isopore membrane filters (Merck Millipore Ltd., Cork, Ireland) instead of Anodisc filters. The viruses and bacteria were stained by addition of 400 µl of 2X SYBR gold (5,000 fold dilution of the stock solution received from Molecular Probes, Eugene, OR) onto the

Anodisc and Isopore filters and kept in dark for 20 min and then rinsed 4 times using autoclaved and 0.1 μm filtered water. The filters were mounted onto slides with anti-fade solution (ref) and a cover slip. The slides were counted immediately at 1000X magnification using a Nikon Eclipse E600 epifluorescence microscopy with FITC filter set.

Bacterial DNA extraction and sequencing

Whole soil DNA was prepared from 0.25 g of moist soil samples by using the PowerLyser PowerSoil DNA isolation kit (Qiagen, Hilden, Germany) following the manufacturer's recommendations. The DNA extractions were quantified with PicoGreen Assay Kit (Invitrogen, Carlsbad, CA). For 16S rRNA gene sequencing, the DNA samples were sent to Genomic Services Lab at HudsonAlpha Institute for Biotechnology (Huntsville, AL, USA barcoded library preparation and sequencing. Briefly, the V3-V4 region of 16S rRNA genes of bacteria was amplified with the primers 341F (5'-CCTACG GGNGGCWGCAG-3') and 785R (5'-GACTACHVGGGTATCTAATCC-3') in PCR to construct libraries (Muyzer et al., 1993). All primers were labeled with adaptor, linker, and 6-bp barcode sequences. The amplified 16S rRNA gene libraries were pooled and sequenced using 300PE (paired-end) on the Illumina MiSeq platform (Illumina, USA) at HudsonAlpha Institute for Biotechnology, Huntsville, AL, USA.

16S rRNA gene sequence analysis

Raw sequence files were run through MUTHUR pipeline (Kozich et al., 2013). Sequence files were demultiplexed and merged into contigs. The resulting 5,131,550 sequences were trimmed of reads containing ambiguous bases and long polymers. Unique sequences were sorted with abundance and all quality-filtered sequences were classified by SILVA alignment (Quast et al., 2013), by which sequences were pre-clustered by 99% similarity followed by removal of chimeric sequences. The divided sequences were classified using the Bayesian classifier and classified into OTUs (operational taxonomic unit) at a 0.03 distance, which resulted in 55,819 OTUs. Sequence files were transferred to

a local computer for subsequent statistical analysis with R software. The raw sequence data was submitted into NCBI under the accession number SRP158136.

Nonmetric multidimensional scaling representing variations in bacterial community composition was built for pairwise comparisons of each microbial community based on Bray-Curtis similarity. The distribution of microbial communities in soil profiles was determined by circular annotated phylogenic and taxonomic tree, stacked bar-plot, boxplot, and heatmap with ggplot2 package (Wickham, 2009). For construction of circular annotated phylogenic and taxonomic tree, the R-processed tree file was further analyzed to produce the figure with GraPhlAn (Asnicar et al., 2015) in Python. Determination of interactions between viral infection and bacteria and between different bacterial taxa by co-occurrence network was completed with SparCC method (Friedman and Alm, 2012) on virus abundance, lysogenic fraction, and the relative abundance of bacterial taxa. Correlations were calculated and averaged with 20 inference interactions, and the pairwise *P*-value was generated by 200 bootstrapping processes. Edges with P-value smaller than 0.01 were considered significant for visualization of networks.

Viral DNA extraction, sequencing, and metagenomic analysis

Viral extracts were concentrated (500-fold) with centrifugal filter units (30KDa cutoff, Amicon Ultra-15, Millipore) at 4,000 g for 20 min. The virus concentrates were treated with DNase I to remove all the free non-encapsulated DNA, and PCR amplification of the 16S rRNA gene was performed with 27F/1492R primers to check for the presence of contaminating bacterial DNA (Yu et al., 2017). These PCR assays were negative indicating the viral concentrates were free of bacterial DNA. Viral DNA was then extracted and purified using the Power Viral Environmental RNA/DNA Isolation Kit (Qiagen, Hilden, Germany). The purified viral DNA samples were submitted to Lucigen Corp. (Middleton, WI, USA) for Library preparation and sequencing. All the following steps were performed by Lucigen corporation. Briefly, DNA samples were amplified with a combination of TthPrimPol Primase and Phi29 DNA polymerase (Sygnis TruePrime WGA kit; catalog no. SYG370025; Picher et al. 2016) and purified using Zymo Research

genomic DNA purification and concentration kit (catalog no. D4010). The prepared viral DNA libraries were sequenced on an Illumina Miseq^{TM} platform by Lucigen corporation.

Raw sequences returned from Lucigen were uploaded to KBase (Arkin et al., 2016) for metagenomic analysis. Reads were demultiplexed, and paired reads were quality-trimmed using Trimmomatic v0.36 (Bolger et al., 2014). The viromic reads were subsequently assembled using Megahit (Li et al., 2015). The assembled sequences were analyzed using Kaiju taxonomic classifier v1.5.0 (Menzel et al., 2016). The taxonomic composition of viromes were computed from Blastp comparison with NCBI NR database and RefSeq complete virus database with a threshold of 10^{-10} on *E*-value. The assembled virome libraries were submitted to VIROME server (Wommack et al., 2012) for prediction of open reading frames (ORFs) and functional annotation. The predicted open reading frames (ORFs) were classified and compared to RefSeq complete viral databases for functional annotations.

Results

Bacterial and viral abundance and prophage induction responses

Surface soil contained significantly higher numbers of viruses and bacteria than subsurface soil ($P < 0.01$, Fig. 5.1a and c). Viral abundance followed bacterial abundance and decreased with soil depth, and the abundance of virus particles in one gram of soil declined from 1.42×10^{10} (0–22 cm) to 8.26×10^{7} (116–140 cm) at MOL site and from 1.97×10^{10} (0–12 cm) to 1.19×10^{8} (108–140 cm) at ALF site. The virus-to-bacteria ratio was highest in surface soils where both viral and bacterial abundances were highest.

Exposure to MC induced notable lysis of bacterial cells and resulted in a large increase of virus particles (data not shown). The lysogenic fractions, ranging from 32.6 to 66.7%, were lowest in surface soils that contained the highest bacterial and viral abundances and highest in C-horizons where both viral and bacterial abundances were lowest in both ALF and MOL soil profiles (Fig. 5.1b and d). The Bz, ranged from 9 to 44, and was highest in surface soil and decreased with soil depth. The lysogenic fraction increased with soil depth and was negatively correlated to bacterial abundance (Pearson

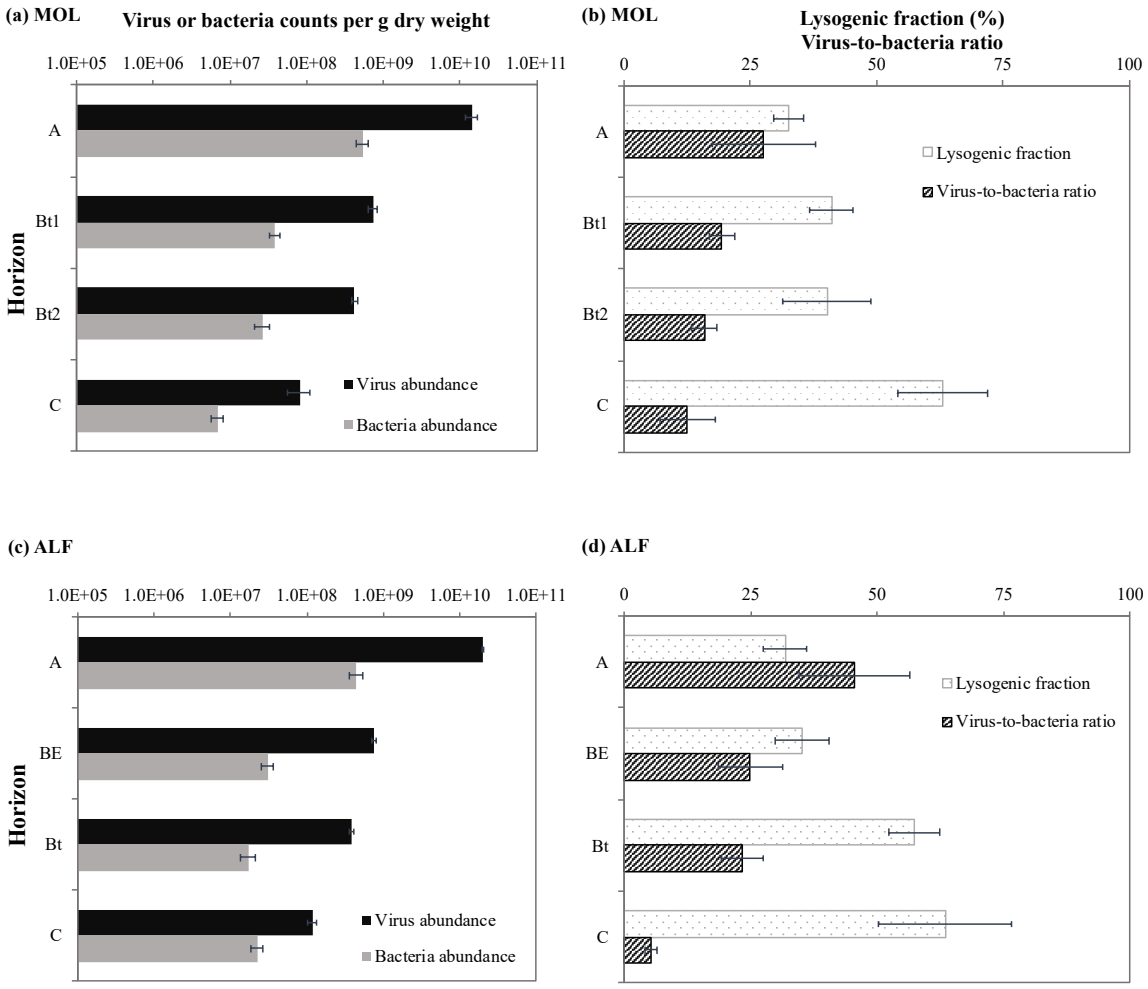

Figure 5.1: Viral abundance, bacterial abundance, virus-to-bacteria ratio, and lysogenic proportions among bacteria populations in soils from different horizons of the soil profiles. Lysogenic fractions were estimated in mitomycin C-induction trials. Each column represents the mean value of triplicate samples, and the error bars show standard deviation.

correlation, r = -0.6, $p < 0.01$; Fig. 5.2a). The correlation analysis also showed that viral abundance had a positive relationship with Bz ($r = 0.7$, $p < 0.0001$; Fig. 5.2b) but a negative relationship with LF (r = 0.6, $p < 0.01$; Fig. 5.2c). Bacterial and viral abundances were positively correlated with each other (r = 0.9, p <0.0001; Fig. 5.2d), and virus-to-bacteria ratio was positively correlated with viral abundance (r = 0.8, $p < 0.0001$; Fig. 5.2e).

Bacterial community diversity and composition

A total of 3,168,746 sequences were obtained from the soil samples after quality filtering, revealing 55,819 OTUs based on a 0.03 distance threshold. Soil samples from all horizons had a similar number of sequences, while A horizons had significantly more OTUs than other horizons. Rarefaction curves showed that the sequencing was sufficient to accurately estimate the species richness in each sample (Appendix Fig. 5.6).

The constrained analysis of the principal coordinates (CAP) showed that the overall bacterial community composition within the various soil horizons were well separated (Fig. 5.3a; Adonis, $P < 0.01$). The bacterial communities in soils of MOL site were also separated from those in soils of ALF site, suggesting that the microbial communities in different landscape position were distinct. The vectors in CAP represent the factors significantly correlated with the variations of bacterial community composition. Soil depth, viral abundance, burst size, bacterial abundance, lysogenic fraction, and virus-to-bacteria ratio were significant factors in separating bacterial communities. PerMANOVA analysis also confirmed that soil depth was the most significant parameter influencing the bacterial community composition, and that viral abundance, lysogenic fraction, and burst size were notable biotic factors in shaping bacterial communities (Appendix Table 5.2).

Fifteen phyla were identified within the bacterial 16S rRNA gene libraries, with the majority (an average of 75% in each sample) of sequences classified into nine major phyla: Acidobacteria (representing 16.4% of all sequences), Planctomycetes (12.5%), Verrucomicrobia (11.8%), Proteobacteria (11.9%), Actinobacteria (9.9%), Cloroflexi (6.6%), Firmicutes (1.8%), Bacteroidetes (1.3%), and Gemmatimonadetes (0.4%). Approximately 20% of the sequences could not be assigned to any known bacterial phylum. Planctomycetes were most abundant in A horizons with abundance gradually

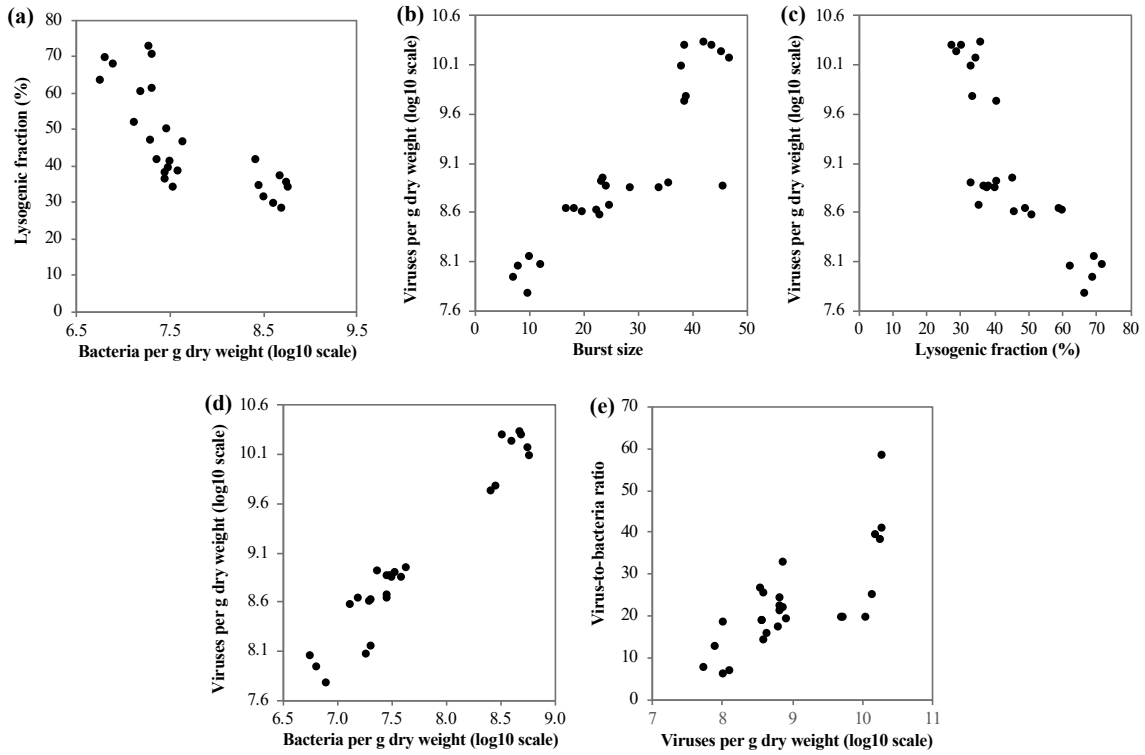

Figure 5.2: Correlation analysis of the traits of viral and bacterial life strategies in soils. (a). The estimated fraction of lysogeny was negatively correlated with bacterial density. (b) Viral abundance was positively correlated with burst size. (c) Viral abundance was negatively correlated with the estimated fraction of lysogeny fraction. (d) Viral abundances were strongly correlated with bacterial abundances. (e) Virus-to-bacteria ratio was positively correlated with viral abundances.

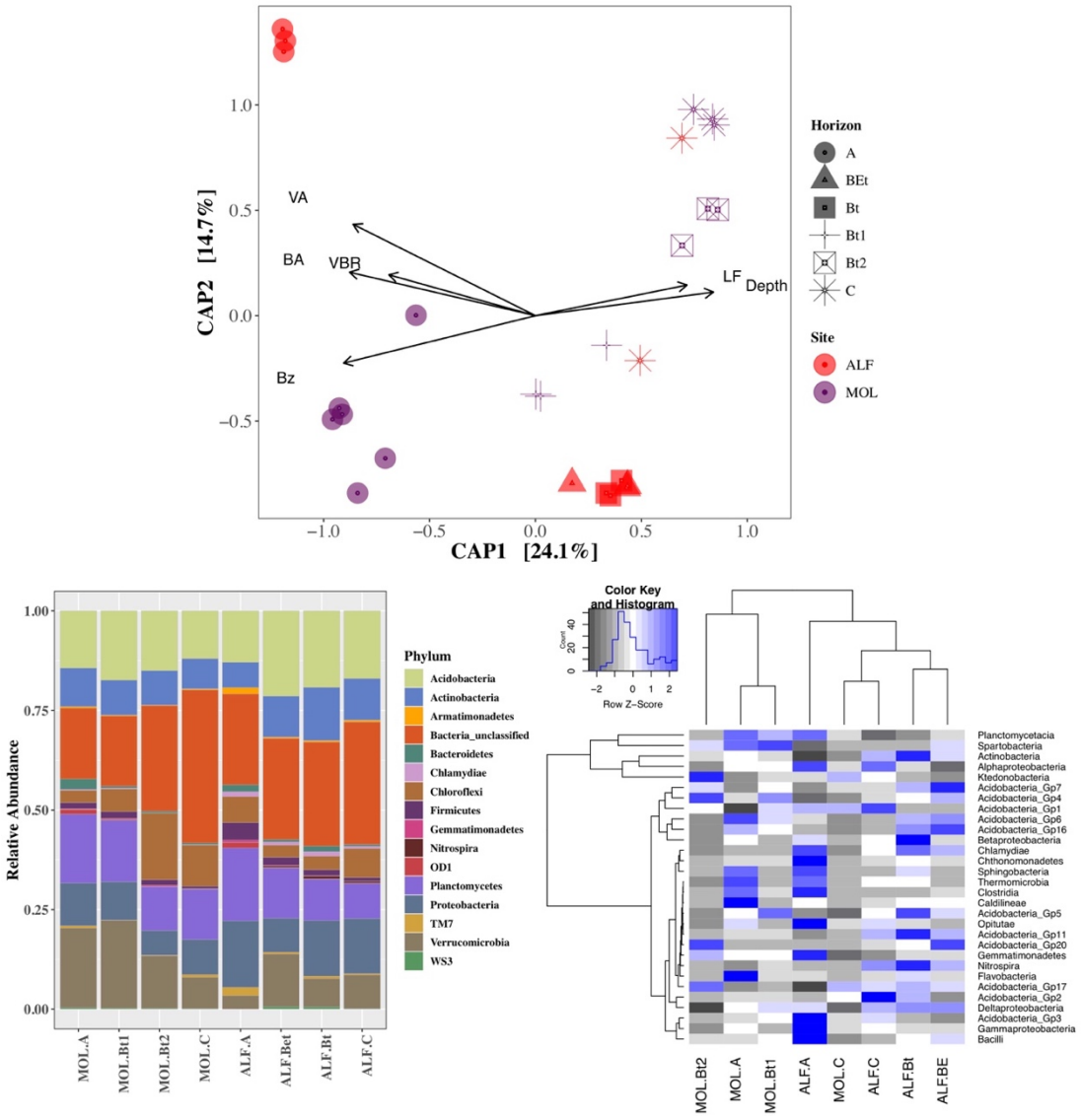

Figure 5.3: Bacterial community composition in soil profiles. (a) Constrained analysis of the principal coordinates (CAP) of bacterial community composition. Samples are color-coded base on sampling site and shape-coded by depth. Arrows indicate notably correlated drivers and the length of the arrow implies the effect size the factor has on the community composition. (b) The relative abundances of major bacterial phylum in soil samples. (c) Heatmap showing the distribution patterns of 30 most abundant OTU groups at class level. The color intensity in each panel indicates the relative abundance per sample. The samples and OTU groups were clustered based on Bray-Curtis distances.

decreasing with depth in both ALF and MOL soil profiles (Fig. 5.3b). The relative abundance of Verrucomicrobia was highest in Bt_1 horizons, while MOL soils as a whole contained substantially higher relative abundance of Verrucomicrobia than ALF soils. The distribution of Acidobacteria was similar in the ALF and MOL soil profiles, with relative abundance increasing from A to Bt1 horizon and decreasing from Bt1 to C horizon. The relative abundance of Proteobacteria decreased from A to B horizons and then increased with depth into the C horizon. Actinobacteria had different distribution patterns in the ALF and MOL soil profiles, and the proportion of Actinobacteria was highest in the A horizon of the MOL soil profile and in the Bt_2 horizon of the ALF soil profile.

The microbial communities in this study were clustered into two major groups based on sampling sites in the hierarchical clustering analysis (Fig. 5.3c). The samples in each group were separated on the basis of soil depth. The Planctomycetacia and Spartobacteria were similarly distributed in the soil samples, with relative abundances highest in the A horizon of the MOL profile yet significantly lower in the A horizon of the ALF profile. Acidobacteria_Gp1, Gp4, Gp6, Gp7, Gp16, and Beta-Proteobacteria were similarly distributed, while Ktedonobacteria, Alpha-Proteobacteria, Actinobacteria, Spartobacteria, and Planctomycetacia were clustered. The relative abundance of Spartobacteria showed a mid-profile peak, highest in Bt_1 horizon (more than 20% relative abundance) of both sites.

Microbiome interactions within soil

Bacterial community richness (based on species number) and diversity (Shannon index) were highest in A horizons and declined with soil depth in both MOL and ALF profiles (Fig. 5.4a). The bacterial richness and diversity were both positively correlated with virus abundance ($r = 0.6$, $p < 0.001$; Fig. 5.4b; Appendix Fig. 5.7). Oppositely, the bacterial species richness was negatively correlated with LF (Appendix Fig. 5.7), while the Shannon diversity showed negative correlation with the fraction of lysogeny in soil ($r = -0.7$, $p < 0.0001$; Fig. 5.4b and c).

Correlation networks were constructed to explore potential connections between metrics of virus populations and the relative abundances of various bacterial classes (Fig.

Figure 5.4: Bacterial community diversity and the relative relationships with viral abundance and lysogenic fraction. a) The bacterial diversity (represented by Shannon index) and species richness decreased with depth in soil profiles. b) Bacterial diversity was positively correlated with viral abundance. The negatively correlation between bacterial diversity and lysogenic fraction. c) The correlation network of virus abundance and lysogenic fraction with bacterial classes. d) The correlations between different nodes were performed with SparCC method. The linkages in the association networks are correlations with *p* value smaller than 0.01 (calculated with 200 bootstrapping processes). The red edges represent negative correlations, and green edges show positive correlations.

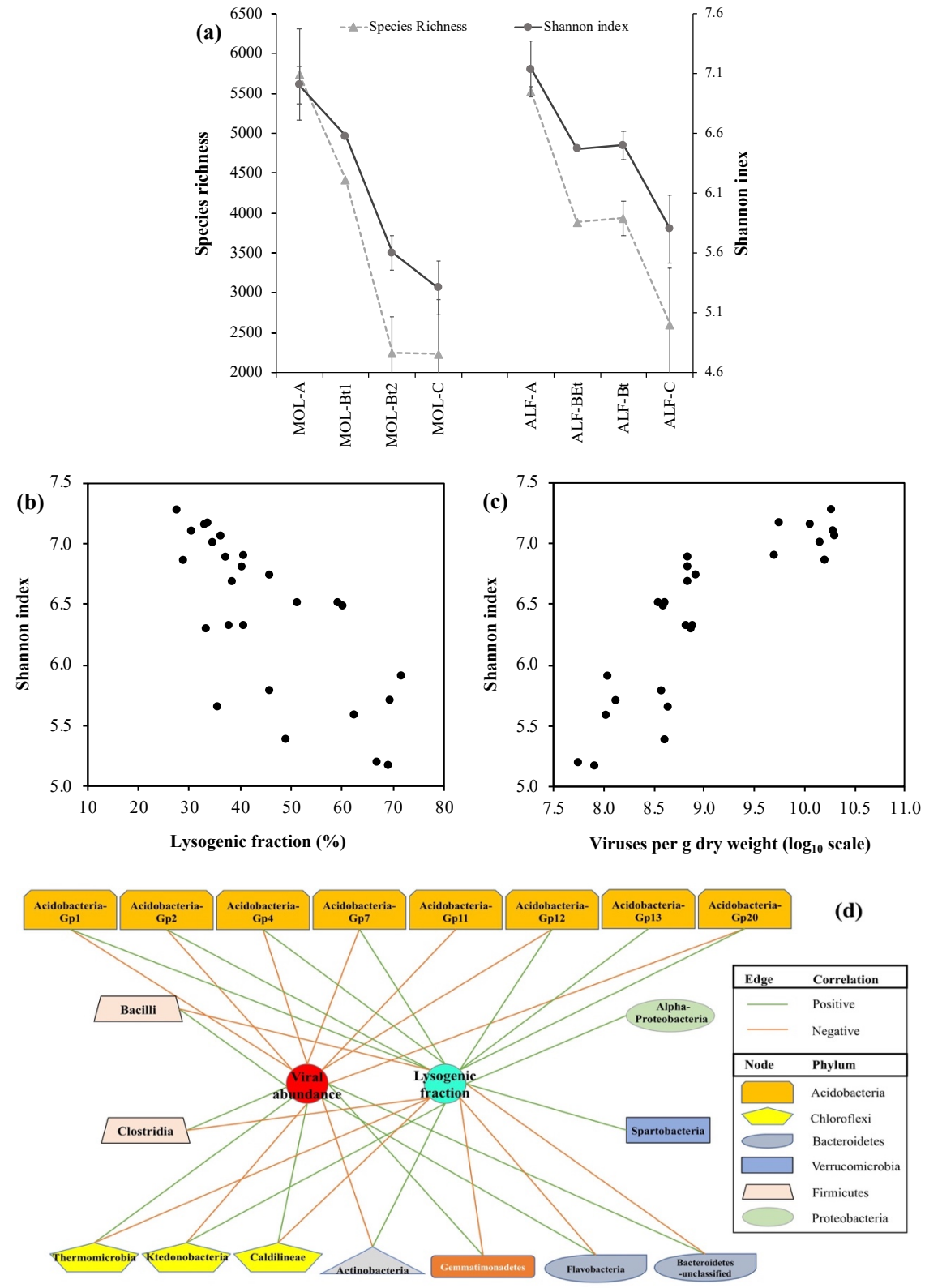

Figure 5.4 continued.

5.4d). All the edges in the network represent correlations with *P* value less than 0.01. Lysogenic fraction was positively related to Acidobacteria classes (Gp1, Gp2, Gp4, Gp7, Gp12, Gp13, Gp20), Alpha-Proteobacteria, Actinobacteria, Spartobacteria, and Kdonobacteria, while viral abundance was negatively related with these classes. Actinobacteria, Spartobacteria, and Ktedonobacteria were also positively correlated with each other and with some of the Acidobacterial classes (Appendix Fig. 5.8). Lysogenic fraction exhibited negative relationships with Flavobacteria, Bacilli, Clostridia, and Caldilineae, yet virus abundance showed positive relationships with these taxa.

The correlation network of bacterial community had the most nodes and edges in the Bt_1 horizon of both ALF and MOL profiles (Appendix Fig. 5.8). The ratio of negative to positive correlations was lowest in A horizon of the MOL profile and in Bt_1 horizon at ALF profile. Members of four bacterial phyla, including Proteobacteria, Acidobacteria, Actinobacteria, and Planctomycetes, were most represented in the bacterial networks.

Virome analysis

A total of 5,025,224 and 2,142,034 sequence reads in surface (0–12 cm) and subsurface (44–108 cm) virome libraries passed through quality control by Trimmomatic, respectively (Table 5.1). Contigs assembled from Megahit were used for taxonomic classification on Kaiju server (Menzel et al., 2016). The virome in surface soil sample (A horizon, 0–22 cm) had more raw sequence reads but less assembled contigs compared with the subsurface soil sample (Bt_2 horizon, 45–116 cm). In general, both soil viromes were dominated by double stranded (ds) DNA tailed phages, while the surface virome also had high relative abundance of single stranded (ss) DNA viruses (Fig. 5.5a). The surface soil virome contained much higher relative abundance (44.5%) of Microviridae, ssDNA viruses, than the subsurface soil virome (0.43%), while the subsurface soil virome had higher relative abundance of dsDNA viruses (97.8%, including *Myoviridae*, *Podoviridae*, and *Siphoviridae*) compared with the surface soil virome (54.9%). The family *Microviridae* were most abundant in the surface soil, and *Myoviridae* were dominant in the subsurface soil. The family-level relative abundance ranking in tailed viruses was *Myoviridae* > *Siphoviridae* > *Podoviridae* in the surface soil and *Myoviridae* > *Podoviridae* >

Table 5.1: Analysis of virome sequence reads in surface (0-12 cm) and subsurface (44-108 cm) soil samples of UP soil profile. The percentage of annotated viral or unclassified sequences was calculated by the number of sequences assigned into the category (annotated as virus or unclassified) divided by the total number of raw sequences reads.

Sample	Number of reads	Total Number of Bases	GC content (%)	Number of contigs generated	Longest contig (bp)	Shortest contig (bp)	Average contig size (bp)	% total abundance	
								Annotated as viral	Unclassified
UP-surface	5,025,224	755,613,621	36.76	1,382	26,072	308	1,161	12.5	87.5
UP-subsurface	2,142,034	322,154,157	35.52	3,171	50,196	301	1,281	7.3	92.7

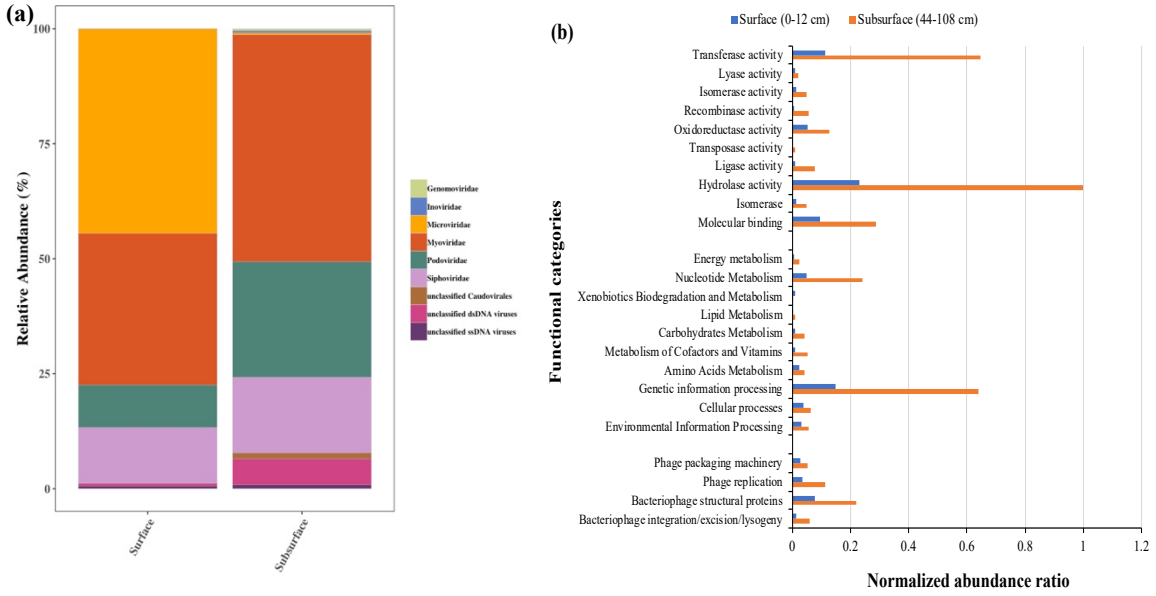

Figure 5.5: Virome annotation. (a) Taxonomic composition of virome in surface (0-12 cm) and subsurface (44-108 cm) soil samples of ALF soil profile. (b) Relative abundance of functional genes in viral metagenomic sequences. Megahit-assembled contigs were used for protein-level sequence classification based on the Burrows-Wheeler transform algorithm in Kaiju server (E-value=1e-10). The predicted ORFs were identified and functionally annotated by VIROME server (compared to the following databases: ACLAME, Clusters of Orthologous Groups of proteins, Gene Ontology Consortium, Kyoto Encyclopedia of Genes and Genomes, SEED) using an E value cutoff of 10^{-5}. Normalized abundance ratio is the abundance of a definite function category divided by the abundance of Hydrolase activity (having the most amounts of prediction ORFs).

Siphoviridae in the subsurface soil.

Viral proteins were predicted from the annotated ORFs on VIROME (Wommack et al., 2015). In general, 37% of the 2,300 predicted viral proteins were functionally annotated in the surface virome, while 44% of the 9,256 predicted viral proteins were functionally annotated in the subsurface virome. Twenty-five functional categories with distinct subsystems were assigned to the libraries (Fig. 5.5b).

The subsurface virome had greater functional abundance in all categories than the surface virome. The categories with the most hits include hydrolase activity, genetic information processing, transferase activity, molecular binding, and bacteriophage structural proteins. The molecular and cellular catalyst activity, especially hydrolase activity, transferase activity, oxidoreductase activity, and ligase activity, were highly represented viral functions in both surface and subsurface viromes. Viromes also contained ORFs with predicted functions for ion-, carbohydrate-, metal cluster-, and protein-binding. The genetic information processing proteins, including proteins for replication and repair, transcription, and translation, were also abundant in the two viromes. Proteins for various metabolic functions (e.g., nucleotide metabolism, amino acid metabolism, and carbohydrate metabolism) were also common. Notably, the predicted proteins associated with bacteriophage integration/excision/lysogeny, phage packaging machinery, and replication were also commonly identified in both sites. However, the subsurface virome had more than 2-fold higher normalized abundance of these predicted proteins than the surface virome.

Discussion

Viral and bacterial abundance

As a fundamental question, viral abundance and distribution in soils has been difficult to address for many years, since the factors influencing the extraction and enumeration are complicated. According to the limited reports, the virus abundance in soils ranges from 2.2×10^3 gdw^{-1} (per gram dry weight) in desert sands to 1.5×10^{10} gdw^{-1} in agricultural soils (Han et al., 2017; Williamson et al., 2017). In this study, the highest virus

abundance was observed in the A horizon (soil surface; 0-10 cm), and the abundance of viruses decreased with depth. Viral infections are believed to be cell-density-dependent, and a higher host density can lead to a larger rate of infection; producing more viruses (Thingstad and Lignell, 1997; Weinbauer and Rassoulzadegan, 2004; Liang and Radosevich, 2019). Viral abundance in this study was positively correlated with bacterial abundance (Pearson correlation, $r = 0.91$, $p < 0.0001$). Our experiments in anaerobic Fe(III)-bioreducing soil columns also showed the positive correlation between viral and bacterial abundances with electron donor (i.e. acetate addition) (Liang et al., 2019). Nutrient stimulation of bacterial growth in soil microcosms also led to a concomitant increase in virus abundance (Srinivasiah et al., 2015).

As the ecological importance of viruses is recognized, research in environmental virology has increasingly attempted to identify their significance in influencing microbial population, productivity, and biogeochemical cycles. The virus-induced effects can be inferred using virus-to-bacteria ratio, proposed as an index reflecting viral reproduction and virus-host interaction patterns (Wigington et al., 2016; Parikka et al., 2017). Previous reports have documented virus-to-bacteria ratio values are highly variable in soils ranging from 0.001 to 8200 (Brum et al., 2016; Wigington et al., 2016; Williamson et al., 2017), yet the mean VBR values in soil ecosystem (Mean = 704) are remarkably higher than in aquatic environments (Mean = 22) (Parikka et al., 2017). In this work, the highest VBR values were detected in the surface soils, and the VBR values decreased with depth in soil profiles and were positively correlated with both viral and bacterial abundance. The positive correlation between the variable virus-to-bacteria ratio and bacterial community diversity observed in these soils are consistent with the potential role of viruses in shaping microbial diversity.

Life strategies of soil viruses

A temperate phage may integrate its genome into the host genome as a prophage entering lysogenic cycle with host cells. Lysogenic reproduction rates are slower than lytic reproduction and may be reflected by low VBR values. However, lysogenic reproduction likely impacts virus-host fitness and coevolution (Bondy-Denomy et al., 2016; Argov et

al., 2017). The lysogenic fractions (LF) among microbes oscillate across different ecosystems and can vary seasonally; usually with higher percentages arising under oligotrophic than eutrophic conditions. Thus, the higher frequency of lysogeny observed in low productivity environments is thought to be associated with nutrient conditions that limit cell growth rates and support low host cell density (Maurice et al., 2010; Thomas et al., 2011; Brum et al., 2016; Silpe and Bassler, 2019). Lysogenic fractions observed in this study were lowest in the A horizons where the host cell densities were greatest, and highest in the C horizons where the lowest host cell densities were measured. The high viral abundance and relatively low lysogenic fraction among bacteria in the A horizons suggest that lytic infection might be dominant in the surface horizon. Lysogenic infection became more prevalent as soil depth increased and bacterial abundance decreased. Similarly, Brum et al. (2016) investigated the temporal changes of viral replication strategies in the Southern Ocean and showed that lysogeny and lytic infections were negatively and positively correlated with bacterial abundance, respectively.

It has been hypothesized that lysogeny is quite common among soil bacteria (Emerson, 2019). A combination of factors rather than one single factor influences the life strategy of viruses and virus-host relationships. MC-based induction of microbial communities from six Delaware soils suggested that approximately 44% of bacteria contained inducible lysogens in surface soils (Williamson et al., 2007), while a cultivation-based experiment found that over 30% of the cultivable bacteria in the same soils contained inducible prophages (Williamson et al., 2008). Some previous studies have shown that lysogeny that enhances the fitness and survival of both viruses and host is associated with low viral and bacterial production rates under less favorable growth conditions, while switching from lysogeny to lytic strategies is associated with increasing bacterial production (Brum et al., 2016; Howard-Varona et al., 2017). However, some studies have proposed the opposite may be true for certain environments in which lysogeny is more prevalent in environments with high host cell densities (e.g., animal gut and near shore ocean environments). The “piggyback-the-winner” model, as it is known, was recently proposed (Knowles et al., 2016), to explain these observations. For example, in some environments such as the animal gut and near shore ocean environments. This research is

the first report of the viral ecology with depth in soil, and the results are consistent with "kill-the-winner" virus-host population dynamics in the heterogeneous soil ecosystems.

With the rapid progress of sequencing technology, whole genome sequencing has been introduced as a promising means of revealing the distribution of lysogeny in nature (Roux et al., 2015; Touchon et al., 2016; 2017). About half of more than 2000 sequenced bacterial genomes were determined to contain prophages (Touchon et al., 2016). The number of prophages in genomes varies widely, with up to 20 contained in certain *Escherichia coli* strains and none in others (Bobay et al., 2012; Roux et al., 2015). Lysogenic conversion plays a key role in the transfer of novel genes between communities, so investigating the ecological consequences of viral replication cycles and conditions driving shifts between lytic and lysogenic strategies is important in microbial ecology.

Viral abundance was negatively related with lysogenic fraction among bacterial populations, suggesting that the extensive lysogeny in soils can maintain the balance of virus-host interactions in the highly heterogeneous conditions of soil. Besides replication strategies of viruses, the number of viruses released per host cell lysed, or burst size, is also an important metric of virus-host interactions (Holmfeldt et al., 2016; Demory et al., 2017; Edwards and Steward, 2017; Maat et al., 2017). Most published studies from aquatic environments report that burst size is positively related to host phenotypes and physiology (e.g., genome size, growth rate, and density) and also subject to environmental conditions, like temperature, oxygen availability and trophic conditions (Parada et al., 2006; Demory et al., 2017; Edwards and Steward, 2017). Estimates of burst size by TEM observation of visibly infected cells range from several to about 500, and the burst size is typically higher under eutrophic conditions than oligotrophic conditions (Bettarel et al., 2004; Parada et al., 2006). Several hypotheses interpreting the variable Bz across different systems have been proposed, suggesting that size and morphology of cells and viruses, environmental conditions, physiological status of hosts, and viral reproduction strategy influence Bz (Parada et al., 2006). In our study, burst size was positively related with VA and BA, and was highest in the A horizons (surface soils) and declined with depth to the lowest in nutrient-poor C horizons (sub-surface). Similar to aquatic environments, both viral abundance and Bz might be related to the trophic conditions in the soil ecosystems.

Bacterial community structure and the interplay with viruses

As sequencing technologies have been increasingly used for studying the microbial communities across an extensive range of soil habitats, pronounced shifts in microbial community structure attributed to contrasting physicochemical and biogeochemical conditions were revealed (Fierer et al., 2003; 2017; Hansel et al., 2008; Ashworth et al., 2017). Viruses, as the most abundant biological entities on earth, play a key role in shaping the microbial communities and influencing nutrient cycling (Emerson et al., 2018; 2019), however, the ecological role of soil viruses has been inadequately studied. To investigate the functions of viral infections in shaping bacterial community, viral abundance, life strategies, and community composition and their correlations with the corresponding bacterial communities need to be considered.

The bacterial communities in the A horizons were most diverse based on species richness and alpha diversity, while the least diverse bacterial communities were observed in the C horizons. Some previous studies have shown similar results that horizon depth has more influence on microbial community composition and diversity than spatially separated sampling sites (Fierer et al., 2003; Eilers et al., 2012; Bai et al., 2017). A recent survey of changes in microbial community structure in response to cropping system and bio-cover also found that the changes of bacterial richness and diversity coincided with soil pH, carbon and nutrient content variability (Ashworth et al., 2017). In contrast, little effort has been made to investigate the impacts of viral infections on microbial communities in soil ecosystems. This study showed that virus abundance, was positively correlated with bacterial diversity indices (Shannon, Inverse Simpson, OTUs), while lysogenic fraction had significant negative correlation with bacterial diversity indices. A recent investigation surveyed the impact of lytic viral infection on freshwater bacterioplankton community structure and suggested that high viral lysis rates supported more diverse community, whereas low viral lysis rates resulted in lower community diversity (Keshri et al., 2017). With respect to the influence of virus infection on microbial diversity, “kill-the-winner” operates on the concept that no one bacterial type can become too numerically dominant because viruses will kill the most abundant bacteria so that the populations stay more even (Thingstad and Lignell, 1997). In contrast, the “piggyback-the-winner” model suggests that

lysogeny is favored at high microbial abundances and growth rates. Considerable efforts have been made in testing the cell density-based paradigms above but no consensus has emerged from these studies (e.g., Maurice et al, 2010; Brum et al., 2016; Keshri et al., 2017; Liang and Radosevich, 2019).

The bacterial community composition changed remarkably with depth in the soil profiles examined. Biotic factors including viral abundance, bacterial abundance, and lysogenic fraction appeared to contribute significantly to the separation of bacterial communities within the soil horizons at the two sampled sites. In previous studies of soil microbial community structure, bottom up environmental factors such as pH, soil texture, oxygen concentration, and resource availability were noted as primary factors influencing microbial community composition and richness in the soil profiles (Fierer et al., 2003; Hansel et al., 2008; Liang et al., 2019). Based the current results, we propose viruses are also major factors impacting the composition and diversity of microbial communities in soil profiles. Viral infection has also been shown to impact microbial community composition in A recent survey in anaerobic digestion of sewage (Zhang et al., 2017).

Our results showed that Bacilli and Gamma-Proteobacteria exhibited the greatest relative abundances in the A horizons (surface soils). These two bacterial classes were determined to be the most widely infected classes in a previous study (Ackermann and Prangishvili, 2012; Kim and Bae, 2018). Host prediction in a recent survey of viral impacts on carbon cycling in thawing permafrost revealed that 45% of linked microbial hosts were Acidobacteria or Verrucomicrobia (members actively involved in organic matter decomposition), and 21% were Proteobacteria, including iron reducers and methane oxidizers (Emerson et al., 2018). Proteobacteria and Acidobacteria16S rRNA genes have been detected within many soil ecosystems, and these two phyla particularly constituted a notable proportion (12 to 21.4% and 6.2 to 18.7%, respectively) of the whole bacterial communities in our study though it cannot be determined if theses taxa were widely infected hosts in the current study based on the data presented. The abundances of Acidobacteria Gp1, Gp2, Gp4, Gp7, Gp11, Gp12, Gp13, Gp20, Spartobacteria, Alpha-Proteobacteria, Actinobacteria, and Ktedonobacteria were positively related with lysogenic fraction, indicating that lysogenic conversions might promote the growth rates and survival

of these bacteria. The increase in viral counts was at the expense of the decrease of some bacterial taxa that were susceptible to viral infection resulting in a decrease in their relative abundance. The relative abundances of Bacilli, Gemmatimonadetes, Clostridia, Sphingobacteria, Flavobacteria, Caldilineae, and Thermomicrobia were positively related with the abundance of free viruses, which might be the indirect response of lysis-based viral infections upon their competitors. However, caution should be used in using correlation networtk analysis to link viruses to predominant host bacteria because the changes in microbial abundances can be derived from multiple governing mechanisms (Alrasheed et al., 2019).

Virome structure and functions

A recent survey in thawing permafrost soils revealed that viral communities differed significantly with soil depth, and the co-occurring microbial community composition, soil moisture, and pH served as predictors of viral community structure (Emerson et al., 2018). In our study, both surface and subsurface viromes were dominated by dsDNA tailed viruses, however the surface soil virome contained much higher relative abundance of ssDNA *Microviridae* than the subsurface virome. The prevalence of *Microviridae* in surface soil viromes coincided with relatively low fractions of lysogeny in surface soil in this study. Previous studies also suggest *Microviridae* tend to be lytic exhibiting rapid infection cycles (Roux et al., 2012; Zhan and Chen, 2019). The dsDNA viruses, including the tailed phages *Myoviridae*, *Siphoviridae*, and *Podoviridae*, accounted for 97.8% of taxonomically assignable sequences in the subsurface virome, and the dominance of dsDNA viruses was consistent with high fractions of lysogeny in deep soils. Kim and Bae (2018) reported high prevalence of lysogeny in murine gut microbiota, and *Myoviridae*, *Siphoviridae*, and *Podoviridae* were most commonly detected prophages in bacterial hosts. The high fraction of lysogeny indicates widespread lysogenic infections which may modulate host gene expression and metabolism through integration and excision of phage genomes. The functional annotation of viromes in this work showed that the subsurface virome contained a higher normalized abundance of functional genes in all categories than the surface virome. The high abundance of functional genes in the

subsurface virome was consistent with the distribution of lysogeny in the soil profiles suggesting lysogenic infections may facilitate gene acquisition from infected host cells by viruses. Notably, genes associated with carbohydrate metabolism, reported in recent studies of soil viruses (Trubl et al., 2018; Jin et al., 2019), were detected in both surface and subsurface viromes, which suggest viruses may be involved in carbon cycling in both surface and subsurface soil environments.

Conclusions

In summary, this study revealed that the virus-bacteria interactions in soil varied with depth and suggested that viruses are an important driver of soil microbial community composition and diversity. The prevalence of lysogeny was positively correlated with soil depth, and the increasing lysogeny fraction coincided with a dominance of dsDNA viruses and higher abundance of functional genes (i.e., AMGs) in the virome. In comparison, ssDNA *Microviridae* were the most abundant viral class in surface soil where viral abundance was highest and lysogenic fraction was lowest. The bacterial community diversity was positively correlated with virus abundance in soil, and the shifts in bacterial taxonomic composition coincides with the varying viral abundances and life strategies in soils. The results collectively showed substantial roles of soil viruses in structuring bacterial communities and potential contribution to microbially-driven processes.

In comparison to progress in aquatic viral ecology, very limited information about bacteria-phage interactions in soils is available. The heterogeneous structure in soil creates diverse microhabitats with potential spatial and temporal isolation of microorganisms from each other and their respective viral predators (Fierer, 2017). The lack of connectivity of individual microbial niches stimulates complicated and differentiated ecological patterns and virus-host strategies with feedbacks into ecosystem functions. The results presented here represent an initial view of the vertical distribution of viral abundance and diversity, and potential impact on bacterial community structure in soil.

Acknowledgements

This work was supported in part by a United States Department of Agriculture project grant to MR (award number: 2018-67019-27792). X.L. also received financial support from China Scholarship Council.

Conflict of Interest

No conflicts of interest are declared.

List of References

Ackermann, H.W. and Prangishvili, D. 2012. Prokaryote viruses studied by electron microscopy. Archives of virology, 157(10),1843-1849.

Alrasheed, H., Jin, R. and Weitz, J.S., 2019. Caution in inferring viral strategies from abundance correlations in marine metagenomes. Nature Communications, 10, 501.

Aminov, R.I. 2011. Horizontal gene exchange in environmental microbiota. Frontiers in microbiology, 2, 158.

Argov, T., Azulay, G., Pasechnek, A., Stadnyuk, O., Ran-Sapir, S., Borovok, I., Sigal, N. and Herskovits, A.A. 2017. Temperate bacteriophages as regulators of host behavior. Current Opinion in Microbiology, 38, 81-87.

Ashworth, A.J., DeBruyn, J.M., Allen, F.L., Radosevich, M. and Owens, P.R. 2017. Microbial community structure is affected by cropping sequences and poultry litter under long-term no-tillage. Soil Biology and Biochemistry, 114, 210-219.

Asnicar, F., Weingart, G., Tickle, T.L., Huttenhower, C. and Segata, N. 2015. Compact graphical representation of phylogenetic data and metadata with GraPhlAn. PeerJ, 3, e1029.

Bettarel, Y., Sime-Ngando, T., Amblard, C. and Dolan, J. 2004. Viral activity in two contrasting lake ecosystems. Applied and Environmental Microbiology, 70(5), 2941-2951.

Bobay, L.M., Rocha, E.P. and Touchon, M. 2012. The adaptation of temperate bacteriophages to their host genomes. Molecular Biology and Evolution, 30(4), 737-751.

Bondy-Denomy, J., Qian, J., Westra, E.R., Buckling, A., Guttman, D.S., Davidson, A.R. and Maxwell, K.L. 2016. Prophages mediate defense against phage infection through diverse mechanisms. The ISME journal, 10, 2854-2866.

Brum, J.R., Ignacio-Espinoza, J.C., Roux, S., Doulcier, G., Acinas, S.G., Alberti, A., Chaffron, S., Cruaud, C., De Vargas, C., Gasol, J.M. and Gorsky, G., 2015. Patterns and ecological drivers of ocean viral communities. Science, 348, 1261498.

Brum, J.R., Hurwitz, B.L., Schofield, O., Ducklow, H.W. and Sullivan, M.B. 2016. Seasonal time bombs: dominant temperate viruses affect Southern Ocean microbial dynamics. The ISME Journal, 10, 437-449.

Coutinho, F.H., Silveira, C.B., Gregoracci, G.B., Thompson, C.C., Edwards, R.A., Brussaard, C.P., Dutilh, B.E. and Thompson, F.L. 2017. Marine viruses discovered via metagenomics shed light on viral strategies throughout the oceans. Nature Communications, 8,15955.

Demory, D., Arsenieff, L., Simon, N., Six, C., Rigaut-Jalabert, F., Marie, D., Ge, P., Bigeard, E., Jacquet, S., Sciandra, A., Bernard, O., Rabouille, S. and Baudoux, A. 2017. Temperature is a key factor in Micromonas–virus interactions. The ISME Journal, 11(3), 601-612.

Dy, R.L., Richter, C., Salmond, G.P. and Fineran, P.C. 2014. Remarkable mechanisms in microbes to resist phage infections. Annual Review of Virology, 1, 307-331.

Edwards, K.F. and Steward, G.F., 2018. Host traits drive viral life histories across phytoplankton viruses. The American Naturalist, 191(5), 566-581.

Eilers, K.G., Debenport, S., Anderson, S. and Fierer, N. 2012. Digging deeper to find unique microbial communities: the strong effect of depth on the structure of bacterial and archaeal communities in soil. Soil Biology and Biochemistry, 50, 58-65.

Emerson, J.B., Roux, S., Brum, J.R., Bolduc, B., Woodcroft, B.J., Jang, H.B., Singleton, C.M., Solden, L.M., Naas, A.E., Boyd, J.A. and Hodgkins, S.B. 2018. Host-linked soil viral ecology along a permafrost thaw gradient. Nature Microbiology, 3, 870-880.

Emerson, J.B. 2019. Soil Viruses: A New Hope. mSystems, 4(3), e00120-19.

Feiner, R., Argov, T., Rabinovich, L., Sigal, N., Borovok, I. and Herskovits, A.A. 2015. A new perspective on lysogeny: prophages as active regulatory switches of bacteria. Nature Reviews Microbiology, 13(10), 641-650.

Fierer, N., Schimel, J.P. and Holden, P.A. 2003. Variations in microbial community composition through two soil depth profiles. Soil Biology and Biochemistry, 35(1), 167-176.

Fierer, N. 2017. Embracing the unknown: disentangling the complexities of the soil microbiome. Nature Reviews Microbiology, 15, 579-590. doi:10.1038/nrmicro.2017.87

Friedman, J. and Alm, E.J. 2012. Inferring correlation networks from genomic survey data. PLoS Computational Biology, 8, e1002687.

Ghosh, D., Roy, K., Williamson, K.E., White, D.C., Wommack, K.E., Sublette, K.L. and Radosevich, M. 2008. Prevalence of lysogeny among soil bacteria and presence of 16S rRNA and trzN genes in viral-community DNA. Applied and Environmental Microbiology, 74(2), 495-502.

Han, L.L., Yu, D.T., Zhang, L.M., Shen, J.P. and He, J.Z. 2017. Genetic and functional diversity of ubiquitous DNA viruses in selected Chinese agricultural soils. Scientific Reports, 7, 45142.

Hansel, C.M., Fendorf, S., Jardine, P.M. and Francis, C.A. 2008. Changes in bacterial and archaeal community structure and functional diversity along a geochemically variable soil profile. Applied and Environmental Microbiology, 74(5), 1620-1633.

Holmfeldt, K., Solonenko, N., Howard-Varona, C., Moreno, M., Malmstrom, R.R., Blow, M.J. and Sullivan, M.B., 2016. Large-scale maps of variable infection efficiencies in aquatic Bacteroidetes phage-host model systems. Environmental Microbiology, 18(11), 3949-3961.

Howard-Varona, C., Hargreaves, K.R., Abedon, S.T. and Sullivan, M.B. 2017. Lysogeny in nature: mechanisms, impact and ecology of temperate phages. The ISME Journal, 11(7), 1511-1520.

Jin, M., Guo, X., Zhang, R., Qu, W., Gao, B. and Zeng, R. 2019. Diversities and potential biogeochemical impacts of mangrove soil viruses. Microbiome 7, 58.

Keshri, J., Ram, A.S.P., Colombet, J., Perriere, F., Thouvenot, A. and Sime-Ngando, T., 2017. Differential impact of lytic viruses on the taxonomical resolution of freshwater bacterioplankton community structure. Water research, 124, 129-138.

Kim, M.S. and Bae, J.W., 2018. Lysogeny is prevalent and widely distributed in the murine gut microbiota. The ISME Journal, 12, 1127-1141.

Kimura, M., JIA, Z.J., Nakayama, N. and Asakawa, S. 2008. Ecology of viruses in soils: past, present and future perspectives. Soil Science & Plant Nutrition, 54(1), 1-32.

Knowles, B., Silveira, C.B., Bailey, B.A., Barott, K., Cantu, V.A., Cobián-Güemes, A.G., Coutinho, F.H., Dinsdale, E.A., Felts, B., Furby, K.A. and George, E.E. 2016. Lytic to temperate switching of viral communities. Nature, 531(7595), 466-470.

Kozich, J.J., Westcott, S.L., Baxter, N.T., Highlander, S.K. and Schloss, P.D. 2013. Development of a dual-index sequencing strategy and curation pipeline for analyzing amplicon sequence data on the MiSeq Illumina sequencing platform. Applied and Environmental Microbiology, 79(17), 5112-5120.

Li, D., Liu, C.M., Luo, R., Sadakane, K., Lam and T.W. 2015. MEGAHIT: an ultra-fast single-node solution for large and complex metagenomics assembly via succinct de Bruijn graph. Bioinformatics 31, 1674-1676.

Liang, X., Zhuang, J., Löffler, F.E., Zhang, Y., DeBruyn, J., Wilhelm, S., Schaeffer, S.M. and Radosevich, M. 2019. Viral and bacterial community responses to stimulated Fe (III)-bioreduction during simulated subsurface bioremediation. Environmental Microbiology, 21, 2043-2055.

Liang, X. and Radosevich, M. 2019. Commentary: A Host-Produced Quorum-Sensing Autoinducer Controls a Phage Lysis-Lysogeny Decision. Frontiers in Microbiology, 10, 1201.

Maat, D., Biggs, T., Evans, C., van Bleijswijk, J., van der Wel, N., Dutilh, B. and Brussaard, C., 2017. Characterization and temperature dependence of arctic *Micromonas polaris* viruses. Viruses, 9(6), 134.

Maurice, C.F., Bouvier, T., Comte, J., Guillemette, F. and Del Giorgio, P.A. 2010. Seasonal variations of phage life strategies and bacterial physiological states in three northern temperate lakes. Environmental microbiology, 12(3), 628-641.

Menzel, P., Ng, K.L. and Krogh, A., 2016. Fast and sensitive taxonomic classification for metagenomics with Kaiju. Nature Communications 7, 11257.

Muyzer, G., De Waal, E.C. and Uitterlinden, A.G. 1993. Profiling of complex microbial populations by denaturing gradient gel electrophoresis analysis of polymerase chain reaction-amplified genes coding for 16S rRNA. Applied and Environmental Microbiology, 59(3), 695-700.

O'Donnell, A.G., Young, I.M., Rushton, S.P., Shirley, M.D. and Crawford, J.W. 2007. Visualization, modelling and prediction in soil microbiology. Nature Reviews Microbiology, 5(9), 689-699.

Pan, D., Nolan, J., Williams, K.H., Robbins, M.J. and Weber, K.A. 2017. Abundance and Distribution of Microbial Cells and Viruses in an Alluvial Aquifer. Frontiers in Microbiology, 8, 1199.

Parada, V., Herndl, G.J. and Weinbauer, M.G. 2006. Viral burst size of heterotrophic prokaryotes in aquatic systems. Journal of the Marine Biological Association of the United Kingdom, 86(3), 613-621.

Parikka, K.J., Le Romancer, M., Wauters, N. and Jacquet, S. 2017. Deciphering the virus-to-prokaryote ratio (VPR): insights into virus–host relationships in a variety of ecosystems. Biological Reviews, 92(2), 1081-1100.

Quast, C., Pruesse, E., Yilmaz, P., Gerken, J., Schweer, T., Yarza, P., Peplies, J. and Glöckner, F.O. 2013. The SILVA ribosomal RNA gene database project: improved data processing and web-based tools. Nucleic Acids Research, 41(D1), D590-D596.

Roux, S., Krupovic, M., Poulet, A., Debroas, D. and Enault, F., 2012. Evolution and diversity of the Microviridae viral family through a collection of 81 new complete genomes assembled from virome reads. PloS One, 7, e40418.

Roux, S., Brum, J.R., Dutilh, B.E., Sunagawa, S., Duhaime, M.B., Loy, A., Poulos, B.T., Solonenko, N., Lara, E., Poulain, J., Pesant, S., et al., 2016. Ecogenomics and potential biogeochemical impacts of globally abundant ocean viruses. Nature, 537, 689-693.

Roux, S., Hallam, S.J., Woyke, T. and Sullivan, M.B. 2015. Viral dark matter and virus–host interactions resolved from publicly available microbial genomes. Elife, 4, e08490.

Silpe, J.E. and Bassler, B.L. 2019. A host-produced quorum-sensing autoinducer controls a phage lysis-lysogeny decision. Cell, 176, 268-280.

Srinivasiah, S., Lovett, J., Ghosh, D., Roy, K., Fuhrmann, J.J., Radosevich, M. and Wommack, K.E. 2015. Dynamics of autochthonous soil viral communities parallels dynamics of host communities under nutrient stimulation. FEMS Microbiology Ecology, 91(7), fiv063.

Thingstad, T.F. and Lignell, R. 1997. Theoretical models for the control of bacterial growth rate, abundance, diversity and carbon demand. Aquatic Microbial Ecology, 13(1), 19-27.

Thomas, R., Berdjeb, L., Sime-Ngando, T. and Jacquet, S. 2011. Viral abundance, production, decay rates and life strategies (lysogeny versus lysis) in Lake Bourget (France). Environmental Microbiology, 13(3), 616-630.

Touchon, M., Bernheim, A. and Rocha, E.P. 2016. Genetic and life-history traits associated with the distribution of prophages in bacteria. The ISME Journal, 10(11), 2744-2754.

Touchon, M., de Sousa, J.A.M. and Rocha, E.P. 2017. Embracing the enemy: the diversification of microbial gene repertoires by phage-mediated horizontal gene transfer. Current Opinion in Microbiology, 38, 66-73.

Trubl, G., Jang, H.B., Roux, S., Emerson, J.B., Solonenko, N., Vik, D.R., Solden, L., Ellenbogen, J., Runyon, A.T., Bolduc, B. and Woodcroft, B.J., 2018. Soil viruses are underexplored players in ecosystem carbon processing. mSystems 3, e00076-18.

Weinbauer, M.G. and Rassoulzadegan, F. 2004. Are viruses driving microbial diversification and diversity?. Environmental Microbiology, 6, 1-11.

Weitz, J.S., Stock, C.A., Wilhelm, S.W., Bourouiba, L., Coleman, M.L., Buchan, A., Follows, M.J., Fuhrman, J.A., Jover, L.F., Lennon, J.T. and Middelboe, M. 2015. A multitrophic model to quantify the effects of marine viruses on microbial food webs and ecosystem processes. The ISME Journal, 9(6), 1352-1364.

Wickham, H. ggplot2: Elegant Graphics for Data Analysis (Springer, 2009).

Wigington, C.H., Sonderegger, D., Brussaard, C.P., Buchan, A., Finke, J.F., Fuhrman, J.A., Lennon, J.T., Middelboe, M., Suttle, C.A., Stock, C. and Wilson, W.H., 2016. Re-examination of the relationship between marine virus and microbial cell abundances. Nature Microbiology, 1, 15024.

Wilhelm, S.W. and Suttle, C.A. 1999. Viruses and nutrient cycles in the sea: viruses play critical roles in the structure and function of aquatic food webs. Bioscience, 49(10), 781-788.

Williamson, K.E., Wommack, K.E. and Radosevich, M. 2003. Sampling natural viral communities from soil for culture-independent analyses. Applied and Environmental Microbiology, 69, 6628-6633.

Williamson, K.E., Radosevich, M. and Wommack, K.E. 2005. Abundance and diversity of viruses in six Delaware soils. Applied and Environmental Microbiology, 71, 3119-3125.

Williamson, K.E., Radosevich, M., Smith, D.W. and Wommack, K.E. 2007. Incidence of lysogeny within temperate and extreme soil environments. Environmental Microbiology, 9, 2563-2574.

Williamson, K.E., Schnitker, J.B., Radosevich, M., Smith, D.W. and Wommack, K.E. 2008. Cultivation-based assessment of lysogeny among soil bacteria. Microbial Ecology, 56, 437-447.

Williamson, K.E., Fuhrmann, J.J., Wommack, K.E. and Radosevich, M. 2017. Viruses in Soil Ecosystems: An Unknown Quantity Within an Unexplored Territory. Annual Review of Virology, 4, 201-219.

Wommack, K.E., Nasko, D.J., Chopyk, J. and Sakowski, E.G. 2015. Counts and sequences, observations that continue to change our understanding of viruses in nature. Journal of Microbiology, 53(3), 181-192.

Zhan, Y. and Chen, F., 2019. The smallest ssDNA phage infecting a marine bacterium. Environmental Microbiology, 21, 1916-1928.

Zhang, J., Gao, Q., Zhang, Q., Wang, T., Yue, H., Wu, L., Shi, J., Qin, Z., Zhou, J., Zuo, J. and Yang, Y. 2017. Bacteriophage–prokaryote dynamics and interaction within anaerobic digestion processes across time and space. Microbiome, 5(1), 57.

Chapter V Appendix

Table 5.2: PerMANOVA analysis showed the correlations between bacterial communities and the driving factors in the soil profiles.

	Site	Depth	Virus abundance	Virus-to-bacteria ratio	Bacterial abundance	Lysogenic fraction	Burst size
R^2	0.23396	0.42049	0.20993	0.15306	0.19852	0.15494	0.19852
p-value	0.001***	0.001***	0.001***	0.001***	0.001***	0.002**	0.001***

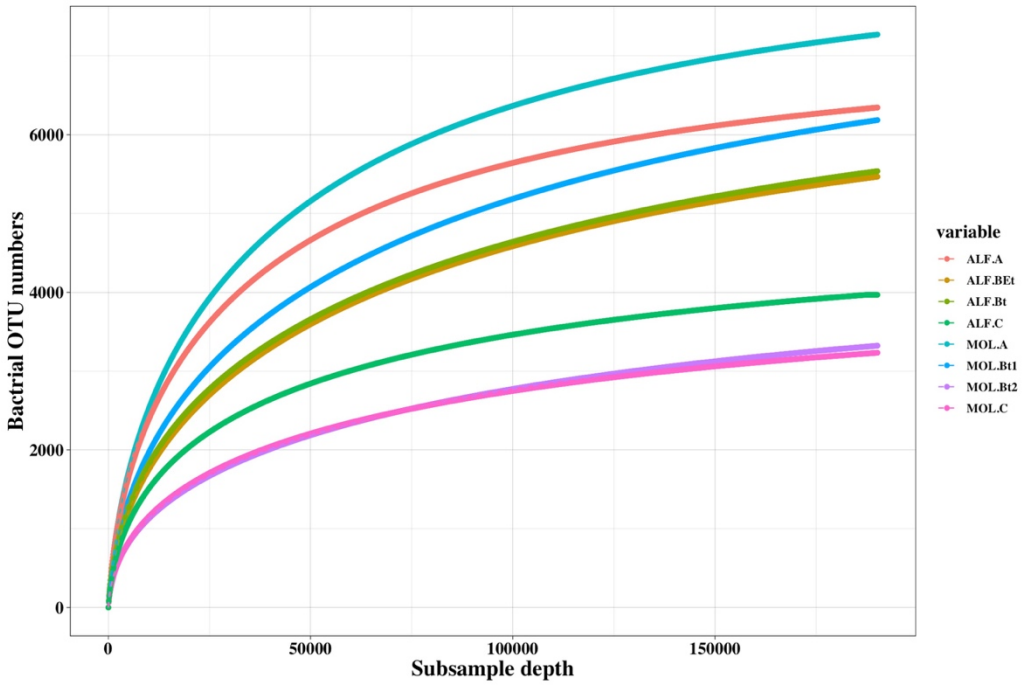

Figure 5.6: Rarefaction curves indicating bacterial 16S rRNA gene richness in soils.

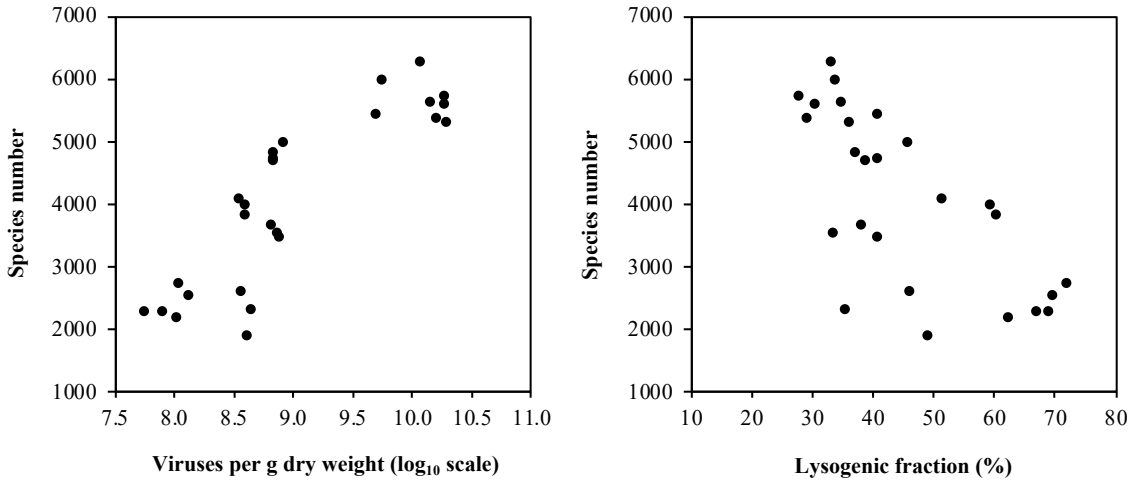

Figure 5.7: Bacterial species (represented by species number) richness was also positively correlated with viral abundance and negatively correlated with the fraction of lysogeny.

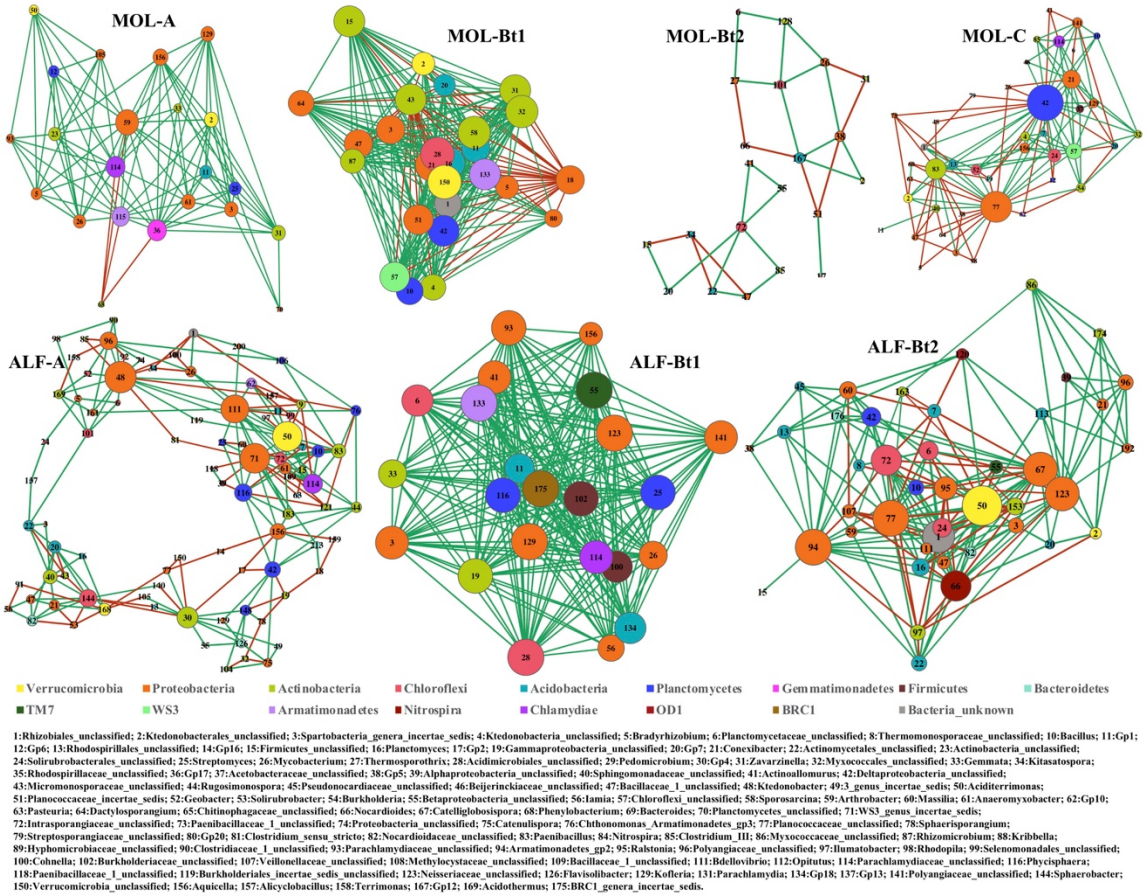

Figure 5.8: The association networks between bacterial taxa in the soil profiles. The co-occurrence correlations between different bacteria were performed with SparCC method, and the edges in the network show correlations with *p* value calculated with 200 bootstrapping processes smaller than 0.01. Negative correlations are shown in red and positive correlations in green. The thickness of the lines represents the strength of the correlations.

CHAPTER VI

Conclusion

While bacterial community structure and activities can be influenced by a variety of environmental factors, viruses shape microbial communities and associated processes through infection and lysis of bacterial hosts across ecosystems. Soil health and subsurface bioremediation are of biogeochemical and economic significance. Increasing efforts are being made to investigate viral abundance and diversity and clarify the functions of viral communities in soil ecosystems. Extremely abundant viruses reside in soil and sedimentary environments, and the genetic diversity of soil viromes also typically exceeds those of other habitats. As obligate parasites of their host, viruses depend on host cells for reproduction. The viral reproductive strategies, i.e. lytic and lysogenic, can have varying effects on host evolution and community structure and function, and have the potential to liberate microbial necromass as a source of soluble carbon and nutrients thereby influencing biogeochemical cycles. The soil heterogeneity and the physical constraints (i.e. pore-scale hydrology and solid-phase adsorption of virus and host cells) exert great impacts on the mobility of viruses and microorganisms and virus-host interactions. Despite the importance of viral ecology in soil systems, research in soil viruses is still rare and even the preliminary information about soil viruses, such as abundance, distribution and diversity, is unknown. We utilized microscopic equipment, molecular tools, high throughput sequencing and bioinformatics tools to study the viral and bacterial communities and virus-host interactions in natural soil environments and a simulated subsurface bioremediation system. The findings of the studies in this dissertation can be summarized as follows.

1. Microbial mediated processes, *i.e.,* anaerobic Fe(III)-bioreduction, contribute to structural breakdown in soil aggregates and may further impact the transport of diffusible ions and molecules and non-diffusible nanoparticles in soil systems. The microbially mediated processes are dependent on the supply of electron donors like acetate, and the microbial effect on the soil aggregate structural breakdown is spatially different in the system.
2. We determined the acetate availability, electron donor in microbial Fe(III)-bioreduction, as an important factor in influencing the viral and bacterial communities in the simulated subsurface bioremediation column system. Notably,

we showed that the genetic composition of viral communities responded to the stimulated Fe(III)-bioreduction in parallel with the bacterial communities. Viral abundance was also an important factor in shaping the bacterial communities in the columns and correlated with the relative abundance of some Fe(III)-reducing bacteria and the total reduced iron.

3. Viral abundance follows bacterial abundance and decreases with depth in a southeastern United States agricultural ultisol. The viral community in surface soils is highly diverse including bacteriophages, amoeba-and eukaryotic-infecting giant viruses and Eukarya dsDNA viruses, while the subsurface viral community is dominated with prokaryote viruses. The complicated viral community composition in surface soils is associated with the high host biodiversity. Surprisingly, the subsurface virome contains higher abundances of potential functional genes than the surface virome.
4. The viral abundances decrease more than bacterial abundances leading to an overall decreasing virus-to-bacteria ratio with soil depth. In comparison, the lysogenic fraction increases with soil depth, indicating lysogeny became the more dominant reproduction strategy for autochthonous soil bacteriophages in deeper soil. The ssDNA *Microviridae* were the predominant viral taxonomic class in the surface soil virome, but had an extremely low relative abundance in the subsurface soil virome. The subsurface soil had higher relative abundances of dsDNA viruses, including *Myoviridae*, *Podoviridae*, and *Siphoviridae*, compared with surface soil. Significant shifts in bacterial community composition and diversity with soil depth were closely correlated with viral abundance, virus-to-bacteria ratio, and lysogenic fraction.

The viral ecology research in soil ecosystems remains in the initial phase, and tremendous work needs to be done to reveal the real picture of soil viruses and their function in terrestrial ecosystem processes. Using the traditional molecular techniques and more contemporary high throughput metagenomics sequencing technology, this dissertation presents a series of studies based on natural soils and laboratory-scale column

experiments to investigate viral abundance, distribution, diversity, and virus-host interactions at nanoscale and ecosystem scale. We identified soil depth-based patterns of viral distribution, diversity and virus-host interactions and shed light on the viral contributions to ecological processes and shaping the microbial communities. The large knowledge gaps in soil viral ecology, such as patterns and ecological drivers of soil viral communities, host linkages, soil virome database, ecological impacts of viral reproductive strategies, community-level biocommunication between viruses in soil systems, and links to soil health and productivity still remain to be filled. However, the rapid development of viral metagenomic approaches and the increasing efforts in viral ecology research laid a solid foundation for future exciting findings.

Soil viral ecology as an exciting new field of treasure in this encouraging era brings new hope and will have significant contribution towards better understanding of the Earth's biosphere. The body of work in this dissertation shed light on the viral ecology in both natural soils and laboratory-scale soil systems and potentially advances the field with the generated new knowledge and hypothesis in it.

VITA

Xiaolong Liang was born in Haiyang, a coastal city in the eastern part of China. He grew up in a small village, where his parents worked very hard to manage their farmland. Xiaolong Liang complete his undergraduate studies in Environmental Engineering from Sichuan Normal University and achieved his MS degree in Microbiology from The University of Chinese Academy of Sciences. He joined he PhD program in UTK in 2015.

Besides being fascinated by the beautiful world in science, he is also passionate about sports. He loved playing soccer, basketball, and badminton. Most importantly, he is a huge fan of Tennessee volunteers and will be Vol for Life.